Implication des canaux sodiques dans la transmission de l'influx nociceptif périphérique et leurs modulations pharmacologiques

Thèse

Olivier Thériault

Doctorat en médecine expérimentale
Philosophiae doctor (Ph.D.)

Québec, Canada

Résumé

Les canaux sodiques dépendant du voltage jouent différents rôles dans la transmission des signaux nociceptifs. Ils participent notamment à la genèse et à la transmission de la douleur. De plus, leur modulation serait impliquée dans les douleurs pathologiques. L'objectif général de ma thèse était d'étudier les impacts de la modulation des canaux Na^+ afin de comprendre les effets sur l'activité des neurones sensitifs. Cette recherche s'est orientée sur 3 axes principaux. Premièrement, nous avons étudié la synergie entre les canaux Na^+ qui mènent aux différents profils électrophysiologiques des neurones. Nous avons observé que les différents canaux Na^+ exprimés dans les neurones de petits diamètres des DRG confèrent des propriétés uniques à chacun des neurones. Le remodelage des canaux Na^+ qui survient dans différents états pathologiques pourrait être responsable de l'hyperexcitabilité de ces neurones. Deuxièmement, nous avons exploré les effets du butamben sur les canaux sodiques. Cette molécule soulage les douleurs pathologiques liées au cancer durant plusieurs semaines sans effet secondaire. Nous avons observé que cette molécule inhibe efficacement les canaux Na^+ exprimés dans les neurones périphériques expliquant partiellement ses effets anesthésiques. De plus, son affinité est plus grande pour les canaux présents au sein des neurones sensitifs périphériques ($Na_v1.7$ et $Na_v1.8$) que pour celui présent dans neurones moteurs ($Na_v1.6$). Cette propriété participerait à la sélectivité du butamben pour l'anesthésie tout en limitant les effets secondaires. Finalement, nous avons étudié les effets sur les canaux Na^+ de trois inhibiteurs sélectifs de la recapture de la sérotonine (SSRI) fréquemment utilisés pour traiter différentes douleurs pathologiques (fluoxétine, paroxétine et citalopram). Nous avons observé que les effets analgésiques de la paroxétine et de la fluoxétine pourraient en partie passer par l'inhibition des canaux Na^+. C'est par ailleurs improbable pour le citalopram compte tenu de sa haute spécificité pour les transporteurs de la sérotonine.

L'étude a permis une meilleure connaissance de l'impact des canaux Na^+ sur l'excitabilité des neurones nociceptifs. Ces avancées permettent notamment de mieux appréhender les mécanismes soutenant l'effet anesthésique des molécules telles que les SSRI et le butamben. Finalement, ces connaissances apparaissent cruciales dans le développement de nouvelles stratégies thérapeutiques.

Abstract

Voltage gated sodium channels (Na^+ channel) play different roles in the transmission of nociceptive signals. They are partially responsible of the genesis and the transmission of the nociceptive action potentials. Moreover, their modulation could be involved in pathological pain. The aim of the study was to investigate the impact of the modulation of sodium channels to understand how it affects nociceptive peripheral neurons excitability. This research was conducted in three phase. First, we were interested in the synergy between the different Na^+ channels leading to multiple electrophysiological profiles of neurons. We observed that the different Na+ channels expressed by the small dorsal root ganglion (DRG) neurons confer unique properties to these neurons. The remodeling which occurs in various pathological conditions may thus be responsible for the increased excitability of those neurons. Second, we explored the effects of butamben on sodium channels. This molecule relieves cancer pain for several weeks without side effects. We found that the drug effectively inhibits Na + channels expressed in peripheral neurons. This partially explains its anesthetic effects. Moreover, its affinity is greater for the channels present in peripheral sensory neurons (Nav1.7 and Nav1.8) than the one present in motor neurons (Nav1.6). This property contributes to the selectivity of butamben for analgesia and limits its secondary effects. Finally, we studied the effects on Na^+ channels of three selective serotonin reuptake inhibitors (SSRI) commonly used in the treatment of various pathological pains (fluoxetine, paroxetine and citalopram). We observed that paroxetine and fluoxetine may partially contribute to the analgesia through the inhibition of Na^+ channels. Citalopram is unlikely to provide anesthesia through this mechanism as it is very selective for serotonin transporter.

The study provides a better understanding of the impact of Na^+ channels on neuronal excitability of nociceptive neurons. These advances contribute to a better understanding of the mechanisms leading to anesthesia by drugs such as SSRIs and butamben. In conclusion, these findings bring fundamental knowledge in the development of new therapeutic strategies.

Table des matières

Liste des tables

Liste des figures

Liste des abréviations

5HT	5-hydroxytryptamine
ADN	Acide désoxyribonucléique
AINS	Anti-inflammatoires non stéroïdiens
AIS	Cone axonique (axon initial segment)
AMPA	Alpha-amino-3-hydroxy-5-methyl-4-isoxazole propionate
ARNm	Acide ribonucléique
ASIC	Canal ionique sensible aux acides
ATP	Adénosine-5'-triphosphate
BAB	Butamben
BZP	*N*-[(*R*)-1-((*R*)-7-chloro-1-isopropyl-2-oxo-2,3,4,5-tetrahydro-1*H*-benzo[*b*]azepin-3-ylcarbamoyl)-2-(2-fluorophenyl)-ethyl]-4-fluoro-2-trifluoromethyl-benzamide
Ca^{++}	Calcium
cAMP	Adénosine monophosphate cyclique
Canal Na^{+}	Canal sodique voltage dépendant
CBZ	Carbamazépine
CCI	Modèle de lésion de nerf par constriction chronique
CFA	Adjuvant complet de Freund
CGRP	Peptide relié au gène calcitonine
CIP	Insensibilité congénitale à la douleur
COX	Cyclo-oxygénase
DAG	Diacylglycérol
DI-DIV	Domaine I à IV du canal Na+
DRG	Ganglion de la racine dorsale
GDNF	Facteur neurotrophe dérivé de la glie
GPCR	Récepteurs couplés aux protéines G
IB4	Isolectin-B4
IFM	Isoleucine, phénylalanine et méthionine
Ig	Immunoglobuline
K+	Potassium
KO	Knock-out
LA	anesthésique local
MAPK	*Mitogen-activated protein kinases*
mGluR	Récepteur glutamatergique métabotrope
MrVIB	µO-conotoxine
Na^{+}	Sodium
$Na_v1.x$	Canal sodiques dépendant du voltage
NGF	Facteur de croissance neuronale

NMDA	N-méthyl-D-aspartate
NSTX	neosaxitoxin
P2X	Récepteur purinergique
PA	Potentiel d'action
PEPD	syndrome de douleur extrême paroxystique
PGE_2	prostaglandines E2
PKA	protéines kinases A
PKC	protéines kinases C
S1-S6	Segment transmembranaire du canal Na+
SCI	Lésion de la moelle épinière
SFN	Neuropathie des petites fibres
SNC	Système nerveux central
SNI	Modèle de lésion de nerf épargné
SNL	Modèle de lésion de nerf par ligature
SNP	système nerveux périphérique
SNRI	inhibiteurs de la recapture de la sérotonine
SSRI	inhibiteurs sélectifs de la recapture de la sérotonine
STX	Saxitoxin
TRP	*transient receptor potential*
TTX	tétrodotoxine
TTX-R	TTX résistant
TTX-S	TTX sensible
V_m	Potentiel de membrane

À ma mère et mon père

Remerciements

Je tiens d'abord à remercier mon directeur de recherche, Professeur Mohamed Chahine. Je lui suis reconnaissant pour la confiance et la liberté qu'il m'a accordées tout au long de ces recherches. Merci aussi pour ta grande disponibilité. Merci Hamid.

Je tiens aussi à remercier le Dr William C. de Groat et le Dr Adrian Sculptoreanu qui m'ont permis de faire un stage à leur laboratoire à l'université de Pittsburgh. Un merci particulier à Adrian pour tout le temps que tu m'as consacré autant au laboratoire qu'à l'extérieur. Merci.

Je tiens aussi à remercier tous les membres du laboratoire Chahine. Merci aux assistants de laboratoire Valérie Pouliot, Hugo Poulin et Karine Drapeau. Je remercie Adrien Moreau et Pascal Gosselin-Badaroudine pour les corrections et les discussions scientifiques, mais particulièrement pour leur amitié. Je ne peux passer sous silence les anciens du laboratoire : Aurélien Chatelier et Rahima Ziane. Je remercie aussi particulièrement Sylvie Pilote et Philipe Chevrier qui m'ont appris l'art de l'électrophysiologie. Je remercie aussi Karine Bachand pour son aide et ses conseils.

Merci à mes amis qui ont su me montrer que derrière les portes du laboratoire se trouve une vie. Merci Étienne, Marie-Pierre, Pierre-Luc, Dominique, Jeff, Marie-Eve, Fredérick, Johannie. Un merci particulier à Bernard pour m'endurer, merci. Merci, Johannie, de m'avoir montré qu'il y a une porte de sortie. Je remercie spécialement Annie d'avoir été si présente tout au long de ma vie, merci.

Merci à mes parents, Francine Gosselin et Gaétan Thériault, qui ont toujours cru en moi et qui m'ont toujours encouragé. Merci aussi à mes frères qui ont toujours su m'inspirer, merci Simon et Mathieu. Merci aussi à Geneviève et Mélanie.

Finalement, je tiens à remercier mes grands-mères, qui m'ont montré force et persévérance.

À vous tous et ceux que j'oublie, Merci!

Avant-Propos

Cette thèse a pour but d'exposer les travaux effectué au cours de mon doctorat effectué sous la supervision du professeur Mohamed Chahine. Ces travaux portent sur l'impact de la modulation des canaux sodiques sur l'excitabilité des neurones de petits diamètres des ganglions dorsaux. La thèse est présentée avec insertion d'articles scientifiques publiés ou soumis à des journaux avec révision par les pairs.

Le manuscrit présenté au chapitre 2, intitulé «Correlation of the electrophysiological profiles and sodium channel transcripts of individual rat dorsal root ganglia neurons » a été publié en 2014 dans *Frontiers in Cellular Neuroscience*. Pour cette étude, j'ai mis au point les différents protocoles de biologie moléculaire et j'ai effectué l'ensemble des expériences électrophysiologiques. Isabel Moreau, sous la supervision du professeure Chantal Mérette, m'a fourni une aide précieuse à l'analyse statistiques des résultats. J'ai rédigé l'article et composé les figures avec les révisions du professeur Mohamed Chahine.

Le manuscrit présenté au chapitre 3, intitulé « Modulation of peripheral Na^+ channels and neuronal firing by n-butyl-p-aminobenzoate» a été publié en 2014 dans la revue *European Journal of Pharmacology*. Pour cette étude, j'ai effectué l'ensemble des expériences électrophysiologiques et de culture cellulaire. Adrian Sculptoreanu a aidé à l'élaboration du manuscrit que j'ai principalement rédigé. Le manuscrit a été révisé par le professeur Mohamed Chahine.

Le manuscrit présenté au chapitre 4, intitulé «Differential modulation of $Na_V1.7$ and $Na_V1.8$ channels by Paroxetine, Fluoxetine and Citalopram » sera soumis pour évaluation au journal *Molecular Pharmacology*. Pour cette étude, j'ai effectué l'ensemble des expériences électrophysiologiques et de culture cellulaire. J'ai

rédigé l'article et j'ai composé les figures. Le professeur Chahine a révisé le manuscrit.

De plus, dans le cadre de mon doctorat j'ai contribués de diverses façons sous forme de collaboration scientifiques selon mon expertise sur les canaux sodiques. L'annexe I contient le manuscrit d'un article publié dans le journal *The Journal of Physiology* intitulé « A distinct de novo expression of Nav1.5 sodium channels in human atrial fibroblasts differentiated into myofibroblasts ». Pour cet article j'ai mis au point, rédigé les protocoles et j'ai fait les expériences de qPCR. L'annexe II est constitué d'un article intitulé « Fluoxetine Blocks Nav1.5 Channels Via a Mechanism Similar to That of Class 1 Antiarrhythmics » publié dans *Molecular Pharmacology.* Pour cet article, j'ai participé à la conception du projet, effectué des expériences et contribuer à la rédaction du manuscrit.

Chapitre I
Introduction générale

La douleur

Nous avons tous une idée de ce qu'est la douleur, mais lorsque nous voulons l'étudier, il est essentiel d'en faire une définition claire. L'Association internationale sur l'étude de la douleur (IASP) définit la douleur comme : « *une expérience sensorielle et émotionnelle désagréable associée à un dommage tissulaire réel ou potentiel, ou décrite en terme d'un tel dommage.* » D'un point de vue physiologique, la douleur est un mécanisme essentiel de protection de l'intégrité corporelle, elle permet de ressentir le danger et ainsi de pouvoir l'éviter. Cependant, lorsqu'elle ne répond plus à un besoin physiologique, la douleur peut devenir pathologique. On distingue ainsi différents types de douleur : la douleur nociceptive, la douleur inflammatoire et la douleur neuropathique (Figure 1).

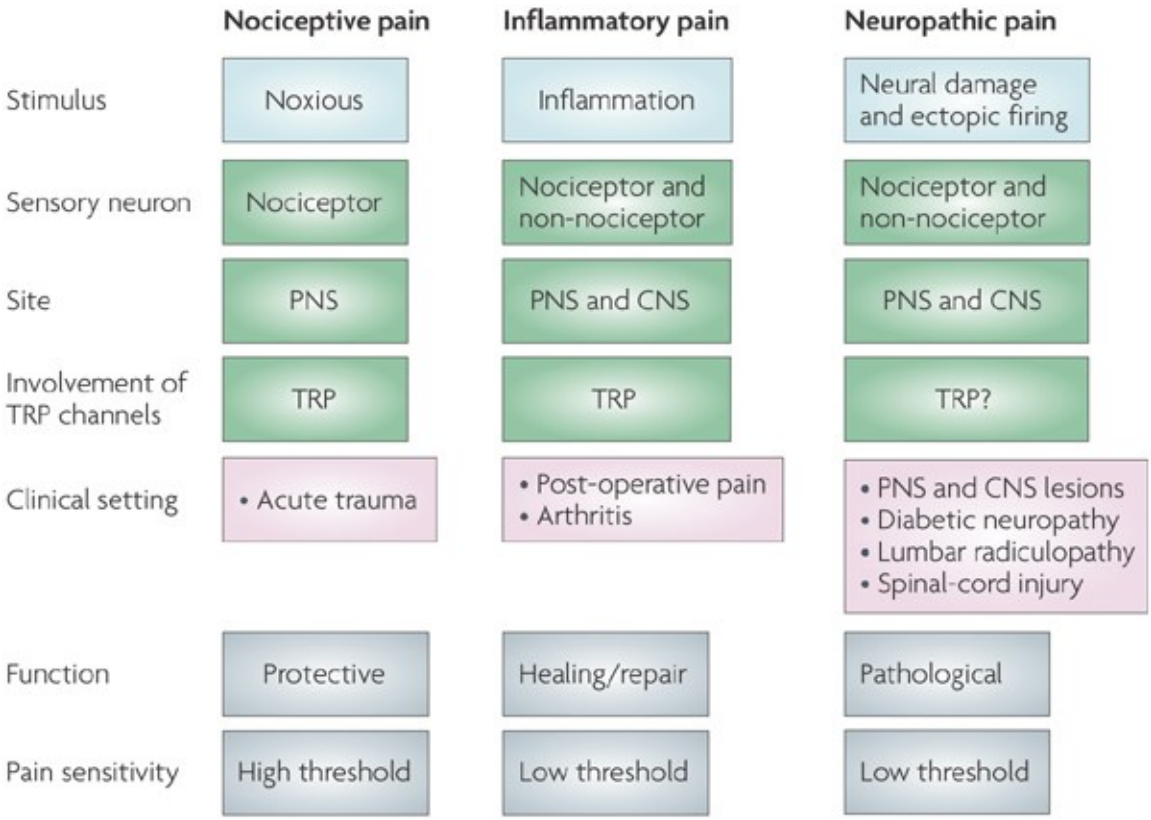

Figure 1. Schéma illustrant certaines caractéristiques des différents types de douleur

Tiré de (Patapoutian *et al.* 2009)

Douleur nociceptive

La douleur nociceptive est aussi dite physiologique ou aiguë. Cette douleur est la réponse normale de l'organisme à un stimulus nocif. C'est celle-ci qui permet à l'organisme de générer une réponse permettant de se protéger. Comme il répond à un stimulus nocif, le seuil pour atteindre la douleur est élevé (Patapoutian *et al.* 2009). La réponse est initiée dans le système nerveux périphérique avant d'être relayée aux aires cérébrales supérieures par la moelle épinière pour être interprétée. Toujours dans un but de protection, la

réponse nociceptive peut aussi provoquer une réponse réflexe, c'est-à-dire sans l'apport des aires cérébrales supérieures (Augustine *et al.* 2001).

Douleur inflammatoire

La douleur inflammatoire est décrite comme une hypersensibilité à la douleur étant causée par l'inflammation résultant d'une lésion. Elle est une condition physiologique qui favorise la guérison. En abaissant le seuil de douleur, l'organisme est forcé de reposer la partie blessée, ce qui permet une meilleure guérison. L'importance de ces douleurs est particulièrement perceptible chez les patients atteints d'insensibilité congénitale à la douleur (CIP). En effet, lors de fracture, les patients atteints d'insensibilité congénitale à la douleur soumettront à des sévices à répétition le membre fracturé, ce qui empêche la guérison et peut finalement conduire à des joints de Charcot (Abdulla *et al.* 2014). La douleur inflammatoire devient cependant pathologique lorsqu'elle persiste au-delà de la guérison.

Suite à une lésion tissulaire, il y aura relargage de différents médiateurs chimiques qui auront pour effet d'abaisser le seuil de la douleur et créer l'hypersensibilité inflammatoire. L'ensemble de ces médiateurs, aussi appelé soupe inflammatoire, est composé entre autres de cytokines, bradykinine, substance P, le facteur de croissance neuronale (NGF), prostaglandines, leucotriènes, endocannabinoides, histamine, protons, ATP, etc. (Woolf 2004; Julius and Basbaum 2001). Ces molécules sont libérées par une panoplie de cellules dont les neurones nociceptifs, cellules endothéliales, kératinocytes, fibroblastes et les cellules du système immunitaire (les mastocytes, les basophiles, plaquettes, macrophages, neutrophiles) (Figure 2).

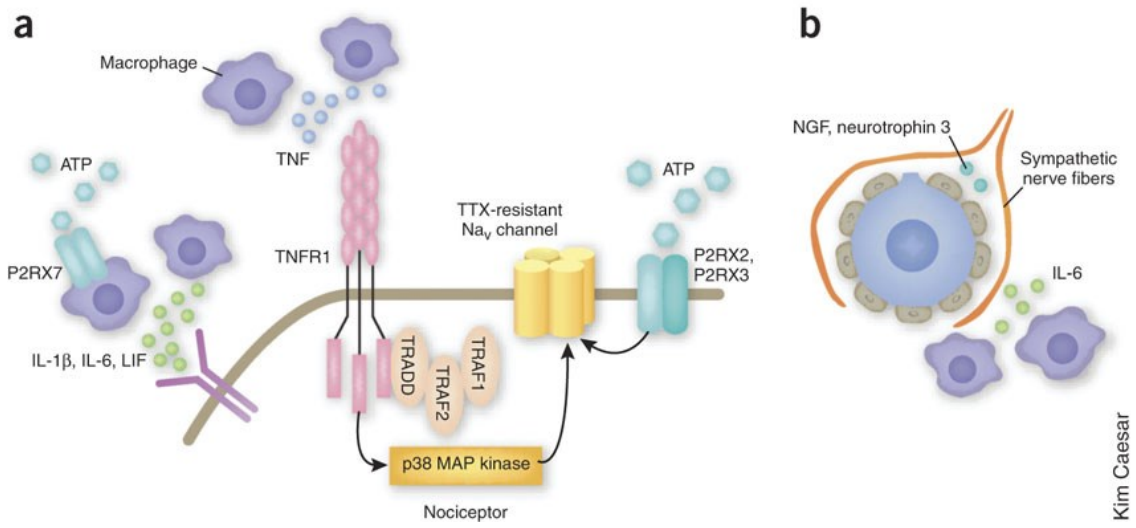

Figure 2. Schématisation des principaux acteurs des douleurs inflammatoires

A) Potentialisation des courants TTX-R par des voies de signalisation impliquant le TNFR1 activé par le TNF. L'activité des nocicepteurs est aussi modulée par les récepteurs purinergiques. B) IL-6 déclenche l'étalement des fibres nerveuses sympathiques dans le DRG. Tiré de (Scholz and Woolf 2007)

Douleur neuropathique

Les douleurs neuropathiques sont des douleurs qui ne répondent plus à un besoin physiologique et qui deviennent donc pathologiques. On définit les douleurs neuropathiques comme : « une douleur qui est la conséquence directe d'une lésion ou d'une maladie affectant le système somatosensoriel » (Treede *et al.* 2008). Pour définir une douleur comme neuropathique, nous devons considérer la durée et la non-réversibilité. Le paramètre de la durée est plutôt arbitraire, mais il est généralement accepté que la douleur chronique est définie comme une douleur qui persiste pendant plus de 3 à 6 mois, ou le temps de "guérison normale" d'une blessure (Debono *et al.* 2013).

Syndromes des douleurs neuropathiques

Hyperalgésie

L'hyperalgésie est le fait de ressentir de façon très douloureuse des stimuli qui sont habituellement ressentis comme inconfortables ou légèrement douloureux (Sandkuhler 2009). Ce phénomène survient fréquemment dans les zones d'inflammations primaires, car les médiateurs de l'inflammation ont pour effet d'abaisser le seuil des neurones nociceptifs. Cependant, ce phénomène survient aussi dans les douleurs pathologiques où il n'y a pas ou peu d'inflammation.

Allodynie

L'allodynie est la perception d'un stimulus inoffensif perçu comme douloureux (Sandkuhler 2009). On ne retrouve pas seulement l'allodynie dans les douleurs neuropathiques, mais aussi dans des conditions physiologiques de douleurs inflammatoires. Par exemple, la sensation d'une caresse perçue douloureuse suite à un coup de soleil.

Douleurs spontanées

Les douleurs spontanées sont des douleurs qui surviennent en l'absence de stimuli extérieurs. Elles peuvent être paroxystiques ou superficielles. La première est décrite par les patients comme une douleur de vive intensité comparable à une décharge électrique et la seconde comme une sensation douloureuse continue souvent comparée à une brûlure (Baron *et al.* 2010). Ces douleurs sont très pénibles chez les patients qui en sont atteints, surtout si elles surviennent la nuit où elles peuvent causer l'insomnie. De plus, nous savons que le manque de sommeil amplifie les douleurs chez les patients atteints de douleurs chroniques (Finan *et al.* 2013).

Fibromyalgie

La fibromyalgie est souvent nommée la douleur chronique généralisée. Les causes de la fibromyalgie sont vagues rendant son diagnostic sujet à débats. Le Collège américain de rhumatologie (ACR) propose que le patient soit atteint de fibromyalgie lorsque celui-ci subit de la douleur depuis au moins trois mois et qu'il ressent de la douleur à la palpation d'au moins 11 des 18 points sensibles (Wolfe *et al.* 1990). Cette maladie est aussi souvent associée à des symptômes secondaires comme la fatigue extrême, des maux de tête, le sommeil non récupérateur et une détresse psychologique. Contrairement à ce qui était initialement pensé, plusieurs preuves montrent une composante neuropathique à cette maladie (Malemud 2009; Sumpton and Moulin 2014), pouvant même impliquer les canaux Na^+ (Vargas-Alarcon *et al.* 2012).

La transmission de l'influx nociceptif

La transmission de l'influx nociceptif est le résultat d'un long processus nerveux qui implique le système nerveux périphérique (SNP) et le système nerveux central (SNC). Cette douleur est initiée par les neurones afférents primaires du SNP et sera relayé au SNC. Le corps cellulaire des neurones afférents primaires se retrouve dans les ganglions de la racine dorsale (DRG). La composante émotionnelle de la douleur étant importante, les étapes précédant l'interprétation sont donc considérées comme la nociception.

Le processus de la perception de la douleur peut se diviser en quatre processus principaux : la transduction, la conduction, la transmission et l'interprétation (Figure 3). Les neurones afférents primaires détecteront un signal potentiellement nocif de la périphérie vers la moelle épinière à l'aide de récepteurs spécifiques et permettront la transduction du signal nociceptif en un signal électrique (transduction). Le courant ainsi généré permettra le déclenchement du potentiel d'action (PA) dans le neurone afférent primaire (conduction). Le potentiel d'action ainsi créé sera conduit jusqu'à l'extrémité

présynaptique où il déclenchera la libération des neurotransmetteurs. Cette libération de neurotransmetteurs (principalement du glutamate) permettra la transmission du signal aux neurones de deuxième ordre de la moelle épinière. Finalement, il y aura transmission du signal au niveau des aires supérieures, où plusieurs régions sont impliquées dans l'intégration et l'interprétation du signal.

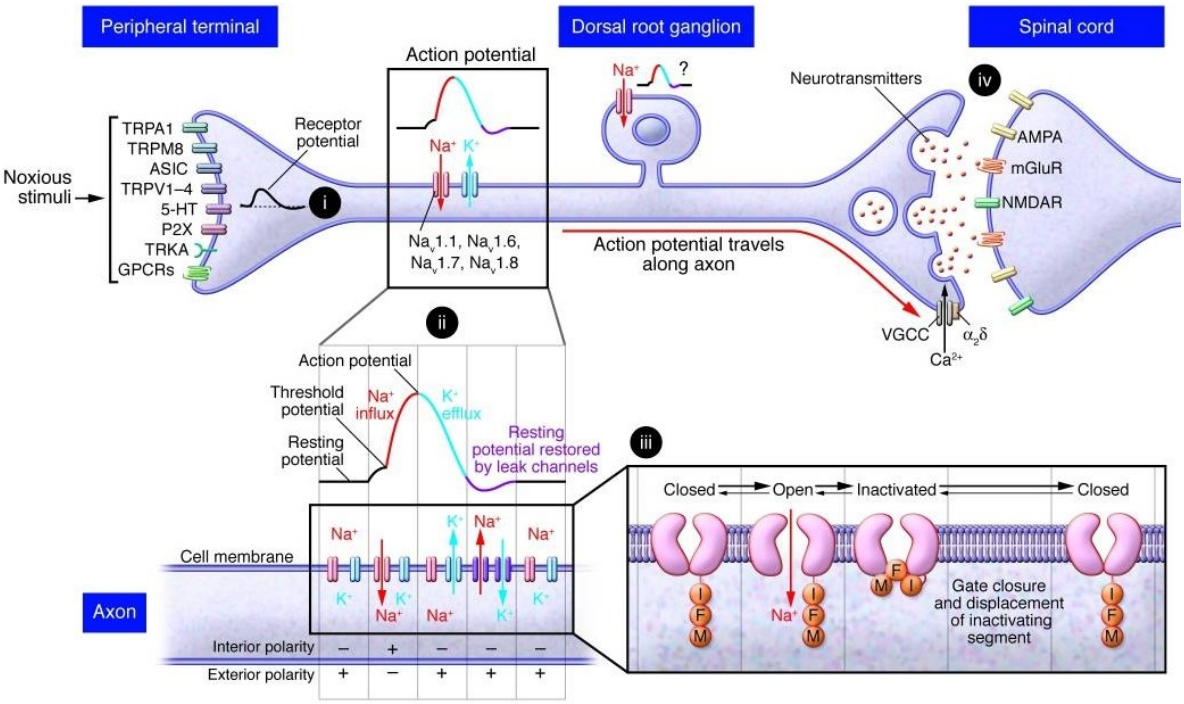

Figure 3. La nociception

Représentation schématique du rôle des canaux sodiques dans la nociception. Les corps cellulaires des nocicepteurs sont contenus dans les DRG et les terminaisons nerveuses libres s'y situent dans les tissus périphériques. Les terminaisons répondent aux stimuli nociceptifs par des récepteurs et des canaux ioniques incluant les TRP, ASIC, les récepteurs 5HT, P2X, TRKA et plusieurs protéines couplées aux protéines G qui activent indirectement des canaux ioniques. Les récepteurs des terminaisons répondent aux stimuli nociceptifs tels la pression et la chaleur (i). Lorsqu'un seuil de dépolarisation est atteint, les canaux Na^+ sont activés et un PA est généré (ii). Durant le PA, les canaux Na^+ s'inactiveront avec la boucle d'inactivation entre 0.5 et 1ms (iii). Dans l'état inactivé, les canaux sodiques ne peuvent être rouverts. Il y aura ouverture des canaux K^+ pour permettre la repolarisation de la membrane. Pendant que la membrane se repolarise, il y aura la réactivation des canaux sodiques (iii). Ce processus est répété pour propager le PA le long de l'axone (ii). Le PA sera propagé jusqu'aux terminaisons présynaptiques des synapses avec les neurones de deuxième ordre dans la moelle épinière. L'influx de Ca^{++} par les canaux Ca^{++} déclenche le relargage des neurotransmetteurs, tel le glutamate, à partir des terminaisons présynaptiques (iv). Le glutamate active les récepteurs ionotropiques AMPA, NMDAR et les récepteurs métabotropiques au glutamate (mGluR) sur les terminaisons postsynaptiques dans la moelle épinière, le signal est transmis par les voies ascendantes aux aires cérébrales supérieures. Tiré de (Raouf *et al.* 2010)

Les neurones afférents primaires

Les neurones afférents primaires des DRG sont classés principalement par le niveau de myélinisation de leurs axones (Figure 4). On distingue les fibres Aβ largement myélinisées qui possèdent une vitesse de conduction de 7 à 50 m/sec voire plus. Ces fibres transmettent principalement de l'information sensorielle non nociceptive. Le dogme selon lequel ces fibres ne peuvent pas être nociceptives est cependant remis en question, mais la littérature sur ce sujet reste anémique (Djouhri and Lawson 2004). On retrouve ensuite les fibres Aδ. Elles sont légèrement myélinisées, conduisent l'influx à une vitesse de 6 à 25 m/sec et sont principalement nociceptives. Finalement, il y a les fibres C non myélinisées qui conduisent l'influx à environs 1m/sec. Ces fibres sont principalement nociceptives.

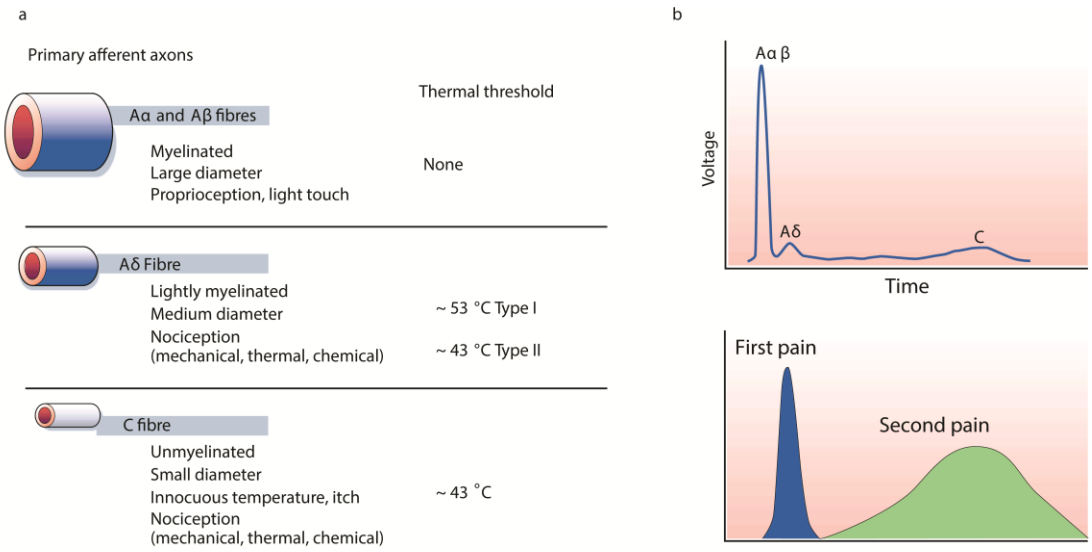

Figure 4. Propriétés des différentes fibres d'afférentes primaires.

Tiré de (Julius and Basbaum 2001)

Les fibres C peuvent être divisées de nouveau en deux groupes. L'isolectine B4 (IB_4) est un marqueur des nocicepteurs non peptidergiques. Ces nocicepteurs expriment généralement le récepteur ionotrope $P2X_3$, les récepteurs au facteur neurotrope dérivé de la glie (GDNFα1-4). Les nocicepteurs non peptidergiques forment la majorité des fibres-C (~70%) et projettent dans la lamina II de la corne dorsale de la moelle épinière (Figure 5). Les neurones peptidergiques diffèrent des non peptidergiques par la réponse au facteur de croissance neuronale (NGF) ainsi que par l'expression de la substance P et du peptide relié au gène calcitonine (CGRP) (Stucky and Lewin 1999; Braz *et al.* 2005).

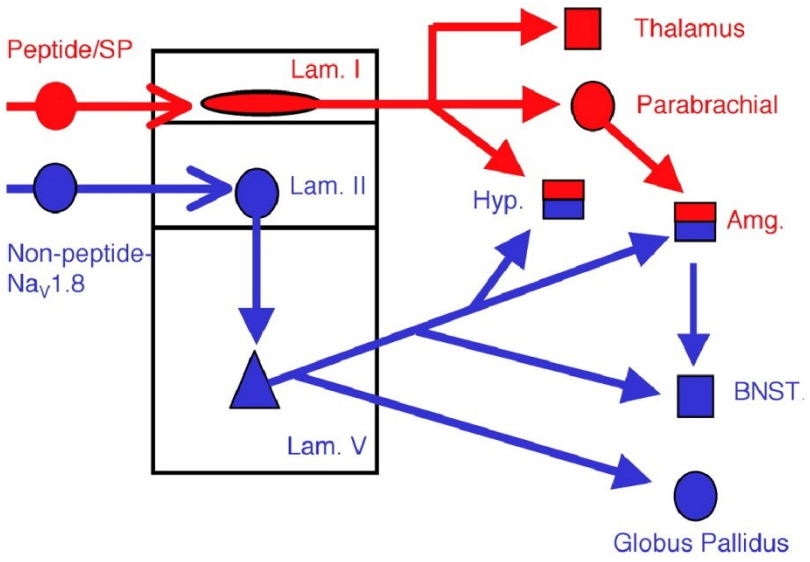

Figure 5. Schéma des circuits des fibres afférentes primaires

Les nocicepteurs peptidergiques projettent dans la lamina I de la moelle épinière alors que les neurones non peptidergiques font connexions aux neurones de deuxième ordre dans la lamina II. Amg, amygdale; BNST, *bed nucleus of the stria terminalis*; Hyp, hypothalamus. Tiré de (Braz *et al.* 2005).

Traitements pharmacologiques de la douleur

Le traitement des douleurs se fait selon l'intensité de la douleur et le type de douleur ressenti. Si les douleurs aiguës suite à un trauma sont assez bien traitées, les douleurs pathologiques demeurent un défi pour les médecins. Les analgésiques existants sont souvent inefficaces ou avec de multiples effets secondaires (Dworkin *et al.* 2007). L'arsenal thérapeutique utilisé a différents mécanismes d'action ciblant différentes composantes des systèmes nerveux périphérique et central (Figure 6).

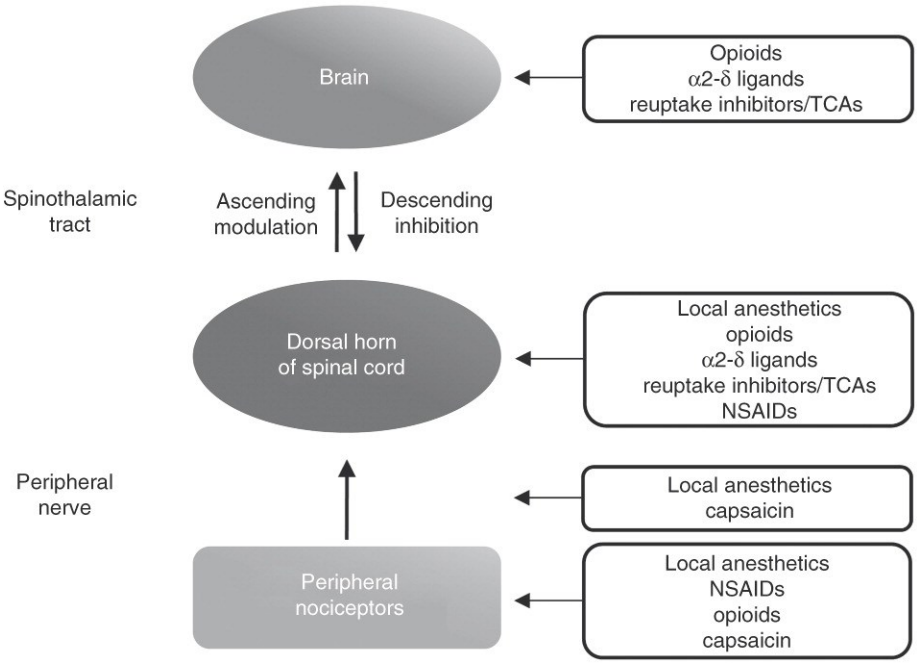

Figure 6. Sites d'actions des principaux analgésiques.

Tiré de (Argoff 2011).

Les anti-inflammatoires non stéroïdiens

Les anti-inflammatoires non stéroïdiens (AINS) avec l'acétaminophène font partie de la première ligne de traitements de la douleur. Ils agissent principalement en inhibant les cyclo-oxygénases COX-1 et COX-2, empêchant la synthèse des prostaglandines. Les AINS ont cependant de nombreux effets secondaires lorsqu'ils sont pris de façon chronique: ulcères, troubles digestifs, hémorragies, complications rénales et risque accru de thrombose (Trelle *et al.* 2011). De plus, leur efficacité est faible à modérée.

Les opioïdes

Les opioïdes sont utilisés dans le traitement des douleurs aiguës et le traitement des douleurs chroniques. Une panoplie de dérivés est maintenant sur le marché ayant des effets plus ou moins puissants. Le principe actif est assez bien connu. Les opioïdes sont en fait des agonistes des récepteurs opiacés diminuant ainsi la libération des neurotransmetteurs (Trescot *et al.* 2008). Les effets secondaires sont multiples, mais ceux limitant leur usage dans le cas des douleurs chroniques sont principalement la sédation, l'euphorie, la tolérance et la dépendance.

Les inhibiteurs de la recapture (SSRI et SNRI)

Les inhibiteurs sélectifs de la recapture de la sérotonine (SSRI) et principalement les inhibiteurs de la recapture de la sérotonine et de la noradrénaline (SNRI) sont couramment utilisés dans le traitement des douleurs neuropathiques et de la fibromyalgie (Dharmshaktu *et al.* 2012; Dworkin *et al.* 2007). Ils sont de plus en plus utilisés dans le traitement des douleurs pathologiques malgré une efficacité modérée en raison de leurs innocuités. Le mécanisme d'action n'est pas entièrement élucidé, mais fonctionne principalement en augmentant l'activation des voies inhibitrices descendantes de la moelle épinière diminuant ainsi la douleur (Rosenberg 2003). Ils pourraient aussi avoir un effet supplémentaire en inhibant les canaux Na^+ (Dick *et al.* 2007; Deffois *et al.* 1996).

Les antidépresseurs tricycliques

Les antidépresseurs tricycliques (TCA) sont largement utilisés dans le traitement des douleurs neuropathiques. Leur efficacité et leur relative innocuité en font un médicament de première ligne dans le traitement des douleurs neuropathiques. Leur mécanisme d'action est cependant inconnu. Il pourrait inclure une inhibition de la recapture de la noradrénaline et de la sérotonine ainsi qu'une inhibition des canaux Na^+ (Bourin *et al.* 2009).

Bloqueur des canaux Na^+

Les bloqueurs des canaux Na^+ ont montré une certaine efficacité dans le traitement des douleurs pathologiques. La principale indication est dans les douleurs localisées. Par exemple, les douleurs liées à la névralgie post-herpétique peuvent être traitées de façon topique avec un gel de lidocaïne (Moulin *et al.* 2007). L'administration intraveineuse, orale et les timbres transdermiques se sont aussi montrés efficaces (Rowbotham *et al.* 1996; Galer *et al.* 1996).

Il existe aussi d'autres gammes de médicaments utilisés pour traiter les douleurs neuropathiques. On retrouve entre autres les anticonvulsifs (gabapentine et prégabaline) et une toxine synthétique (ω-conotoxin) qui agissent en bloquant les canaux Ca^{++}. Malgré cette pharmacopée impressionnante, seulement de 40 à 60% des patients obtiennent un soulagement complet ou partiel de la douleur (Dworkin *et al.* 2007). Cela illustre comment il est primordial d'améliorer le traitement de ces douleurs. La compréhension des différents mécanismes menant aux douleurs neuropathiques permettra l'élaboration de nouvelles stratégies thérapeutiques.

Les canaux sodiques

Les canaux sodiques dépendants du voltage (canaux Na^+) sont des protéines transmembranaires qui se retrouvent dans les cellules excitables. À ce jour, dix sous-types de canaux sodiques dépendants du voltage ont été clonés. Les rôles et les distributions tissulaires des différents canaux Na^+ sont variés (Chahine *et al.* 2005). Ces protéines sont essentielles à l'initiation et à la propagation des potentiels d'action dans les cellules excitables comme les neurones, les myocytes et certaines cellules endocrines. Nous nous intéresserons particulièrement aux sous-types se retrouvant dans les neurones sensitifs périphériques ou ayant été liés aux douleurs pathologiques.

Potentiel de membrane et potentiel d'action

Le potentiel de membrane (V_m) au repos des cellules est le fruit d'un déséquilibre ionique entre le milieu intracellulaire et le milieu extracellulaire. Le V_m au repos est en fonction de la concentration des ions de part et d'autre de la membrane, de leur perméabilité et de la température. L'équation de Goldman–Hodgkin–Katz permet le calcul du potentiel membranaire (Goldman 1943). Comme au repos la perméabilité membranaire est nettement plus élevée pour le K^+, le V_m se situe près de la valeur d'équilibre de ce dernier. Le V_m se situe généralement autour de -65mV dans les neurones sensitifs des fibres C et Aδ. Un mouvement d'ions de part et d'autre de la membrane influencera donc le V_m.

Le potentiel d'action se définit comme la modification transitoire du V_m. Il survient lorsque les cellules excitables sont stimulées et permet la transmission d'un signal électrique. Les PAs sont créés par le mouvement rapide d'ions entre le milieu intracellulaire et extracellulaire. Tel que décrit par Hodgkin & Huxley, le potentiel d'action est un événement tout ou rien (Hodgkin and Huxley 1939). C'est-à-dire qu'il sera déclenché par un stimulus, mais que ce dernier n'influence pas l'amplitude du PA. De façon générale, une fois le seuil

atteint, il y a la phase de dépolarisation rapide, suivi de la repolarisation, de l'hyperpolarisation et du retour au potentiel de repos (Augustine *et al.* 2001).

De façon simplifiée, voici la séquence générique d'un potentiel d'action. De faibles variations de potentiels de membrane par différents stimuli (Figure 3 ii) permettront d'atteindre le potentiel seuil, c'est-à-dire le potentiel où il y aura ouverture des canaux Na^+ et dépolarisation rapide de la membrane. L'activation des canaux Na^+ étant si rapide que le voltage atteint sera près du potentiel d'équilibre des ions Na^+. En quelques dixièmes de millisecondes, il y aura fermeture des canaux sodiques et ouverture des canaux potassiques qui permettront l'entrée de potassium et ainsi la repolarisation de la cellule. La fermeture des canaux potassiques étant lente, une entrée supérieure de potassium créera une hyperpolarisation de la membrane. La pompe Na^+-K^+ ATPase permettra le retour aux conditions ioniques initiales par le transport actif de 3 ions Na^+ vers l'extérieur pour 2 ions K^+ vers l'intérieur de la cellule par ATP dégradé.

Diversité et localisation des canaux Na^+

La famille des canaux Na^+ comprend à ce jour 10 sous-types chacun encodé par un gène unique. Comme nous le verrons dans la section suivante, les canaux Na^+ partagent une structure tridimensionnelle et plusieurs composantes fonctionnelles. La nomenclature des canaux Na^+ est simple : elle commence par l'ion qui lui est perméable (Na^+) suivi du mécanisme qui le régule en indice (v pour voltage) et se termine par le numéro du sous type (Catterall *et al.* 2005). On dénote ainsi les canaux $Na_v1.1$ à $Na_v1.9$ ainsi que le canal atypique Na_x qui est indépendant du voltage.

Malgré une structure similaire, les différents sous-types de canaux Na^+ diffèrent par leurs propriétés biophysiques, leur distribution, leurs sensibilités aux toxines et aux différents agents pharmacologiques (Table 1). Ainsi, on

retrouve des canaux Na^+ qui sont principalement exprimés dans le système nerveux central (SNC), le système nerveux périphérique (SNP) ou les muscles squelettiques sans toutefois s'y restreindre. Par exemple, on retrouve différents variants issus de l'épissage alternatif dans le cortex cérébral du canal $Na_v1.5$ qui a longtemps été cru exclusivement cardiaque (Wu *et al.* 2002; Wang *et al.* 2009). Le muscle squelettique exprime principalement $Na_v1.4$ et le muscle cardiaque $Na_v1.5$. On retrouve les canaux $Na_v1.1$, $Na_v1.2$, $Na_v1.3$, $Na_v1.6$ et Na_x principalement dans le SNC alors que les canaux $Na_v1.7$ à $Na_v1.9$ se retrouvent dans le SNP.

Table 1. Summary of DRG sodium channels

Na^+ channel Isoform	Type (Pharmacology/ kinetics)	Distribution	Unique biophysical characteristics in DRG	Role in AP generation
$Na_v1.1$	TTX-S, fast	Widespread	Unknown	Unknown
$Na_v1.2$	TTX-S, fast	Embryonic	Depolarized activation/inactivation for a TTX-S channel; can produce resurgent current	May maintain firing when misexpressed in MS damaged neurons
$Na_v1.3$	TTX-S, fast	Embryonic	Rapid repriming, ramp current, persistent current	Ectopic firing when misexpressed in axotomy/SCI.
$Na_v1.4$	TTX-S, fast	Not present	N/A	N/A
$Na_v1.5$	TTX-R, fast	Embryonic	Not fully characterized	Unknown
$Na_v1.6$	TTX-S, fast	Widespread	Rapid repriming; persistent current; can produce resurgent current	Maintains high frequency firing when present
$Na_v1.7$	TTX-S, fast	Widespread	Slow onset of inactivation leading to ramp current, slow repriming	Ramp current amplifies small inputs
$Na_v1.8$	TTX-R, slow	Widespread	Very depolarized activation/ inactivation, rapid repriming	Major contributor to action potential upstroke and repetitive firing in small neurons
$Na_v1.9$	TTX-R, persistent	Most small cells (esp. IB4+)	Hyperpolarized activation, overlapping activation/inactivation curves, ultra-slow inactivation	May be involved in setting RMP, amplification of inputs and/or maintaining activation of $Na_v1.8$.

Table 1. Localisation et rôles des canaux Na^+ dans des DRG

Tiré de (Rush *et al.* 2007).

À ce jour, plusieurs maladies ont comme origine les canaux ioniques ou leur régulation, ces maladies sont nommées canalopathies. Par exemple, des mutations retrouvées sur le gène SCN1A (codant pour $Na_v1.1$) provoquent l'épilepsie généralisée avec convulsions fébriles (Wallace *et al.* 2001) et les migraines hémiplégiques. (Weller *et al.* 2014). $Na_v1.5$ est la source de diverses maladies cardiaques comme le syndrome du QT long, le syndrome de Brugada ou plus récemment la cardiomyopathie dilatée (Acharfi *et al.* 2002; Wang *et al.* 2004; Gosselin-Badaroudine *et al.* 2013). Récemment, il a été montré que des mutations sur le gène SCN3A ($Na_v1.3$) sont associées à l'épilepsie focale (Vanoye *et al.* 2014). De plus, il existe une multitude de canalopathies provoquant des douleurs (Figure 7). Comme le sujet est très vaste, nous nous attarderons seulement aux canaux Na^+ qui sont impliqués dans la transmission de la douleur.

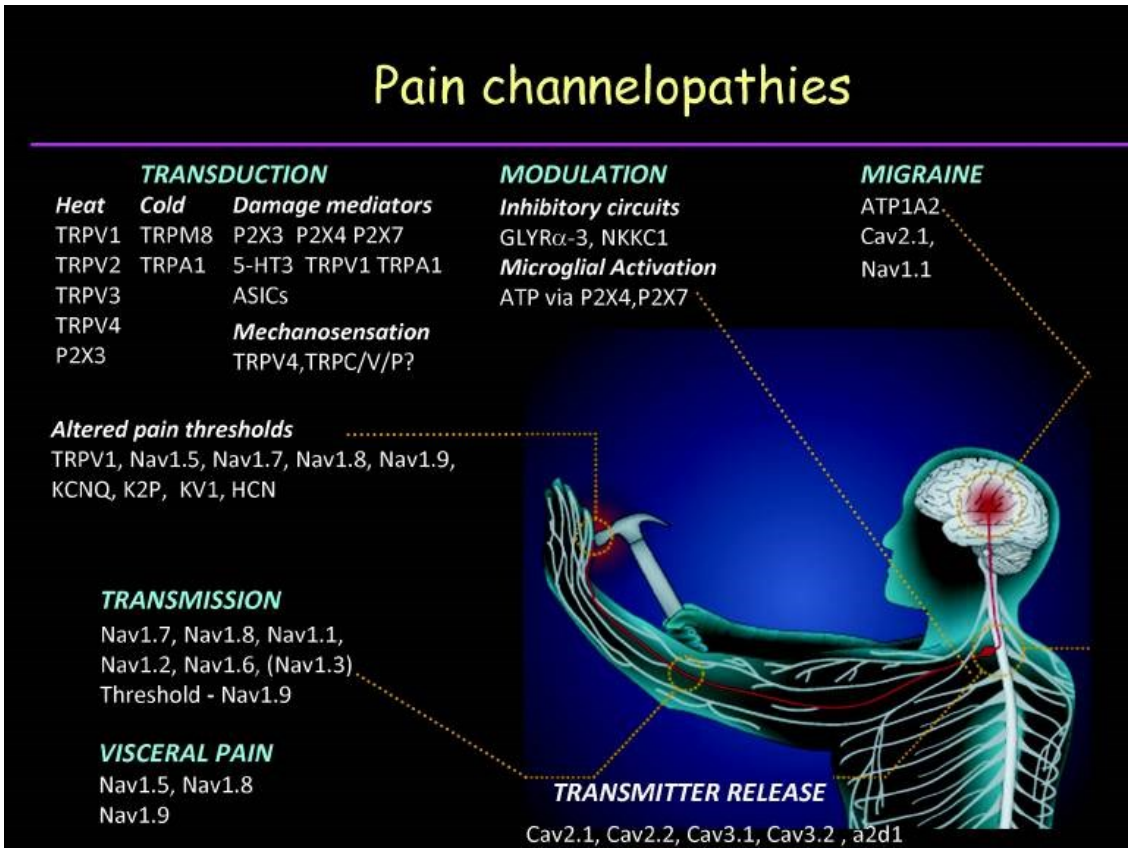

Figure 7. Canalopathies associées à des syndromes douloureux

Tiré de (Cregg *et al.* 2010)

Structure fonction

Sous-unité α

Les canaux Na^+ sont composés d'une sous-unité α de 260kDa qui est en soi suffisante à l'expression d'un canal fonctionnel (Armstrong and Hille 1998). La sous-unité α est formée de quatre domaines homologues (DI à DIV) chacun composé de 6 segments transmembranaires (Figure 8). Les segments transmembranaires sont composés d'une hélice α transmembranaire. Les segments sont nommés selon le domaine et leur rang, par exemple le segment 4 du domaine I se nomme DIS4.

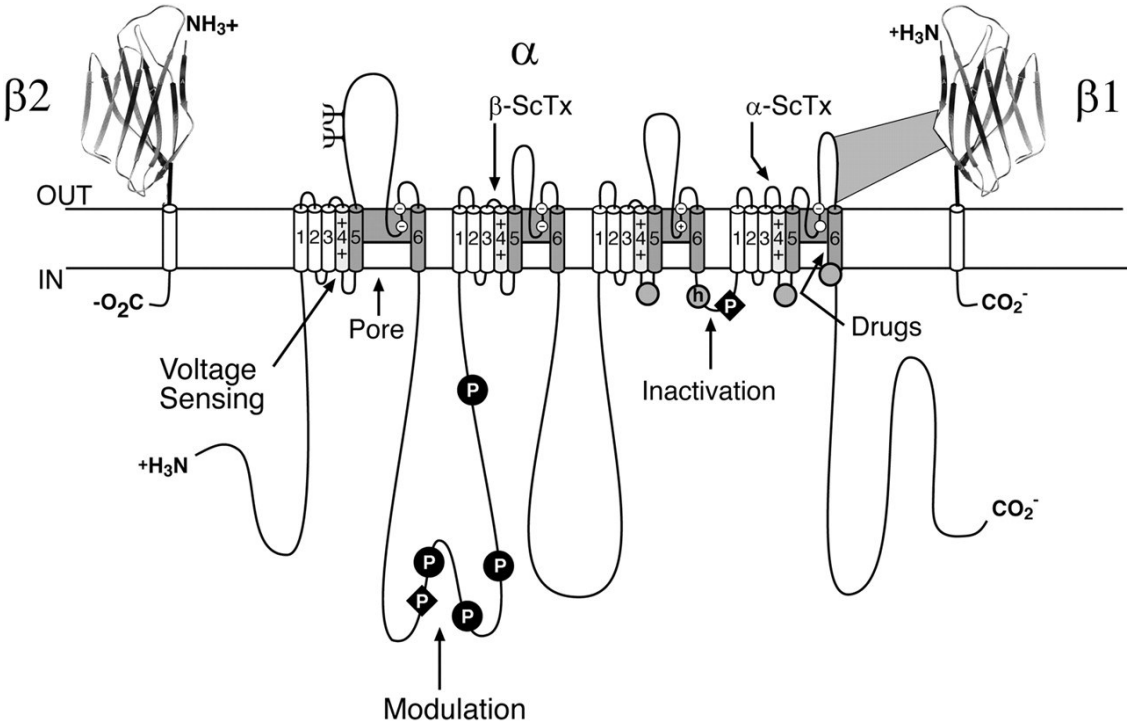

Figure 8. Représentation schématique d'un canal Na^+

Organisation transmembranaire d'un canal sodique. Les cylindres représentent les hélices α transmembranaires. Ψ: sites probables de N-glycosylation. P: sites de phosphorylation par les PKA (cercles) et PKC (losange); Zone ombragée: segments S5-P-S6 Cercles blancs : l'anneau extérieur (EEDD) et l'anneau intérieur (DEKA) du filtre de sélectivité et du site de liaison de la TTX. ++: Senseur de voltage S4; h dans un cercle gris: boucle d'inactivation (IFM) Cercles gris: sites impliqués dans l'ancrage de la boucle d'inactivation. Les sites de liaisons des toxines α- et β de scorpion sont indiqués par des flèches. Tiré de (Catterall *et al.* 2005)

Le senseur de voltage

Une fois assemblé on distingue plusieurs composantes essentielles pour former un canal fonctionnel. Les segments S1-S4 de chacun des quatre domaines du canal Na^+ forment le domaine senseur de voltage (VSD) de ces canaux. Cette structure est conservée parmi plusieurs protéines voltages dépendantes (Yu *et al.* 2005). Le segment S4 joue un rôle central dans la dépendance au voltage de l'activation du canal Na^+. Les acides aminés chargés positivement (3 à 7 résidus) des segments S4, les arginines et les lysines, permettent un changement de conformation de la protéine suite aux variations de voltage menant à l'ouverture du pore (Stühmer *et al.* 1989; Kontis *et al.* 1997). Les segments S1-S3 possèdent aussi plusieurs acides aminés conservés qui sont essentiels au maintien du segment S4 dans différents états conformationnels (Tao *et al.* 2010; Pless *et al.* 2011; Moreau *et al.* 2014).

Il existe 3 principaux modèles quant à la façon dont le S4 pourrait bouger pour mener à l'ouverture du canal. Le premier modèle est l'hélice α de S4 qui glisserait de façon perpendiculaire à la membrane pour permettre l'activation (Catterall 1986). Le second est le modèle à vis hélicoïdale, l'hélice α se déplacerait vers l'extérieure en effectuant un mouvement de rotation telle une vis (Guy and Seetharamulu 1986). Le troisième modèle a été évoqué par le professeur McKinnon suite à la cristallisation de KvAP (Aggarwal and MacKinnon 1996). Ce modèle propose que le segment S4 soit perpendiculaire à la membrane et qu'une dépolarisation le fasse bouger pour devenir presque parallèle à la membrane selon un mouvement nommé « *paddle »*. Cependant, chacun de ces modèles comporte des défauts et n'explique pas certaines données expérimentales (Delemotte *et al.* 2011).

Le pore

Le pore des canaux Na^+ est un élément essentiel qui assure plusieurs fonctions cruciales. En plus de permettre aux ions de traverser la membrane, il

est responsable de la sélectivité aux différents ions et permet la liaison de certaines toxines et des anesthésiques locaux.

La boucle liant les segments S5 et S6 est appelée la boucle-P, elle est composée de 2 courts segments : SS1 et SS2 (short segment). SS1 entre dans la membrane tandis que SS2 en ressort pour former l'embouchure du pore (Pérez-garcía *et al.* 1996; Yamagishi *et al.* 1997). On retrouve sur le segment P le motif DEKA qui permet la sélectivité aux ions Na^+ (Favre *et al.* 1996; Tikhonov and Zhorov 2005). La modification de ces acides aminés permet de changer la sélectivité du canal. Par exemple, une simple mutation dans ce motif rend le canal sodique perméable aux ions Ca^{++} (Heinemann *et al.* 1992b). De plus, le site 1 de liaison des neurotoxines (*neurotoxin binding site 1*) se situe aussi à l'embouchure du pore (Backx *et al.* 1992; Heinemann *et al.* 1992a; Cestèle and Catterall 2000). Ce site permet entre autre la liaison de la tétrodotoxine (TTX), saxitoxin (STX), neosaxitoxin (NSTX) et de la μ-conotoxine. Il est constitué de plusieurs acides aminés chargés négativement nécessaires à la liaison des toxines (Terlau *et al.* 1991; Lipkind and Fozzard 1994). Les neurotoxines se lieraient à ce site et auraient un effet de bouchon empêchant ainsi l'entrée des ions.

L'embouchure interne du pore joue un rôle crucial dans l'inactivation des canaux Na^+. En effet, la boucle reliant les domaines DIII et DIV du canal Na^+ est appelé la porte d'inactivation et comporte le motif IFM essentiel à l'inactivation (isoleucine, phénylalanine et méthionine) (Deschênes *et al.* 1999; McPhee *et al.* 1995). Cette boucle agit comme un couvercle à charnière et bloque le pore du côté intracellulaire Figure 8. Le site de liaison du motif IFM est situé sur plusieurs régions telle que la boucle S4-S5 des domaines DIII et DIV ainsi que la partie intracellulaire de S6 DIV (Kellenberger *et al.* 1997; McPhee *et al.* 1995; Lerche *et al.* 1997).

On retrouve aussi différents sites de liaison aux anesthésiques locaux et à différentes toxines (Ragsdale *et al.* 1996; Kambouris *et al.* 1998; Cestèle and Catterall 2000). Ces aspects seront traités en détails dans les sections traitant de la pharmacologie des canaux Na^+ (p. 29).

Sous-unité β

À la sous-unité α viennent se greffer une ou plusieurs sous-unités β. Les sous-unités β permettent de moduler les caractéristiques biophysiques ainsi que de modifier et de réguler l'expression des canaux Na^+ (Zhao *et al.* 2011; Chahine and O'Leary 2011). Il y a 4 gènes qui codent les différentes sous-unités β_{1-4} actuellement identifiées et clonées (SCN1B à SCN4B) (Chahine *et al.* 2008). On retrouve aussi 2 variants issus de l'épissage alternatif de β1 qui augmentent la complexité fonctionnelle : β1a et β1b (Kazen-Gillespie *et al.* 2000; Qin *et al.* 2003). Leur expression est différentielle selon les types cellulaires et le stade de développement (Table 2) (Ho *et al.* 2012; Chahine and O'Leary 2011). La sous-unité β est une protéine de 22 à 36 kDa. Elle comprend un domaine transmembranaire, une longue queue N-terminale extracellulaire et une courte queue C-terminale intracellulaire (Figure 9). Les sous-unités β1 et β3 se lient de façon non-covalente alors que β2 et β4 se lient de façon covalente au canal Na^+ via un pont disulfure sur une cystéine extracellulaire (Morgan *et al.* 2000; Yu *et al.* 2003).

Table 2 | Tissue distribution of auxiliary β subunits.

Subunit	Apparent M_r (kDa)	Tissue expression	Expression in DRG sensory neurons
β_1	36	Heart, skeletal muscle, CNS, glial cells, PNS	Large, intermediate diameter, and low levels in small-diameter
β_{1A}	45	Heart, skeletal muscle, adrenal gland, PNS	Large, intermediate, and small
β_{1B}	30.4	Human brain, spinal cord, DRG, cortical neurons, and skeletal muscle	Large, intermediate, and small
β_2	33	CNS, PNS, heart	Large, intermediate, and small
β_3	—	CNS, adrenal gland, kidney, PNS	Predominately in small-diameter
β_4	38	Heart, skeletal muscle, CNS, PNS	Large-diameter very low levels in intermediate and small

Table 2. Distribution des sous-unités β dans le système nerveux

(Chahine and O'Leary 2011)

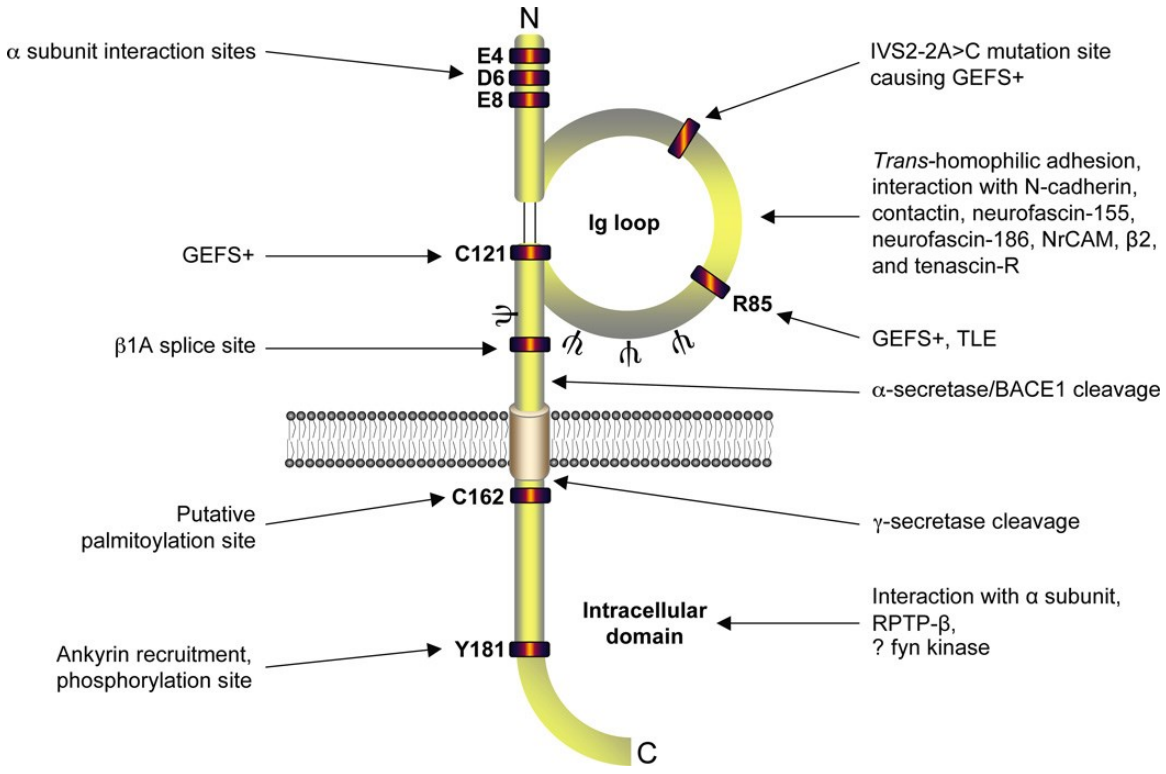

Figure 9. Représentation schématique d'une sous-unité β.

Représentation d'une sous-unité β avec les principaux sites d'interaction. Ψ : sites de N-glycosylation; GEFS+ : Épilepsie généralisée avec convulsions fébriles; TLE : Épilepsie du lobe temporal. Tiré de (Brackenbury *et al.* 2008).

En plus de modifier les propriétés biophysiques, les sous-unités β possèdent un motif immunoglobuline (Ig) dans le domaine N-terminal et forment une famille de protéines d'adhésion cellulaire (Isom 2001; Isom and Catterall 1996). Il a été montré que la sous-unité β permet l'agrégation cellulaire via une interaction homophile et qu'elle se lie physiquement à l'ankyrine au niveau des cônes axoniques et des nœuds de Ranvier (Malhotra *et al.* 2000). β1 et β3 se lient à la neurofascine par le domaine Ig aux nœuds de Ranvier dans les neurones en développement (Ratcliffe *et al.* 2001). De plus, les sous-unités β

interagissent avec des protéines de la matrice extracellulaire telles la ténascine-C et la ténascine-R (TN-C et TN-R), ces dernières sont importantes dans le développement, la migration et la régénération neuronale.

Propriétés biophysiques des canaux sodiques

Chacun des 9 canaux Na^+ possède des propriétés biophysiques différentes qui vont influencer la réponse neuronale. Les canaux sodiques peuvent se retrouver dans différents états : au repos (fermé), activé (ouvert) ou inactivé (ouvert non-conducteur). L'état inactivé peut être subdivisé en 3 états : inactivé rapide (millisecondes), inactivé lent (secondes) et en récupération. Les cinétiques de transition entre ces états sont uniques pour chaque canal Na^+. Dans cette section, nous définirons brièvement les différentes propriétés biophysiques des canaux Na^+ et leurs effets physiologiques sur l'activité neuronale.

Activation

Comme mentionné précédemment, sous l'effet du voltage le S4 se déplace vers l'extérieur et provoque le changement de conformation du canal Na^+ qui permet l'ouverture du pore permettant l'entrée massive d'ions Na^+ (Yang and Horn 1995; Yang *et al.* 1996). La dépendance au voltage de l'activation est un paramètre essentiel qui détermine le seuil d'activation des PA. Ainsi, plus le canal est apte à s'ouvrir à des potentiels hyperpolarisés, plus le neurone est susceptible d'être actif (Dib-Hajj *et al.* 2009) (Figure 10).

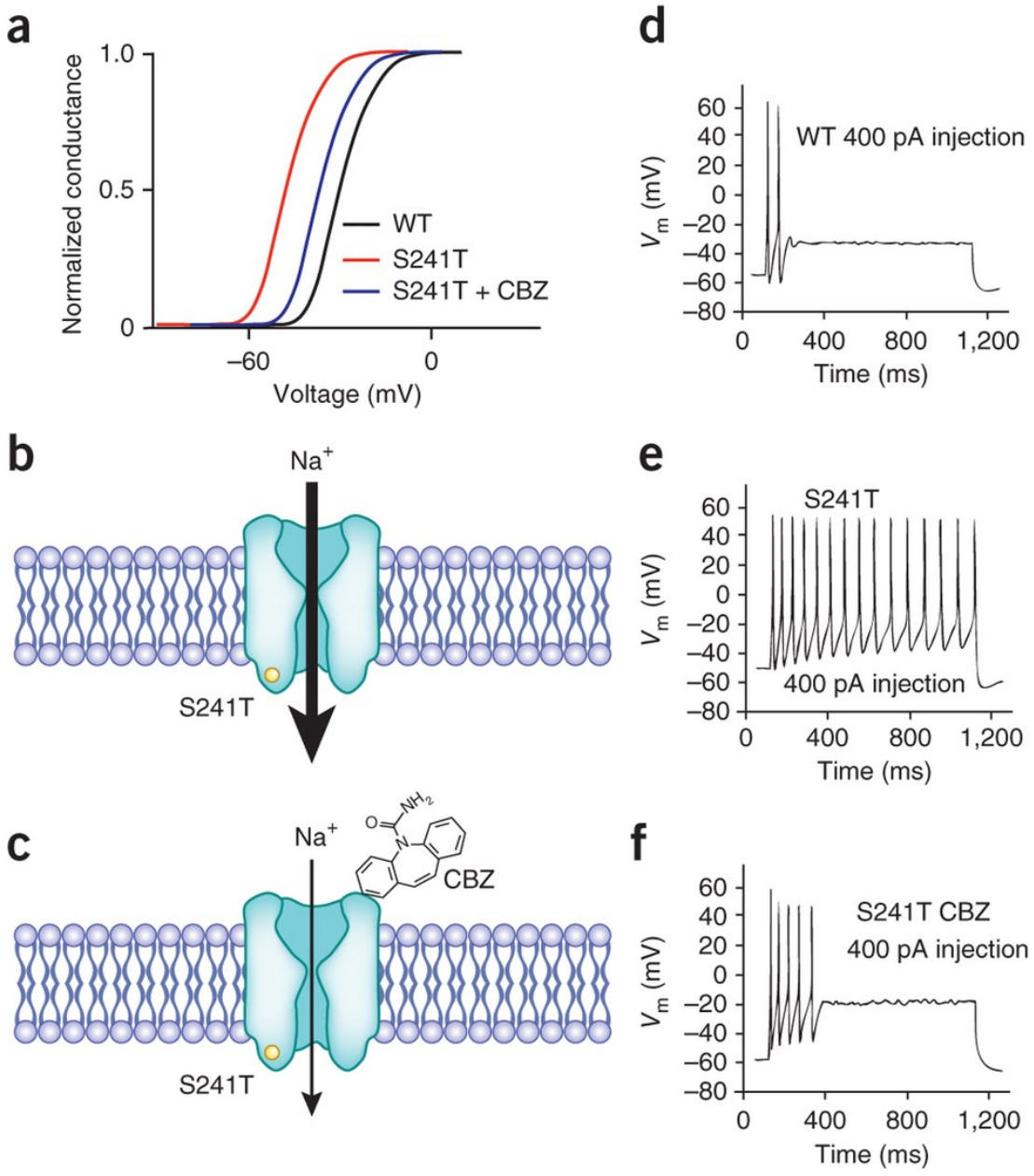

Figure 10. Effet de l'activation du canal Na^+ sur les potentiels d'action

Illustration de l'effet d'un shift de l'activation de $Na_v1.7$ sur les propriétés électrophysiologiques d'un neurone de DRG. (a) Analyse de « *voltage-clamp* » montrant un shift de l'activation du mutant $Na_v1.7$ S241T qui est partiellement compensé par l'application de carbamazépine (CBZ).(b,c) Gain de fonction créé par la mutation S241T b) qui est normalisé par le CBZ c). (d-f) L'analyse en « current-clamp » de cellules de DRG transfecté avec $Na_v1.7$ WT montre une

faible activité(d). La mutation S241T réduit le seuil d'activation et augmente la fréquence des PA (e), l'ajout de CBZ permet le retour à des propriétés similaires au WT. Tiré de (Waxman and Zamponi 2014)

Inactivation rapide

La boucle d'inactivation qui est responsable de l'inactivation rapide permet l'inactivation du canal Na^+ dans l'ordre de la milliseconde. On sait cependant que la queue C-terminale du canal Na^+ est importante dans les cinétiques de l'inactivation rapide. Interchanger le domaine C-terminale du canal $Na_v1.5$ sur le canal $Na_v1.2$ confère à ce dernier une cinétique d'inactivation plus lente similaire à celle de $Na_v1.5$ (Mantegazza *et al.* 2001). La période dans laquelle le canal est inactivé est connue comme la période réfractaire, c'est un état non-conducteur dans lequel une dépolarisation ne permet pas l'ouverture du canal. Cette période permet au potentiel d'action d'être unidirectionnelle. La période réfractaire détermine la fréquence maximale à laquelle un neurone peut déclencher des potentiels d'action. Un déplacement de la dépendance au voltage de l'inactivation rapide vers des potentiels plus hyperpolarisés permettra aux canaux d'être plus actifs et inversement en modifiant la quantité de canaux Na^+ à l'état de repos disponible (Eberhardt *et al.* 2014). La récupération de l'état inactivé influencera aussi la disponibilité des canaux à l'état de repos et par conséquent l'activité des neurones.

Inactivation lente

L'inactivation lente est un état non-conducteur qui survient après une dépolarisation prolongée, cet état peut persister pendant plusieurs secondes. Plusieurs sections du canal Na^+ sont impliquées. Les acides aminés en C-terminal (Veldkamp *et al.* 2000), le motif IFM de la boucle d'inactivation (Richmond *et al.* 1998) et certaines portions du pore (Wang and Wang 1997; Xiong *et al.* 2003) sont importants pour moduler l'entrée dans l'inactivation lente. Cette propriété est importante pour réguler l'activité des neurones étant

donné qu'elle sera directement liée à la disponibilité de l'état de repos des canaux Na^+.

Pharmacologie des canaux Na^+

Les canaux sodiques peuvent être modulés par différents agents pharmacologiques et par différentes toxines qui se lient à des endroits spécifiques. On reconnait six sites de liaisons aux toxines et un site de liaison aux anesthésiques locaux. Ils agissent sur les canaux sodiques de différentes façons afin de les bloquer ou d'en modifier les propriétés biophysiques.

Anesthésiques locaux

Les études initiales sur l'interaction des anesthésiques locaux (LA) et des canaux Na^+ ont montré que le site de liaison se situe du côté intracellulaire (Catterall 2000). Sur le canal $Na_v1.2$, les acides aminés F1764 et Y1771 sont essentiels à la liaison des LAs (Ragsdale *et al.* 1994). Ces acides aminés sont dans DIVS6 vers l'intérieur du pore (Figure 11) (Catterall 2000). On sait maintenant que des acides aminés conservés sur les segments S6 des domaines DI, DIII et DIV sont aussi essentiels à la liaison des LAs. Ce site est aussi le site de liaison des antiarythmiques, des anticonvulsant et des antidépresseurs. L'inhibition des LAs et des molécules qui se fixent sur ce site sont dépendant de l'état du canal et agissent comme modulateurs allostériques. En effet, l'affinité de la lidocaïne est plus grande sur le canal inactivé, présente une inhibition fréquence-dépendante en plus de modifier les propriétés d'inactivation (Chevrier *et al.* 2004).

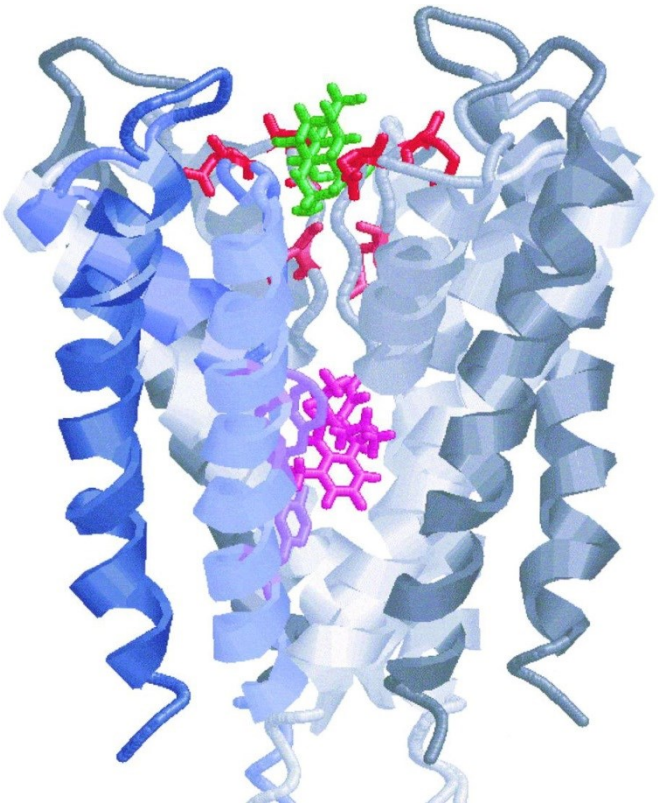

Figure 11. Modélisation du pore du canal sodique

Le modèle du canal potassique Kcsa est utilisé pour représenter le pore du canal Na^+. Le domaine IV du canal sodique est représenté en bleu, les autres segments sont en gris. Les segments S6 sont représentés en bleu clair ou en gris clair alors que les segments S5 sont foncés. Les acides aminés du filtre de sélectivité sont représentés en rouge. La TTX est représenté en vert. Les acides aminés Phe-1764 et Tyr-1771 du site de liaison des anesthésiques locaux sont représentés en bleu sur le segment IVS6. L'étidocaine est représenté en violet à l'intérieur du pore, près du site de liaison des anesthésiques locaux. Tiré de (Catterall 2000)

Les neurotoxines

On retrouve 6 sites de liaisons des neurotoxines sur les canaux Na^+ (Figure 12). Les neurotoxines peuvent se distinguer par les effets qu'elles ont sur les canaux Na^+ (Table 3). On peut ainsi les classer en 3 groupes : les bloqueurs du pore (site 1), les toxines affectant les propriétés biophysiques des canaux par des récepteurs situés dans la membrane (sites 2 et 5) et les toxines affectant les propriétés biophysiques des canaux par des sites extracellulaires (sites 3, 4 et 6) (Cestèle and Catterall 2000). Les toxines du premier groupe bloquent le canal en bouchant l'ouverture du canal Na^+ tel un bouchon empêchant ainsi l'entrée des ions. Les toxines affectant les propriétés biophysiques des canaux sont couplées de façon allostérique. Le changement induit par leur liaison modifie les propriétés biophysiques et permet aussi de modifier l'équilibre entre les états.

Table 1 | Overview of neurotoxin binding sites according to the revised model.

Site	Neurotoxins	Examples	Peptide	Main binding area known up to date	Result
1	Guanidinium toxins	TTX, STX	–	DI–IV P-loop	Block of Na^+ conduction
	μ-Conotoxins	KIIIA, SIIIA, PIIIA	x		
2	Small lipid-soluble toxins	Batrachotoxin	–	DI DIV S6	Negative shift in voltage-dependency of activation
		Veratridine	–		Slowing down of inactivation
		Grayanotoxins	–		Block of Na^+ conductance
		Aconitine	–		Altering ion selectivity
3	Scorpion α-toxins	AaH II, LqhaIT, BMK M1	x	DIV S3–S4	Slowing down of inactivation
	Sea anemone toxins	ATX-II, AFTII	x		
4	Scorpion β-toxins	Css4, Tsγ, AahIT	x	DII S3–S4	Negative shift in voltage-dependency of activation
	Spider β-toxins	Magi 5, HWTX-IV	x		Block of Na^+ conductance
	μO-conotoxins	MrVIA	x		
5	Cyclic polyether compounds	Brevetoxins	–	DI S6	Negative shift in voltage-dependency of activation
		Ciguatoxins	–		Slowing down of inactivation
6	δ-Conotoxins		x	DIV S4	Slowing down of inactivation

Table 3. Sites de liaisons des neurotoxines et leurs effets principaux.

Modifié de (Stevens *et al.* 2011)

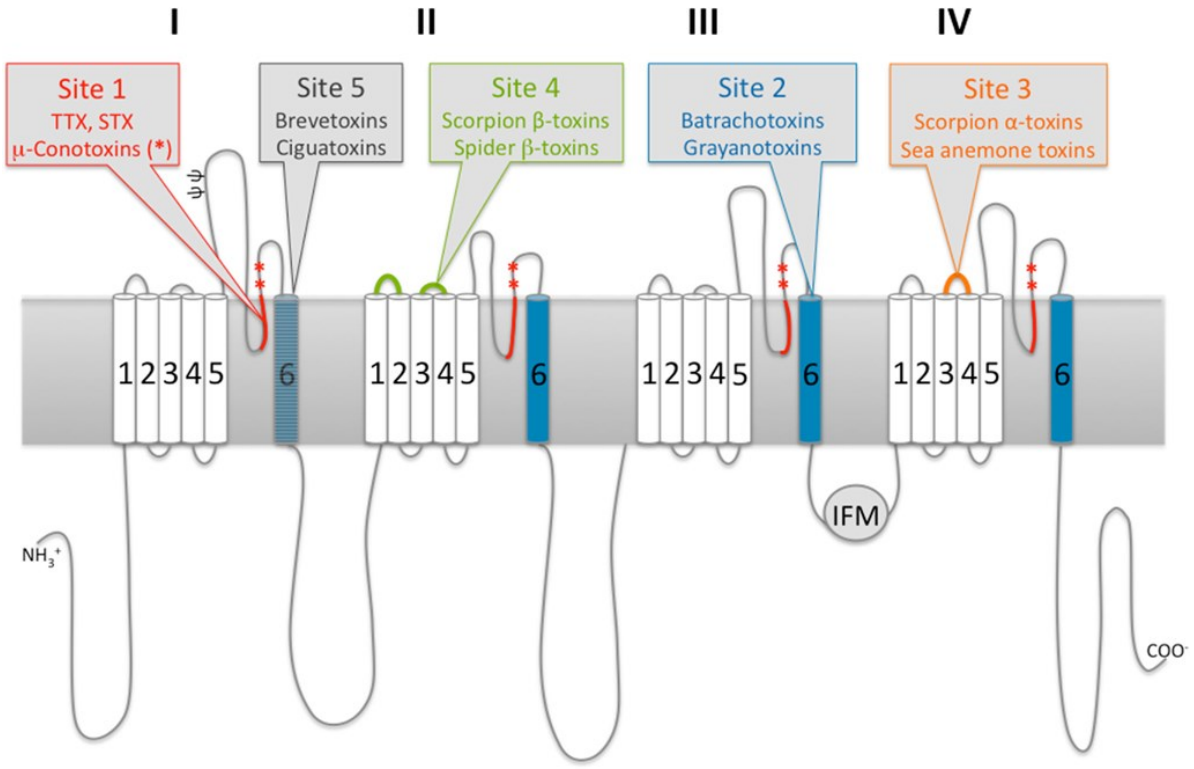

Figure 12. Sites de liaisons des neurotoxines sur les canaux Na^+

Tiré de (Stevens *et al.* 2011)

Développement de nouveaux bloqueurs des canaux Na^+

Les canaux Na^+ semblent une cible de prédilection pour traiter les douleurs chroniques (Dib-Hajj *et al.* 2009; Moldovan *et al.* 2013). Actuellement, les bloqueurs des canaux sodiques ne sont pas spécifiques ce qui implique de nombreux effets secondaires et dangereux. Leur utilisation dans le traitement des douleurs pathologiques est donc limitée. Les chercheurs académiques et industriels concentrent leurs efforts à retrouver des composés qui pourraient être plus spécifiques. Dans les dernières années, différentes molécules

chimiques, toxines et leurs dérivés ont été criblés (Table 4). Malgré quelques essais cliniques, leurs utilisations demeurent essentiellement un outil de laboratoire (Theile and Cummins 2011).

Table 2 | Summary of voltage-gated sodium channel blockers.

Compound	Selectivity	Likely mechanism of action	References
Benzazepinone series	Nav1.7 > Nav1.5 ≫ Nav1.8	State-dependent inhibition	Hoyt et al. (2007a,b)
Pyrazole 20	Nav1.7 > Nav1.8	State-dependent inhibition	Tyagarajan et al. (2010)
ProTx-II	Nav1.7 ≫ Nav1.2-Nav1.6, Nav1.8	Voltage-sensor trapper	Schmalhofer et al. (2008)
2,4-diaminotriazine 52	Nav1.7 ≈ Nav1.3, Nav1.4 > Nav1.5, Nav1.8	State-dependent inhibition	Bregman et al. (2011)
MrVIB	Nav1.8 ≈ Nav1.4 > Nav1.2, Nav1.3, Nav1.5, Nav1.7 ≫ Nav1.9	Blocks conduction pathway	Ekberg et al. (2006), Zorn et al. (2006)
A-803467	Nav1.8 ≫ Nav1.2, Nav1.3, Nav1.5, Nav1.7	State-dependent inhibition	Jarvis et al. (2007)
Ambroxol	Nav1.8 ≥ TTX-S channels	State-dependent inhibition	Leffler et al. (2010)
Capsaicin + QX-314	TRPV1 expressing neurons	TRPV1 activation paired with state-dependent inhibition	Binshtok et al. (2007)
Lacosamide	Chronically depolarized channels	Enhanced slow-inactivation	Errington et al. (2008)
Z123212	Chronically depolarized channels	Enhanced slow-inactivation	Hildebrand et al. (2011)
Riluzole	Persistent currents	Enhanced fast inactivation	Urbani and Belluzzi (2000)
Ranolazine	Persistent currents	Open-channel block	Wang et al. (2008)

Table 4. Nouveaux bloqueurs des canaux sodiques

Tiré de (Theile and Cummins 2011)

Localisation et propriétés des canaux Na^+ impliqués dans la transmission de la douleur

Les canaux Na^+ jouent différents rôles essentiels dans la transmission des signaux nociceptifs. Les canaux sodiques dépendants du voltage sont partiellement responsables de la genèse et de la transmission de la douleur. Les neurones de DRG adultes expriment principalement les canaux $Na_v1.1$, $Na_v1.6$, $Na_v1.7$, $Na_v1.8$ et $Na_v1.9$, mais on retrouve aussi en faible quantité les isoformes $Na_v1.2$, $Na_v1.3$ et $Na_v1.5$. Les sous-types $Na_v1.7$, $Na_v1.8$ et $Na_v1.9$ sont les principaux canaux associés à la perception de la douleur dans les

neurones périphériques (Rogers *et al.* 2006). Dans cette section, nous verrons les sous-types de canaux Na^+ présents dans les neurones de DRG et leur implication spécifique dans la nociception/douleur.

$Na_v1.1$

Le canal $Na_v1.1$ est largement exprimé dans le PNS et le CNS. Les cinétiques des courants TTX-S créés par ce canal sont caractérisées par une activation et une inactivation rapide (Smith and Goldin 1998). Dans les neurones de DRG, l'hybridation in situ a révélé que ce canal est principalement exprimé dans les neurones de large et de moyens diamètres (Black *et al.* 1996). Il n'y a que très peu d'évidences qui impliquent ce canal dans la génération des douleurs. Seule une étude basée sur un modèle de rat SNL montre une surexpression de la protéine par western blot et un nombre augmenté de neurones exprimant la protéine par immunohistochimie avec un anticorps anti-$Na_v1.1$ après la lésion du nerf (Wang *et al.* 2011). Les modèles de douleurs montrent généralement une diminution des ANR_m de ce canal (Berta *et al.* 2008; Fukuoka *et al.* 2012).

$Na_v1.2$

Le canal sodique $Na_v1.2$ est principalement exprimé dans le SNC. Il est exprimé dans le PNS au stade embryonnaire, mais l'expression diminue pour n'être que très faiblement exprimée dans le PNS adulte (Chahine *et al.* 2008). Il ne semble pas être impliqué dans les douleurs périphériques (Cummins *et al.* 2007).

$Na_v1.3$

Le canal $Na_v1.3$ est largement exprimé dans le PNS et le CNS au stade embryonnaire, mais son expression chute par la suite. Il demeure toutefois répandu dans le SNC, alors qu'il est pratiquement absent du SNP (Whitaker *et al.* 2001; Lindia and Abbadie 2003). On le retrouve en particulier au niveau des

lamina I/II de la moelle épinière (Hildebrand *et al.* 2011a). Malgré sa faible abondance dans les neurones de DRG adultes, une surexpression des protéines et des ARNm de ce canal fut l'un des premiers indices qu'il serait impliqué dans la génération de douleurs pathologiques. Il a été montré qu'il est surexprimé dans les modèles de douleurs neuropathiques comme la SNL (Kim *et al.* 2001), l'axotomie des nerfs périphériques (Waxman *et al.* 1994; Xiao *et al.* 2002), la CCI (Dib-Hajj *et al.* 1999) et l'élongation des nerfs (Ohno *et al.* 2010).

Les cinétiques des courants TTX-S créés par ce canal sont caractérisées par une activation et une inactivation rapide typique des canaux TTX-S. Il est à noter que la récupération de l'inactivation est trois fois plus rapide que le canal $Na_v1.7$ et qu'il génère un large courant de rampe suite à une lente rampe de dépolarisation (Cummins *et al.* 2001; Cummins *et al.* 1998). Les propriétés de $Na_v1.3$ favoriseraient une hyperexcitabilité des neurones. En effet, la récupération rapide de l'inactivation favorise une augmentation de la fréquence de décharge (Cummins *et al.* 2007). De plus, la surexpression de $Na_v1.3$ dans les modèles de douleurs neuropathiques induit un courant persistant. Le courant persistant jumelé au large courant de rampe favorise la diminution du seuil de déclenchement des PAs (Lampert *et al.* 2006). L'augmentation de l'excitabilité neuronale par $Na_v1.3$ est suspectée de jouer un rôle dans les décharges ectopiques qui provoqueraient des douleurs spontanées (Lampert *et al.* 2006). $Na_v1.3$ est suspecté de jouer un rôle important dans la sensibilisation centrale. En plus de la surexpression dans les neurones de DRG, il a été montré que les neurones de la moelle épinière (neurones de 2è ordre) et les neurones du thalamus (les neurones de 3è ordre) surexpriment aussi le canal $Na_v1.3$ suite à une lésion de la moelle épinière (Lampert *et al.* 2006). Cela aurait pour effet d'augmenter l'excitabilité neuronale.

Des études utilisant des oligonucléotides antisens et des souris $Na_v1.3$ KO ($Na_v1.3^{-/-}$) montrent des résultats qui semblent contradictoires. L'administration

intrathécale d'oligonucléotides antisens pour $Na_v1.3$ a montré une diminution de l'allodynie associé au CCI et au SCI (Hains *et al.* 2003; Hains *et al.* 2004). Cependant, l'administration intrathécale d'oligonucléotides antisens sur un modèle SNI a montré une diminution d'environ 50% de $Na_v1.3$, mais sans incidence sur l'allodynie au froid ou l'allodynie mécanique (Lindia and Abbadie 2003). De plus, les souris $Na_v1.3^{-/-}$ ayant subi le SNL développent de l'allodynie et des décharges ectopiques (Nassar *et al.* 2006). Les auteurs concluent donc que le canal sodique $Na_v1.3$ n'est pas nécessaire ni suffisant pour provoquer l'hypersensibilité. Le développement de bloqueurs spécifique à $Na_v1.3$ permettrait finalement de définir son implication spécifique dans le développement des douleurs neuropathiques.

$Na_v1.6$

Le canal $Na_v1.6$ est largement exprimé dans le PNS et le CNS. On le retrouve principalement aux nœuds de Ranvier où il permet la conduction saltatoire des PAs (Caldwell *et al.* 2000) et dans les axones des neurones non myélinisés où il permet la conduction continue (Black *et al.* 2002). On le retrouve aussi au niveau des cônes axoniques (AIS), aux dendrites et aux synapses (Shirahata *et al.* 2006; Caldwell *et al.* 2000). La dépendance au voltage de l'activation et de l'inactivation de $Na_v1.6$ ainsi que les cinétiques rapides du courant sont similaires à celles d'autres canaux Na^+ TTX-S ($Na_v1.1$, $Na_v1.2$, $Na_v1.7$) (Smith *et al.* 1998). Cependant, le canal $Na_v1.6$ récupère environ 5 fois plus vite de l'inactivation que le canal $Na_v1.7$ et l'inactivation à l'état fermé de $Na_v1.6$ qui se produit à des potentiels plus hyperpolarisés que $Na_v1.7$ (Herzog *et al.* 2003). La récupération de l'état inactivé aurait pour effet de permettre les décharges à très haute fréquence des neurones de gros diamètres des DRG pouvant être supérieures à 100Hz. L'inactivation à l'état fermé de $Na_v1.6$ aurait pour effet d'atténuer la réponse aux petites dépolarisations aux nœuds de Ranvier. $Na_v1.6$, dans certaines conditions, peut montrer un courant résurgent. Le courant résurgent se produit lorsque les canaux Na^+ s'ouvrent durant la phase de récupération de l'inactivation (Raman and Bean 1997). Il est estimé que le

courant résurgent provoqué par le canal $Na_v1.6$ augmente la fréquence de PAs dans les cellules de Purkinje (Khaliq *et al.* 2003).

L'apport de $Na_v1.6$ dans les douleurs pathologiques est supporté par des preuves indirectes depuis plusieurs années. Des études ont montré une surexpression des ARNm de $Na_v1.6$ dans les DRG chez un modèle de neuropathie diabétique (Craner *et al.* 2002) et une augmentation de la protéine au site lésé suite à une lésion du nerf sous-orbitale (Henry *et al.* 2007). Plus récemment, l'utilisation d'un modèle animal d'allodynie au froid induit par l'oxaliplatine montre un rôle important de $Na_v1.6$. En effet, un bloqueur de $Na_v1.6$ inhibe l'allodynie au froid (Deuis *et al.* 2013). Finalement, le knock-down par l'injection de siRNA diminue l'allodynie mécanique et les décharges ectopiques provoquées par un modèle d'inflammation du ganglion dorsal L5 (Xie *et al.* 2013)

$Na_v1.7$

Le canal $Na_v1.7$ est largement exprimé dans les neurones du SNP où il se situe principalement dans les terminaisons nerveuses et dans les neurones du système nerveux sympathique. Il est particulièrement exprimé dans les fibres C et les fibres $A\delta$, mais on le retrouve aussi dans certains neurones des fibres $A\alpha/\beta$ (~40%) (Toledo-Aral *et al.* 1997; Ho and O'Leary 2011; Djouhri and Lawson 2004). Les cinétiques des courants produits par $Na_v1.7$ sont caractéristiques des courants TTX-S, c'est-à-dire avec une activation et une inactivation rapide. Ils diffèrent cependant de $Na_v1.6$ par une entrée en inactivation à l'état fermé beaucoup plus lente et une récupération environ 5 fois plus lente (Cummins *et al.* 1998; Herzog *et al.* 2003; Vijayaragavan *et al.* 2001). À l'inverse de $Na_v1.6$, la lente entrée dans l'inactivation à l'état fermé permet la génération d'un grand courant de rampe facilitant le déclenchement des PAs suite à de petites variations du V_m (Cummins *et al.* 2007). Ainsi, $Na_v1.7$ serait important pour amplifier les dépolarisations infraliminaires du canal $Na_v1.8$ et permettre le déclenchement des PAs (Blair and Bean 2002).

$Na_v1.8$ est le principal responsable du PA dans les fibres C et certaines fibres Aδ. De plus, la relativement lente fréquence de décharge des neurones de DRG serait en partie causée par la lente récupération de $Na_v1.7$ (Herzog *et al.* 2003).

Nous savons que $Na_v1.7$ est en partie responsable de la genèse et de la transmission du PA dans les neurones sensitifs primaires (Toledo-Aral *et al.* 1997). Il serait aussi en partie responsable de l'hyperexcitabilité des neurones nociceptifs dans les douleurs inflammatoires et pathologiques. L'induction de l'inflammation par l'injection de carraghénane (Black *et al.* 2004) ou d'adjuvant complet de Freund (CFA) (Strickland *et al.* 2008) provoquent une augmentation des ARN_m et de la protéine qui sont corrélés avec l'hyperalgésie. Le BZP, un bloqueur plus puissant sur les canaux $Na_v1.7$ que $Na_v1.8$ et qui ne traverse pas la barrière hémato-encéphalique, permet de réduire l'hyperalgésie provoquée par l'administration de CFA et le modèle SNL (McGowan *et al.* 2009). Plusieurs études montrent aussi que les molécules du cocktail inflammatoires modulent les canaux Na^+, pour éviter d'être redondant, cette partie est traitée dans la section *Régulation des canaux Na^+* (p. 52). Chez la souris, la délétion complète du gène SCN9A codant pour $Na_v1.7$ est létale. Nassar et coll. ont donc utilisé le système Cre-loxP pour créer une souris knock-out nocicepteurs spécifiques de $Na_v1.7$, qui est viables et d'apparence normale (Nassar *et al.* 2004). Ils ont remarqués une douleur inflammatoire réduite ou abolie suite à l'administration de composés pro-inflammatoires tels la formalin, la carraghénane, de CFA ou le NGF.

Diverses études minimisent le rôle de $Na_v1.7$ dans les douleurs neuropathiques. En effet, il a été montré qu'il y a une diminution des ARN_m de $Na_v1.7$ dans le modèle de douleur SNL (Kim *et al.* 2002) et un modèle SNI (Berta *et al.* 2008). De plus, les souris knock-out nocicepteurs spécifiques de $Na_v1.7$ et double KO $Na_v1.7$ et $Na_v1.8$ développent des douleurs neuropathiques dans un modèle SNL (Nassar *et al.* 2005). Il est probable que

l'implication de $Na_v1.7$ soit différente entre les modèles de douleurs et les différentes espèces.

Canalopathies liées à $Na_v1.7$

Il existe diverses canalopathies dans le canal $Na_v1.7$ qui provoquent les douleurs pathologiques. L'érythromélalgie, le syndrome de douleur extrême paroxystique (PEPD), l'insensibilité congénitale à la douleur (CIP) et la neuropathie des petites fibres (SFN) ont permis d'établir un rôle crucial et non redondant de $Na_v1.7$ dans la douleur chez l'humain (Figure 13).

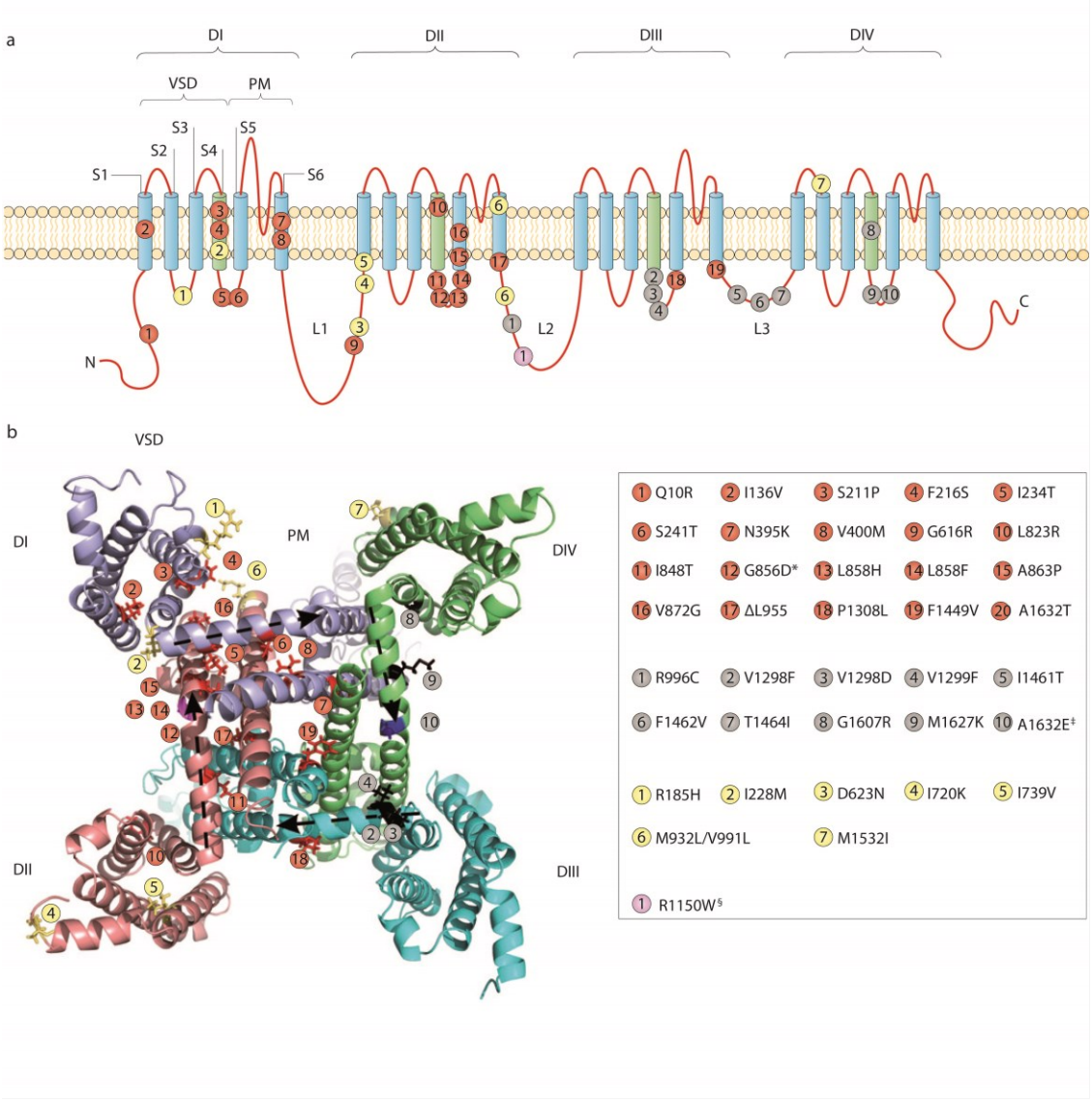

Figure 13. Canalopathies liées à $Na_v1.7$

a) Localisation des mutations sur une représentation linéaire de $Na_v1.7$. b) Localisation des mutations sur une représentation 3D de $Na_v1.7$ basé sur la cristallisation du canal Na^+ bactérien. Érythromélalgie (rouge), PEPD (gris), SFN (jaune). La mutation A1632T n'est pas représentée, mais se situe au même endroit que A1632E. ‡ le patient avec cette mutation présente des symptômes communs à la PEPD et l'érythromélalgie. § Polymorphisme présent dans 30% de la population caucasienne de descendance européenne. Modifié de (Dib-Hajj *et al.* 2013)

Érythromélalgie

L'érythromélalgie est une maladie héréditaire qui cause chez le patient des douleurs de type brûlure, des rougeurs de la peau et de l'allodynie. Elle a été identifiée en 2004 chez des familles chinoises (Yang *et al.* 2004). L'érythromélalgie est liée à des mutations dans le gène SCN9A qui code pour le canal $Na_V1.7$. Il existe à ce jour une vingtaine de mutations liées à cette maladie (Figure 13) (Dib-Hajj *et al.* 2013). D'un point de vue fonctionnel, les mutations liées à l'érythromélalgie provoquent un gain de fonction impliquant shift de l'activation vers les potentiels plus hyperpolarisés (Figure 14 a-c) (Cummins *et al.* 2004; Waxman 2013). Cette modification de la dépendance au voltage de l'activation facilite ainsi la genèse d'un potentiel d'action et est suspectée de causer l'hypersensibilité chez les patients souffrant de cette maladie (Cummins *et al.* 2004; Sheets *et al.* 2007).

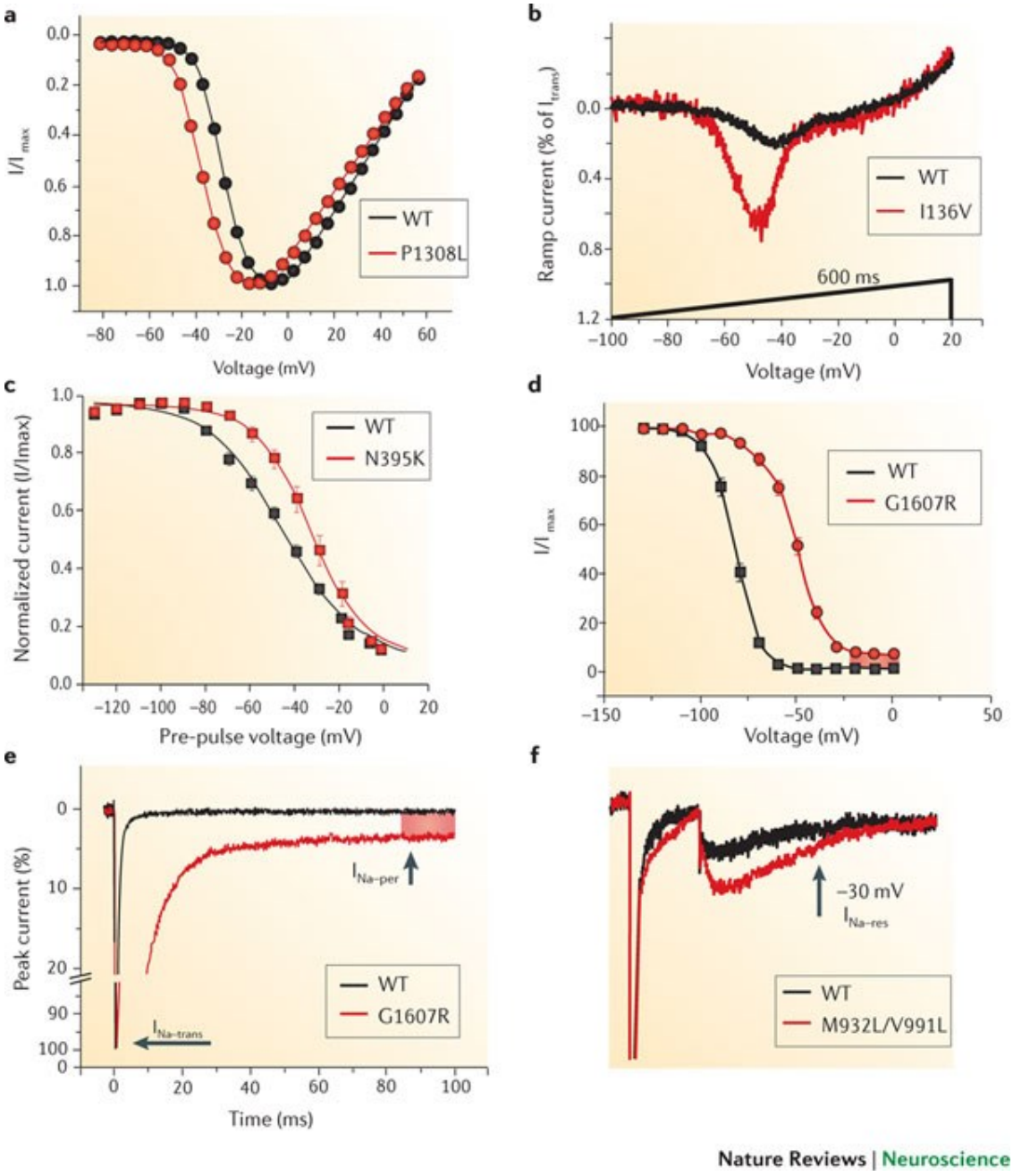

Figure 14. Propriétés électrophysiologiques des mutations menant à l'érythromélalgie et au PEPD

(a) Mutation de SCN9A menant à l'érythromélalgie. La mutation montre une activation hyperpolarisée de 10mV comparé à $Na_v1.7$ WT. (b) Mutation de SCN9A menant à

l'érythromélalgie provoquant un courant de rampe augmenté. (c) Mutation de SCN9A réduisant l'entrée en inactivation lente. Ces mutations augmentent la fréquence des PAs dans les neurones de DRG. (d) Cette mutation PEPD provoque une inactivation hyperpolarisée typique des mutations PEPD. (e) Mutation PEPD empêchant l'inactivation complète des canaux, provoquant un courant persistant. (f) Mutation d'un patient SFN montrant un courant résurgent. Ces courants supportent les rafales de PAs. (Dib-Hajj *et al.* 2013)

PEPD

Un autre exemple de l'implication de $Na_v1.7$ dans les douleurs neuropathiques provient de la PEPD, anciennement connu sous le nom de douleur rectale familiale. On retrouve au moins 10 mutations sur le gène SCN9A provoquant la PEPD (Figure 13). Cette maladie est caractérisée par des douleurs de type brûlures rectales, péri-oculaire et péri-mandibulaire (Dib-Hajj *et al.* 2008). Les effets des mutations causant cette maladie sont distincts de ceux causant l'érythromélalgie tant au niveau des symptômes qu'au niveau fonctionnel. Les effets de cette maladie sont dus à un déplacement vers des potentiels plus dépolarisés de la dépendance au voltage de l'inactivation et une inactivation incomplète menant à des courants persistants prolongés (Figure 14 d-f) (Fertleman *et al.* 2006).

Érythromélalgie, PEPD et chevauchement des syndromes

Malgré que l'érythromélalgie et le PEPD soient caractérisés par des symptômes cliniques distincts, il se pourrait qu'ils soient en fait les extrémités d'un continuum. Une mutation retrouvée chez une patiente présentant des symptômes de l'érythromélalgie et de la PEPD présente des caractéristiques des 2 maladies. La mutation A1632E produit une hyperpolarisation de la dépendance au voltage de l'activation, ralentit la désactivation et montre un courant de rampe augmenté similaire aux mutations provoquant l'érythromélalgie. Cependant, elle montre aussi une dépolarisation de

l'inactivation, une inactivation rapide ralentie et une inactivation incomplète similaires aux mutations provoquant la PEPD (Estacion *et al.* 2008).

La modification de l'inactivation étant associée au PEPD, il est intéressant de noter que récemment une mutation présentant des défauts d'inactivation provoque l'érythromélalgie (Han *et al.* 2014). La mutation A1632T induit un shift vers les potentiels plus dépolarisés de l'inactivation rapide et une récupération accélérée de l'inactivation. Cette mutation (A1632T) se retrouve au même endroit sur $Na_v1.7$ que celle provoquant un syndrome hybride entre l'érythromélalgie et le PEPD, mais n'induit pas de courant résurgent. Les auteurs proposent que le déplacement de l'inactivation sans induire de courant résurgent provoque l'érythromélalgie et que le PEPD soit lié au courant résurgent.

SFN

La neuropathie des petites fibres est un syndrome relativement commun qui affecte les petites fibres légèrement ou non myélinisées. Le début de la maladie survient habituellement à l'âge adulte est caractérisé par des douleurs de type brûlure. Il a été découvert que certains patients atteints de cette maladie sont porteurs de mutation sur le gène SCN9A. En tout, huit mutations différentes ont été trouvées. L'analyse fonctionnelle de ces mutations a révélé de légers gains de fonction du canal $Na_v1.7$ rendant les neurones de DRG hyperexcitable (Faber *et al.* 2012a).

CIP

La CIP indique un rôle crucial du canal $Na_v1.7$ dans la transmission de la douleur. Comme le nom l'indique, les patients atteints de la CIP sont incapables de ressentir la douleur. Cette maladie est due à une perte de fonctionnalité du canal sodique $Na_v1.7$ (Cox *et al.* 2006; Goldberg *et al.* 2007). Cependant, la proprioception, le toucher, la sensation chaude ou froide, la

vision et l'ouïe ne sont pas affectés. La CIP démontre un rôle essentiel de $Na_v1.7$ dans la nociception chez l'humain.

$Na_v1.8$

Le canal sodique $Na_v1.8$ est très largement exprimé dans les DRG et dans les ganglions trijumeaux. On le retrouve principalement dans les fibres C et Aδ ainsi qu'une expression marginale dans fibres Aβ (Akopian *et al.* 1996; Djouhri *et al.* 2003). $Na_v1.8$ est responsable de la majorité du courant Na^+ provoquant la dépolarisation des neurones lors des PAs dans les neurones nociceptifs (Renganathan *et al.* 2001; Blair and Bean 2002). Les petits neurones des DRG provenant des souris $Na_v1.8$ KO ($Na_v1.8^{-/-}$) produisent de faibles potentiels gradués lors de l'injection de courant dépolarisant alors que l'injection de courant provoque des PAs de type tout ou rien chez les souris WT (Renganathan *et al.* 2001). De façon fonctionnelle, les cinétiques d'activation et d'inactivations de $Na_v1.8$ sont relativement lentes comparés aux canaux TTX-S. Son activation et son inactivation sont dépolarisées comparées aux canaux TTX-S retrouvés dans les DRG, environ 30 mV (Vijayaragavan *et al.* 2001; Caffrey *et al.* 1992; Ogata and Tatebayashi 1993). $Na_v1.8$ présente une récupération rapide de l'état inactivé qui permet aux neurones de maintenir une fréquence de décharge rapide (Renganathan *et al.* 2001; Cummins and Waxman 1997). L'entrée en inactivation lente de $Na_v1.8$ est rapide, ce qui est responsable de la réduction des courants TTX-R observés lors de stimulations répétées (Rush *et al.* 1998; Vijayaragavan *et al.* 2001; Tripathi *et al.* 2006). Il est intéressant de noter que le refroidissement augmente l'inactivation lente des canaux TTX-S et provoque l'accumulation de ces derniers dans un état inactivé alors que $Na_v1.8$ est insensible au refroidissement (Zimmermann *et al.* 2007). $Na_v1.8$ est ainsi le seul canal capable de provoquer un PA et de transmettre l'information nociceptive au CNS dans les conditions de basse température.

Plusieurs études montrent un rôle majeur de l'implication de $Na_v1.8$ dans la transmission de la douleur et son implication dans l'hyperactivité neuronale suite à l'inflammation ou dans les douleurs neuropathiques. Il a été montré que différents médiateurs de l'inflammation provoquent une augmentation des courants liés à $Na_v1.8$ dans les neurones de DRG. Des études ont montré que la douleur liée à l'inflammation suite à l'injection des molécules pro-inflammatoire CFA et prostaglandines E2 (PGE_2) ou dans un modèle d'inflammation de la vessie est réduite suite à l'injection d'oligonucléotides antisens (Porreca *et al.* 1999; Yoshimura *et al.* 2001). Les souris $Na_v1.8^{-/-}$ présentent une anesthésie complète aux stimuli mécaniques alors qu'elles présentent une anesthésie partielle aux stimuli thermiques suite à l'inflammation provoquée par l'injection intraplantaire de carraghénane (Akopian *et al.* 1999). L'implication de $Na_v1.8$ dans la transmission nociceptive serait dépendante de la modalité des stimuli et serait plus impliqués dans la transmission des stimuli nociceptifs mécanique que thermique (Matthews *et al.* 2006).

En plus de la transmission et de son implication dans les douleurs inflammatoires, plusieurs études montrent un rôle important de $Na_v1.8$ dans le développement et le maintien des douleurs neuropathiques. Il a été montré que $Na_v1.8$ subit une redistribution suite à différents modèles de douleurs neuropathiques et contribuerait ainsi à ces douleurs. En effet, l'immunoréactivité de $Na_v1.8$ diminue au niveau des corps cellulaires des cellules de DRG, mais augmente au niveau de la lésion CCI (Novakovic *et al.* 1998). Après la ligature L5/L6 (SNL), il y a une redistribution de $Na_v1.8$ dans les axones L4 des neurones non lésés qui sont accompagnés de décharges ectopiques (Gold *et al.* 2003). Chez un modèle de douleur créé par le sectionnement de la veine saphène, les souris $Na_v1.8^{-/-}$ ne développent pas d'activité spontanée contrairement aux souris WT (Roza *et al.* 2003). L'allodynie tactile et thermale induite chez les modèles de rats SNL est

réversible suite à l'injection d'oligonucléotides antisens contre $Na_v1.8$ (Lai *et al.* 2002).

Malgré plusieurs études montrant un rôle pour $Na_v1.8$ dans le développement des douleurs chroniques, certaines études remettent en question ce rôle. Par exemple, il a été montré que l'allodynie thermique et mécanique se développe normalement chez un modèle de douleurs neuropathique SNI chez les souris $Na_v1.8^{-/-}$ (Kerr *et al.* 2001). De plus, la souris double KO $Na_v1.7$ et $Na_v1.8$ montre le même niveau d'allodynie mécanique que les souris WT suite chez les souris SNL (Nassar *et al.* 2005). Il existe quelques hypothèses pouvant expliquer ces différences, on sait que des mécanismes compensatoires peuvent survenir dans les souris KO, par exemple les souris $Na_v1.8^{-/-}$ montrent une surexpression de $Na_v1.7$ (Akopian *et al.* 1999). Il est aussi possible que les divergences entre les études proviennent de différences entre les espèces, les études knock-out et knock-down ont été effectuées respectivement sur les souris et sur les rats.

Quoi qu'il en soit, $Na_v1.8$ semble une cible de choix dans le traitement des douleurs pathologiques. En effet, la μO-conotoxine (MrVIB) isolé d'un coquillage de mer (conus marmoreus) a montré une réduction des symptômes neuropathiques chez les souris lorsqu'injectée de façon intrathécale, cette toxine est près de 10 fois plus puissante pour bloquer $Na_v1.8$ que les autres canaux neuronaux TTX-S (Ekberg *et al.* 2006). De plus, il a été montré que le A-803467, un bloqueur spécifique à $Na_v1.8$, procure une anesthésie aux douleurs neuropathiques et inflammatoires (Jarvis *et al.* 2007).

SFN

Il a été montré que la SFN est dans certains cas causée par une mutation du canal $Na_v1.7$ qui provoque un gain de fonction. Mais ces mutations ne représentent qu'environ 30% des cas de SFN. En 2012 et 2013, il a été identifié trois mutations sur le canal $Na_v1.8$ (L554P, A1304T et I1707V) qui

provoquent la SFN en causant un gain de fonction de $Na_v1.8$ (Faber *et al.* 2012b; Huang *et al.* 2013). L554P provoque un courant de rampe augmenté ainsi qu'une récupération accélérée. A1304T provoque une augmentation de l'activation et shift le courant de rampe vers des potentiels hyperpolarisés. I1707V provoque une hyperpolarisation de l'activation et du courant de rampe. Ainsi, ces trois mutations affectent l'activation pour provoquer l'hyperexcitabilité des neurones nociceptifs et contribuer ainsi aux neuropathies périphériques. Plus récemment, il a été montré que la SFN peut induite par une mutation déplaçant la dépendance au voltage de l'inactivation (Han *et al.* 2014). Cette mutation (G1662S) provoque l'hyperexcitabilité des neurones de DRG en augmentant la proportion de canaux en état fermé disponible à la membrane. La SFN peut donc être causée par une panoplie d'altération des paramètres biophysiques de $Na_v1.8$ qui induisent l'hyperexcitabilité des neurones de DRG.

$Na_v1.9$

Le canal sodique $Na_v1.9$ est exprimé dans les neurones de DRG ainsi que dans les neurones des ganglions trijumeaux où on le retrouve principalement dans les neurones IB_4^+ (Dib-Hajj *et al.* 1998b; Fang *et al.* 2002; Fang *et al.* 2006). Les propriétés fonctionnelles de ce canal sont uniques. $Na_v1.9$ présente un courant TTX-R dont les cinétiques d'activation et d'inactivation sont très lentes, elles sont trop lentes pour participer au PA (Vanoye *et al.* 2013; Cummins *et al.* 1999). Il a en effet été montré que les potentiels d'action sont identiques chez les souris $Na_v1.9^{-/-}$ comparées au WT (Priest *et al.* 2005; Amaya *et al.* 2006). L'enregistrement des courants TTX-R de souris $Na_v1.8$ KO nous apprend que le $V_{1/2}$ d'activation de ce canal est -47 mV, mais commence à s'ouvrir à un voltage très hyperpolarisé, dès -70 mV. Le $V_{1/2}$ d'inactivation se situe à -47 mV et est inactivé à environ 95% au potentiel de membrane (-65 mV) (Cummins *et al.* 1999). Cependant, l'activation très hyperpolarisée est responsable d'un courant Na^+ persistant qui contribue à moduler le V_m pouvant aussi modifier la réponse neuronale aux stimuli infraliminaires (Herzog *et al.* 2001).

Plusieurs études montrent un rôle majeur de l'implication de $Na_v1.9$ dans l'hyperactivité neuronale suite à l'inflammation. L'injection intraplantaire des composés pro-inflammatoires formaline et CFA chez les souris $Na_v1.9^{-/-}$ montre une hyperalgésie thermique réduite comparée au souris WT alors que l'hyperalgésie mécanique n'est pas réduite (Priest *et al.* 2005; Amaya *et al.* 2006). L'étude de la modulation de $Na_v1.9$ chez les souris $Na_v1.8^{-/-}$ par des médiateurs de l'inflammation montre une régulation de ces canaux. Par exemple, la préincubation avec PGE_2 déplace l'activation et l'inactivation vers les potentiels plus hyperpolarisés en plus de causer une augmentation de l'amplitude de deux fois (Rush and Waxman 2004). Cependant, l'application directe des molécules pro-inflammatoires ne provoque pas ces modifications (Zheng *et al.* 2007; Maingret *et al.* 2008).

Les études concernant l'implication dans les douleurs pathologiques de $Na_v1.9$ à partir des expériences sur les animaux sont souvent contradictoires. Il est par exemple montré que l'expression de $Na_v1.9$ diminue après l'axotomie (Dib-Hajj *et al.* 1998a) et que les symptômes de douleurs neuropathiques sont inchangés chez les souris $Na_v1.9$ KO comparées aux souris WT dans des modèles de douleurs chroniques (Amaya *et al.* 2006). À l'opposé, les souris $Na_v1.9^{-/-}$ ne développent pas d'allodynie au froid dans les modèles SNI et CCI (Leo *et al.* 2010).

Canalopathies de $Na_v1.9$

Différentes mutations rapportées sur le gène SCN11A sont reconnues pour provoquer des effets opposés. Il a été rapporté qu'une mutation sur ce gène provoque une perte de perception de la douleur (Leipold *et al.* 2013) alors que d'autres mutations sont rapportées pour provoquer des neuropathies douloureuses (Zhang *et al.* 2013; Huang *et al.* 2014). Paradoxalement, toutes ces mutations sont décrites comme provoquant un gain de fonction.

L'étude de Leipold supporte son hypothèse d'une étude biophysique satisfaisante. Cette étude est supportée par un modèle de souris transgénique montrant cette mutation. Ces souris montrent des symptômes similaires aux humains atteints de cette maladie telle les blessures auto-infligées et un manque de perception de la douleur. De plus, cette étude en « voltage-clamp » montre clairement plusieurs différences biophysiques entre les canaux mutés et ceux de type sauvage. Il appert que l'inactivation à l'état d'équilibre de cette mutation est déplacée vers des potentiels plus hyperpolarisés. Cela aurait pour effet de créer une fuite de sodium provoquant une augmentation du potentiel de membrane des neurones. Le potentiel de membrane élevé favoriserait l'entrée en inactivation des canaux sodiques causant la perte d'excitabilité de ces neurones. Il est cependant intéressant de noter qu'une dépolarisation similaire du V_m a été rapportée et provoque une hyperexcitabilité des nocicepteurs (Faber *et al.* 2012b; Faber *et al.* 2012a).

L'étude génétique de 2 familles chinoises atteintes de douleurs épisodiques par l'équipe de Zhang et coll. a permis de trouver deux mutations dans le canal $Na_v1.9$ (R225C et A808G). Les enregistrements de « *voltage-clamp »* ont permis de montrer une densité de courant augmenté chez les mutants et une excitabilité neuronale augmentée par la technique du « *current-clamp »*. Récemment, le criblage génétique de patients atteints de SFN et la caractérisation en « *voltage-clamp »* a permis de trouver 2 mutations sur $Na_v1.9$ montrant des gains de fonction (L1158P et I381T). Ensuite, par la technique du « *current-clamp »* ils ont montré que l'excitabilité neuronale est augmentée.

Ces études contradictoires montrent clairement le niveau de sophistication des mécanismes de régulation, la complexité de l'analyse des résultats électrophysiologiques et leur pertinence clinique. Néanmoins, ces observations montrent que le canal $Na_v1.9$ pourrait jouer un rôle pathologique dans la génération des douleurs neuropathiques.

Les sous-unités β

Comme les sous-unités β des canaux sodiques ont un rôle important dans la régulation des canaux Na^+, il est probable qu'ils aient une implication indirecte en modulant les canaux Na^+ dans le développement et le maintien des douleurs inflammatoires et pathologiques (Isom 2001; Chahine and O'Leary 2011).

Peu de données sur l'expression de la sous-unité β_1 sont disponibles. L'expression des ARN_m de sous-unité β_1 n'est pas modulée dans les modèles de neuropathie diabétique induite par la streptozocine (Shah *et al.* 2001a) et de neuropathie induite par l'axotomie (Takahashi *et al.* 2003) alors que son expression est augmentée dans un modèle CCI dans la corne dorsale de la moelle épinière (Blackburn-Munro and Fleetwood-Walker 1999). De plus, l'expression de cette sous-unité est principalement exprimée dans les neurones de larges diamètres (Oh *et al.* 1995; Zhao *et al.* 2011). En prenant en considération la faible expression dans les neurones de petits diamètres et sa faible modulation dans les modèles de douleurs, il est peu probable que cette sous-unité contribue significativement aux douleurs neuropathiques (Chahine and O'Leary 2011).

Des études sur la régulation de l'expression de la sous-unité $\beta 2$ ont montré des résultats différents selon les modèles utilisés. L'expression de la protéine est augmentée dans les neurones de DRG dans les modèles de rats neuropathiques SNI (Pertin *et al.* 2005) alors qu'elle n'est pas modifiée suivant un modèle SNI (Takahashi *et al.* 2003). Cependant, les souris β_2 KO montrent une diminution de l'allodynie mécanique comparé aux souris WT suite au modèle SNI (Pertin *et al.* 2005). De plus, les souris β_2 KO montrent une diminution des courants TTX-S et une réduction de l'hyperalgésie suite à l'injection intra-plantaire de formaline (Lopez-Santiago *et al.* 2006).

L'expression de la sous-unité β_3 est intimement liée à l'expression des canaux $Na_v1.8$ et $Na_v1.9$ qui sont exprimés principalement dans les nocicepteurs. (Shah *et al.* 2000; Shah *et al.* 2001b). Il a été montré que l'expression de la sous-unité β_3 est augmentée dans les fibres C dans les modèles pathologiques CCI (Shah *et al.* 2000) et SNL (Takahashi *et al.* 2003). De plus, l'expression des ARNm de la sous-unité β_3 sont aussi augmenté dans les fibres Aδ dans les modèles de neuropathie diabétique induite par la streptozocine (Shah *et al.* 2001a). L'augmentation de l'expression de la sous-unité β_3 se fait de façon parallèle à l'expression de $Na_v1.3$ dans les modèles de douleurs (Takahashi *et al.* 2003). Les études d'expression hétérologue ont montré quel la co-expression de la sous-unité β_3 et de $Na_v1.3$ dépolarise l'activation et l'inactivation, accélères la récupération de l'inactivation et ralentit les cinétiques (Cummins *et al.* 2001).

Peu d'évidence lie la sous-unité β_4 à un rôle dans les douleurs pathologiques. Une hypothèse est cependant digne de mention. Le courant résurgent provoqué par une mutation sur $Na_v1.7$ a été impliqué dans l'hyperexcitabilité neuronale menant au PEPD (Theile and Cummins 2011). La sous-unité β_4 est sans doute nécessaire aux courants résurgents produits par $Na_v1.6$ (Grieco *et al.* 2005; Cummins *et al.* 2005). Ainsi, β_4 pourrait favoriser l'hyperexcitabilité neuronale en favorisant l'apparition de courants résurgents (Chahine and O'Leary 2011).

Régulation des canaux Na^+

Il y a une fine régulation des canaux Na^+ dans les neurones sensitifs périphériques qui permettent de réguler l'excitabilité de ces neurones. Dans cette section, nous traiterons de différents mécanismes de régulation des canaux Na^+ qui influence l'excitabilité des neurones en condition physiologique,

mais aussi dans les cas de lésions des nerfs périphériques, de l'inflammation et de différents désordres métaboliques.

Régulation des canaux Na^+ par les kinases

Les protéines kinases A

Les protéines kinases A (PKA) forment une famille de kinases dépendante de l'adénosine monophosphate cyclique (cAMP). Ces protéines sont impliquées de plusieurs façons dans la régulation des canaux Na^+ et régulent différemment les sous-types de canaux Na^+. En effet, lorsqu'ils sont exprimés de façon hétérologue, l'activation des PKA par des activateurs (forskolin et 8-bromo cAMP) réduit l'amplitude des courants de $Na_v1.2$, et $Na_v1.7$ (Vijayaragavan *et al.* 2004; Smith and Goldin 1996) alors qu'elle augmente celle des canaux $Na_v1.5$ et $Na_v1.8$ (Zhou *et al.* 2000; Vijayaragavan *et al.* 2004).

On retrouve 5 sites consensus de phosphorylation par la PKA dans la boucle liant les DI et DII de $Na_v1.2$ qui permettent la régulation par la PKA. Ces sites sont reconnus par les motifs suivant RRXS/T et KRXXS/T où seulement quatre de ces sites sont phosphorylés (Rossie and Catterall 1989; Murphy *et al.* 1993). $Na_v1.8$ possède aussi cinq sites consensus reconnus par la PKA où, lorsque ces sites sont éliminés, $Na_v1.8$ n'est plus modulé par la PKA (Fitzgerald *et al.* 1999). $Na_v1.4$ qui ne possède pas ces sites n'est pas modulé par la PKA (Frohnwieser *et al.* 1997). En plus de moduler les niveaux d'expression, la PKA permet de modifier les propriétés biophysiques de certains canaux. On remarque entre autres qu'elle modifie la dépendance au voltage vers des potentiels plus hyperpolarisés de l'activation des courants TTX-R (England *et al.* 1996). Le rôle de $Na_v1.9$ dans les douleurs inflammatoires est supporté par les études montrant l'augmentation de $Na_v1.9$ par les molécules inflammatoires (Gold *et al.* 1998) qui est en partie inhibé dans les souris $Na_v1.9$ KO (Maingret *et al.* 2008). L'inflammation qui survient après la lésion des tissus provoque différentes cascades qui résultent à

l'hyperexcitabilité des fibres afférentes primaires (Gold 1999; Woolf and Ma 2007). Les différents mécanismes inflammatoires augmentant l'activité de la PKA seraient en partie liés à l'hyperexcitabilité périphérique en modulant les canaux Na^+, en particulier $Na_v1.8$ (Gold 1999; England *et al.* 1996; Cheng and Ji 2008; Woolf and Ma 2007).

Les protéines kinases C

La famille des PKC est aussi reconnue pour moduler les canaux Na^+. Les PKC se divisent en trois sous-familles : les PKC conventionnelles (nPKC), les nouvelles PKC (nPKC) et les PKC atypiques (aPKC). On différencie les sous-familles par les différences dans les mécanismes d'activation. Les cPKC sont activées par le diacylglycérol (DAG) et le Ca^{++}, nPKC sont activés seulement par le DAG alors que l'activation des aPKC ne nécessite ni le DAG ni le Ca^{++} (Dempsey *et al.* 2000). En plus de deux sites consensus pour la liaison des PKC dans la boucle DI-II (S554 et S573) on reconnait un site de phosphorylation dans la boucle des domaines DIII-IV (S1506) (Cantrell *et al.* 2002). L'activation des PKC ne module pas les canaux du muscle squelettiques $Na_v1.4$, car les sites de phosphorylation sont absents (Smith and Goldin 1996).

L'activation des PKC par le phorbol 12-myristate, 13-acetate (PMA) des canaux $Na_v1.8$ exprimés de façon hétérologue montre une réduction du courant (Vijayaragavan *et al.* 2004) alors qu'il montre une augmentation dans les modèles où $Na_v1.8$ est exprimé de façon endogène (Cang *et al.* 2009).

La modulation par les PKC des canaux $Na_v1.8$ semble impliquée dans l'hyperexcitabilité neuronale suite à l'inflammation. L'application de PGE_2 potentialise les courants TTX-R des neurones sensitifs primaires (Gold *et al.* 1996). L'application d'activateurs des PKC (PMA et PDBu) provoque une augmentation des courants TTX-R et un déplacement de l'activation et de l'inactivation vers les potentiels hyperpolarisés (Cang *et al.* 2009). De plus,

l'augmentation de l'activité de nPKC$_\varepsilon$ et cPKCβII est impliquée dans les processus d'hyperalgésies inflammatoires (Aley *et al.* 2000; Igwe and Chronwall 2001).

MAPK

Une autre famille formée de protéines kinases connues sous le nom de MAPK pour « *mitogen-activated protein kinases* » régule les canaux Na^+. Il a été rapporté que l'activation de p38 augmente les densités de courant sans altérer les propriétés biophysiques de $Na_v1.6$ et de $Na_v1.8$ (Wittmack *et al.* 2005; Hudmon *et al.* 2008). Cependant, les différentes kinases de cette famille n'ont pas nécessairement les mêmes effets sur les canaux Na^+. En effet, les kinases ERK1 et ERK2 provoquent un déplacement de l'activation et de l'inactivation de $Na_v1.7$ sans changement dans la densité de courant, ce qui a pour effet d'augmenter la fréquence de décharges des neurones de DRG (Stamboulian *et al.* 2010).

Les MAPK seraient impliqués dans la modulation des douleurs inflammatoires et chroniques, entre autres, par la modulation des canaux Na^+ (Price and Dussor 2013). Plusieurs modèles animaux de douleurs ont montré une régulation anormale des MAPKs. ERK, p38 and JNK augmentent après la ligature des nerfs spinaux et de l'axotomie (Jin *et al.* 2003; Kim and Choi 2010). L'expression de p38 provoquerait l'augmentation des courants TTX-R et TTX-S dans les neurones de DRG (Obata *et al.* 2004; Jin and Gereau IV 2006).

Ankyrines

Les ankyrines sont des protéines adaptatrices qui permettent la liaison des protéines membranaires aux protéines du cytosquelette. Leurs architectures modulaires permet l'interaction de plusieurs protéines et de former des complexes de protéines membranaires, de molécules de signalisation et de

protéines du cytosquelette. Ces complexes permettent le guidage, l'ancrage et la stabilisation des protéines membranaires (Cunha and Mohler 2009).

Dans le système nerveux, nous savons que les ankyrines permettent la localisation des canaux Na^+ dans l'AIS (Zhou *et al.* 1998). L'ankyrine G permet aussi d'empêcher la diffusion des canaux Na^+ avant la formation de la barrière de diffusion (Brachet *et al.* 2010). Le transport axonal des canaux sodiques demeure une question importante en neurobiologie à laquelle nous n'avons que peu d'indices. Récemment, il a été montré que l'ankyrine G se lie directement au complexe KIF5/kinesin 1 pour permettre le transport de $Na_v1.2$ dans l'axone (Barry *et al.* 2014). Il a aussi été montré que l'ankyrine G peut influencer les paramètres d'inactivation du canal Na^+ $Na_v1.6$ (Shirahata *et al.* 2006). Les auteurs avancent donc que l'ankyrine pourrait moduler l'activité des neurones non seulement en permettant le regroupement des canaux Na^+ dans l'AIS, mais en modulant les propriétés biophysiques des canaux Na^+.

D'un point de vue pathologique, il a été démontré que l'ankyrine pouvait provoquer des troubles cardiaques suite à des défauts d'adressage dans diverses protéines électrogéniques (Mohler *et al.* 2003; Mohler *et al.* 2004). Leur implication dans les douleurs pathologiques n'est pas aussi claire. Cependant, il a été avancé que l'ankyrine pourrait jouer un rôle dans certaines douleurs pathologiques en modulant les canaux Na^+ (Kretschmer *et al.* 2002). Il a été observé dans des névromes associés de douleurs que les niveaux d'ankyrines étaient supérieurs. L'augmentation de l'expression d'ankyrine pourrait faciliter le regroupement des canaux Na^+ dans l'AIS et donc l'hyperexcitabilité des neurones (Kretschmer *et al.* 2002).

Objectifs

L'objectif général de la thèse était d'étudier les impacts de la modulation des canaux Na^+ afin de comprendre les effets sur l'activité des neurones périphériques. La compréhension fine des mécanismes provoquant la modulation des canaux Na^+ est un outil important dans la compréhension des mécanismes menant au développement et au maintien des douleurs pathologiques. C'est aussi un outil important dans le développement de nouvelles avenues thérapeutiques et dans la compréhension de celles existantes.

L'objectif du chapitre 2 était de comprendre comment les différentes sous-unités α des canaux Na^+ présentes dans les neurones sensitifs périphériques interagissent pour moduler l'activité électrique de ces neurones et provoquer les multiples profils électrophysiologiques. Pour ce faire, nous avons jumelé les techniques de PCR quantitative et de patch-clamp. Nous pouvions ainsi connaître le contenu de la cellule et le corréler au profile électrophysiologique.

Dans le chapitre 3, on s'est intéressé à la modulation pharmacologique des canaux Na^+. Le but est de comprendre comment les molécules au pouvoir anesthésiques modulent les canaux sodiques pour provoquer l'anesthésie. Pour ce faire, nous avons étudié le mécanisme d'action du butamben (BAB sur les canaux Na^+ présents dans les neurones périphériques.

Finalement, le chapitre 4 porte sur la compréhension des effets anesthésiques des SSRI dans le traitement des douleurs pathologiques. Comme la compréhension des effets anesthésiques des SSRI est encore incomplète, nous avons étudié les effets provoqués par différents SSRI sur les canaux Na^+.

Chapitre 2

Correlation of the electrophysiological profiles and sodium channel transcripts of individual rat dorsal root ganglia neurons

Frontiers in Cellular Neuroscience. 2014

Correlation of the electrophysiological profiles and sodium channel transcripts of individual rat dorsal root ganglia neurons

Olivier Thériault[1] and Mohamed Chahine[1*]

[1]Centre de recherche de l'institut universitaire en santé mentale de Québec, Department of Medicine, Université Laval, Quebec City, QC, Canada

Number of words: 6 543

Number of figures: 6

Number of table: 2

Running title: Sodium channels and neuronal excitability

Correspondence:

Mohamed Chahine, PhD

Centre de Recherche de l'Institut Universitaire en Santé Mentale de Québec

2601 chemin de la Canardière

Québec City, QC, Canada G1J 2G3

Telephone: 1-418-663-5747, #4723

Fax: 1-418-663-8756

Email: mohamed.chahine@phc.ulaval.ca

Keywords: voltage-gated sodium channel, neuronal excitability, pain, biophysical properties, dorsal root ganglia neurons

Abstract

Voltage gated sodium channels (Na_v channels) play an important role in nociceptive transmission. They are intimately tied to the genesis and transmission of neuronal firing. Five different isoforms ($Na_v1.3$, $Na_v1.6$, $Na_v1.7$, $Na_v1.8$, and $Na_v1.9$) have been linked to nociceptive responses. A change in the biophysical properties of these channels or in their expression levels occurs in different pathological pain states. However, the precise involvement of the isoforms in the genesis and transmission of nociceptive responses is unknown. The aim of the present study was to investigate the synergy between the different populations of Na_v channels that give individual neurons a unique electrophysical profile.

We used the patch-clamp technique in the whole-cell configuration to record Na_v currents and action potentials from acutely dissociated small diameter DRG neurons (<30 μm) from adult rats. We also performed single cell qPCR on the same neurons.

Our results revealed that there is a strong correlation between Na_v currents and mRNA transcripts in individual neurons. A cluster analysis showed that subgroups formed by Na_v channel transcripts by mRNA quantification have different biophysical properties. In addition, the firing frequency of the neurons was not affected by the relative populations of Na_v channel.

The synergy between populations of Na_v channel in individual small diameter DRG neurons gives each neuron a unique electrophysiological profile. The Na_v channel remodeling that occurs in different pathological pain states may be responsible for the sensitization of the neurons.

Introduction

Voltage gated sodium channels (Na_v channels) play an important role in nociceptive transmission and are intimately tied to the genesis and transmission of neuronal action potentials. Five isoforms ($Na_v1.3$, $Na_v1.6$, $Na_v1.7$, $Na_v1.8$, and $Na_v1.9$) have been linked to nociceptive responses (Garrison *et al.* 2014; Dib-Hajj *et al.* 2009; Xie *et al.* 2013). The diversity of the biophysical properties and expression patterns of Na_v channels point to functional specialization (Hu *et al.* 2009). Moreover, previous studies emphasized the importance of different properties of Na_v in the neuronal excitability. For instance, the slow closed-state inactivation of $Na_v1.7$ is thought to play an important role in the amplification of subthreshold depolarization and initiate AP firing in neurons (Cummins *et al.* 2007; Blair and Bean 2002). The fast recuperation from the inactivated state of $Na_v1.8$ is thought to sustain the relatively high frequency firing of small DRG neurons (Cummins and Waxman 1997; Renganathan *et al.* 2001) while the current induced by the hyperpolarized activation of $Na_v1.9$ could modulate the membrane voltage and alter the neuronal excitability (Herzog *et al.* 2001).

Furthermore, defect in biophysical properties of peripheral Na_v channels lead to diverse pain syndromes. Two inherited human neuropathic pain conditions, erythermalgia(Black *et al.* 2004) and paroxysmal extreme pain disorder (PEPD)(Fertleman *et al.* 2006), are associated with various missense (gain of function) mutations in SCN9A, the gene encoding the human $Na_v1.7$ channel. PEPD is associated with defective fast inactivation, whereas erythermalgia is associated with a negative-shifted voltage-dependence of activation of $Na_v1.7$ channels (Estacion *et al.* 2008). More recently, a remarkable congenital indifference to pain (CIP) (Ahmad *et al.* 2007) was described in consanguineous Pakistani and Canadian individuals, who are homozygous for a null mutation (complete loss of function) of $Na_v1.7$ (Ahmad *et al.* 2007; Cox *et al.* 2006). It has also been reported that humans can harbour single nucleotide polymorphisms in SCN9A, which apparently confer different thresholds for pain susceptibility, depending on the functionality of the inherited alleles (Reimann *et al.* 2010). A variant of $Na_v1.8$ has been reported in a family with painful peripheral

neuropathy (Faber *et al.* 2012). Gain-of-functions mutations on Nav1.9 were reported to induce either loss of pain (Leipold *et al.* 2013) or episodic pain (Zhang *et al.* 2013).

The regulation of Na_v channels in sensory neurons is complex and may be a mechanism for conferring unique biophysical properties on the neurons (Chahine *et al.* 2005). Changes in the voltage-dependence, kinetics, and expression of Na_v channel subtypes in several models of nerve injury and inflammation used in pain research have been reported (Black *et al.* 2004; Moore *et al.* 2002; Gold and Flake 2005; Gold *et al.* 1998; Gold *et al.* 2003; Thakor *et al.* 2009). These changes have been shown to induce hyperexcitability in primary afferent neurons (Moore *et al.* 2002; Song *et al.* 2003).

The aim of the study was to understand how the different Na_v channel α-subunits present in peripheral neurons interact to modulate neuronal excitability and induce the various electrophysiological profiles seen in these neurons. We hypothesized that individual Na_v paralogs contribute to their different biophysical properties to shape the action potential waveforms and overall excitability of peripheral neurons. Clarifying interactions between Na_v subtypes is an important step toward understanding the development of neuropathic pain, and the maturation and diversifications of neurons.

We used the patch-clamp technique in the whole-cell configuration to record Na_v currents and action potentials from acutely dissociated small diameter DRG neurons from adult rats (<30 μm). We also performed single cell qPCR on the same neurons. We compared Na_v channel transcripts in individual neurons and correlated them to the electrophysiological profiles of the neurons to assess their impact on excitability.

The ratio of the expression of mRNA reflected the proportion of Na_v channels at the membrane of the neurons. Moreover, the ratio of the different Na_v channel subtypes expressed in each neuron conferred a unique electrophysiological profile on the neuron. For instance, compared to the $Na_v1.8$ and $Na_v1.9$ channel subtypes, $Na_v1.7$ channel

displayed faster AP kinetics and shorter AP. Moreover, the presence of $Na_v1.7$ decreased the threshold potential and accelerates the rise and the decay of the AP.

Materials and methods

DRG neuron dissection and culture

Neurons were isolated from L4-L5 DRG of adult male Sprague–Dawley rats weighting from 250 g to 350 g(Wilmington, MA). Briefly, freshly removed ganglia were de-sheathed and enzymatically digested at 37°C for 20 min in DMEM containing 2 $mg \cdot ml^{-1}$ of type 4 collagenase (Worthington Biochemical Corp.). Trypsin (2.5 $mg \cdot ml^{-1}$, Sigma) was added, and the neurons were incubated for an additional 15 min. The ganglia were then dissociated mechanically by trituration using fire-polished Pasteur pipettes. The cell suspensions were centrifuged for 5 min at 1000 rpm at room temperature. The cell pellets were re-suspended in DMEM containing 4 $mg \cdot ml^{-1}$ of type 2S trypsin inhibitor (Sigma), layered on 7.5% BSA in Dulbecco's phosphate buffered saline (DPBS), and centrifuged at 1000 rpm for 5 min. After removing the supernatant, the pellet containing the neurons was re-suspended in DMEM containing 10% heat-inactivated horse serum and 5% FBS. The neurons were plated on poly-d-lysine-coated dishes and were kept in a 5% CO_2 incubator at 37°C. The patch-clamp recordings were performed within 18 h. All experiments were performed according to the guidelines of the Canadian Council on Animal Care and were approved by the Université Laval Animal Care Committee.

Whole-cell patch-clamp recording

Neurons ranging in diameter from 20-30 μm (mean short and long axis) measured using a graduated ocular were selected for recording. Whole-cell Na_v currents in DRG neurons were recorded using an Axopatch 200B (Molecular Devices) with the whole-cell configuration of the patch-clamp technique. pClamp v10 (Molecular Devices) was used for the pulse stimulations and recordings. Currents were filtered at 5 kHz, digitized at 100 kHz using a Digidata 1200 series AD converter (Molecular devices), and stored on a personal computer for later offline analysis. Series resistance was compensated 70-80%. When needed, linear leak current artifacts were removed by online leak subtraction. Capillaries used for electrodes were silanized prior to fashioning to reduce mRNA adsorption. The capillaries were soaked in a 5% (v/v) solution of dimethyldichlorosilane (Sigma) in chloroform for 20 min in a fume hood. They were then sterilized (15 min) and dried (15 min) in an autoclave (Lin *et al.* 2007). Fire-polished low-resistance electrodes (1MΩ) were pulled from 8161 glass (Corning) and were coated with Sylgard (Dow-Corning) to minimize pipette capacitance.

AP recordings were obtained from DRG neurons using the whole-cell configuration of the patch-clamp technique. APs were generated by 5-ms, 50 to 300-pA rectangular current pulse injections followed by a 100-ms interpulse at the holding potential and then a 600-ms pulse. The sequence consisted of at least two recordings of evoked APs before and after the addition of 1 μM TTX.

For whole-cell voltage-clamp recordings, the intracellular pipette solution contained 10 mM NaCl, 140 mM CsF, 1 mM EGTA, and 10 mM HEPES. The pH was adjusted to pH 7.3 with 1 mM CsOH. The external solutions contained, the bath solution contained 35 mM NaCl, 105 mM choline chloride, 3 mM KCl, 1 mM $CaCl_2$, 1.0 mM $MgCl_2$, 10 mM glucose, 10 mM HEPES, and 100 nM $CdCl_2$ to block calcium channels. The pH was adjusted to 7.3 with 1 M NaOH.

For the current-clamp recordings, the intracellular solution contained 122 mM KCl, 10 mM NaCl, 1.0 mM $MgCl_2$, 1.0 mM EGTA, and 10 mM HEPES. The pH was adjusted to 7.3 with 1 M KOH. The extracellular solution contained 154 mM NaCl, 5.6 mM KCl, 2.0 mM $CaCl_2$, 1.0 mM $MgCl_2$, 10 mM glucose, and 8.0 mM HEPES. The pH was adjusted to 7.4 with 1 M NaOH.

RT-qPCR

RNA extraction

We used two-step RT-qPCR to evaluate the mRNA in each DRG neuron tested. After the patch-clamp recording, the neuron was drawn into the recording pipette, expelled into a thin wall PCR tube, and stored in liquid nitrogen until the RT-PCR was performed. The RT-PCR reagents were added directly to the tube.

Total RNA for primer validation and standard curves was extracted from the DRG neurons using TRIZOL® (Invitrogen). RNA integrity was evaluated by ethidium bromide staining of 1% agarose gels. Total RNA was quantified by recording the optical density at 260 and 280 nm.

RT-PCR

RT-PCR was performed using Transcriptor First Strand cDNA Synthesis kits (Roche) according to the supplier's protocol. Briefly, lysed cells or 1 μg of total RNA was added to 60 pmol random hexamer primer and water was added to bring the volume to 13 µL. The template-primer mixture was denatured for 10 min at 65˚C. Reaction buffer, RNase inhibitor (20 U final concentration), DNTP (1 mM each), and Transcriptor Reverse Transcriptase (1 U final concentration) were added to the mixture (20 µL). cDNA was synthesized at 50˚C for 1 h. The enzymes were heat-deactivated at 85˚C for 2 min. cDNA from DRG was stored at –80˚C until used. Single cell qPCR was performed on the same day as the electrophysiological recordings.

qPCR

The qPCR assays were performed using a previously described protocol (Chatelier *et al.* 2012). Briefly, amplification products were detected with SYBR Green I and a LightCycler® 480 platform (Roche) using the supplier's protocol. Primers were designed using PerlPrimer v1.1.19 (Marshall 2007). The qPCR samples were run at least in duplicate. A non-template control (NTC) and a positive control for each primer pair were included in each qPCR run. The qPCR conditions were as follows: an initial 7-min step at 95°C to activate the Taq polymerase and 45 cycles of 10 s at 95°C and 10 s at 58°C, followed by a 12-s elongation step at 72°C.

qPCR efficiency was determined using a series of known cDNAs, and the Cq values were plotted against the relative cDNA concentrations. qPCR efficiency was calculated using the slope of the regression line using the following equation: E = 10^[-1/slope]. The analyses were performed using LightCycler® 480 SW 1.5 software. Quantifications were corrected for efficiency and run-to-run variations were adjusted using a known standard:

$$Normalized\ ratio = \left(\frac{[Target]}{[Reference]}\right)_{sample} \div \left(\frac{[Target]}{[Reference]}\right)_{calibrator}$$

Target represents Cp of sodium channels and reference represents Cp of GAPDH (Gudrun 2006). This is an efficient and accurate method to compensate for efficiency and run-to-run variations without the need of a standard curve in every run (Bustin 2004). The specificity of the amplification for each run was monitored by melting curve analysis and was performed immediately following the PCR by continuously reading the fluorescence while slowly heating the reaction mixture from 65°C to 95°C.

Data analysis

Electrophysiological data were analyzed using a combination of pCLAMP software v10.0 (Molecular Devices), Microsoft Excel, and SigmaPlot 12.0 (Systat Software, Inc.).

Unless otherwise stated, statistical analyses were performed using SAS/STAT software v9.2 (SAS Institute Inc.). The results of Pearson analyses are expressed as coefficients of Pearson (ρ). Values are expressed as means ± SEM. When required for clarity, results are expressed as z-scores (z-scores=(x-mean)/SD).

Cluster analyses were performed to identify homogenous subsets of neurons based on the mRNA each subset expressed. mRNA quantifications were entered into the cluster analysis based on a Gaussian mixture model implemented in the R software with the Mclust package (available at http://cran.r-project.org/web/packages/mclust/index.html). Since we did not want to define a number of a priori subgroups of neurons, we compared the adjustments of different clustering solutions with 1, 2, 3, 4, and 5 clusters using the Bayesian Information Criterion (BIC). The inspection of the BIC values showed that the five-cluster solution worked best. However, given that there were very slight differences between two pairs of clusters, we opted for a three-cluster solution. Each subject was then assigned to a most probable cluster.

Results

qPCR amplification efficiency and single-cell qPCR validation

We validated the selectivity of the qPCR reaction using ethidium bromide-stained agarose gels. We observed single bands on the agarose gels, indicating that each primer pair produced one amplicon. The amplicons were validated by sequencing (data not shown). qPCR amplification was assessed using a melting curve analysis to ensure that it gave rise to a single PCR product. We evaluated the efficiency of the qPCR by generating standard curves over a wide range of mRNA copies using serial dilutions of known concentrations of cDNA (Supplement Fig. 2A). Each primer pair had an efficiency superior to 1.90 in the 5-log range and was efficient with a low copy number (<100 copies) of mRNA (Table 1).

Since the quantification was relative to a reference gene, we verified the stability of the selected gene in individual cell experiments. We selected three references genes that are frequently used in qPCR experiments: GAPDH (Glyceraldehyde 3-phosphate dehydrogenase), ACTB (beta-actin), and PPIA (peptidylprolyl isomerase A). We first determined whether the ratio of the genes was stable in single neurons. Supplement Figures 1 A and B show the cell-to-cell variations of the ACTB/GAPDH and PPIA/GAPDH gene ratios, respectively. The variations are expressed as (x-mean)/mean. We observed a marked cell-to-cell variation in the ACTB/GAPDH gene ratio of 59% with a mean error of 34%. The variation in the PPIA/GAPDH gene ratio was generally under 20% with a mean error of 12%. There was little correlation between the Ct values for ACTB and GAPDH, indicating that there was a large variation in the amount of mRNA among cells (Supplement Fig. 1A). As such, GAPDH and ACTB could not be used as references genes. Supplement figure 1 D shows the correlation between the Ct values of GAPDH and PPIA for different cells. The high correlation (R^2=0.98) and the slope value approaching one indicated that there was a low cell-to-cell variation for these two genes. Since GAPDH levels appeared to be stable in individual neurons, we used GAPDH as a reporter gene in our experiments.

We also ensured that the selectivity and efficiency were conserved in our experimental conditions by quantifying serial 1:1 dilutions (up to 1:32) of mRNA from single cells (Supplement fig. 2A). We observed very good quantification at all dilutions, with an error of less than10%. Every amplification product was monitored with a melting curve to ensure that we had a single amplification product.

RT-PCR is often inefficient and can be a source of error (Stahlberg *et al.* 2004). The relative quantification of the GAPDH reference gene minimizes the risk of error by reducing the influence of variation in the efficiency of the RT-PCR. We assumed that the efficiency was similar for each gene tested and, as such, that the ratios of the Na_v channel transcripts to the reference gene were similar, regardless the efficiency of the

RT-PCR. The small amount of mRNA in a single cell and the small volume may also have induced an error. However, any loss of mRNA could be assumed to be the same for each gene we tested and, as such, would also be also minimized by the relative quantification.

mRNAs reflect electrophysiological properties

The voltage-clamp approach can discriminate between TTX-sensitive and resistant Na_v channels. TTX-sensitive Na_v channels (TTX-S) are completely blocked by TTX at low nM concentrations while TTX-resistant Na_v channels (TTX-R) are insensitive to TTX (IC_{50}>40 μM) (Caffrey *et al.* 1992). Figure 1A shows an example of a representative Na_v current recorded from a small neuron before (left) and after (right) the addition of 1 μM TTX. The TTX-R Na_v current was probably due to $Na_v1.8$ and $Na_v1.9$ channels. The TTX-S current-voltage relationship (I/V) curve was obtained by subtracting the I/V-curve of the TTX-R Na_v current from the total Na_v current (Fig. 1B). Figure 1C shows the GV curves of TTX-R current and TTX-s current obtain from data of figure 1B. (Fig. 1A). The proportions of the TTX-S and TTX-R Na_v currents were strongly correlated (R^2=0.92) with the relative expression of mRNA by the TTX-S and TTX-R Na_v channels (Fig. 1D). In these experiments $Na_v1.6$ was not quantified due to low levels of transcripts in less than 35% of neurons (16 out of 46 neurons), data not shown. These results are similar to the study by Ho and O'leary where $Na_v1.6$ is 6 to 8 time less abundant than $Na_v1.7$, $Na_v1.8$ and $Na_v1.9$ (Ho and O'Leary 2011).

Impacts on AP properties

We analyzed the parameters of APs recorded from small diameter DRG neurons in the current-clamp mode and quantified the mRNA in the neurons by single-cell qPCR. Neurons ranging in diameter from 20-30 μm exhibited marked differences in sensitivity to TTX. Twenty-one of the 49 neurons were sensitive to 1 μM TTX and exhibited no AP firing. Figure 2A shows a typical neuron in which AP firing was resistant to TTX. The left panel of Figure 2A show a representative AP recording under control conditions and the right panel shows a representative AP recording in the presence of 1 μM TTX. The protocol is shown in the inset. Figure 2B shows a neuron

whose AP firing was inhibited by TTX. The left panel shows AP firing prior to the addition of TTX and the right panel show that the firing was abolished after the addition of 1 μM TTX. The first AP was not abolished by TTX.

Table 2 shows Pearson correlations between mRNAs and several biophysical properties of the AP. The correlations are expressed as negative or positive r values, which were considered significant at $p<0.05$ (*$p<0.05$, **$p<0.01$). There was a significant correlation between $Na_v1.7$ mRNA and the overshoot, threshold (in mV and in pA), rise time (dV/dT), and time of decay as well as between $Na_v1.8$ and $Na_v1.9$ mRNA and the half AP width (duration of the AP at 50% amplitude), current threshold, and overshoot. There was also a significant correlation between $Na_v1.9$ mRNA and a slowing of the rise and decay of dV/dT.

Cluster analysis

We performed another post hoc analysis of the data by plotting the amounts of mRNA in order to visualize their distributions (Fig. 3A). $Na_v1.7$ mRNA was plotted against $Na_v1.8$ mRNA in $Na_v1.3$ mRNA-positive (red) and $Na_v1.3$ mRNA-negative cells (blue). We observed a marked difference between the two types of cell, with $Na_v1.3$ mRNA-positive cells expressing more $Na_v1.7$ mRNA than $Na_v1.3$ mRNA-negative cells.

We also performed a cluster analysis to determine whether there were different subgroups of neurons (Fig. 3B). Interestingly, the cluster analysis revealed that there were three subgroups of neurons that differed in the expression of Na_v channel mRNA. The first subgroup (red) expressed large numbers of TTX-R $Na_v1.8$ and $Na_v1.9$ channels. The second subgroup (orange) made up 8% of all the neurons tested and expressed a combination of TTX-S Na_v channels ($Na_v1.7$) and TTX-R Na_v channels ($Na_v1.8$ and $Na_v1.9$). The third subgroup (green) made up 43% of all the neurons tested and mainly expressed TTX-S $Na_v1.7$ Na_v channels.

We performed statistical analyses to determine whether there were any differences in AP parameters between the subgroups. Results are expressed as z-scores on the y axis (Fig. 3C). We also performed multiple comparisons when the Anova p-value was less than 0.05 ($p<0.05$). We observed significant differences between subgroups 1 and 3 (*) and subgroups 2 and 3 (¤). There was a significant difference between subgroups 1 and 2 versus subgroup 3 in terms of half AP width, overshoot, current threshold, and maximum dV/dt rise. There was also a significant difference between groups 1 and 3 in terms of dV/dt decay. The figure 4 illustrates the AP properties of a representative neurons from each groups.

Discussion

One concern with qPCR is that the amount of amplified mRNA is not proportional to the amount of functional protein (Maier *et al.* 2009; Greenbaum *et al.* 2003). We recorded voltage-clamp currents and performed single-cell qPCR to measure the expression of functional Na_v channels and mRNA (Lin *et al.* 2007; Sucher *et al.* 2000). Adding TTX makes it possible to discriminate between TTX-R and TTX-S Na_v channels and, as such, correlate the expression of functional TTX-R and TTX-S Na_v channels and their mRNAs. We observed a strong correlation between the proportion of mRNA and the expression of functional Na_v channels (Fig. 1D), indicating that the expression of mRNA was a good representation of the amount of functional protein in our study and could thus be used to quantify the amount of proteins.

There was a significant correlation between Na_v channel mRNA and AP parameters. It has been shown that faster Na_v channel kinetics may result in faster AP kinetics (Schild and Kunze 2012; Cummins *et al.* 2007). The presence of $Na_v1.7$ channels increased the rise in dV/dT, decreased the decay in dV/dT, and reduced the half AP width of the AP. The correlation analysis also showed that $Na_v1.7$ channels had a lower threshold and a higher overshoot than $Na_v1.8$ and $Na_v1.9$ channels while $Na_v1.8$ and $Na_v1.9$ channels displayed slower AP kinetics than $Na_v1.7$ channels. This is in agreement with the hypothesis that $Na_v1.7$ amplifies subthreshold stimuli to evoked

AP (Blair and Bean 2002). Moreover, those results can be linked to studies that indicate a role for the upregulation of $Na_v1.7$ in neuropathic pain (Black *et al.* 2004; Cummins *et al.* 2004).

In our study, the presence of $Na_v1.9$ and $Na_v1.8$ channels significantly slowed dV/dT rise and decay ($p=0.06$ for $Na_v1.9$ and $p=0.05$ for $Na_v1.8$). The half AP width was also correlated with the proportion of $Na_v1.8$ and $Na_v1.9$ Na_v channels, which is in agreement with their slower kinetics (Vijayaragavan *et al.* 2001). Those results are in accordance with studies which concluded that the sodium channels subtypes have different roles in the electrogenesis within DRG neurons (Rush *et al.* 2007; Ho and O'Leary 2011).

Pearson analysis does not show any correlation between Na_v channels transcripts and firing frequency of the neurons (Table 2). It has been assumed that slowly inactivating $Na_v1.8$ channels support high frequency firing in small C-fiber neurons (Renganathan *et al.* 2001). However, our data showed that both $Na_v1.7$ and $Na_v1.8$ channels can support high frequency tonic firing in DRG neurons. Indeed, $Na_v1.7$ supports high frequency neurons in SCG neurons (Rush *et al.* 2006).

The plot of the distributions of $Na_v1.7$ and $Na_v1.8$ mRNA showed marked differences depending on whether $Na_v1.3$ mRNA was present or not, which together with prior observations indicated that there are several subtypes of neurons (Ho and O'Leary 2011; Fornaro *et al.* 2008). We thus performed a cluster analysis of mRNA distributions, which revealed that there are three subgroups of neurons in small diameter DRG neurons (<30 μm) that we tested. One subgroup mainly expressed $Na_v1.8$ and $Na_v1.9$ mRNA, the second subgroup expressed similar amounts of $Na_v1.7$, $Na_v1.8$, and $Na_v1.9$ mRNA, while the third subgroup mainly expressed $Na_v1.7$ mRNA.

The three subgroups displayed significant differences in AP properties. The frequency and threshold (in mV) were the only parameters that were the same for all three subgroups. The half AP width, overshoot, current threshold, dV/dT decay, and

dV/dT rise of the third group differed from those of the first and the second subgroups. The lack of significant differences between the first and second subgroups may be due to the very low proportions of these two subgroup and greater differences between them.

It is interesting that the biophysical properties of the three subgroups were similar to the results of the Pearson correlations. The third subgroup, which had a greater proportion of $Na_v1.7$, had a faster AP, a shorter half AP width, and a faster dV/dT decay and rise than the first and second subgroups. The third subgroup also had a greater overshoot and a lower current threshold than the first and second subgroups. The first and seconds subgroups, which had more $Na_v1.8$ and $Na_v1.9$ channels than $Na_v1.7$ channels, exhibited slower kinetics than the third subgroup as well as a lower overshoot and a higher current threshold.

Potassium and calcium channels also have a major impact on the firing pattern (Winlove and Roberts 2012; Deister *et al.* 2009). It is thus possible that the changes we observed were caused by more than one contributing factor (ion channels, pumps, exchangers, etc.). Nevertheless, the strong linear correlation indicated that Na_v channels play a major role in the biophysical properties of DRG neurons. It's important to keep in mind that electrophysiological properties of a neuron are the results of the equilibrium between the different ion channels present and therefore changes might not lead to the same outcome. As shown by Rush et al., a gain of function mutation of $Na_v1.7$ that lead to erythermalgia render the sensory neurons hyperexcitable and sympathetic neurons hypoexcitable (Rush *et al.* 2006).

Our results also have major implications during development since the different expression patterns that occur during the maturation of the nervous system (Beckh 1990) are associated with changes in the electrical excitability of the neurons (Benn *et al.* 2001). Our results contribute to understanding how the different subtypes of Na_v channels affect the maturation and excitability of sensory neurons.

While there are numerous reports in the literature on the modulation of Na_v channels and the changes in the excitability of sensory neurons during different pathological conditions, little is known about how this affects the excitability of neurons (Berta *et al.* 2008; Cummins and Waxman 1997; Thakor *et al.* 2009). We showed that the modulation of Na_v channels has an impact on the firing properties of acutely dissociated DRG sensory neurons. It now remains to be determined how changes in Na_v channel expression in pathological conditions affect the excitability of neurons.

We concluded that the different Na_v channel subtypes in small diameter DRG neurons point to complex physiological interactions and that their modulation affects the biophysical properties of these neurons. Further studies are needed to unravel the roles of the Na_v channel subtypes during development and in pathological conditions.

Acknowledgements

This work was supported by grants from the Canadian Institutes of Health Research (CIHR, MOP-111072), and the Heart and Stroke Foundation of Quebec (HSFQ).

References

Ahmad, S., Dahllund, L., Eriksson, A.B., Hellgren, D., Karlsson, U., Lund, P.E. et al. (2007). A stop codon mutation in SCN9A causes lack of pain sensation. Hum. Mol. Genet. 16, 2114-2121.

Beckh, S. (1990). Differential expression of sodium channel mRNAs in rat peripheral nervous system and innervated tissues. FEBS Lett. 262, 317-322.

Benn, S.C., Costigan, M., Tate, S., Fitzgerald, M., and Woolf, C.J. (2001). Developmental expression of the TTX-resistant voltage-gated sodium channels Nav1.8 (SNS) and Nav1.9 (SNS2) in primary sensory neurons. J. Neurosci. 21, 6077-6085.

Berta, T., Poirot, O., Pertin, M., Ji, R.R., Kellenberger, S., and Decosterd, I. (2008). Transcriptional and functional profiles of voltage-gated Na(+) channels in injured and non-injured DRG neurons in the SNI model of neuropathic pain. Mol. Cell Neurosci. 37, 196-208.

Black, J.A., Liu, S., Tanaka, M., Cummins, T.R., and Waxman, S.G. (2004). Changes in the expression of tetrodotoxin-sensitive sodium channels within dorsal root ganglia neurons in inflammatory pain. Pain 108, 237-247.

Blair, N.T. and Bean, B.P. (2002). Roles of tetrodotoxin (TTX)-sensitive Na+ current, TTX-resistant Na+ current, and Ca2+ current in the action potentials of nociceptive sensory neurons. J. Neurosci. 22, 10277-10290.

Bustin, S.A. (2004). A to Z of Quantitative PCR.

Caffrey, J.M., Eng, D.L., Black, J.A., Waxman, S.G., and Kocsis, J.D. (1992). Three types of sodium channels in adult rat dorsal root ganglion neurons. Brain Res. 592, 283-297.

Chahine, M., Ziane, R., Vijayaragavan, K., and Okamura, Y. (2005). Regulation of Na(v) channels in sensory neurons. Trends Pharmacol. Sci. 26, 496-502.

Chatelier, A., Mercier, A., Tremblier, B., Theriault, O., Moubarak, M., Benamer, N. et al. (2012). A distinct de novo expression of Nav1.5 sodium channels in human atrial fibroblasts differentiated into myofibroblasts. J. Physiol 590, 4307-4319.

Cox, J.J., Reimann, F., Nicholas, A.K., Thornton, G., Roberts, E., Springell, K. et al. (2006). An SCN9A channelopathy causes congenital inability to experience pain. Nature 444, 894-898.

Cummins, T.R., Dib-Hajj, S.D., and Waxman, S.G. (2004). Electrophysiological properties of mutant Nav1.7 sodium channels in a painful inherited neuropathy. J. Neurosci. 24, 8232-8236.

Cummins, T.R., Sheets, P.L., and Waxman, S.G. (2007). The roles of sodium channels in nociception: Implications for mechanisms of pain. Pain 131, 243-257.

Cummins, T.R. and Waxman, S.G. (1997). Downregulation of tetrodotoxin-resistant sodium currents and upregulation of a rapidly repriming tetrodotoxin-sensitive sodium current in small spinal sensory neurons after nerve injury. J. Neurosci. 17, 3503-3514.

Deister, C.A., Chan, C.S., Surmeier, D.J., and Wilson, C.J. (2009). Calcium-activated SK channels influence voltage-gated ion channels to determine the precision of firing in globus pallidus neurons. J. Neurosci. 29, 8452-8461.

Dib-Hajj, S.D., Black, J.A., and Waxman, S.G. (2009). Voltage-gated sodium channels: therapeutic targets for pain. Pain Med. 10, 1260-1269.

Estacion, M., Dib-Hajj, S.D., Benke, P.J., te Morsche, R.H., Eastman, E.M., Macala, L.J. et al. (2008). NaV1.7 gain-of-function mutations as a continuum: A1632E displays physiological changes associated with erythromelalgia and paroxysmal extreme pain disorder mutations and produces symptoms of both disorders. J. Neurosci. 28, 11079-11088.

Faber, C.G., Lauria, G., Merkies, I.S., Cheng, X., Han, C., Ahn, H.S. et al. (2012). Gain-of-function Nav1.8 mutations in painful neuropathy. Proc. Natl. Acad. Sci. U. S. A 109, 19444-19449.

Fertleman, C.R., Baker, M.D., Parker, K.A., Moffatt, S., Elmslie, F.V., Abrahamsen, B. et al. (2006). SCN9A mutations in paroxysmal extreme pain disorder: allelic variants underlie distinct channel defects and phenotypes. Neuron 52, 767-774.

Fornaro, M., Lee, J.M., Raimondo, S., Nicolino, S., Geuna, S., and Giacobini-Robecchi, M. (2008). Neuronal intermediate filament expression in rat dorsal root ganglia sensory neurons: an in vivo and in vitro study. Neuroscience 153, 1153-1163.

Garrison, S.R., Weyer, A.D., Barabas, M.E., Beutler, B.A., and Stucky, C.L. (2014). A gain-of-function voltage-gated sodium channel 1.8 mutation drives intense hyperexcitability of A- and C-fiber neurons. Pain

Gold, M.S. and Flake, N.M. (2005). Inflammation-mediated hyperexcitability of sensory neurons. Neurosignals. 14, 147-157.

Gold, M.S., Levine, J.D., and Correa, A.M. (1998). Modulation of TTX-R INa by PKC and PKA and their role in PGE2-induced sensitization of rat sensory neurons in vitro. J. Neurosci. 18, 10345-10355.

Gold, M.S., Weinreich, D., Kim, C.S., Wang, R., Treanor, J., Porreca, F. et al. (2003). Redistribution of Nav1.8 in uninjured axons enables neuropathic pain. J. Neurosci. 23, 158-166.

Greenbaum, D., Colangelo, C., Williams, K., and Gerstein, M. (2003). Comparing protein abundance and mRNA expression levels on a genomic scale. Genome Biol. 4, 117.

Gudrun, T. (2006). The E-Method: a highly accurate technique for gene-expression analysis. Nature Methods 3

Herzog, R.I., Cummins, T.R., and Waxman, S.G. (2001). Persistent TTX-resistant Na+ current affects resting potential and response to depolarization in simulated spinal sensory neurons. J. Neurophysiol. 86, 1351-1364.

Ho, C. and O'Leary, M.E. (2011). Single-cell analysis of sodium channel expression in dorsal root ganglion neurons. Mol. Cell Neurosci. 46, 159-166.

Hu, W., Tian, C., Li, T., Yang, M., Hou, H., and Shu, Y. (2009). Distinct contributions of Na(v)1.6 and Na(v)1.2 in action potential initiation and backpropagation. Nat. Neurosci. 12, 996-1002.

Laird, J.M.A., Souslova, V., Wood, J.N., and Cervero, F. (2002). Deficits in visceral pain and referred hyperalgesia in Nav1.8 (SNS/PN3)-null mice. J. Neurosci. 22, 8352-8356.

Leipold, E., Liebmann, L., Korenke, G.C., Heinrich, T., Giesselmann, S., Baets, J. et al. (2013). A de novo gain-of-function mutation in SCN11A causes loss of pain perception. Nat. Genet. 45, 1399-1404.

Lin, D.M., Loveall, B., Ewer, J., Deitcher, D.L., and Sucher, N.J. (2007). Characterization of mRNA expression in single neurons. Methods Mol. Biol. 399, 133-152.

Maier, T., Guell, M., and Serrano, L. (2009). Correlation of mRNA and protein in complex biological samples. FEBS Lett. 583, 3966-3973.

Marshall, O. (2007). Graphical design of primers with PerlPrimer. Methods Mol. Biol. 402, 403-414.

Moore, B.A., Stewart, T.M., Hill, C., and Vanner, S.J. (2002). TNBS ileitis evokes hyperexcitability and changes in ionic membrane properties of nociceptive DRG neurons. Am. J. Physiol Gastrointest. Liver Physiol 282, G1045-G1051.

Reimann, F., Cox, J.J., Belfer, I., Diatchenko, L., Zaykin, D.V., McHale, D.P. et al. (2010). Pain perception is altered by a nucleotide polymorphism in SCN9A. Proc. Natl. Acad. Sci. U. S. A 107, 5148-5153.

Renganathan, M., Cummins, T.R., and Waxman, S.G. (2001). Contribution of Nav1.8 sodium channels to action potential electrogenesis in DRG neurons. J. Neurophysiol. 86, 629-640.

Rush, A.M., Cummins, T.R., and Waxman, S.G. (2007). Multiple sodium channels and their roles in electrogenesis within dorsal root ganglion neurons. J. Physiol. 579, 1-14.

Rush, A.M., Dib-Hajj, S.D., Liu, S., Cummins, T.R., Black, J.A., and Waxman, S.G. (2006). A single sodium channel mutation produces hyper- or hypoexcitability in different types of neurons. Proc. Natl. Acad. Sci. U. S. A 103, 8245-8250.

Schild, J.H. and Kunze, D.L. (2012). Differential distribution of voltage-gated channels in myelinated and unmyelinated baroreceptor afferents. Auton. Neurosci. 172, 4-12.

Song, X.J., Zhang, J.M., Hu, S.J., and LaMotte, R.H. (2003). Somata of nerve-injured sensory neurons exhibit enhanced responses to inflammatory mediators. Pain 104, 701-709.

Stahlberg, A., Hakansson, J., Xian, X., Semb, H., and Kubista, M. (2004). Properties of the reverse transcription reaction in mRNA quantification. Clin. Chem. 50, 509-515.

Sucher, N.J., Deitcher, D.L., Baro, D.J., Warrick, R.M., and Guenther, E. (2000). Genes and channels: patch/voltage-clamp analysis and single-cell RT-PCR. Cell Tissue Res. 302, 295-307.

Thakor, D.K., Lin, A., Matsuka, Y., Meyer, E.M., Ruangsri, S., Nishimura, I. et al. (2009). Increased peripheral nerve excitability and local NaV1.8 mRNA up-regulation in painful neuropathy. Mol. Pain 5, 14.

Vijayaragavan, K., O'Leary, M.E., and Chahine, M. (2001). Gating properties of Nav1.7 and Nav1.8 peripheral nerve sodium channels. J. Neurosci. 21, 7909-7918.

Winlove, C.I. and Roberts, A. (2012). The firing patterns of spinal neurons: in situ patch-clamp recordings reveal a key role for potassium currents. Eur. J. Neurosci. 36, 2926-2940.

Xie, W., Strong, J.A., Ye, L., Mao, J.X., and Zhang, J.M. (2013). Knockdown of sodium channel NaV1.6 blocks mechanical pain and abnormal bursting activity of afferent neurons in inflamed sensory ganglia. Pain 154, 1170-1180.

Zhang, X.Y., Wen, J., Yang, W., Wang, C., Gao, L., Zheng, L.H. et al. (2013). Gain-of-Function Mutations in SCN11A Cause Familial Episodic Pain. Am. J. Hum. Genet. 93, 957-966.

Gene (protein)	Amplification length (pb)	Primer sequence
SCN3A ($Na_v1.3$)	158	F : 5'- AACGAAAGACGATCAAGACC-3' R : 5'-CCAAAGAAACATCAACGATCAG-3'
SCN9A ($Na_v1.7$)	163	F : 5'- GGGAACTTGATCTTTACAGGG-3' R : 5'-ACTGATAATCCTTCCACATCTG-3'
SCN10A ($Na_v1.8$)	189	F : 5'- TAGACATGGAGAAGAGGGAC-3' R : 5'-TTCAAGCTCCTCAATGACAG-3'
SCN11A ($Na_v1.9$)	196	F : 5'- AAATGATCCTGAAGTGGGTG-3' R : 5'-GTAGACGACAACCTTCATTCC-3'
GAPDH	152	F : 5'- AGTATGTCGTGGAGTCTACTG-3' R : 5'-GGGAGTTGTCATATTTCTCGT-3'
ACTB	175	F : 5'- AGATCAAGATCATTGCTCCTCC-3' R : 5'-AACGCAGCTCAGTAACAGTC-3'
PPIA	160	F : 5'- TTTATCTGCACTGCCAAGAC-3' R : 5'-AATTAGAGTTGTCCACAGTCGG-3'

Table 1: qPCR primers used

Table2: Pearson correlations of Na^+ channels mRNA and electrophysiological properties measured.

	Frequency	Half AP width	Overshoot	Threshold (mV)	Threshold (pA)	dV/dT (decay)	dV/dT (rise)
$Na_v1.7$	-	-0.46**	0.43**	-0.32*	-0.46**	-0.30*	0.46**
$Na_v1.8$	-	0.31*	-0.31*	-	0.45**	-	-
$Na_v1.9$	-	0.34*	0.38**	-	0.32*	0.29*	-0.37**

Data are presented as the correlation coefficient of Pearson correlations (ρ). Significant values are presented with *; *p-value < 0.05; ** p-value < 0.01. -, no significant correlation.

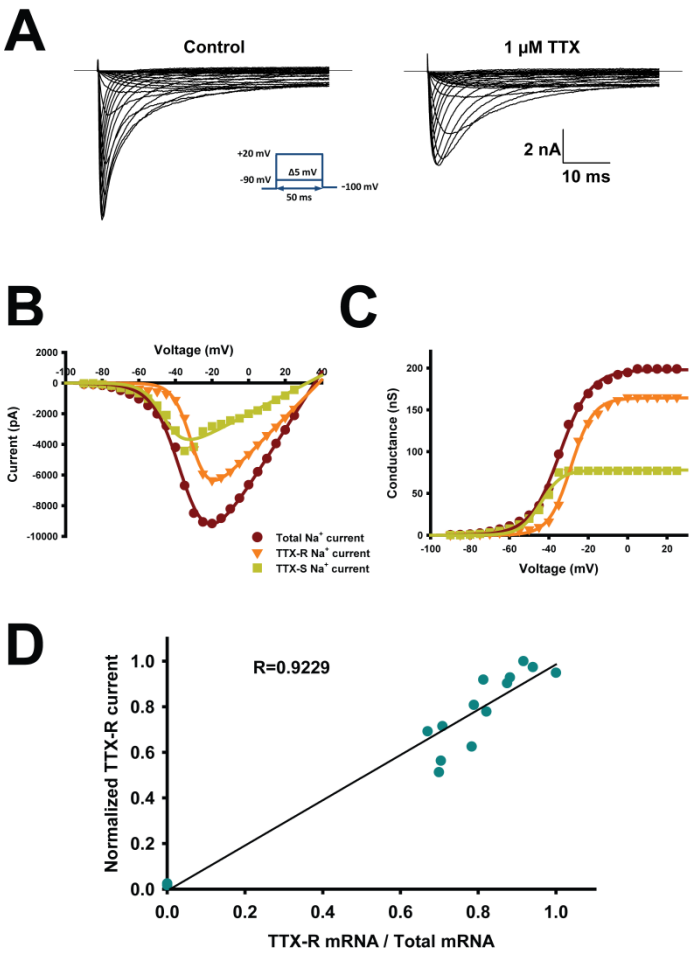

Figure 1. mRNAs reflect electrophysiological properties

(A) Representative current-traces recorded from small diameter DRG neurons (28 µm in diameter) before (right) and after (left) the addition of 1 µM TTX. The protocol is shown in the inset. **(B)** Example of current-voltage (I-V) relationships obtained from the small diameter DRG neuron shown in (A). The dark red trace is the total current recorded under control conditions, the orange trace is the total TTX-R current recorded in presence of 1 µM TTX, and the green trace is the TTX-S current obtained by subtracting the TTX-R Na_v current (orange) from the total Na_v current (dark red). I-V are fitted using a Hodgkin–Huxley-like equation: $f=G_{max}*(V-V_{rev})/(1+\exp((V-V_{1/2})/k))$, where G_{max} is the maximal conductance, V the potential, $V_{1/2}$ is the voltage at which half of the channels are in the open state, V_{rev} is the reversal potential, and k is the slope factor. **(C)** Activation curves obtained from B illustrating the conductance of total Na_v current (dark red), TTX-R current (orange) and TTX-S current (green). The conductance was calculated using the following equation: $G_{Na} = I_{Na}/(V_m - V_{rev})$, where G_{Na} is the conductance, I_{Na} is the peak current for the test potential V_m, and V_{rev} is the reversal potential estimated from the current-voltage curve. **(D)** Correlation of normalized TTX-R Na_v currents to normalized mRNA coding for TTX-R channels ($Na_v1.8+Na_v1.9/(Na_v1.7+Na_v1.8+Na_v1.9)$). Currents were normalized to the maximal current. n=17 from 8 animals.

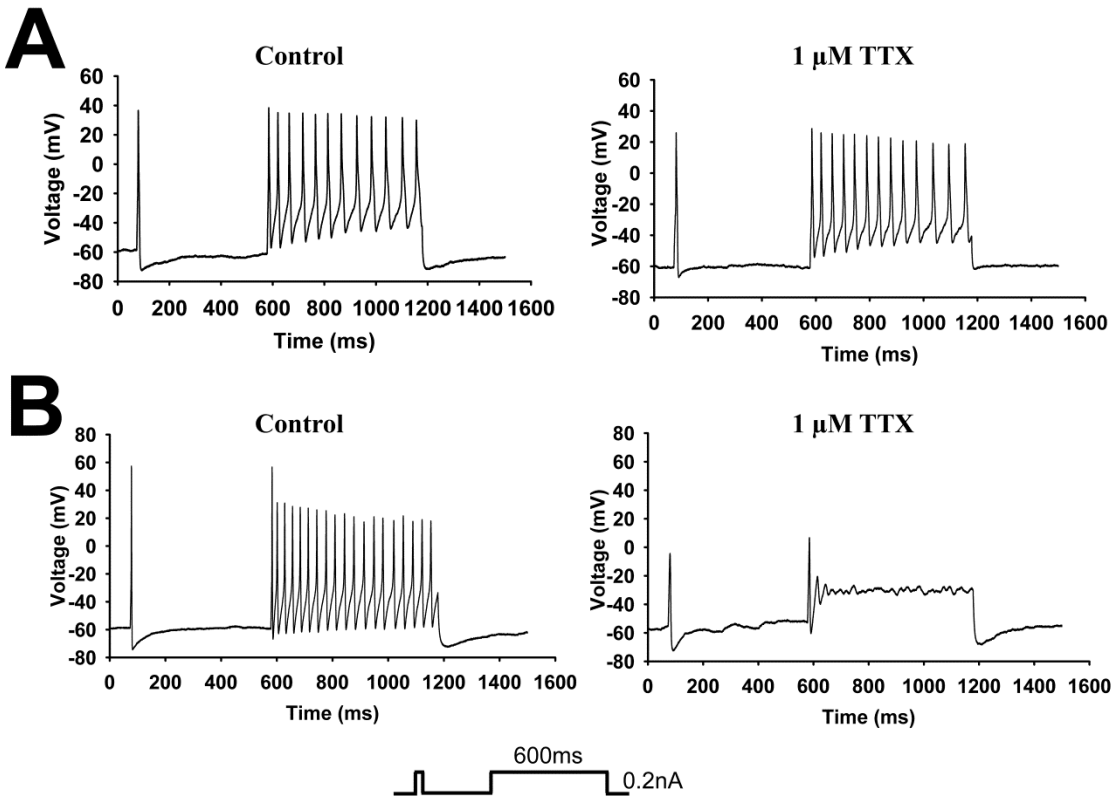

Figure 2. Current-clamp analysis

(A) Examples of AP firing (see protocol in inset) recorded from a 27-μm-diameter TTX-R neuron. The left panel shows the recording of AP firing before the addition of TTX, and the right panel shows the recording of AP firing by the same neuron after the addition of 1 μM TTX. **(B)** Examples of AP firing recorded from a 30-μm-diameter TTX-S neuron. The left panel shows the recording of AP firing before the addition of TTX, and the right panel show the recording of AP firing by the same neuron after the addition of 1 μM TTX.

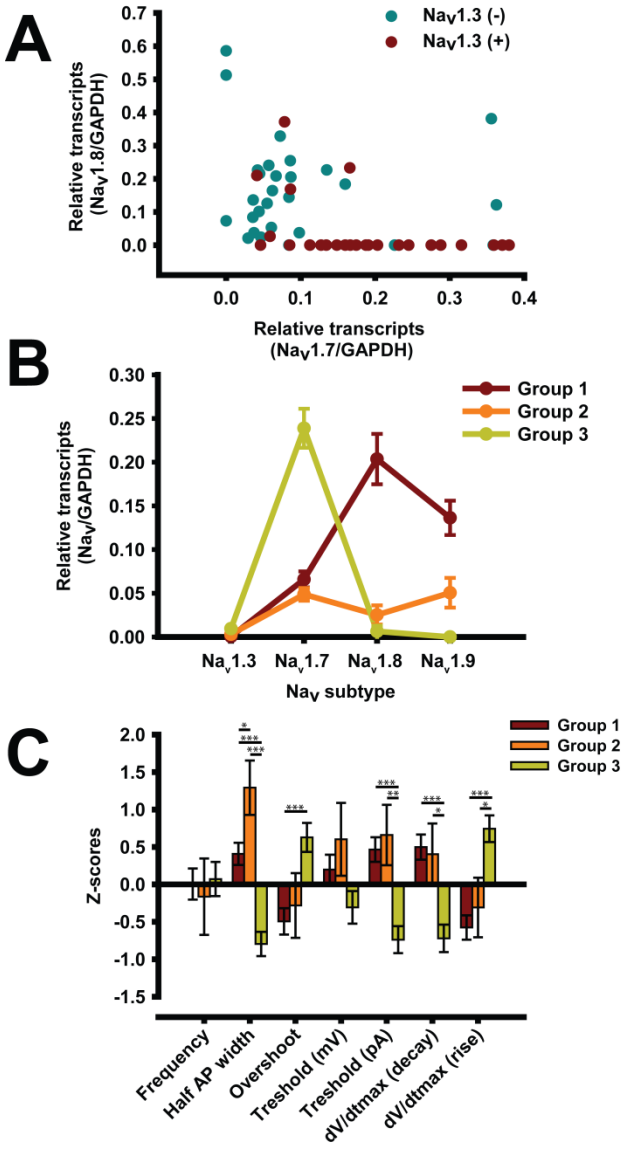

Figure 3. Cluster analysis

(A) Graphical representation of the distribution of Na_v mRNA as a function of the presence of $Na_v1.3$ mRNA. **(B)** Cluster analyses of mRNA from single DRG neurons revealed three profiles that represent 49%, 8%, and 43% of all the small diameter DRG neurons tested (<30 µm). **(C)** Electrophysiological characterization of the three profiles expressed as z-scores ± SEM. Neurons are recorded without TTX. z-scores=(x-mean)/SD; * p< 0.05; ** p< 0.01;*** p<0.001, n=49 from 16 animals.

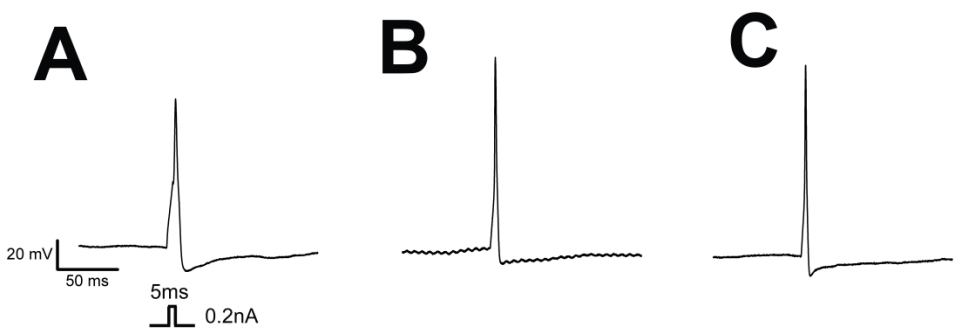

Figure 4. Action potential properties of distinct groups

(A) Example of single AP firing elicited from a 5 ms pulse recorded from a neuron of the first group expressing principally TTX-R Na_v channel. **(B)** Example of single AP firing elicited from a 5 ms pulse recorded from a neuron of the second group, expressing a combination of TTX-S and TTX-R Na_v channel. **(C)** Example of single AP firing elicited from a 5 ms pulse recorded from a neuron of the third group, expressing principally TTX-S Na_v channel. Protocol is shown in inset.

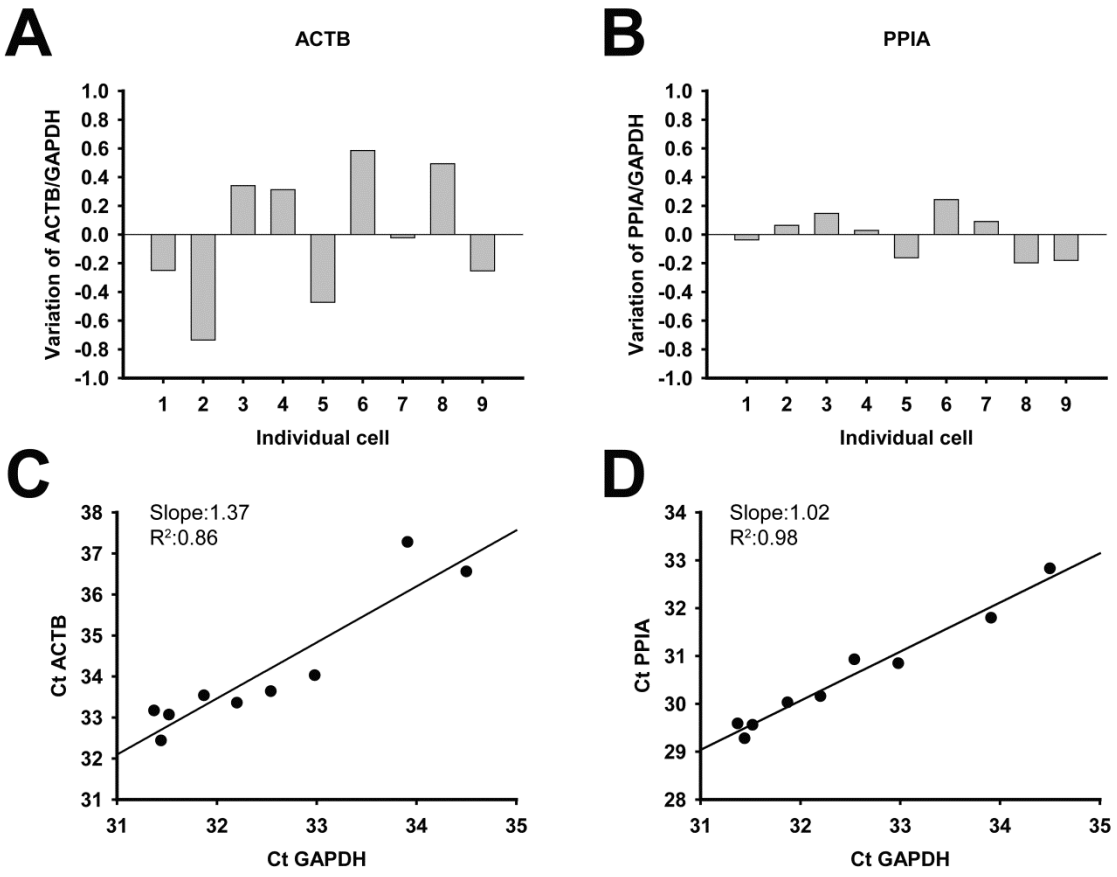

Supplement figure 1. Validation of reference genes

(A) Cell-to-cell variations in the C_t value of the ACTB/GAPDH ratio. The Y axis represents the variation: (x-mean)/mean. **(B)** Cell-to-cell variations in C_t value of the PPIA/GAPDH ratio. The Y axis represents the variation: (x-mean)/mean. (**C)** Conservation of the quantification when the C_t value changes. The X axis represents the C_t value of GAPDH in a single cell, and the Y axis represents the C_t value of ACTB in the same cell. **(D)** Conservation of the quantification when the C_t value changes. The X axis represents the C_t value of GAPDH in a single cell and the Y axis represents the C_t value of PPIA in the same cell. (n=9)

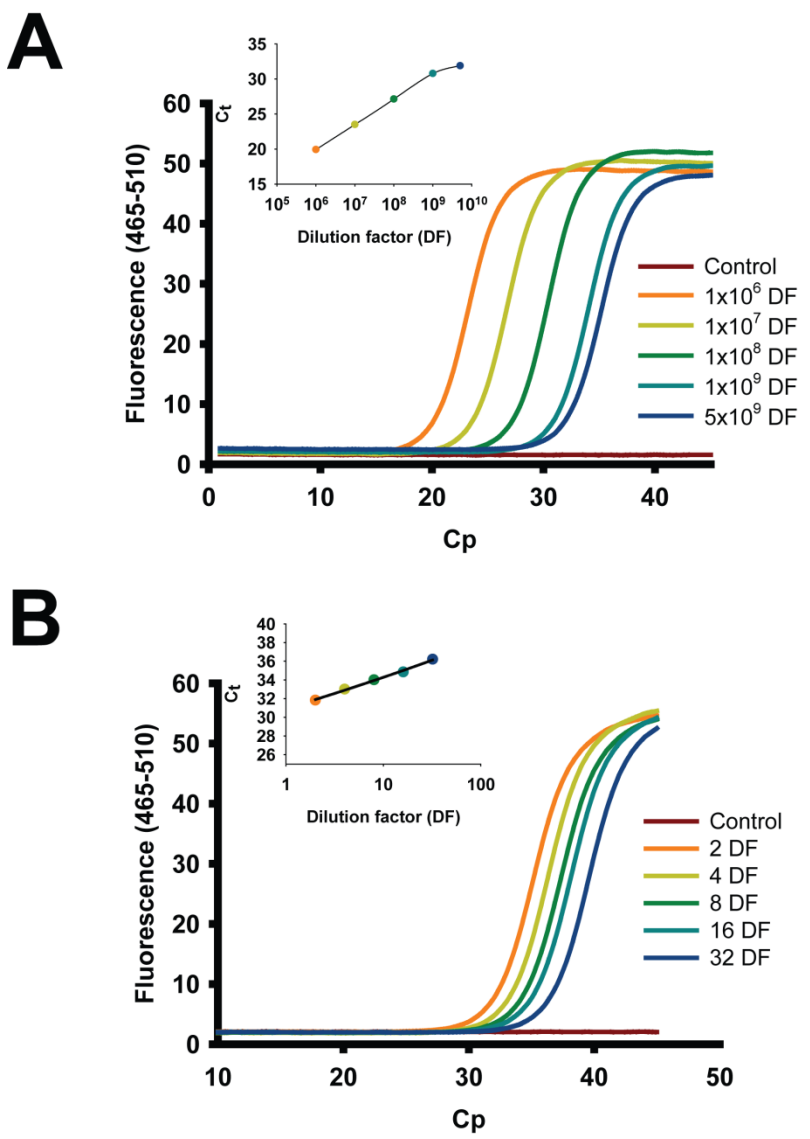

Supplement figure 2. qPCR validation and quantification

(A) Example of an amplification curve of serial 1:9 dilutions of GAPDH used to calculate the efficiency. The inset is the linear plot of the Cp values calculated from the dilutions and shows that the efficiency is conserved for low copy numbers (efficiency 1.90) Efficiency is calculated using the following function: E = 10^[1/slope]; when C_t is plotted against log(dilution). DF: Dilution factor. **(B)** Example of an amplification plot of serial 1:1 dilutions of GAPDH from a single cell RT-qPCR. The inset is the linear plot of the Cp values calculated from the serial dilutions of a single cell and shows that the efficiency is conserved up to a 1:32 dilution (efficiency 1.98).

Chapitre 3

Modulation of peripheral Na+ channels and neuronal firing by n-butyl-p-aminobenzoate

Eur. J. Pharmacol. 2014

Modulation of peripheral Na^+ channels and neuronal firing by n-butyl-p-aminobenzoate

[a]Olivier Thériault, [a]Hugo Poulin, [b,1]Adrian Sculptoreanu, [b]William C. de Groat, [c]Micheal E. O'Leary, [a]Mohamed Chahine

[a]Le Centre de recherche de l'Institut universitaire en santé mentale de Québec, Université Laval, Quebec City, QC, Canada;[b]Department of Pharmacology & Chemical Biology, University of Pittsburgh Medical School, Pittsburgh, PA, USA. [c]Department of Biomedical Sciences, Cooper Medical School of Rowan University, Camden, NJ, USA

[1] *Present address:*

Neurobiology of Learning Unit, Universita' Vita-Salute San Raffaele, Milan, Italy

Corresponding author:

Mohamed Chahine, Ph.D.

Le Centre de recherche de l'Institut universitaire en santé mentale de Québec

2601 chemin de la Canardière

Quebec City, QC, Canada G1J 2G3

Telephone: 418-663-5747 #4723

Fax: 418-663-8756

Email: mohamed.chahine@phc.ulaval.ca

Résumé

Le n-butyl-p-aminobenzoate (BAB), un anesthésique local, administré de façon péridurale chez les patients cancéreux a montré une analgésie pouvant durer plusieurs semaines. Le but de cette étude était de découvrir le mécanisme sous-jacent à l'anesthésie sans effet secondaire du BAB. Nous avons utilisé la méthode du *patch-clamp* pour enregistrer les courants Na^+ et les potentiels d'actions dans les neurones nociceptifs des ganglions dorsaux de rat. De plus, nous avons enregistré les effets du BAB sur deux canaux Na^+ des neurones sensitifs ($Na_v1.7$ et $Na_v1.8$) et d'un canal Na^+ des neurones moteurs ($Na_v1.6$) exprimés dans les cellules HEK293. Le BAB provoque une réduction de la dépolarisation induite par les potentiels d'actions, des courants induits par les trois différents canaux Na^+ exprimés dans les cellules HEK293 et le courant TTX-R des neurones de DRG. Le BAB provoque une inhibition fréquence-dépendante et un déplacement vers des potentiels hyperpolarisés de l'inactivation. De plus, le BAB accélère l'entrée en inactivation lente de Nav1.7 et Nav1.8, mais pas celle de Nav1.6. À des concentrations cliniquement pertinentes (1-100μM BAB), le BAB est un inhibiteur plus puissant des canaux Na^+ des neurones sensitifs (Nav1.7 et Nav1.8) que le canal des neurones moteurs (Nav1.6). Les effets du BAB sont similaires sur les canaux Na^+ TTX-R des neurones de ganglions dorsaux de rat et $Na_v1.8$ exprimés de façon hétérologue dans les cellules HEK293. La sélectivité du BAB chez les patients cancéreux proviendrait en partie de la plus forte affinité des canaux Na^+ exprimés dans les neurones sensitifs envers l'anesthésique que le canal $Na_v1.6$.

Abstract:

n-butyl-p-aminobenzoate (BAB), a local anesthetic, is administered epidurally in cancer patients to treat pain that is poorly controlled by other drugs that have a number of adverse effects. The purpose of the study was to unravel the mechanisms underlying the apparent selective pain suppressant effect of BAB. We used the whole-cell patch-clamp technique to record Na^+ currents and action potentials (APs) in dissociated, nociceptive dorsal root ganglion (DRG) cells from rats, two types of peripheral sensory neuron Na^+ channels ($Na_v1.7$ and $Na_v1.8$), and the motor neuron-specific Na^+ channel ($Na_v1.6$) expressed in HEK293 cells. BAB (1-100 μM) inhibited, in a concentration-dependent manner, the depolarization evoked repetitive firing in DRG cells, the three types of Na^+ current expressed in HEK293 cells, and the TTXr Na^+ current of the DRG neurons. BAB induced a use-dependent block that caused a shift of the inactivation curve in the hyperpolarizing direction. BAB enhanced the onset of slow inactivation of $Na_v1.7$ and $Na_v1.8$ currents but not of $Na_v1.6$ currents. At clinically relevant concentrations (1-100 μM), BAB is thus a more potent inhibitor of peripheral TTX-sensitive (TTXs, $Na_v1.7$) and TTX-resistant ($Na_V1.8$) Na^+ channels than of motor neuron axonal $Na_v1.6$ Na^+ channels. BAB had similar effects on the TTXr Na^+ channels of rat DRG neurons and $Na_v1.8$ channels expressed in HEK293 cells. The observed selectivity of BAB in treating cancer pain may be due to an enhanced and selective responsiveness of Na^+ channels in nociceptive neurons to this local anesthetic.

1. Introduction

The pharmacological management of chronic pain is often limited by the occurrence of side effects and the development of dependence and/or tolerance (Dworkin *et al.* 2007). However, the epidural administration of n-butyl-p-aminobenzoate (BAB) has been shown to produce long-lasting (≥4 weeks) analgesia to chronic pain patients with no significant adverse effects or loss of motor function (McCarthy *et al.* 2002; Shulman *et al.* 1998; Shulman *et al.* 2000). These observations raised the possibility that BAB inhibits subtypes of voltage gated sodium channels (VGSCs) in peripheral neurons and the spinal cord with different affinities. This idea was supported by the fact that BAB has different inhibitory effects on tetrodotoxin-resistant(TTXr) and tetrodotoxin-sensitive (TTXs) Na^+ channels in isolated rat DRG neurons (Van den Berg *et al.* 1996; Van den Berg *et al.* 1995). The interpretation of the findings from these early studies is complicated by the many Na^+ channel subtypes expressed in afferent neurons. The interpretation of the results is made even more challenging by the difficulty in determining the exact identity of Na^+ channel subtypes using pharmacological and electrophysiological methods.

Various Na^+ channel subtypes are upregulated and their subcellular distribution is changed following nerve injury or inflammation, which results in chronic pain. Hyperexcitability in primary afferents induced by noxious stimuli occurs in several models of nerve injury, inflammation, and nociceptive sensitization (Moore *et al.* 2002; Song *et al.* 2003) due to changes in the kinetics, voltage-dependence, and expression of VGSCs (Black *et al.* 2004; Moore *et al.* 2002; Gold and Flake 2005; Gold *et al.* 1998; Gold *et al.* 2003; Thakor *et al.* 2009). In addition, the inhibition of K^+ channels has also been implicated in the induction of both acute (Sculptoreanu and De Groat 2007) and chronic nociceptive sensitization (Sculptoreanu *et al.* 2005).

In the present study, we used the patch-clamp method to investigate the actions of BAB on the properties of sensory neuron Na^+ channel subtypes, TTXs $Na_v1.7$, TTXr $Na_v1.8$, and the motor neuron axonal subtype $Na_v1.6$ stably

transfected in HEK293 cells. We compared the effects on these channels to the effects on TTXr Na^+ channels in a select group of small to medium-sized, 20 to 35 μm in diameter, putative nociceptive DRG neurons of adult rats. We also examined the effect of BAB on the depolarization-evoked firing of the DRG neurons

We hypothesized that $Na_v1.6$ channels are less sensitive to BAB than $Na_v1.7$ and $Na_v1.8$ channels, which would account for the greater selectivity of BAB for sensory versus motor pathways, and that BAB might produce a use-dependent block that would make hyperactive neurons more sensitive to its suppressant action. An understanding of the action of BAB on Na^+ channels might provide new insights into the pathophysiological mechanisms of afferent sensitization and lead to new approaches for the treatment of neuropathic pain. The long-term and selective anesthesia induced by BAB may be due to a faster entry in the slow-inactivated state of Na^+ channels and a better selectivity to Na^+ channels expressed in sensory neurons ($Na_v1.7$ and $Na_v1.8$) than motor axons ($Na_v1.6$).

2. Materials and methods

2.1. Cell culture and cell lines

The stable cell lines were grown in Dulbecco's minimal essential medium (DMEM, Gibco BRL Life Technologies) supplemented with fetal bovine serum (FBS, 10%), L-glutamine (2 mM), penicillin (100 U/ml), streptomycin (10 mg/ml), and 75 μg/ml hygromycin (Gibco BRL Life Technologies). The cells were incubated at 37ºC in a 5% CO_2 humidified atmosphere.

To study the effect of BAB on the various Na^+ channels, we used three different cell lines that stably express $Na_v1.6$, $Na_v1.7$, or $Na_v1.8$. Briefly, to generate the cell lines, HEK293 cells were transfected with the pIRESneo3/Na_v vector using calcium phosphate method. One day after the transfection, the

cells were divided at various dilutions. On day 2, 800 µg/ml of neomycin was added. Three weeks after the transfection, individual clones were tested using the patch-clamp technique to ensure that they expressed the selected Na^+ channels. Clones that generated currents >500 pA were selected for study, and the neomycin concentration was lowered to 400 µg/ml. Two days before the recordings, the cells were transfected with pIRES/CD8/β_1 to include the regulatory subunit. Cells that bound to CD8 antibody-coated beads (Dynabeads M-450 CD8-a) were considered to express the β_1 subunit and were selected for recording.

2.2. DRG neuron culturing and dissection

Experiments were performed on male Sprague–Dawley rats purchased from Charles River Laboratories (Wilmington, MA). Animals were housed under conditions 12:12 h light–dark cycle and constant room temperature and humidity. Food and water provided *ad libitum*. All experiments were performed according to the guidelines of the Canadian Council on Animal Care and were approved by the Animal Care Committee of Laval University.

Neurons were isolated from the L4-L5 DRG of adult male rats. Briefly, freshly removed ganglia were de-sheathed and enzymatically digested at 37°C for 20 min in DMEM containing 2 mg/ml of type 4 collagenase (Worthington Biochemical Corp.). Trypsin (2.5 mg/ml, Sigma) was then added and the neurons were incubated for an additional 15 min. The ganglia were then dissociated mechanically by trituration using fire-polished Pasteur pipettes. The cell suspension was centrifuged for 5 min at 200g at room temperature. The cells were re-suspended in DMEM containing 4 mg/ml of type 2S trypsin inhibitor (Sigma), layered on 7.5% BSA in Dulbecco's phosphate buffered saline (DPBS), and centrifuged at 200g for 5 min. After removing the supernatant, the pellet containing the neurons was re-suspended in DMEM containing 10% heat-inactivated horse serum and 5% FBS. The neurons were

plated on poly-d-lysine-coated dishes and were kept in a 95% air-5% CO_2 incubator at 37°C until the patch-clamp recordings were performed 1 to 2 days later.

2.3. Whole-cell patch-clamp recording

Whole-cell Na^+ currents in HEK293 cells were recorded using an Axopatch 200B with the whole-cell configuration of the patch-clamp technique (Molecular Devices). pClamp v9.0 or later was used for the pulse stimulations and recordings (Molecular Devices). Currents were filtered at 5 kHz, digitized at 100 kHz using a Digidata 1200 series AD converter (Molecular devices), and stored on a personal computer for later offline analysis. Series resistance was compensated by 70-80%. When needed, linear leak current artifacts were removed using on-line leak subtraction. Fire-polished low-resistance electrodes (1MΩ) were pulled from 8161 glass (Corning) and were coated with Sylgard (Dow-Corning) to minimize pipette capacitance.

GigaOhm-seal recordings of Na^+ currents were obtained in DRG neurons using the whole-cell patch-clamp technique. Immediately before the recordings, the serum-containing medium was replaced with current-clamp recording solution. APs were generated by 5 ms, 50-300 pA rectangular current pulse injections followed by a 100 ms interpulse at the holding potential and then a 600 ms pulse. In general, the sequence consisted of at least two control recordings of evoked APs followed by pharmacological studies where increasing concentrations of BAB were sequentially applied prior to recording the APs. In some experiments, the time courses of the effects of TTX and BAB were monitored by repeating the above sequence at a stimulus intensity just above that required to evoke an AP.

2.4. Solutions and reagents

For the voltage-clamp recordings from HEK293 cells, the bath solution for the $Na_v1.8$ and $Na_v1.6$ current recordings contained 150 mM NaCl, 2 mM KCl, 1.5 mM $CaCl_2$, 1.0 mM $MgCl_2$, 10 mM glucose, and 10 mM HEPES. The pH was adjusted to 7.4 with 1 M NaOH. To reduce the voltage-clamp error due to the large current evoked by $Na_v1.7$, the extracellular solution was supplemented with 20 mM NaCl and 130 mM choline chloride to reduce the maximum current and increase the clamp speed. For the DRG neuron recordings, the bath solution contained 35 mM NaCl, 105 mM choline chloride, 3 mM KCl, 1 mM $CaCl_2$, 1.0 mM $MgCl_2$, 10 mM glucose, 10 mM HEPES, and 100 nM $CdCl_2$.

For the HEK293 cells, the intracellular pipette solution for $Na_v1.6$ and $Na_v1.7$ contained 35 mM NaCl, 105 mM CsF, 10 mM EGTA, and 10 mM HEPES. The pH was adjusted to pH 7.4 with 1 M CsOH. Since $Na_v1.8$ currents are small, the driving force was increased by reducing the intracellular Na^+ concentration to 5 mM (30 mM NaCl was replaced with 30 mM CsF). For the DRG neurons, the intracellular pipette solution contained 10 mM NaCl, 140 mM CsF, 1 mM EGTA, and 10 mM HEPES. The pH was adjusted to pH 7.3 with 1 M CsOH.

For the current-clamp recordings, the extracellular solution contained 154 mM NaCl, 5.6 mM KCl, 2.0 mM $CaCl_2$, 1.0 mM $MgCl_2$, 10 mM glucose, and 8.0 mM HEPES. The pH was adjusted to 7.4 with 1 M NaOH. The pipette (intracellular) solution contained 122 mM KCl, 10 mM NaCl, 1.0 mM $MgCl_2$, 1.0 mM EGTA, and 10 mM HEPES. The pH was adjusted to 7.3 with 1 M KOH.

BAB was applied by superfusion using a ValveLink8.2® perfusion system (Automate Scientific) through a 250 µM needle. Fresh stock solutions of BAB dissolved in EtOH was prepared weekly. The stock solutions contained 0.1% EtOH and the desired concentration of BAB. Due to the very low solubility of BAB in water, no concentrations over 600 µM BAB were tested. All chemicals were purchased from Sigma Aldrich.

2.5. Data analysis

The data were analyzed using a combination of pCLAMP software v10.0 (Molecular Devices), Microsoft Excel, and SigmaPlot 11.0 (Systat Software, Inc.). All P-values are two-tailed, and $P<0.05$ was considered statistically significant. Statistical values are expressed as means ± SEM. Statistical testing was carried out using a stepwise procedure depending upon the number of groups being compared. When only two means were compared, a two-tailed t-test with unequal variances was used. When more than two means were involved, a one-way analysis of variance was first carried out to obtain a global test of the null hypothesis. If the global *P*-value for the test of the null hypothesis was <0.05, we performed post-hoc comparisons between the different groups using the Holm-Sidak test (Glantz, 2005).

The conductance was calculated using the following equation: ($G_{Na} = I_{Na}/(V_m - V_{rev})$), where G_{Na} is the conductance, I_{Na} is the peak current for the test potential V_m, and V_{rev} is the reversal potential estimated from the current-voltage curve. Conductance values were then fitted to a Boltzmann equation: $I/I_{max}=1/(1+\exp((V + V_{1/2})/k))$, where I_{max} is the maximal evoked current, $V_{1/2}$ is the voltage at which half of the channels are in the open state, and k is the slope factor. Steady-state inactivation values were fitted using a similar Boltzmann equation. Slow inactivation was fitted with the sum of two exponential curves, with a fast time constant (τ_f) and a slow time constant (τ_s).

3. Results

3.1. Effect of BAB on APs in isolated rat DRG neurons

APs were recorded from cultured lumbar DRG neurons ranging from 20 to 35 μm in diameter (average of long and short axes). TTX applied at the end

of the experiments had little or no effect on firing at a holding potential of -60 mV (data not shown) (Yamane *et al.* 2007). When the resting potential was held at -60 mV, the DRG neurons fired with a mean numbers of APs of 13.0 ± 0.9 in response to a long 600 ms, 0.2 pA depolarizing pulse (Fig. 1; n = 12). The superfusion of 1 or 10 μM BAB did not decrease the AP (Fig. 2A). The superfusion of 100 μM BAB decreased the AP generated by a 0.2 pA pulse from 13.0 ± 0.9 to 9.0 ± 1.7. The first overshoot (OS) (Fig. 2C) was not significantly different. The superfusion of 10 μM BAB significantly reduced the maximum rate of rise (Fig. 2D, $P<0.05$). The OS decreased quickly in a dose-dependent manner in the presence of BAB (Fig. 2E). The superfusion of 1 μM BAB decreased the OS of the last evoked AP by 12.5 mV from 33.9 ± 6.1 mV to 21.4 ± 5.4 mV. The superfusion of 100 μM BAB led to a greater decrease in the OS (28.1 mV). 100 μM BAB increase the duration of the AP from 1.43 ms to 1.52 ms (Fig. 2F).

3.2. Tonic block by BAB of Na^+ channels expressed in HEK293 cells

The tonic effect of BAB on heterologously expressed Na^+ channels in HEK293 cells was tested using 40 ms depolarizing pulses at a voltage that evoked the maximum current. The voltage was different for each Na^+ channel subtype (Fig. 3). $Na_v1.6$, $Na_v1.7$, and $Na_v1.8$ were tested at -20 mV, -40 mV, and +10mV, respectively. Representative current traces from control experiments, 400 μM BAB superfusion and washout are shown in Figure 3A-C. The inset shows the holding potential and test pulse in each experiment. $Na_v1.6$ and $Na_v1.7$ heterologously expressed in HEK293 cells displayed a similar block in the presence of 100 μM BAB (15 ± 2% for $Na_v1.6$, 18 ± 5% for $Na_v1.7$), while $Na_v1.8$ displayed the highest degree of inhibition (30 ± 4% block), which was significantly different from the inhibition of $Na_v1.6$ ($P<0.05$) and $Na_v1.7$ ($P<0.01$). In the presence of 600 μM BAB, $Na_v1.8$ also displayed a significantly greater inhibition (80 ± 4% block) than that of $Na_v1.6$ (42 ± 3%) and $Na_v1.7$ (49 ± 3%) ($P<0.01$).

3.3. Effect of BAB on the activation of heterologously expressed Na^+ channels

Figure 4A,B,C shows the effect of BAB on the voltage-dependence of activation of $Na_v1.6$, $Na_v1.7$, and $Na_v1.8$, respectively. Values are plotted as relative membrane conductances as explained in Materials and methods. The different biophysical properties of the Na^+ channel subtypes meant that the voltage protocols had to be adjusted for each subtype. Briefly, short 50 ms depolarizing pulse were applied in increments starting from a holding potential at -140 mV. Pulses ranging from -80 mV to +90 mV in 5 mV increments were used for $Na_v1.6$ (Fig. 4A) and $Na_v1.8$ (Fig. 4C) and from -90 mV to +15 mV for $Na_v1.7$ (Fig. 4B). The protocols are shown in the insets. BAB did not alter the voltage dependence of the Na^+ channels (see Table 1).

3.4. Effect of BAB on fast inactivation

The voltage-dependences of $Na_v1.6$, $Na_v1.7$, and $Na_v1.8$ were determined using the protocols shown in the insets in Figure 4D-F. The values were then fitted with a Boltzmann equation. For $Na_v1.6$, a conditioning pulse was applied from -150 mV to -5 mV in 5 mV increments followed by a test pulse to -20 mV. BAB (100 µM) caused a 17.8 mV hyperpolarizing shift in the $V_{1/2}$ from -71.5 ± 5.1 mV in the control condition to -89.3 ± 2.6 mV after the superfusion of BAB (Fig. 4D). The slope factor was also significantly shifted from 5.1 ± 0.2 to 6.1 ± 0.4. For $Na_v1.7$, conditioning pulses were applied from -150 mV to -35 mV, and currents were determined with a test pulse to -40 mV (Fig. 4E). Figure 4F shows the inactivation curve of $Na_v1.8$ determined with a conditioning pulse from -140 mV to +5 mV and a test pulse to 0 mV. $Na_v1.7$ and $Na_v1.8$ also exhibited significant hyperpolarizing shifts of 17.1 mV ($P<0.01$) and 9.6 mV ($P<0.05$), respectively. The effects of BAB on the parameters of inactivation are summarized in Table 1.

3.5. Effect of BAB on slow inactivation

We previously showed that the local anesthetic lidocaine differentially modulates the slow inactivation of $Na_v1.7$ and $Na_v1.8$ (Chevrier *et al.* 2004). In the present study, we tested the effect of BAB on slow inactivation using a similar protocol, which consisted of a conditioning pulse of variable duration (1 ms to 10 s) followed by a 10 ms pulse to allow for recovery from fast inactivation and then a 40 ms test pulse. The conditioning pulse and the test pulse were to -10 mV for $Na_v1.6$, -20 mV for $Na_v1.7$, and +15 mV for $Na_v1.8$. BAB did not affect the time constants of $Na_v1.6$ slow inactivation (Fig. 5A). The slow inactivation curve of $Na_v1.7$ was much steeper in the presence of 100 μM BAB, which was mainly a result of a marked (50%) reduction in the slow time constant (τ_s was 7428 ± 1006 ms in the control and 3658 ± 264 ms after the superfusion of 100 μM BAB) (Fig. 5B). A similar effect was observed for $Na_v1.8$ (Fig. 5C), which was also due to an acceleration of the slow time constant, with little or no change in the rapid time constant (Table 1).

3.6. Frequency-dependent block

Stimulation frequencies up to 20 Hz were used to test the frequency-dependent block of Na^+ channels by BAB (100 μM). Fifty stimulus pulses were applied at the voltage that elicited the maximum current for each channel subtype (-20 mV for $Na_v1.6$, -40 mV for $Na_v1.7$, and +10 mV for $Na_v1.8$). Currents were normalized to the first pulse in the sequence. $Na_v1.6$ currents exhibited a slight frequency-dependent block in the presence of BAB. At 20 Hz there was a further reduction in the normalized current (Fig. 6A, 7.5%, $P<0.05$). $Na_v1.7$ displayed the highest sensitivity to the frequency-dependent block (Fig. 6B, a significant 7% reduction at 10 Hz ($P<0.01$) and a 20% reduction at 20 Hz ($P<0.01$)). The frequency-dependent block of $Na_v1.8$ was similar to that of $Na_v1.6$ (Fig. 6C, 7.4% at 20 Hz).

3.7. Effect of BAB on the TTXr Na+ channels of rat DRG neurons

The tonic block of TTXr Na^+ currents was measured using a 50 ms test pulse to 0 mV that was repeated every 10 s until the current reached a steady-state which occurs between 3 to 5 minutes. BAB was applied sequentially at concentrations of 1, 10, and 100 μM, and the steady-state inhibition at each concentration was compared to the control current before applying BAB (Fig. 7A, n = 10). The inhibition of the TTXr Na^+ currents of DRG neurons was greater (48 ± 6%, Fig. 7A) than the inhibition (31 ± 4%, Fig. 3D) of $Na_v1.8$ currents in HEK293 cells.

As observed with HEK293 cells expressing $Na_v1.8$, 100 μM BAB had no effect on the voltage-dependence of activation of TTXr Na^+ currents (Fig. 7B). However, 100 μM BAB provoked a 16 mV ($P<0.001$) hyperpolarized shift of the voltage-dependence of inactivation of the TTXr Na^+ current of DRG neurons compared to 10 mV in transfected cells (Table 1).

The frequency-dependent block of the TTXr Na^+ current of DRG neurons was studied by adjusting the frequency of stimulation from 2 to 20 Hz in the absence or presence of 100 μM BAB (Fig. 7 C). At 10 Hz, there was a 5% increase in the frequency-dependent inhibition of the TTXr Na^+ current of DRG neurons ($p>0.01$), while at 20 Hz, the inhibition increased to 9%.

4. Discussion

The experiments described in the present study were designed to shed light on the mechanisms underlying the prominent analgesic effect of epidural BAB that occurs with relatively few adverse effects. We observed substantial differences in the BAB sensitivity of the three types of currents generated by Na^+ channels expressed in HEK293 cells. TTXr Na^+ currents ($Na_v1.8$) in these neurons were also sensitive to BAB at similar concentrations. Currents generated by TTXr $Na_v1.8$ channels expressed in HEK293 cells were also more sensitive to BAB

than currents generated by TTXs $Na_v1.6$ and $Na_v1.7$ channels, although the heterologously expressed channels were less sensitive to BAB than native channels. An analysis of the frequency and time dependent inactivation of currents also revealed differences in the effect of BAB on the different channels. These results suggested that the clinical usefulness of epidural BAB in treating pain may be related to the targeting of specific subtypes of Na^+ channels in sensitized, small diameter, nociceptive afferent neurons.

The clinical efficacy occurs with a series of 4 epidural injection of 5% BAB in suspension (Shulman *et al.* 1998). A study on the diffusion of few local anesthetics through the human dura-arachnoid supports the hypothesis that the selective action of BAB suspension can be attributed to the spatial confinement into the epidural space (Grouls *et al.* 2000). The prolonged analgesia produced by BAB can in large part be attributed to the physiochemical properties of the drug (water solubility, partition coefficient) that enable its formulation as a hydrophobic suspension. After injection into the epidural space BAB slowly leaches out of suspension onto the adjacent nerve roots thereby producing a selective inhibition of sensory nerve fibers.

In DRG neurons, concentrations of BAB as low as 1 μM elicited prominent changes in the OS of the last AP evoked by depolarizing current pulses and in the tonic block. The effect in the OS of the last AP evoked is most likely because more Na^+ channels enter the slow inactivated state in the presence of BAB. At least part of this effect of BAB on nociceptive neuron excitability may be due to its effect on TTXr Na^+ channels. Indeed, BAB produced a concentration-dependent steady-state inhibition and a frequency-dependent inhibition of TTXr Na^+ currents and a hyperpolarizing shift in the inactivation curve of the TTXr Na^+ currents in these neurons. These effects occurred with no change in the activation curve. Furthermore, we showed that the effects of BAB are completely reversible within a minute after the washout on sodium channels expressed in HEK293 cells.

However, it has been reported that BAB affects multiple ion channels, including a block of potassium channels (Beekwilder *et al.* 2003; Winkelman *et al.* 2005), which suggests that it may depolarize the resting membrane potential and lead to greater Na^+ channel inactivation (slow and fast). Calcium channels (Beekwilder *et al.* 2005) and TRP channels (Bang *et al.* 2012) have also been reported to be blocked by BAB. It is thus possible that the effect on AP parameters results from a combination of effects on Na^+ and other ion channels.

To compare the effects of BAB on TTXr and TTXs Na+ channels, we expressed the channels in HEK293 cells. In the absence of BAB, we observed significant differences in the biophysical properties of native TTXr Na^+ currents (presumed to reflect primarily $Na_v1.8$) recorded in DRG neurons and the $Na_v1.8$ currents recorded in HEK293 cells. The native TTXr Na^+ currents exhibited a significant 8 mV hyperpolarized shift in activation parameters and an even greater 20 mV depolarizing shift in inactivation parameters. We also observed a significant difference in the frequency dependent block above 10 Hz between TTXr Na^+ currents of DRG neurons and $Na_v1.8$ transiently expressed in HEK293 cells. The reason for the differences between heterologously expressed Na^+ channels and DRG Na^+ channels is uncertain, but may be due to other regulatory processes in native tissue but absent in HEK293 cells. However, BAB had a similar effect on $Na_v1.8$ channels in DRG neurons and $Na_v1.8$ channels heterologously expressed in HEK293 cells despite the differences in basal biophysical properties. The shift in inactivation parameters and the frequency-dependent inhibition caused by BAB was similar for native TTXr currents and $Na_v1.8$ currents in HEK293 cells.

A difference in the affinity of BAB for the different Na^+ channel subtypes does not entirely explain why BAB causes selective analgesia without reducing motor function or touch perception. We only observed a small tonic block of the total Na^+ current in transfected cells with 100 μM BAB (18% $Na_v1.7$, 31% $Na_v1.8$, and 15% $Na_v1.6$). Since the affinity is low and the inhibition is probably

partial, it was not possible to extrapolate these data to an IC_{50} for BAB or explain the clinical efficacy of BAB based on differences in the tonic blocks of $Na_v1.8$, $Na_v1.6$, and $Na_v1.7$ channels stably expressed in HEK293 cells. We thus investigated the modulation by BAB of the activation and inactivation of the channels. BAB did not affect the activation parameters, but shifted inactivation to hyperpolarized values. Similar effects have been observed with other local anesthetics (Chevrier *et al.* 2004; Scholz 2002). This means that more Na^+ channels are likely to be in the inactivated state and will not open when the membrane is depolarized. However, there was no significant difference in the effect of BAB on the inactivation of the three types of Na^+ channels, and this cannot thus account for the selective action of BAB on pain pathways.

We observed a small reduction in frequency-dependent inhibition. The higher sensitivity to frequency-dependent inhibition of $Na_v1.7$ in the presence of BAB probably contributes to reducing firing in sensory neurons. This channel is mainly expressed in small C fiber sensory neurons and is thought to play a major role in pain transmission (Cox *et al.* 2006).

The role of slow inactivation in nociceptive fibers is relatively well known and appears to be important in neuronal excitability. A mutation in $Na_v1.7$ that reduces the kinetics of slow inactivation has been reported to exacerbate pain in patients with small fiber neuropathy (Han *et al.* 2012). Furthermore, the entry of $Na_v1.8$ into slow inactivation reduces firing in small diameter DRG neurons (Blair and Bean 2003). It has also been reported that molecules that stabilize Na^+ channels in the slow inactivated state attenuate neuropathic pain (Hildebrand *et al.* 2011b). It is thus likely that the increase in the onset of slow inactivation of $Na_v1.7$ and $Na_v1.8$ in the presence of BAB contributes to the anesthesia induced by this drug.

$Na_v1.6$ is thought to be a major component of the motor axon AP. It is also preferentially expressed in sensory A-fibers and is localized at the nodes of Ranvier, dendrites, and synapses (Fukuoka *et al.* 2008; Caldwell *et al.* 2000).

$Na_v1.6$ has a significantly lower affinity than $Na_v1.8$ for BAB and the onset of slow inactivation of $Na_v1.6$ is not affected at all by BAB, both of which might, in part, explain its selectivity.

In summary, we propose that the mechanism by which BAB induces long-term anesthesia may include an effect on the slow inactivation of Na^+ channels. The selectivity of the anesthetic may, in part, be due to more pronounced effects on channels expressed in small-medium diameter nociceptive sensory neurons ($Na_v1.7$ and $Na_v1.8$) than on channels expressed in large diameter non-nociceptive sensory neurons and motor axons ($Na_v1.6$).

Acknowledgements

This work was supported by grants from the Canadian Institutes of Health Research (CIHR, MT-13181); the Heart and Stroke Foundation of Quebec (HSFQ).

References

Bang,S., Yang,T.J., Yoo,S., Heo,T.H., Hwang,S.W., 2012. Inhibition of sensory neuronal TRPs contributes to anti-nociception by butamben. Neurosci.Lett. 506, 297-302.

Beekwilder,J.P., O'Leary,M.E., van den Broek,L.P., van Kempen,G.T., Ypey,D.L., Van den Berg,R.J., 2003. Kv1.1 channels of dorsal root ganglion neurons are inhibited by n-butyl-p-aminobenzoate, a promising anesthetic for the treatment of chronic pain. J.Pharmacol.Exp.Ther. 304, 531-538.

Beekwilder,J.P., Winkelman,D.L., van Kempen,G.T., Van den Berg,R.J., Ypey,D.L., 2005. The block of total and N-type calcium conductance in mouse sensory neurons by the local anesthetic n-butyl-p-aminobenzoate. Anesth.Analg. 100, 1674-1679.

Black,J.A., Liu,S., Tanaka,M., Cummins,T.R., Waxman,S.G., 2004. Changes in the expression of tetrodotoxin-sensitive sodium channels within dorsal root ganglia neurons in inflammatory pain. Pain 108, 237-247.

Blair,N.T., Bean,B.P., 2003. Role of tetrodotoxin-resistant Na+ current slow inactivation in adaptation of action potential firing in small-diameter dorsal root ganglion neurons. J.Neurosci. 23, 10338-10350.

Caldwell,J.H., Schaller,K.L., Lasher,R.S., Peles,E., Levinson,S.R., 2000. Sodium channel Na(v)1.6 is localized at nodes of Ranvier, dendrites, and synapses. Proc.Natl.Acad.Sci.U.S.A 97, 5616-5620.

Chevrier,P., Vijayaragavan,K., Chahine,M., 2004. Differential modulation of Nav1.7 and Nav1.8 peripheral nerve sodium channels by the local anesthetic lidocaine. Br.J.Pharmacol. 142, 576-584.

Cox,J.J., Reimann,F., Nicholas,A.K., Thornton,G., Roberts,E., Springell,K., Karbani,G., Jafri,H., Mannan,J., Raashid,Y., Al-Gazali,L., Hamamy,H., Valente,E.M., Gorman,S., Williams,R., McHale,D.P., Wood,J.N., Gribble,F.M.,

Woods,C.G., 2006. An SCN9A channelopathy causes congenital inability to experience pain. Nature 444, 894-898.

Dworkin,R.H., O'Connor,A.B., Backonja,M., Farrar,J.T., Finnerup,N.B., Jensen,T.S., Kalso,E.A., Loeser,J.D., Miaskowski,C., Nurmikko,T.J., Portenoy,R.K., Rice,A.S., Stacey,B.R., Treede,R.D., Turk,D.C., Wallace,M.S., 2007. Pharmacologic management of neuropathic pain: evidence-based recommendations. Pain 132, 237-251.

Fukuoka,T., Kobayashi,K., Yamanaka,H., Obata,K., Dai,Y., Noguchi,K., 2008. Comparative study of the distribution of the alpha-subunits of voltage-gated sodium channels in normal and axotomized rat dorsal root ganglion neurons. J.Comp Neurol. 510, 188-206.

Gold,M.S., Flake,N.M., 2005. Inflammation-mediated hyperexcitability of sensory neurons. Neurosignals. 14, 147-157.

Gold,M.S., Levine,J.D., Correa,A.M., 1998. Modulation of TTX-R INa by PKC and PKA and their role in PGE2-induced sensitization of rat sensory neurons in vitro. J.Neurosci. 18, 10345-10355.

Gold,M.S., Weinreich,D., Kim,C.S., Wang,R., Treanor,J., Porreca,F., Lai,J., 2003. Redistribution of Nav1.8 in uninjured axons enables neuropathic pain. J.Neurosci. 23, 158-166.

Grouls,R., Korsten,E., Ackerman,E., Hellebrekers,L., van,Z.A., Breimer,D., 2000. Diffusion of n-butyl-p-aminobenzoate (BAB), lidocaine and bupivacaine through the human dura-arachnoid mater in vitro. Eur.J.Pharm.Sci. 12, 125-131.

Han,C., Hoeijmakers,J.G., Ahn,H.S., Zhao,P., Shah,P., Lauria,G., Gerrits,M.M., te Morsche,R.H., Dib-Hajj,S.D., Drenth,J.P., Faber,C.G., Merkies,I.S., Waxman,S.G., 2012. Nav1.7-related small fiber neuropathy: impaired slow-inactivation and DRG neuron hyperexcitability. Neurology 78, 1635-1643.

Hildebrand,M.E., Smith,P.L., Bladen,C., Eduljee,C., Xie,J.Y., Chen,L., Fee-Maki,M., Doering,C.J., Mezeyova,J., Zhu,Y., Belardetti,F., Pajouhesh,H., Parker,D., Arneric,S.P., Parmar,M., Porreca,F., Tringham,E., Zamponi,G.W., Snutch,T.P., 2011. A novel slow-inactivation-specific ion channel modulator attenuates neuropathic pain. Pain 152, 833-843.

McCarthy,R.J., Kerns,J.M., Nath,H.A., Shulman,M., Ivankovich,A.D., 2002. The antinociceptive and histologic effect of sciatic nerve blocks with 5% butamben suspension in rats. Anesth.Analg. 94, 711-716.

Moore,B.A., Stewart,T.M., Hill,C., Vanner,S.J., 2002. TNBS ileitis evokes hyperexcitability and changes in ionic membrane properties of nociceptive DRG neurons. Am.J.Physiol Gastrointest.Liver Physiol 282, G1045-G1051.

Scholz,A., 2002. Mechanisms of (local) anaesthetics on voltage-gated sodium and other ion channels. Br.J.Anaesth. 89, 52-61.

Sculptoreanu,A., De Groat,W.C., 2007. Neurokinins enhance excitability in capsaicin-responsive DRG neurons. Exp.Neurol. 205, 92-100.

Sculptoreanu,A., De Groat,W.C., Buffington,C.A., Birder,L.A., 2005. Abnormal excitability in capsaicin-responsive DRG neurons from cats with feline interstitial cystitis. Exp.Neurol. 193, 437-443.

Shulman,M., Harris,J.E., Lubenow,T.R., Nath,H.A., Ivankovich,A.D., 2000. Comparison of epidural butamben to celiac plexus neurolytic block for the treatment of the pain of pancreatic cancer. Clin.J.Pain 16, 304-309.

Shulman,M., Lubenow,T.R., Nath,H.A., Blazek,W., McCarthy,R.J., Ivankovich,A.D., 1998. Nerve blocks with 5% butamben suspension for the treatment of chronic pain syndromes. Reg Anesth.Pain Med. 23, 395-401.

Song,X.J., Zhang,J.M., Hu,S.J., LaMotte,R.H., 2003. Somata of nerve-injured sensory neurons exhibit enhanced responses to inflammatory mediators. Pain 104, 701-709.

Thakor,D.K., Lin,A., Matsuka,Y., Meyer,E.M., Ruangsri,S., Nishimura,I., Spigelman,I., 2009. Increased peripheral nerve excitability and local NaV1.8 mRNA up-regulation in painful neuropathy. Mol.Pain 5, 14.

Van den Berg,R.J., Van Soest,P.F., Wang,Z., Grouls,R.J., Korsten,H.H., 1995. The local anesthetic n-butyl-p-aminobenzoate selectively affects inactivation of fast sodium currents in cultured rat sensory neurons. Anesthesiology 82, 1463-1473.

Van den Berg,R.J., Wang,Z., Grouls,R.J.E., Korsten,H.H.M., 1996. The local anesthetic, n-butyl-p-aminobenzoate, reduces rat sensory neuron excitability by differential actions on fast and slow Na+ current components. Eur.J.Pharmacol. 316, 87-95.

Winkelman,D.L., Beck,C.L., Ypey,D.L., O'Leary,M.E., 2005. Inhibition of the A-type K+ channels of dorsal root ganglion neurons by the long-duration anesthetic butamben. J.Pharmacol.Exp.Ther. 314, 1177-1186.

Yamane,H., De Groat,W.C., Sculptoreanu,A., 2007. Effects of ralfinamide, a Na+ channel blocker, on firing properties of nociceptive dorsal root ganglion neurons of adult rats. Exp.Neurol. 208, 63-72.

Table 1
Effects of BAB on fast activation, inactivation and slow inactivation parameters.

	$Na_v1.6$ (HEK293)		$Na_v1.7$ (HEK293)		$Na_v1.8$ (HEK293)		(DRG)	
	Control	100 μM BAB	Control	100 μM BAB	Control	100 μM BAB	Control	100 μM BAB
Activation								
$V_{1/2}$ (mV)	−35.8 ± 1.4	−38.4 ± 1.8(NS)	−48.1 ± 1.5	−48.5 ± 3.2(NS)	−21.6 ± 1.3	−16.2 ± 3.1(NS)	−29.0 ± 1.1	−24.1 ± 5.1(NS)
k_v	−6.1 ± 0.3	−6.3 ± 0.4(NS)	−5.5 ± 0.3	−6.0 ± 0.3(NS)	−12.0 ± 0.4	−13.0 ± 0.8(NS)	−5.0 ± 0.5	−6.4 ± 0.8(NS)
n	8	7	10	4	31	7	6	5
Inactivation								
$V_{1/2}$ (mV)	−71.5 ± 5.1	−89.3 ± 2.6[b]	−92.8 ± 2.0	−109.9 ± 2.4[b]	−58.5 ± 1.6	−68.1 ± 3.8[a]	−38.8 ± 0.9	−54.7 ± 2.5[b]
k_v	5.1 ± 0.2	6.1 ± 0.4[b]	7.4 ± 0.8	7.0 ± 0.4(NS)	7.9 ± 0.7	7.8 ± 0.7(NS)	4.3 ± 0.2	4.5 ± 0.2(NS)
n	8	6	10	4	10	7	7	9
Slow-inactivation								
τ_f (ms)	2069 ± 683	871 ± 285(NS)	70.3 ± 26.6	76.1 ± 5.5(NS)	248 ± 85	173 ± 15(NS)	–	–
τ_s (s)	18.8 ± 3.5	19.1 ± 5.2(NS)	7.4 ± 1.0	3.6 ± 0.26[b]	43.6 ± 6.1	29.2 ± 3.4[a]	–	–
n	4	5	4	6	5	7	–	–

τ_f = fast inactivation time constant; τ_s = slow inactivation time constant; n = number of experiments; NS: not significant.

[a] $P < 0.05$.

[b] $P < 0.01$.

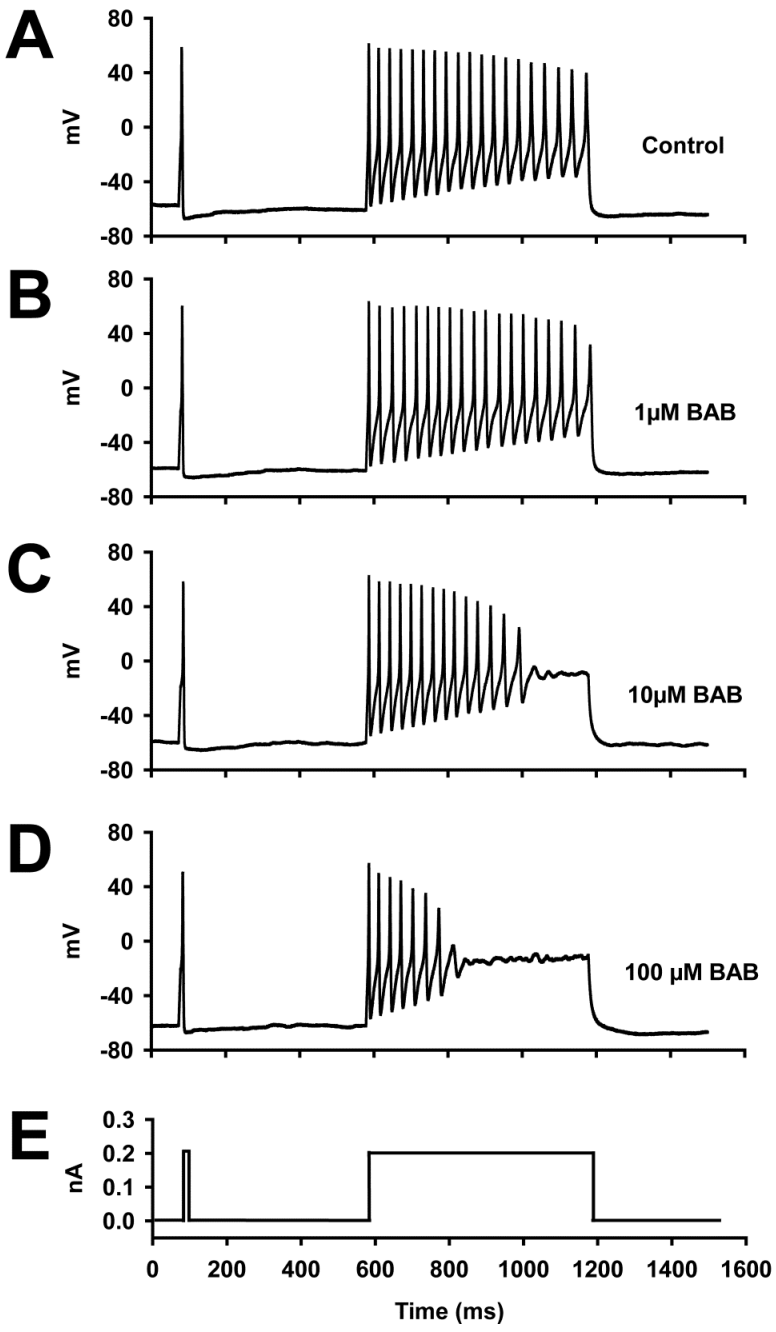

Fig. 1. *Effect of BAB on firing*.

Representative AP traces of firing triggered by a 600 ms depolarizing pulse (control) (A), and in the presence of 1 μM BAB (B), 10 μM BAB (C), and 100 μM BAB (D). (E) Shows the current-clamp protocol used to generate single APs and the long spike trains in A to D.

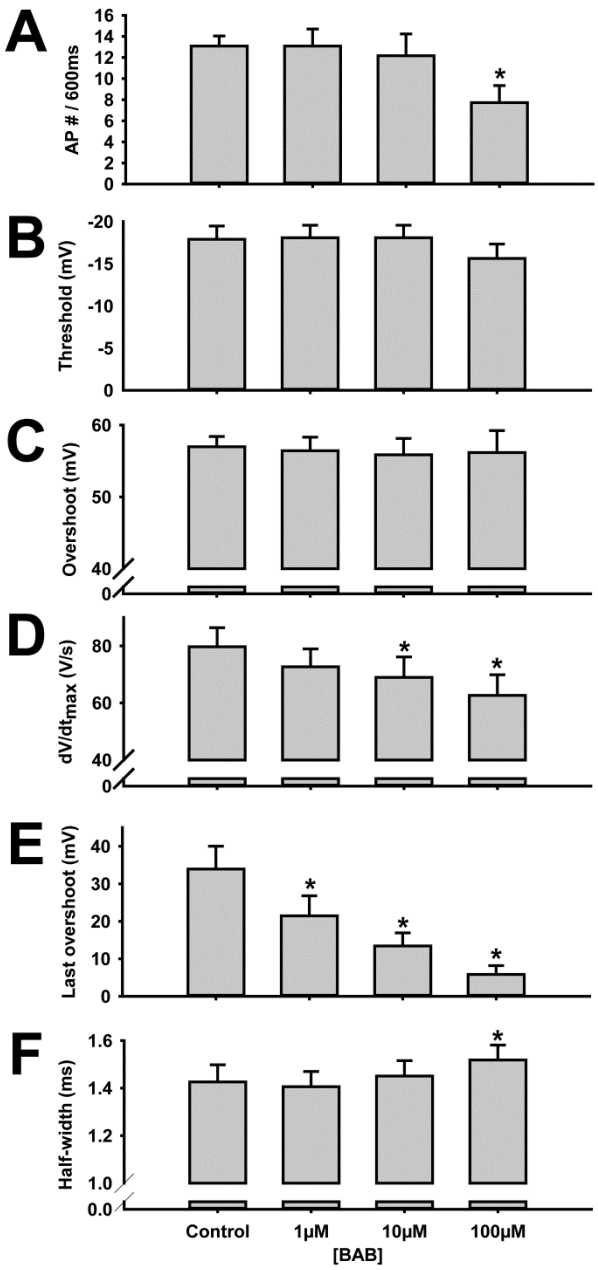

Fig. 2. *Effect of BAB on AP parameters.*

In a separate series of experiments, a 200 pA current injection (as shown in Fig. 1E) was used to generate single APs and long 600 ms spike trains, and the following parameters were measured: AP no./600ms (A); voltage-threshold for firing (B); OS (C); maximum rate of rise, dV/dt_{max} (D); last generated OS/first OS (E); and duration of AP at 50%, AP_{50} (F). 1, 10, and 100 μM BAB applied in that sequence. (* $p>0.05$, **$p>0.001$, n=12)

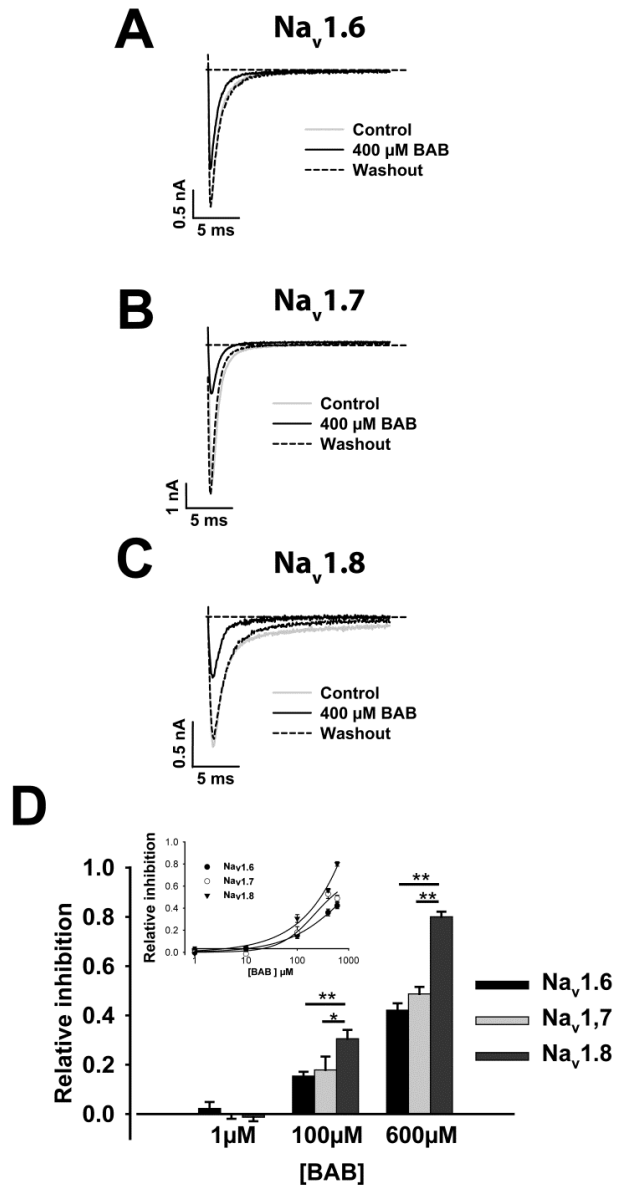

Fig. 3. *Concentration-dependent suppression of Na$_v$1.6, Na$_v$1.7, and Na$_v$1.8 currents by different concentrations of BAB.*

Whole-cell Na^+ currents in HEK293 cells were evoked by a 40 ms depolarizing pulse to -20 mV for Na$_v$1.6, -40 mV for Na$_v$1.7, and +10 mV for Na$_v$1.8 (holding potential of -140 mV). (A-C) Representative trace-currents of Na$_v$1.6, Na$_v$1.7, and Na$_v$1.8, respectively, in control conditions (gray), 400 µM of BAB (black) and washout (dotted line). (D) Representation of the relative inhibition by BAB of the different Na^+ channels. The inset of (D) shows concentration-response curves for Na$_v$1.6 (filled circle), Na$_v$1.7 (open circle), and Na$_v$1.8 (filled triangle). (*,P<0.05; **, P<0.01; n= 4-10).

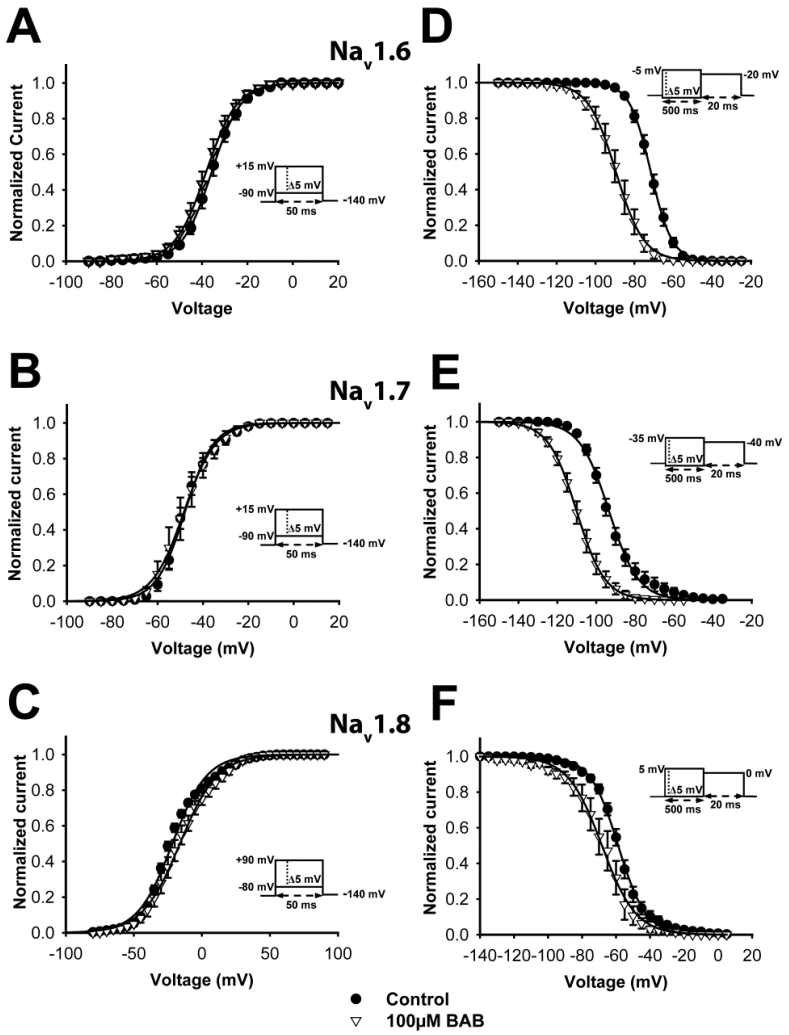

Fig. 4. *Effect of BAB on the steady-state activation and inactivation of Na$_v$1.6, Na$_v$1.7, and Na$_v$1.8.*

(A-C) Steady-state activation of Na$_v$1.6, Na$_v$1.7, and Na$_v$1.8, respectively, in the presence of 100μM BAB (open triangles) or in control conditions (filled circles). The stimulus protocols are shown in the figure insets. Conductance was derived from the maximum amplitude for each voltage obtained from the IV curves. (D-F) Steady-state inactivation of Na$_v$1.6, Na$_v$1.7, and Na$_v$1.8, respectively. Steady-state inactivation was determined using 500 ms conditioning pulses followed by a standard test pulse. The test current was normalized and plotted against the conditioning voltage. The voltages are indicated in the protocol shown in the inset of each panel. Control condition (filled circles) and 100 μM BAB (open triangles). Values and significance are listed in Table 1. See Material and methods for details.

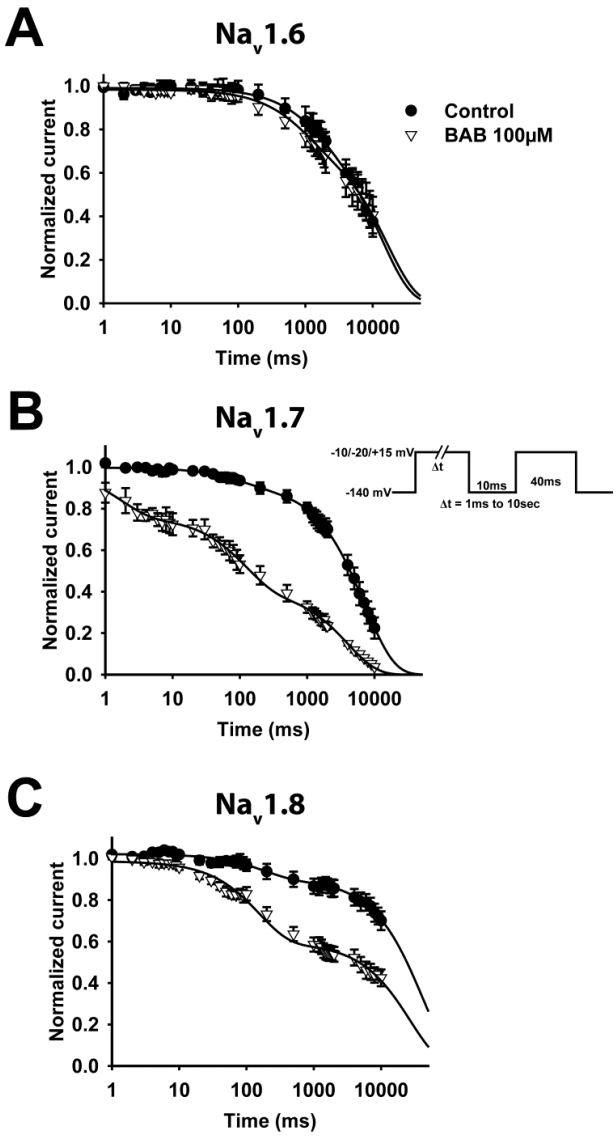

Fig. 5. *Impact of BAB on the slow inactivation of Na$_v$1.6, Na$_v$1.7, and Na$_v$1.8.*

(A-C) The slow activation of Na$_v$1.6 (A), Na$_v$1.7 (B), and Na$_v$1.8 (C) was studied in control condition (filled circles) and in the presence of 100 µM BAB (open triangles). The entry into the slow inactivation state was measured using a double-pulse protocol consisting of a conditioning first test pulse of variable duration (1 ms to 10 s), a 10 ms interpulse to -140 mV, and a second test pulse. The voltages used in the first and second test pulses were -10 mV for Na$_v$1.6, -20 mV for Na$_v$1.7, and +15 mV for Na$_v$1.8. The currents were normalized and were plotted against the duration of the conditioning pulse. The values were fitted with the sum of two exponentials in all cases. See Table 1 for the time constant values.

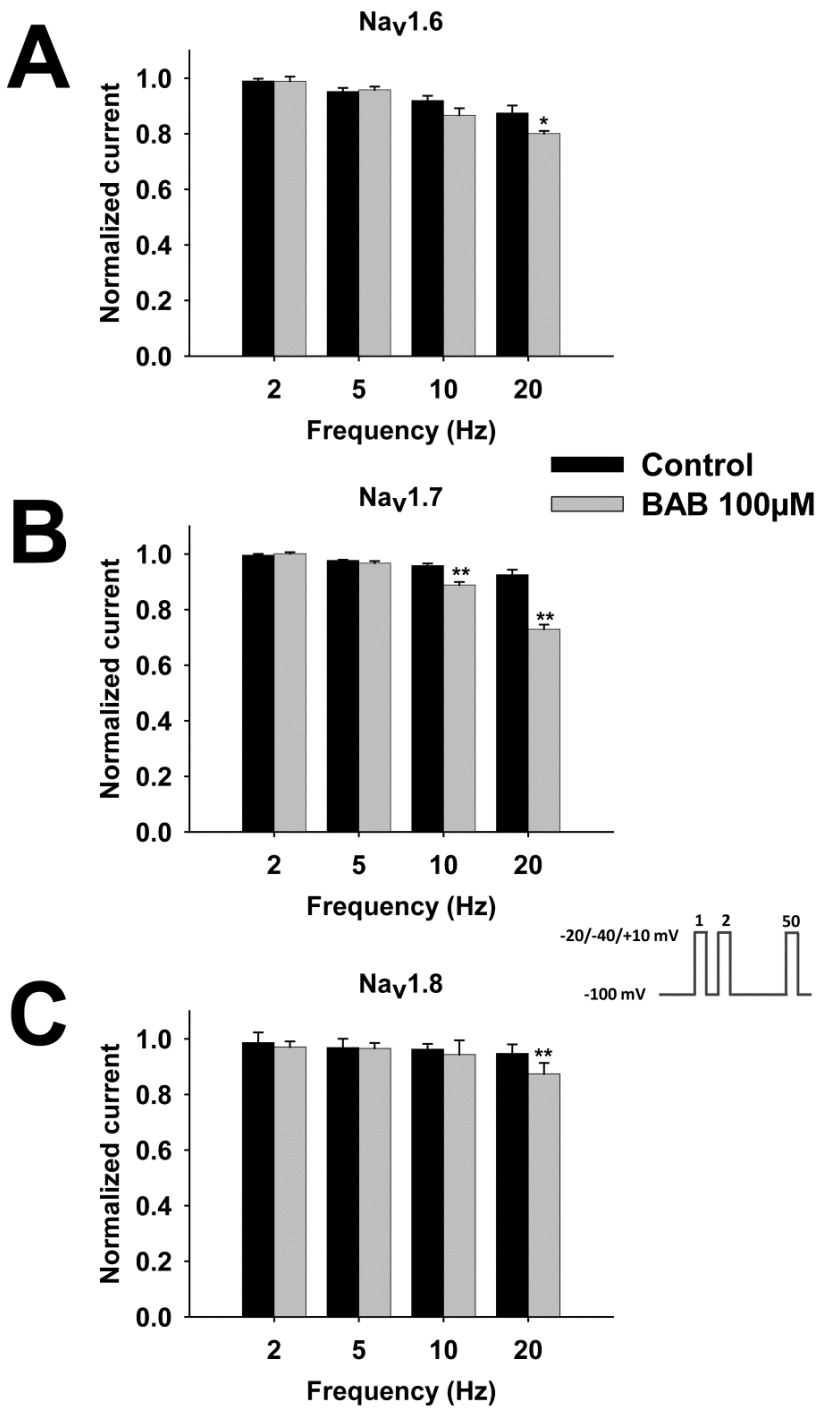

Fig. 6. *Use-dependent inhibition of $Na_v1.6$, $Na_v1.7$, and $Na_v1.8$ by BAB.*

Currents were evoked by test pulses at different frequencies. The black columns are the control condition and the gray columns are in presence of 100μM BAB. Test pulses were -20 mV for $Na_v1.6$ (A), -40 mV for $Na_v1.7$ (B), and +10 mV for $Na_v1.8$ (C). See the inset for the protocols. (*,P<0.05; **, P<0.01; n = 5-7).

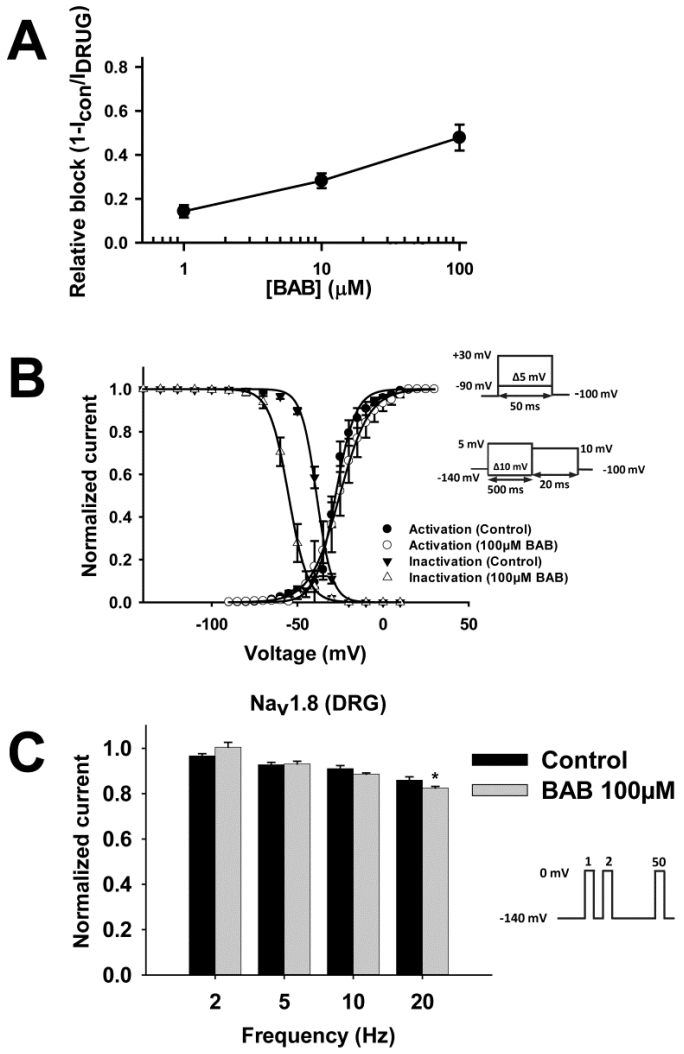

Fig. 7. *Effect of BAB on the TTXr Na⁺ channels of DRG neurons*.

(A) Tonic block of TTXr I_{Na} in the presence of 1, 10, and 100 μM BAB (n = 10). The time-course of the effect of each BAB concentration was determined using a 50 ms pulse from -80 mV to 0 mV applied every 10 s until the steady-state effect of the drug was reached (between 3-5 minutes, data not shown). (B) Steady-state activation (circles) and inactivation (triangles) of TTXr Na^+ channels of DRG neurons in the presence of 100 μM BAB (open symbols) and the control condition (filled symbols). The protocols are shown in the inset. (C) The use-dependent block of the TTXr Na^+ current was determined as described in Materials and methods by applying pulses to 0 mV at either 2 Hz, 5 Hz, 10 Hz, or 20 Hz in the presence of 100 μM BAB. The black columns are the control condition and the gray columns are in presence of 100μM BAB.

Chapitre 4

Differential modulation of Nav1.7 and Nav1.8 channels by antidepressant drugs

En préparation

Differential modulation of Nav1.7 and Nav1.8 channels by antidepressant drugs

Olivier Thériault[1,3], Hugo Poulin[1], Jean-Martin Beaulieu[1,2] and Mohamed Chahine[1,3]

[1]Centre de recherche de l'institut universitaire en santé mentale de Québec, Quebec City, QC, Canada G1J 2G3

[2]Department of Psychiatry and Neuroscience

[3]Department of Medicine, Université Laval, Quebec City, QC, Canada G1K 7P4

Correspondence to:

Mohamed Chahine, PhD

Centre de recherche,

Institut universitaire en santé mentale de Québec

2601 chemin de la Canardière

Quebec City, QC, Canada G1J 2G3

Telephone: 1-418-663-5747, ext. 4723

Fax: 1-418-663-8756

Email: mohamed.chahine@phc.ulaval.ca

Authorship Contributions:

O Thériault and M Chahine conducted the experiments

O Thériault, M Chahine, JM Beaulieu and H Poulin participated in research design

O Thériault and M Chahine analysed the data

O Thériault, JM Beaulieu and M Chahine wrote or contributed to the writing of the manuscript

Running title: Effects of antidepressants on sodium channels

Keywords: sodium channels, $Na_v1.7$, $Na_v1.8$, fluoxetine, paroxetine, citalopram, antipsychotics, serotonin re-uptake, SSRI, peripheral sodium channels

Abstract

BACKGROUND AND PURPOSE

Antidepressant drugs of the SSRI family are used as a third-line treatment for neuropathic pain. In contrast MAOi antidepressants, that also increase extracellular serotonin bioavailability have little or no effects on this condition. In addition to their action of the serotonin transporter, some SSRI have been shown to inhibit voltage gated sodium channels. Here we investigated the potential inhibition of SSRIs and MAOi antidepressants on $Na_v1.7$ or $Na_v1.8$, which are expressed in sensory neurons and play an important role in pain sensation.

EXPERIMENTAL APPROACH

We used the whole-cell patch-clamp technique on HEK293 cells expressing either $Na_v1.7$ or $Na_v1.8$, and evaluated the effects of the SSRIs fluoxetine, paroxetine, and citalopram as well as one MAOi antidepressants on the electrophysiological properties of the Na^+ channels.

KEY RESULTS

Paroxetine exhibited the greatest affinity for Na^+ channels. In ascending order of affinity for $Na_v1.7$ were paroxetine (IC_{50}=10 μM), followed by fluoxetine (IC_{50}=66 μM), then citalopram (IC_{50}=174 μM). In ascending order of affinity for $Na_v1.8$ were paroxetine (IC_{50}=9 μM), followed by fluoxetine (IC_{50}=49 μM), then citalopram (IC_{50}=100 μM). Paroxetine and fluoxetine accelerated the onset of slow-inactivation and delayed the time-course of recovery from inactivation for both channels. Paroxetine and fluoxetine also had a prominent effect on the frequency-dependent inhibition, with a greater effect on $Na_v1.7$. In contrast to SSRIs, MAOi did not affect Na^+ channels currents.

CONCLUSIONS AND IMPLICATIONS

These results suggest that, in certain conditions, the analgesic effect of SSRIs may in part be due to their interactions with Na^+ channels.

Abbreviations:

CNS, central nervous system; IC_{50}, dose producing 50% maximum current inhibition; MAOi, Monoamine oxidase inhibitors; NSAID, nonsteroidal anti-inflammatory drug; SERT, serotonin transporter; SSRI, selective serotonin re-uptake inhibitor

Introduction

Pathological pain, including neuropathic pain and fibromyalgia, is a frequent condition and is very challenging to manage. Neuropathic pain is described as "*pain arising as a direct consequence of a lesion or disease affecting the somatosensory system*" (Treede *et al.*, 2008). The definition and causes of fibromyalgia are vague. Fibromyalgia is often referred to as chronic widespread pain and is often accompanied by other symptoms such as extreme fatigue, impaired cognition, and non-restorative sleep. There is currently few evidence linking fibromyalgia to a neuropathic component (Malemud, 2009;Sumpton & Moulin, 2014). The management of neuropathic pain and fibromyalgia usually includes non-steroidal anti-inflammatory drugs (NSAIDs) and opioids that are often ineffective. Moreover, patients can have multiple side effects and develop dependence and/or tolerance (Dworkin *et al.*, 2007).

As they have few adverse effects and are relatively well tolerated, selective serotonin reuptake inhibitors (SSRIs) are widely used to treat neuropathic pain and fibromyalgia (Lee & Chen, 2010;Dharmshaktu *et al.*, 2012). These drugs, which are commonly prescribed for depression and anxiety, are used as a third-line treatment for neuropathic pain and fibromyalgia (Dworkin *et al.*, 2007). The effects of SSRIs on depression and anxiety are relatively well established. SSRIs inhibit serotonin transporter (SERT), which is responsible for the re-uptake of serotonin into the presynaptic cell, increasing the level of serotonin in the synaptic cleft (Rosenberg, 2003). However, their role in the treatment of pathological pain remains unclear. On the one hand, these effects may involve increase bioavailability of extracellular serotonin. Pain is modulated by serotonin and noradrenalin in the descending inhibitory pathway while SSRIs have a reduced analgesic effect in conditional KO mice that lack central serotoninergic neurons (Zhao *et al.*, 2007). The overactivation of this pathway by SSRIs may thus prevent excessive pain by negative feedback in the spinal cord. On the other hand, some evidence also point toward the involvement of additional mechanisms. Indeed, activation of different serotonin receptors has been shown to have divergent affects by either decreasing or increasing pain perception (Millan, 2002). Furthermore, some SSRIs such as citalopram, and MAOi antidepressants, that also

increase extracellular serotonin availability, have shown little or no efficacy in the treatment of chronic pain and are not efficient for fibromyalgia (Tort *et al.*, 2012;Mika *et al.*, 2013).

Na^+ channels are widely expressed throughout the nervous system, and several subtypes are linked to pain sensation in normal and pathological conditions (Garrison *et al.*, 2014). $Na_v1.7$ and $Na_v1.8$ are widely expressed in sensory neurons, and play a major role in pain transmission (Cox *et al.*, 2006). It has been suggested that these Na^+ channels may be good therapeutic targets for managing neuropathic pain (Dib-Hajj *et al.*, 2009). It is possible that the inhibition of Na^+ channels by SSRIs may contribute to their analgesic effect. Indeed, several studies haves shown that SSRIs can inhibit some Na^+ channels (Dick *et al.*, 2007;Lenkey *et al.*, 2010;Deffois *et al.*, 1996), but the anemic literature on the effect of antidepressant on Na^+ channels render the comprehension of the implication of Na+ channels difficult.

We used the patch-clamp technique to investigate the effects of SSRIs fluoxetine, paroxetine and citalopram as well as the MOAi moclobemide on the electrophysiological properties of two Na^+ channels ($Na_v1.7$ and $Na_v1.8$) that are expressed in peripheral sensory neurons. A better understanding of the action of SSRIs may provide new insights into the pathophysiological mechanisms of neuropathic pain and fibromyalgia and lead to the development of new approaches for the treatment of neuropathic pain.

Materials and methods

Cell culture and cell lines

We used two cell lines stably expressing $Na_v1.7$ or $Na_v1.8$ (Theriault *et al.*, 2014) to study the effect of fluoxetine, paroxetine, and citalopram on two peripheral Na^+ channels. Briefly, the cell lines were generated using the calcium phosphate method. HEK293 cells were transfected with a pIRESneo3/Na_v vector. The day after the transfection, the cells were diluted to obtain a pure cell line, and 800 µg •ml^{-1} of neomycin was added on the second day. Three weeks after the transfection, individual clones were tested using PCR and the patch-clamp technique to ensure that they expressed the selected Na^+ channel. Clones that generated currents exceeding 500 pA were selected for the study, and the neomycin concentration was lowered to 400 µg •ml^{-1}.

The cell lines were grown in Dulbecco's minimal essential medium (DMEM, Gibco BRL Life Technologies) supplemented with fetal bovine serum (FBS, 10%), L-glutamine (2 mM), penicillin (100 U·ml^{-1}), streptomycin (10 mg·ml^{-1}), and hygromycin (75 µg·ml^{-1}) (Gibco BRL Life Technologies). The cells were incubated at 37ºC in a 5% CO_2 humidified atmosphere. The cell lines were then transfected with pIRES/CD8/β_1 to add the β_1 subunit 2 days prior to the recordings. Cells that bound CD8 antibody-coated beads (Dynabeads M-450 CD8-a) were considered to be β_1-positive and were selected for the recordings.

Whole cell patch-clamp recordings

Na^+ currents were recorded from HEK293 stable cell lines using the whole-cell configuration of the patch-clamp technique. Stimulations and recordings were done using pCLAMP software (version 10.0), an Axopatch 200 amplifier, and a Digidata 1200 series AD converter (Molecular Devices). The recordings were stored on a personal computer for later offline analysis. Currents were filtered at 5 kHz and were digitized at 100 kHz. Series resistance was compensated by 70-80%. When needed, linear leak current artifacts were removed using online leak subtraction.

Recordings were done 10 min after gigaohm seals were obtained to stabilize the current. Fire-polished low-resistance electrodes (1MΩ) were pulled from 8161 glass (Corning) and were coated with Sylgard (Dow-Corning) to minimize pipette capacitance. The glass electrodes were filled with pipette solution.

Drugs and solutions

Different internal and external solutions were used for the $Na_v1.7$ and $Na_v1.8$ recordings in order to reduce or increase the driving force. The $Na_v1.7$ bath recording solution contained 20 mM NaCl, 130 mM choline chloride, 2 mM KCl, 1.5 mM $CaCl_2$, 1.0 mM $MgCl_2$, 10 mM glucose, and 10 mM HEPES. The pH was adjusted to 7.4 with 1 M NaOH. For $Na_v1.7$ recordings the pipette solution contained 35 mM NaCl, 105 mM CsF, 10 mM EGTA, and 10 mM HEPES. The pH was adjusted to pH 7.4 with 1 M CsOH.

The $Na_v1.8$ bath recording solution contained 150 mM NaCl, 2 mM KCl, 1.5 mM $CaCl_2$, 1.0 mM $MgCl_2$, 10 mM glucose, and 10 mM HEPES. The pH was adjusted to 7.4 with 1 M NaOH. The $Na_v1.7$ pipette solution contained 5 mM NaCl, 135 mM CsF, 10 mM EGTA, and 10 mM HEPES. The pH was adjusted to pH 7.4 with 1 M CsOH.

The drugs were applied by superfusion using a ValveLink8.2® perfusion system (Automate Scientific) through a 250 µm needle. Silicone-free tubing was used since Poulin et al. had observed that fluoxetine adheres to silicone, which may considerably change the applied concentrations (Poulin *et al.*, 2014). Fresh drugs working solutions were prepared daily from the stock solution. Paroxetine and moclobemide stock solutions were made in EtOH. The stock solutions of the drugs were kept at –80°C. All the chemicals were from Sigma-Aldrich.

Data analysis

Data was analyzed using a combination of pCLAMP software v10.0 (Molecular Devices), Microsoft Excel, and SigmaPlot 11.0 (Systat Software, Inc.). All p-values are two-tailed, and $p<0.05$ was considered statistically significant. Statistical values are expressed as means ± SEM.

The following equation was used to calculate the conductance: ($G_{Na} = I_{Na}/(V_m - V_{rev})$, where G_{Na} is the conductance, I_{Na} is the peak current for the test potential V_m, and V_{rev} is the reversal potential estimated from the current-voltage curve. Conductance values were then fitted to the following Boltzmann equation: $I/I_{max}=1/(1+\exp((V + V_{1/2})/k))$, where I_{max} is the maximal evoked current, $V_{1/2}$ is the voltage at which half of the channels are in the open state, and k is the slope factor. Steady-state inactivation values were fitted using a similar Boltzmann equation. Recovery from inactivation values were fitted to the sum of the following two-exponent equation: $f=a*(1-\exp(x/-\tau_f))+(1-a)*(1-\exp(x/-\tau_s))$. For $Na_v1.7$, the onset of slow-inactivation values were fitted to a single exponential: $f = a_s*\exp(-\tau_s *x)$. For $Na_v1.8$, the onset of slow-inactivation were fitted to the sum of two exponentials: $f=a_f*\exp(-\tau_f *x)+a_s*\exp(-\tau_s *x)$.

Results

Tonic inhibition of $Na_v1.7$ and $Na_v1.8$ by fluoxetine, paroxetine, and citalopram

The tonic inhibition by the three SSRIs were assessed on $Na_v1.7$ Na^+ channels heterologously expressed in HEK293 cells. Figure 1A-C shows representative current traces for controls and after superfusion of fluoxetine, paroxetine, and citalopram. Tonic inhibition were assessed at –20mV. We observed marked differences in IC_{50} for the three drugs (Figure 2D). In descending effectiveness were paroxetine (IC_{50} = 9.6 μM), followed by fluoxetine (IC_{50} = 65.5 μM), and then citalopram (IC_{50} = 174.2 μM). The effect was fully reversible upon washout (Figure 1A-C).

Figure 2 shows the tonic inhibition of $Na_v1.8$ by fluoxetine, paroxetine, and citalopram. Figure 2A-C shows representative current traces for the control channels and after superfusion of fluoxetine, paroxetine and citalopram respectively. Figure 2D shows the dose responses of $Na_v1.8$ to the drugs. The tonic inhibition of $Na_v1.8$ were similar to those observed with $Na_v1.7$: paroxetine (IC_{50} = 9.1 μM), fluoxetine (IC_{50} = 48.7 μM), and citalopram (IC_{50} = 100.9 μM). The effect was fully reversible upon washout (Figure 2A-C). Interestingly, the MAOi moclobemide have no effects on $Na_v1.7$ and $Na_v1.8$ with concentrations up to 500 μM (Figure 1 and 2).

Effect of fluoxetine and paroxetine on steady-state activation and inactivation

Figures 3 and 4 show the effect of fluoxetine and paroxetine, respectively, on steady-state activation and inactivation. Due to differences in the biophysical properties of $Na_v1.7$ and $Na_v1.8$, the voltage protocols were slightly different for each channel. Steady-state activation was assessed on $Na_v1.7$ and $Na_v1.8$ using a 50-ms depolarizing pulse with 5 mV increments (from –90 to +25 mV for $Na_v1.7$ and from –80 to +55 mV for $Na_v1.8$) from a –140-mV holding potential. Conductances were derived from these currents and were plotted against voltages. Data were fitted using a Boltzmann equation (see Materials and methods). Steady-state inactivation was assessed using a two-pulse protocol consisting of –140-mV to –10-mV conditioning pulses in 10 mV

increments for $Na_v1.7$ and –140-mV to +10-mV conditioning pulses in 10 mV increments for $Na_v1.8$ followed by a –30-mV test pulse for $Na_v1.7$ and a 10-mV test pulse for $Na_v1.8$. A 4-s interval between sweeps was used for the control condition and a 15-s interval between sweeps was used in presence of the drugs to allow full recovery from inactivation between sweeps. The currents were then normalized to a current evoked at –140 mV and were fitted using a Boltzmann equation. The protocols are shown in the insets of each figure.

In figures 3 and 4, activation and inactivation parameters are represented in black for control conditions and in gray for test conditions. Figure 3 shows that paroxetine did not affect the activation (rising curve) or inactivation (falling curve) of either $Na_v1.7$ (Fig. 3A) or $Na_v1.8$ (Fig. 3B). We observed similar results for both channels with paroxetine (Fig. 4). The only significant difference was the slope of the activation parameters of $Na_v1.7$ in the presence of paroxetine. None of the other steady-state activation or inactivation parameters were affected by paroxetine (Table 1).

Effect of fluoxetine and paroxetine on the onset of slow inactivation

Fluoxetine and paroxetine sped up the onset of slow inactivation of both $Na_v1.7$ and $Na_v1.8$ (Fig. 5). The protocol used to investigate the effect on the onset of the slow inactivation of $Na_v1.7$ consisted of a –20 mV inactivating pulse of increasing duration (1 ms to 10 s) followed by a –140 mV recovery pulse , which allowed recovery from fast inactivation, then a –20 mV test pulse. Normalized currents were then plotted against the duration of the conditioning pulse. A single exponential function gave the best fit with the onset of slow inactivation of $Na_v1.7$. The time constant of the control condition was 15 s, but was significantly lower in presence of 25 μM fluoxetine (0.80 s) and 10 μM paroxetine (1.3 s) (Fig. 5C).

Fluoxetine and paroxetine also sped up the onset of slow inactivation of $Na_v1.8$. The protocol was similar to that used for $Na_v1.7$. However, the voltages were adjusted to take the differences in the biophysical properties of the two channels into consideration. The inactivating and test pulses were 0 mV. The protocol is shown in the inset of Fig. 5. The sum of two exponentials, one with a fast time constant (τ_f) and the

other with a slow time constant (τ_s), gave the best fit for the onset of slow inactivation of $Na_v1.8$. The weight of the fast time constant was much higher, which accelerated the onset of the slow inactivation of $Na_v1.8$ (Fig. 5B). The weight of the slow time constant was 0.15 for the control condition and rose to 0.48 and 0.34 in the presence of fluoxetine and paroxetine, respectively (Table 2).

Effect of fluoxetine and paroxetine on the recovery from inactivation

The recovery from inactivation of $Na_v1.7$ was tested using a three-step protocol that consisted of a 40 ms inactivating pulse at –20 mV, a variable duration (0.1 ms to 4 s) recovery pulse of –140 mV, followed by a –20 mV test pulse. The current of the test pulse was normalized to the current elicited by the inactivating pulse and was then plotted against the recovery time. The data were fit to the sum of two exponentials (see equation in Material and methods). Fluoxetine and paroxetine increased the time of recovery from inactivation of $Na_v1.7$ (Fig. 6A). The fast time constant (τ_f) was significantly slower in the presence of both drugs, increasing from 1.6 ms in the control condition to 4.7 and 3.7 ms in the presence of fluoxetine and paroxetine, respectively. The slow time constant was also slower in the presence of both drugs, increasing from 0.04 s in the control condition to 1.29 s and 1.4 s in the presence of 25 μM fluoxetine and 10 μM paroxetine, respectively.

The recovery from inactivation of $Na_v1.8$ was assessed using a similar three-pulse protocol. However, the voltages used were adjusted to take the differences in the biophysical properties of the two channels into consideration. The inactivating and test pulses were 0 mV. The data were fit either with a single exponential (control condition) or the sum of two exponentials (in presence of the drugs). Figure 6B shows a recovery process in presence of the drugs that include a second time constant and accounts for about 20%. The effects of fluoxetine and paroxetine on the inactivation parameters are summarized in Table 2.

Frequency-dependent inhibition caused by fluoxetine and paroxetine

The frequency-dependent inhibition of Na^+ channels by fluoxetine and paroxetine was tested using three stimulation frequencies (2, 5, and 10 Hz) at –20 mV

for $Na_v1.7$ and 0 mV for $Na_v1.8$ (Fig. 7). The 50th pulse was normalized to the first pulse and was then plotted as a histogram. While $Na_v1.7$ did not display a frequency-dependent inhibition at 2 Hz, 25 μM fluoxetine caused a 30% inhibition ($P<0.001$) and 10 μM paroxetine caused a 46% inhibition ($P<0.001$) (Fig. 7A). At 10 Hz, the frequency-dependent inhibition was only 7% in the control condition but increased to 47% ($P<0.001$) in the presence of 25 μM fluoxetine and 60% ($P<0.001$) in presence of 10 μM paroxetine.

The two drugs also caused a significant frequency-dependent inhibition of $Na_v1.8$. In control conditions, 2 Hz caused no inhibition while 5 Hz and 10 Hz only caused frequency-dependent inhibition s of 2% and 5%, respectively. Fluoxetine (25 μM) caused a 15% inhibition at 2 Hz ($P<0.01$) and a 22% inhibition at 10 Hz ($P<0.001$) while 10 μM paroxetine caused a 28% inhibition at 2 Hz ($P<0.001$) and a 39% inhibition at 5 Hz and 10 Hz ($P<0.001$).

Discussion

The present study was designed to improve our understanding of the analgesic effect of the SSRIs used to treat neuropathic pain and fibromyalgia. We examined and compared the effects of three commonly prescribed SSRIs and one MAOi on two peripheral nerve sodium channels that are known to play an important role in pain sensation. As mentioned, previous studies also attempted to assess the selectivity of fluoxetine and paroxetine on Nav1.7 but didn't fully characterize those effects (Dick *et al.*, 2007). Moreover, the efficacy of those drugs on $Na_v1.8$ were never assessed. Our study filled the gap in the literature and increased our understanding of those compounds in the anesthesia evoked by antidepressant drugs.

Similar to what was reported in the literature for central nervous system (CNS) and cardiac Na^+ channels, we observed that fluoxetine, paroxetine, and citalopram inhibited the $Na_v1.7$ and $Na_v1.8$ channels in a dose-dependent manner (Deffois *et al.*, 1996;Lenkey *et al.*, 2006). We observed significant differences in the affinities of the three SSRIs, with paroxetine displaying the greatest affinity and citalopram displaying very low affinity.

Since Na^+ channel blockers may have different effects in different functional states and since measuring tonic inhibition is insufficient for evaluating the impacts of drugs (Chevrier *et al.*, 2004;Hildebrand *et al.*, 2011;Choi *et al.*, 2009;Ragsdale *et al.*, 1994;Lenkey *et al.*, 2010), we evaluated the impact of fluoxetine and paroxetine on different functional states. Na^+ channel blockers commonly trap Na^+ channels in the inactivated state, increasing the number of Na^+ channels in the inactivated state following repeated stimulation (Chevrier *et al.*, 2004;Choi *et al.*, 2009). $Na_v1.7$ and $Na_v1.8$ both exhibited strong frequency-dependent inhibition in the presence of fluoxetine and paroxetine. This effect may reduce firing by sensory neurons. While Na^+ channel blockers commonly shift the steady-state inactivation of these channels, we observed very small or no impact on the two channels by paroxetine and fluoxetine (Theriault *et al.*, 2014;Scholz, 2002).

The onset of slow inactivation of Na^+ channels is a very important component of neuron excitability and can modulate pain (Han *et al.*, 2012;Blair & Bean, 2003). Lenkey et al. postulated that the affinity of two SSRIs (fluoxetine and desipramine) for the slow-inactivated state greatly contribute to the inhibition on Na^+ channels in hippocampal neurons (Lenkey *et al.*, 2006). We observed a marked acceleration of the onset of slow-inactivation of the two peripheral Na^+ channels we tested. We also observed a delay in the recovery from the inactivation, with a more pronounced effect on $Na_v1.7$. The great affinity for the slow-inactivated state may trap the channel in this state and contribute to the delay in the recovery from inactivation, increase the onset of slow-inactivation, and enhance use-dependent inhibition.

The effect of SSRIs is unclear since many studies have reported conflicting results on the effectiveness of SSRIs in treating neuropathic pain (Saarto & Wiffen, 2007;Lee & Chen, 2010;Dworkin *et al.*, 2007;Dharmshaktu *et al.*, 2012). However, randomized control trials have shown that SSRIs are effective in treating neuropathic pain. However, each compounds have distinct efficacy in the treatment of different neuropathic pain syndrome (Lee & Chen, 2010). Those differences in effectiveness might be explained by the specific mechanism leading for those neuropathic pains. Na^+ channels might be more involved in some type of neuropathic pain and less in others. For example, paroxetine and citalopram have been shown to provide better pain relief than placebos in the treatment of painful diabetic neuropathy (Sindrup *et al.*, 1990;Sindrup *et al.*, 1992). Since citalopram appears to be effective in treating painful diabetic neuropathy, the inhibition of Na^+ channels by SSRIs may play a secondary role in reducing neuropathic pain.

Several SSRIs, including fluoxetine and paroxetine, have been shown to be effective in managing fibromyalgia pain (Roskell *et al.*, 2011) while citalopram, which has very low affinity for Na^+ channels, is not effective (Norregaard *et al.*, 1995). Interestingly, lidocaine, a Na^+ channel blocker and a local anesthetic, also alleviates fibromyalgia pain (Raphael *et al.*, 2003;Schafranski *et al.*, 2009). However, MAOi, which do not inhibit $Na_v1.7$ and $Na_v1.8$, while increasing central and peripheral serotonin tones are not efficient for the treatment of several types of pathological pain,

including fibromyalgia (Tort *et al.*, 2012). The high affinities of fluoxetine and paroxetine for Na^+ channels may therefore also contribute to their analgesic effect while the low affinity of citalopram, which is more specific for SERT, may explain its lack of effectiveness. These results suggested that the clinical effectiveness of paroxetine and fluoxetine may, in part, be due to a combination of enhanced serotonin neurotransmission with Na^+ channels inhibition.

In conclusion, we showed that paroxetine and fluoxetine cause a state-dependent and use-dependent inhibition of $Na_v1.7$ and $Na_v1.8$. We propose that the mechanism by which SSRIs reduce fibromyalgia pain may include the inhibition of Na^+ channels. Further studies are essential to unravel the implication of Na+ channels in neuropathic pain.

Acknowledgements

This work was supported by grants from the Canadian Institutes of Health Research (CIHR, MOP-111072) and the Heart and Stroke Foundation of Quebec (HSFQ).

Conflict of interest

None

References

Blair, N.T. and Bean, B.P. 2003. Role of tetrodotoxin-resistant Na+ current slow inactivation in adaptation of action potential firing in small-diameter dorsal root ganglion neurons. J. Neurosci. 23(32): 10338-10350

Chevrier, P., Vijayaragavan, K. and Chahine, M. 2004. Differential modulation of Nav1.7 and Nav1.8 peripheral nerve sodium channels by the local anesthetic lidocaine. Br. J. Pharmacol. 142(3): 576-584

Choi, J.S., Zhang, L., Dib-Hajj, S.D., Han, C., Tyrrell, L., Lin, Z. et al. 2009. Mexiletine-responsive erythromelalgia due to a new Na(v)1.7 mutation showing use-dependent current fall-off. Exp. Neurol. 216(2): 383-389

Cox, J.J., Reimann, F., Nicholas, A.K., Thornton, G., Roberts, E., Springell, K. et al. 2006. An SCN9A channelopathy causes congenital inability to experience pain. Nature 444(7121): 894-898

Deffois, A., Fage, D. and Carter, C. 1996. Inhibition of synaptosomal veratridine-induced sodium influx by antidepressants and neuroleptics used in chronic pain. Neurosci. Lett. 220(2): 117-120

Dharmshaktu, P., Tayal, V. and Kalra, B.S. 2012. Efficacy of antidepressants as analgesics: a review. J. Clin. Pharmacol. 52(1): 6-17

Dib-Hajj, S.D., Black, J.A. and Waxman, S.G. 2009. Voltage-gated sodium channels: therapeutic targets for pain. Pain Med. 10(7): 1260-1269

Dick, I.E., Brochu, R.M., Purohit, Y., Kaczorowski, G.J., Martin, W.J. and Priest, B.T. 2007. Sodium channel blockade may contribute to the analgesic efficacy of antidepressants. J. Pain 8(4): 315-324

Dworkin, R.H., O'Connor, A.B., Backonja, M., Farrar, J.T., Finnerup, N.B., Jensen, T.S. et al. 2007. Pharmacologic management of neuropathic pain: evidence-based recommendations. Pain 132(3): 237-251

Garrison, S.R., Weyer, A.D., Barabas, M.E., Beutler, B.A. and Stucky, C.L. 2014. A gain-of-function voltage-gated sodium channel 1.8 mutation drives intense hyperexcitability of A- and C-fiber neurons. Pain

Han, C., Hoeijmakers, J.G., Ahn, H.S., Zhao, P., Shah, P., Lauria, G. et al. 2012. Nav1.7-related small fiber neuropathy: impaired slow-inactivation and DRG neuron hyperexcitability. Neurology 78(21): 1635-1643

Hildebrand, M.E., Smith, P.L., Bladen, C., Eduljee, C., Xie, J.Y., Chen, L. et al. 2011. A novel slow-inactivation-specific ion channel modulator attenuates neuropathic pain. Pain 152(4): 833-843

Lee, Y.C. and Chen, P.P. 2010. A review of SSRIs and SNRIs in neuropathic pain. Expert. Opin. Pharmacother. 11(17): 2813-2825

Lenkey, N., Karoly, R., Kiss, J.P., Szasz, B.K., Vizi, E.S. and Mike, A. 2006. The mechanism of activity-dependent sodium channel inhibition by the antidepressants fluoxetine and desipramine. Mol. Pharmacol. 70(6): 2052-2063

Lenkey, N., Karoly, R., Lukacs, P., Vizi, E.S., Sunesen, M., Fodor, L. et al. 2010. Classification of drugs based on properties of sodium channel inhibition: a comparative automated patch-clamp study. PLoS. One. 5(12): e15568

Malemud, C.J. 2009. Focus on pain mechanisms and pharmacotherapy in the treatment of fibromyalgia syndrome. Clin. Exp. Rheumatol. 27(5 Suppl 56): S86-S91

Norregaard, J., Volkmann, H. and Danneskiold-Samsoe, B. 1995. A randomized controlled trial of citalopram in the treatment of fibromyalgia. Pain 61(3): 445-449

Poulin, H., Bruhova, I., Timour, Q., Theriault, O., Beaulieu, M., Frassati, D. et al. 2014. Fluoxetine Blocks Nav1.5 Channels Via a Mechanism Similar to That of Class 1 Antiarrhythmics. Mol. Pharmacol.

Ragsdale, D.S., McPhee, J.C., Scheuer, T. and Catterall, W.A. 1994. Molecular determinants of state-dependent block of Na+ channels by local anesthetics. Science 265(5179): 1724-1728

Raphael, J.H., Southall, J.L. and Kitas, G.D. 2003. Adverse effects of intravenous lignocaine therapy in fibromyalgia syndrome. Rheumatology. (Oxford) 42(1): 185-186

Rosenberg, M. 2003. Goodman and Gilman's The Pharmacological Basis of Therapeutics, 10th Edition. Anesth. Prog. 50(4): 190-191

Roskell, N.S., Beard, S.M., Zhao, Y. and Le, T.K. 2011. A meta-analysis of pain response in the treatment of fibromyalgia. Pain Pract. 11(6): 516-527

Saarto, T. and Wiffen, P.J. 2007. Antidepressants for neuropathic pain. Cochrane. Database. Syst. Rev. (4): CD005454

Schafranski, M.D., Malucelli, T., Machado, F., Takeshi, H., Kaiber, F., Schmidt, C. et al. 2009. Intravenous lidocaine for fibromyalgia syndrome: an open trial. Clin. Rheumatol. 28(7): 853-855

Scholz, A. 2002. Mechanisms of (local) anaesthetics on voltage-gated sodium and other ion channels. Br. J. Anaesth. 89(1): 52-61

Sindrup, S.H., Bjerre, U., Dejgaard, A., Brosen, K., Aaes-Jorgensen, T. and Gram, L.F. 1992. The selective serotonin reuptake inhibitor citalopram relieves the symptoms of diabetic neuropathy. Clin. Pharmacol. Ther. 52(5): 547-552

Sindrup, S.H., Gram, L.F., Brosen, K., Eshoj, O. and Mogensen, E.F. 1990. The selective serotonin reuptake inhibitor paroxetine is effective in the treatment of diabetic neuropathy symptoms. Pain 42(2): 135-144

Sumpton, J.E. and Moulin, D.E. 2014. Fibromyalgia. Handb. Clin. Neurol. 119: 513-527

Theriault, O., Poulin, H., Sculptoreanu, A., De Groat, W.C., O'Leary, M.E. and Chahine, M. 2014. Modulation of peripheral Na(+) channels and neuronal firing by n-butyl-p-aminobenzoate. Eur. J. Pharmacol. 727: 158-166

Treede, R.D., Jensen, T.S., Campbell, J.N., Cruccu, G., Dostrovsky, J.O., Griffin, J.W. et al. 2008. Neuropathic pain: redefinition and a grading system for clinical and research purposes. Neurology 70(18): 1630-1635

Zhao, Z.Q., Chiechio, S., Sun, Y.G., Zhang, K.H., Zhao, C.S., Scott, M. et al. 2007. Mice lacking central serotonergic neurons show enhanced inflammatory pain and an impaired analgesic response to antidepressant drugs. J. Neurosci. 27(22): 6045-6053

Table 1 : Effect on steady-state activation and inactivation of fluoxetine and paroxetine

	Activation			Inactivation		
	$V_{1/2}$	k_v	n	$V_{1/2}$	k_v	n
Nav1.7						
Control	-31.3±1.0	-6.1±0.4	6	-80.4±1.4	7.9±1.1	7
Fluoxetine	-32.0±1.6	-6.8±0.3	13	-84.6±1.8	8.8±0.6	11
Paroxetine	-31.5±1.4	-7.4±0.3*	6	-83.9±1.3	6.7±0.3	7
Nav1.8						
Control	-8.2±1.6	9.4±0.4	21	-41.1±2.1	6.7±0.8	9
Fluoxetine	-9.1±2.0	8.1±0.4	8	-41.2±3.2	6.3±0.7	9
Paroxetine	-13.8±2.2	10.4±0.8	6	-44.2±2.0	7.9±0.8	7

* = P<0.05; ** = P<0.01;*** = P<0.001.

	Onset of slow inactivation					Recovery			
	a_f	τ_f (ms)	a_s	τ_s (s)	n	τ_f (ms)	τ_s (s)	a	n
$Na_v1.7$									
Control	---	---	1.00±0.01	15±2.1	6	1.6±0.3	0.04±0.02	0.78±0.06	6
Fluoxetine	---	---	0.81±0.01***	0.80±0.05***	8	4.7±0.2***	1.29±0.03***	0.71±0.01	10
Paroxetine	---	---	0.74±0.05***	1.3±0.1**	5	3.7±0.2***	1.400±0.2***	0.68±0.02	6
$Na_v1.8$									
Control	0.15±0.06	650±150	0.86±0.07	7±2	4	1.1±0.1	---	0.98±0.01	9
Fluoxetine	0.48±0.06*	200±20**	0.52±0.03**	10.3±0.4***	3	1.5±0.3	1.6±0.1	0.82±0.02	7
Paroxetine	0.34±0.08*	400±200	0.60±0.06*	5±2*	4	1.6±0.3	2.0±0.5	0.82±0.04	4

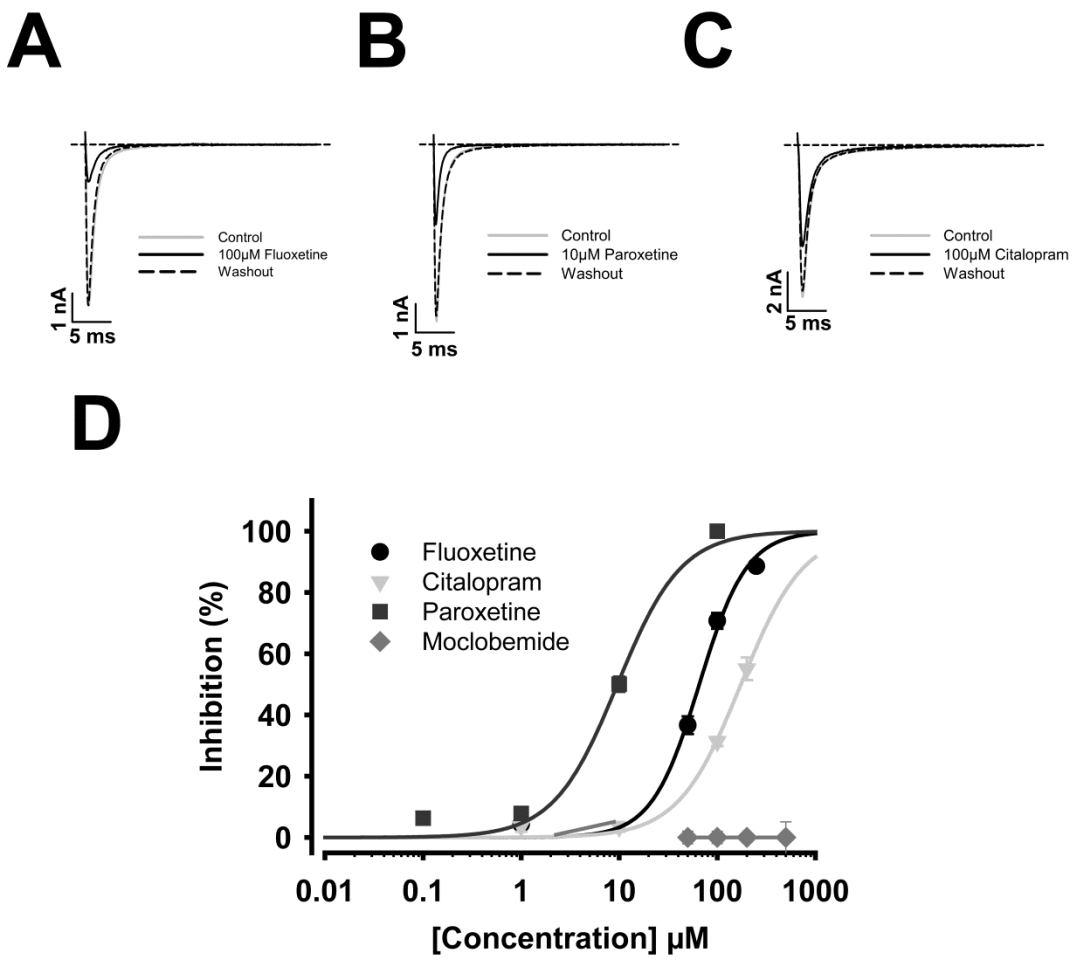

Figure 1

Tonic inhibition of heterologously expressed $Na_v1.7$ channels by fluoxetine, paroxetine, and citalopram. Whole-cell Na^+ currents in HEK293 cells were evoked by a 40 ms depolarizing pulse to –25 mV from a holding potential of –140 mV). (A-C) Representative current traces of $Na_v1.7$ in the presence of 100 μM fluoxetine (A), 10 μM paroxetine (B), and 100 μM citalopram (C). Control (gray), drug (black), and washout (dotted line). (D) Dose-response curves of $Na_v1.7$ in the presence of fluoxetine (black dot), paroxetine (gray square), and citalopram (gray triangle). Data were fitted using a three-parameter logistic fit. The IC_{50} were 65.5 μM, 9.6 μM, and 174.2 μM for fluoxetine, paroxetine, and citalopram, respectively.

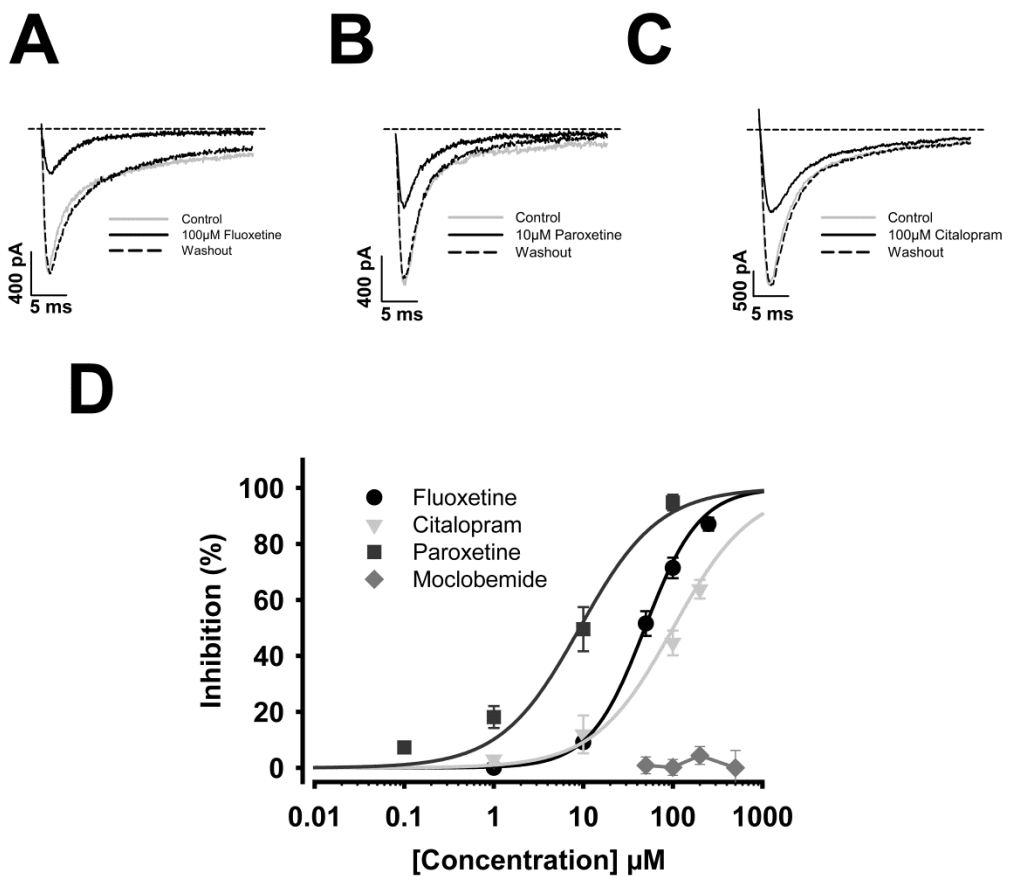

Figure 2

Tonic inhibition of heterologously expressed $Na_v1.8$ channels by fluoxetine, paroxetine, and citalopram. Whole-cell Na^+ currents in HEK293 cells were evoked by a 40 ms depolarizing pulse to 0 mV from a holding potential of –140 mV). (A-C) Representative current traces of $Na_v1.8$ in the presence of 100 μM fluoxetine (A), 10 μM paroxetine (B), and 100 μM citalopram (C). Control (gray), drug (black), and washout (dotted line). (D) Dose-response curves of $Na_v1.8$ in the presence of fluoxetine (black dot), paroxetine (gray square), and citalopram (gray triangle). Data were fitted using a three-parameter logistic fit. The IC_{50} were 48.7 μM, 9.1 μM, and 100.9 μM for fluoxetine, paroxetine, and citalopram, respectively.

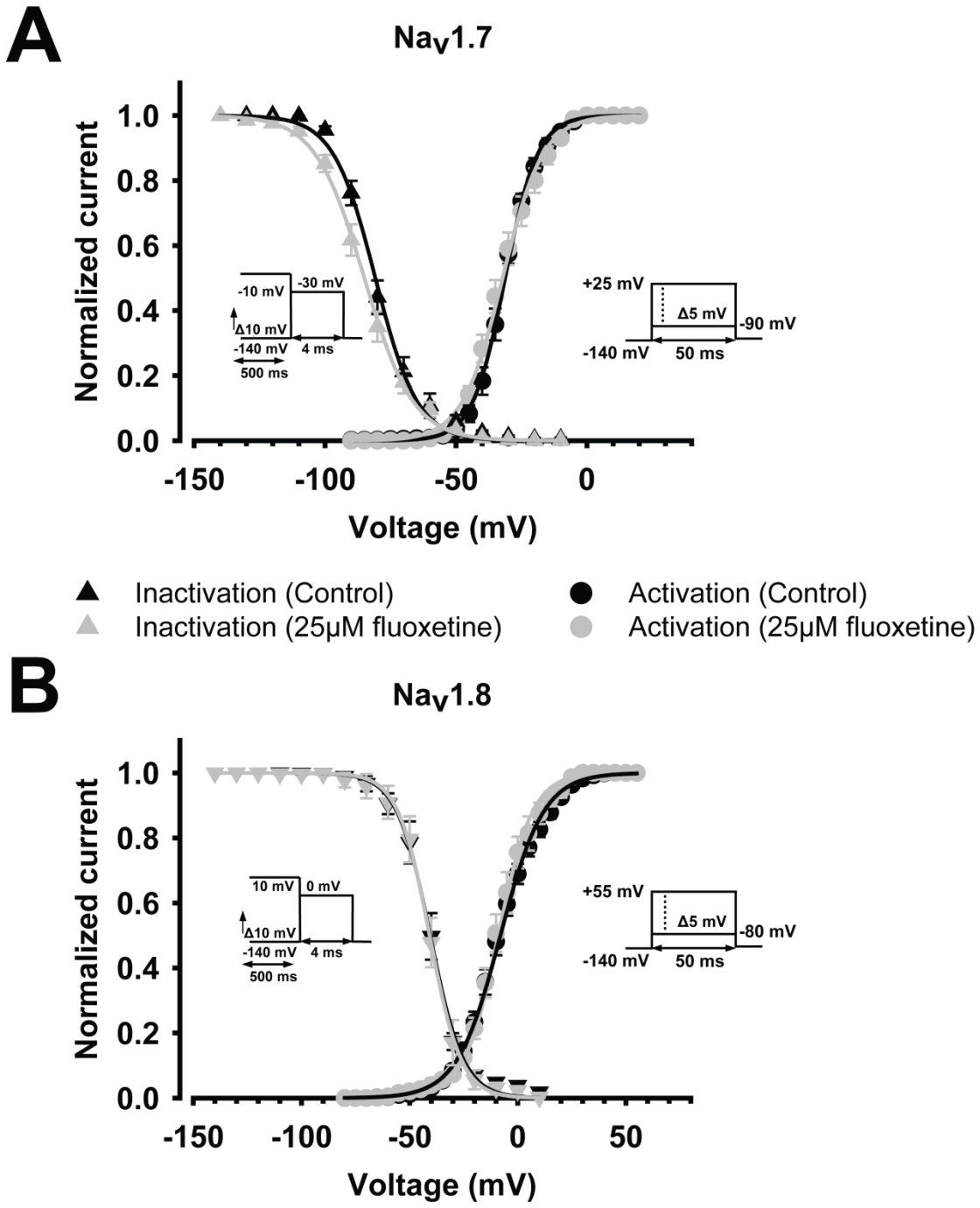

Figure 3

Effects of fluoxetine on heterologously expressed Na^+ channels. (A) Effects of fluoxetine on steady-state activation (circles) and steady-state inactivation of $Na_V1.7$ in the absence of fluoxetine (black) and in the presence of 25 μM fluoxetine (gray). The voltage-dependence of activation was determined by eliciting depolarizing pulses from

a holding potential of –140 mV to potentials ranging from –90 mV to +25 mV in 5 mV increments. Current activation curves were plotted using a Boltzmann equation (see Methods). Steady-state inactivation was determined using a 500 ms conditioning pulse from –140 mV to –10 mV, with a –30 mV test pulse. See the inset for the steady-state inactivation protocol. The test current was normalized, plotted against the conditioning voltage, and fitted with a Boltzmann equation. The $V_{1/2}$ of activation was –31.3 mV in absence of fluoxetine and 32.0 mV in the presence of 25 μM fluoxetine. The $V_{1/2}$ of inactivation was –80.4 mV in the absence of fluoxetine and –84.8 mV in presence of 25 μM fluoxetine. No significant shift in steady-state activation or inactivation was observed. (B) Effects of fluoxetine on the steady-state activation (circles) and steady-state inactivation of $Na_v1.8$ in the absence of fluoxetine (black) or the presence of 25 μM fluoxetine (gray). The voltages used for the activation and inactivation protocols were adjusted to take the differences in the biophysical properties of the Na^+ channels into consideration. See the inset for the protocols. The $V_{1/2}$ of activation was –8.2 mV in the absence of fluoxetine and –9.1 mV in the presence of 25 μM fluoxetine. The $V_{1/2}$ of inactivation was –41.1 mV in absence of fluoxetine and –41.2 in presence of 25 μM fluoxetine. No significant shifts in activation or inactivation were observed. All values are given in Table 1. See Materials and methods for details.

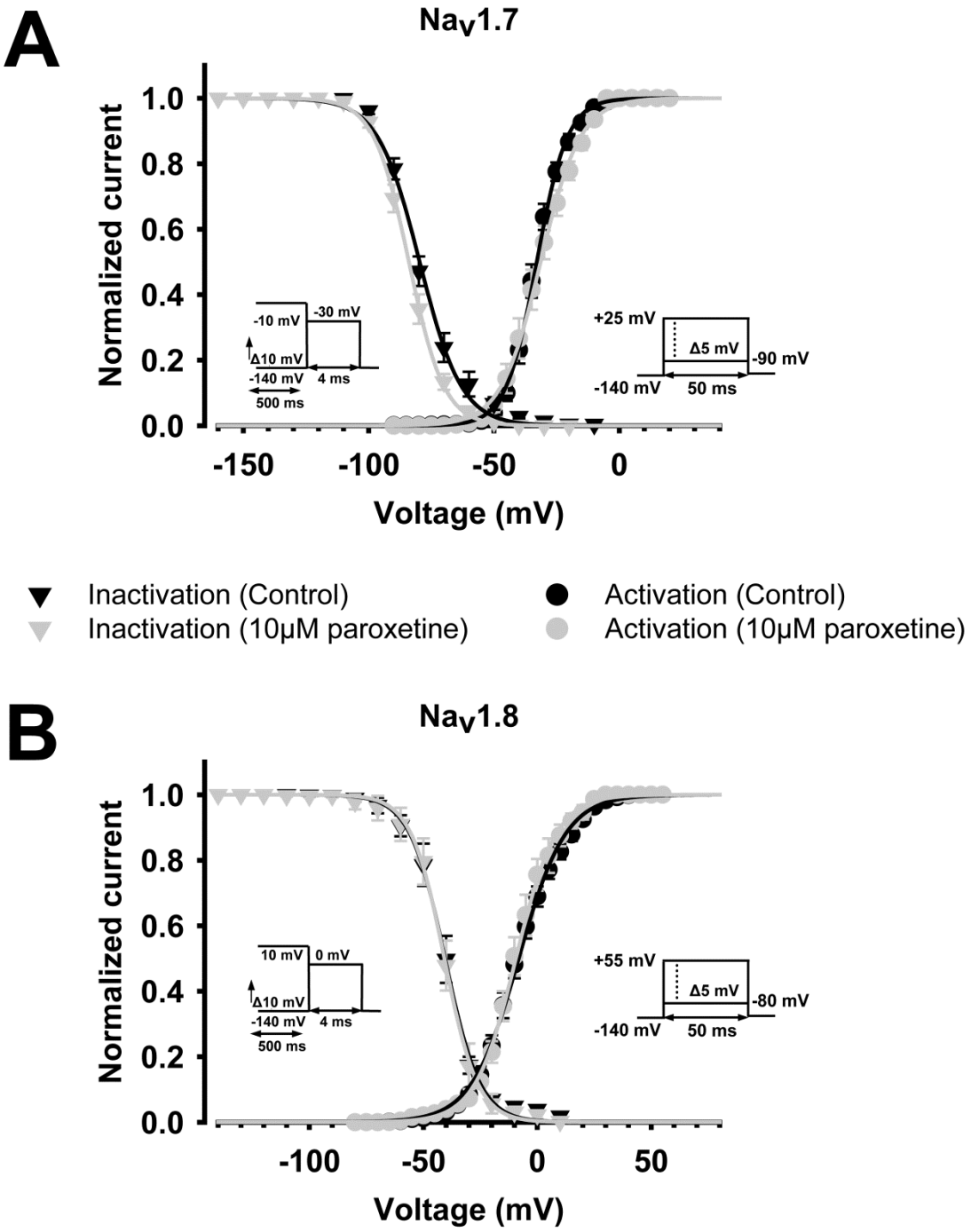

Figure 4

Effects of paroxetine on heterologously expressed Na^+ channels. (A) Effects of paroxetine on the steady-state activation (rising curve) and inactivation of $Na_v1.7$ in the absence of paroxetine (black) or the presence of 10 μM paroxetine (gray). The protocols are shown in inset and are identical to those in Figure 3 (A). The $V_{1/2}$ of

activation was –31.5 mV in the presence of 10 μM fluoxetine. The $V_{1/2}$ of inactivation was –83.9 mV in presence of 10 μM paroxetine. No significant shifts in steady-state activation or inactivation were observed. (B) Effects of fluoxetine on the steady-state activation and inactivation of $Na_v1.8$ in absence of paroxetine (black) or the presence of 10 μM paroxetine (gray). The protocols are shown in the inset and are identical to those in Figure 3B. The $V_{1/2}$ of activation was 8.2 mV in the absence of paroxetine and –13.8 mV in the presence of 10 μM paroxetine. The $V_{1/2}$ of inactivation was 41.1 mV in the absence of paroxetine and –44.2 mV in the presence of 10 μM paroxetine. No significant shifts in steady-state activation or inactivation were observed. All values are given in Table 1. See Material and methods for details.

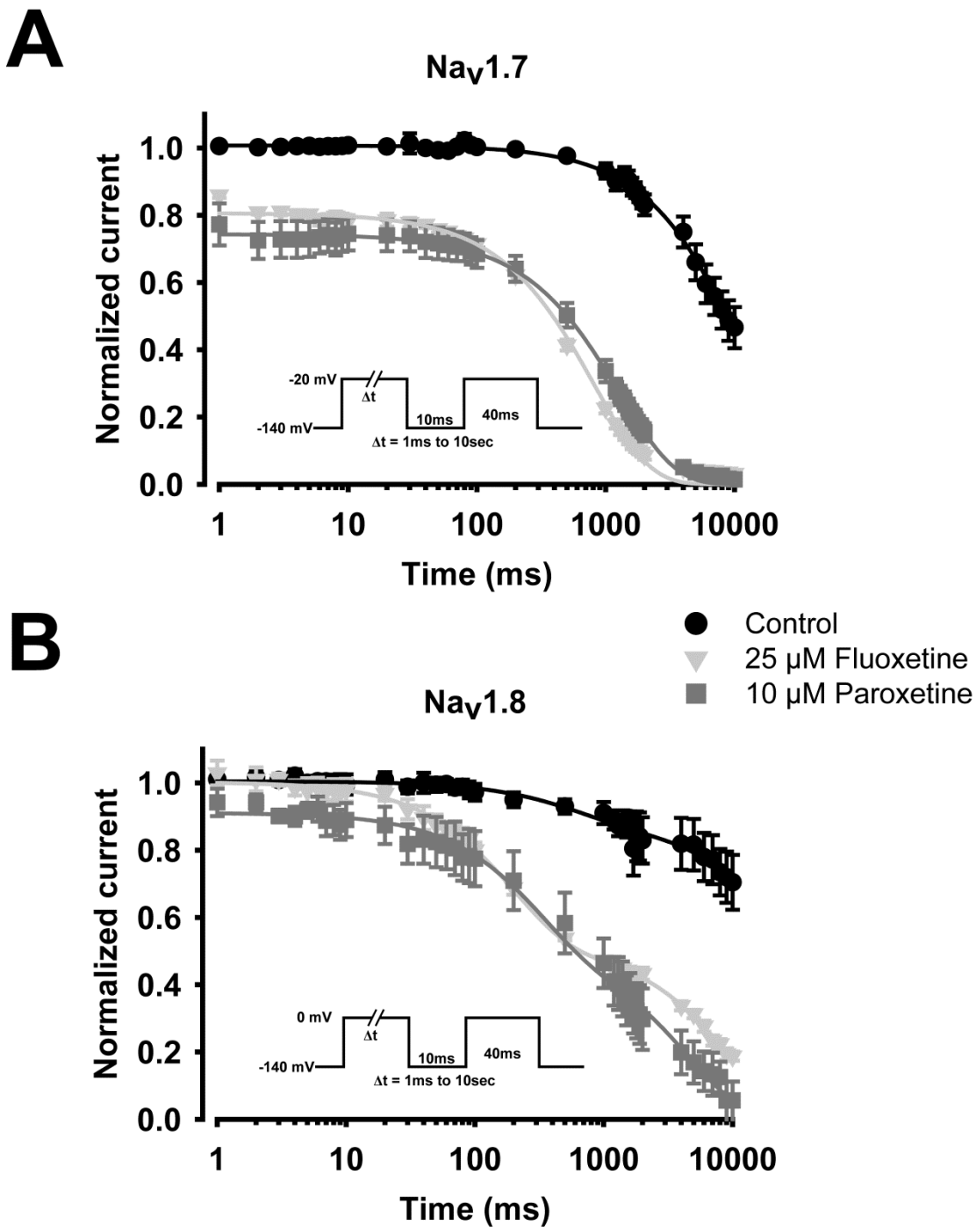

Figure 5

Effects of fluoxetine and paroxetine on the onset of slow inactivation. The onset of slow-inactivation for $Na_v1.7$ (A) and $Na_v1.8$ (B) in the absence of drug (black circles), the presence of 25 μM fluoxetine (light gray triangles), and the presence of 10 μM

paroxetine (dark gray squares). The protocol used to measure the time course of the onset of slow inactivation consisted of a triple-pulse protocol: a conditioning pulse of variable duration (1 ms to 10 s), a 10 ms interpulse to –140 mV, and a test pulse (see inset). The voltages used for the conditioning and test pulses were –20 mV for $Na_v1.7$ (A) and 0 mV for $Na_v1.8$ (B). The test currents were normalized and were plotted against the conditioning pulse interval. $Na_v1.7$ was best fitted to a single exponential while $Na_v1.8$ was best fitted with the sum of two exponentials. All values are given in Table 2.

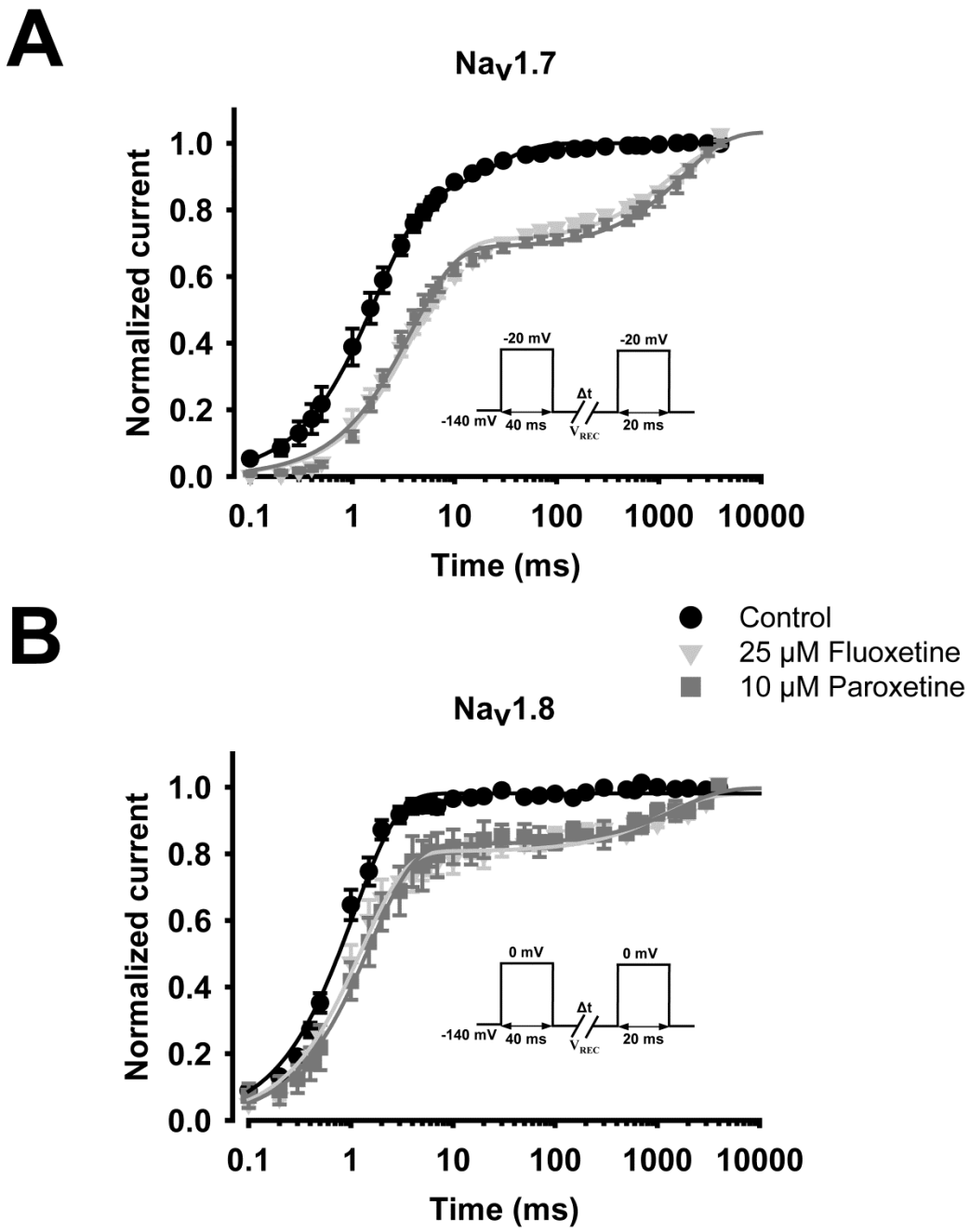

Figure 6

Effects of fluoxetine and paroxetine on the time course of recovery from inactivation.

The effects of the SSRIs on the recovery from inactivation were tested on $Na_v1.7$ (A) and $Na_v1.8$ (B). The protocol used to measure the time course of the onset of slow inactivation consisted of a triple-pulse protocol: a 40 ms inactivating pulse, a –140-mV

hyperpolarizing pulse of variable duration (0.1 ms to 4 s) to allow the recovery, and a test pulse to assessed the fraction of current that recovered. See the inset for the protocol. The inactivating and test pulses were –20 mV for $Na_v1.7$ and 0 mV for $Na_v1.8$. The test currents were normalized to the current evoked by the inactivating pulse and were plotted against the recovery interval. The data for the control condition (no drug) for $Na_v1.8$ were best fitted to a single exponential equation, while the other data were fitted to the sum of two exponentials with fast and slow time constants. All values are given in Table 2.

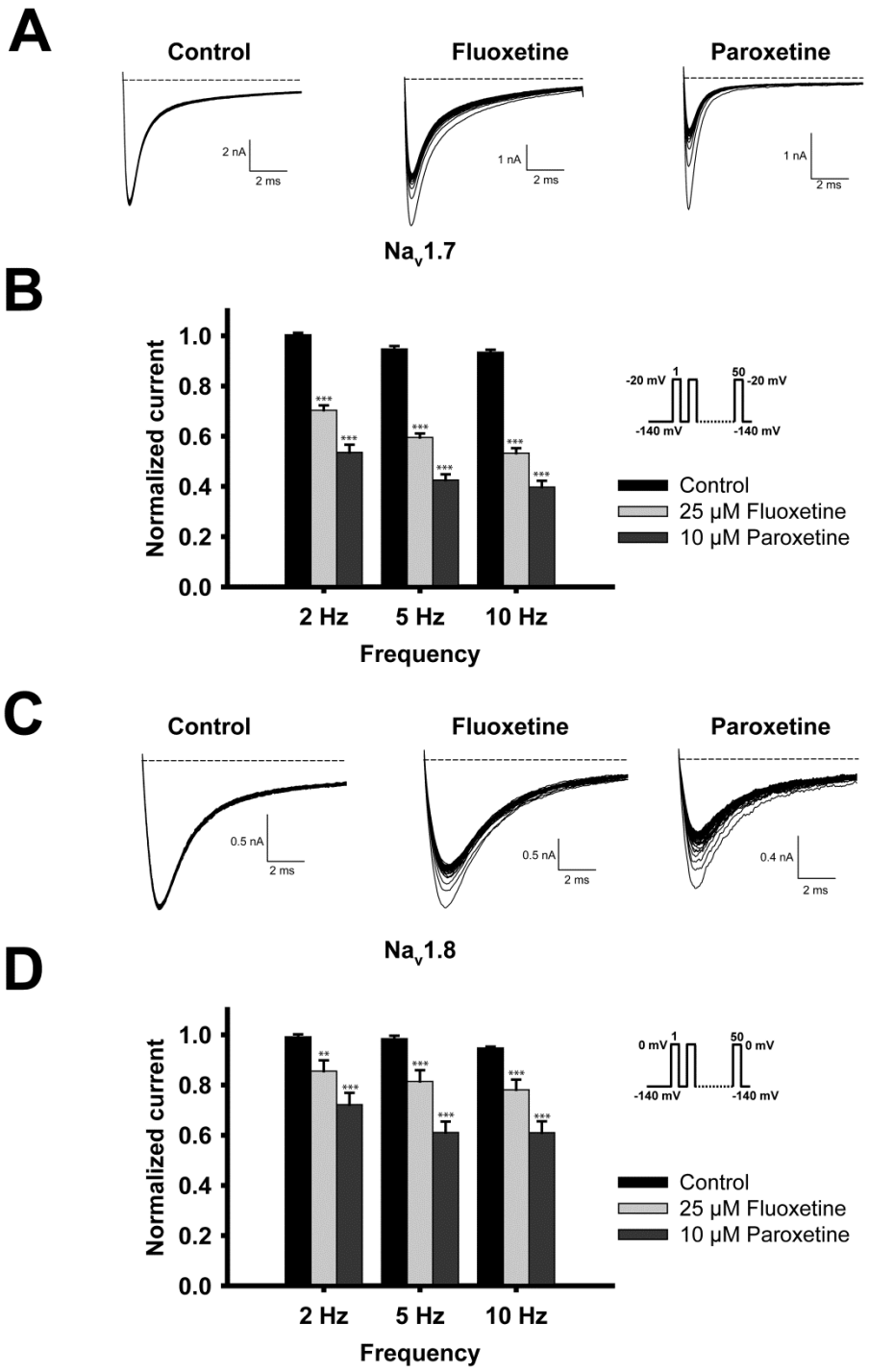

Figure 7

Effects of fluoxetine and paroxetine on use-dependent inhibition. (A, C) Representative whole-cell traces recorded from Na$_v$1.7 (A) and Nav1.8 (C) in control condition, in presence of 25 µM fluoxetine, and 10 µM paroxetine at 5 Hz. (B, D) Use-

dependent inhibition of $Na_v1.7$ (B) and Nav1.8 (D) in the absence of fluoxetine (black), the presence of 25 μM fluoxetine (light gray), and the presence of 10 μM paroxetine (dark gray). Currents were evoked with a train of depolarizing pulses (0.5 Hz, 2 Hz, or 5 Hz). The 50th pulse was normalized against the first pulse and was plotted as a normalized current. The test pulse voltages were –20 mV for $Na_v1.7$ (A, B) and 0 mV for $Na_v1.8$ (C, D). See the insets for the protocols. (*, $P<0.05$; **, $P<0.01$; ***, $P<0.001$; n=5-7).

Chapitre 5
Discussion

Bilan de l'étude

L'approche expérimentale utilisée dans cette thèse contribue à une meilleure compréhension de l'impact des modulations des canaux Na^+ sur l'activité électrique des neurones nociceptifs.

Impact des canaux Na^+ sur le profil électrophysiologique de neurones de DRG

Dans la première partie, nous avons clairement montré que les différents transcrits de sous-unités α des canaux Na^+ présentes dans les neurones sensitifs périphériques modulent l'activité électrique et contribuent ainsi aux multiples profils électrophysiologiques de ces neurones. Pour ce faire, nous avons dû commencer par montrer que les ARN_m présents à l'intérieur des neurones reflètent la quantité de protéine. Par la méthode de la PCR quantitative sur cellule unique et le *patch-clamp* en mode voltage imposé, il a été possible de corréler les niveaux de protéines fonctionnelles aux niveaux d'ARN_m. Nous avons donc pu utiliser ce rapprochement entre les ARN_m et les protéines afin de montrer que les ARN_m (et donc les canaux Na^+) sont linéairement corrélés avec les différents paramètres électrophysiologiques des neurones. En effet, nous avons montré un rôle important de $Na_v1.7$ dans l'initiation du PA puisque la présence de ce canal Na^+ diminue le seuil d'activation des PA. Ces résultats confirment d'ailleurs l'importance de $Na_v1.7$ dans l'amplification des stimuli sous-liminaire (Blair and Bean 2002). Nous avons aussi montré que les cinétiques des PAs sont étroitement liées aux cinétiques des canaux Na^+ présents dans le neurone. Alors que les cinétiques d'activation et d'inactivation rapides de $Na_v1.7$ favorisent un PA court et rapide, les canaux $Na_v1.8$ et $Na_v1.9$ soutiennent des PAs ayant des cinétiques plus lentes. Nous avons aussi montré que la fréquence de décharge n'est que peu régulée par la présence des isoformes $Na_v1.7$ et $Na_v1.8$. Plusieurs études avaient cependant proposé que la récupération rapide de $Na_v1.8$ pourrait favoriser une fréquence de décharge rapide alors que la lente récupération de

$Na_v1.7$ était responsable d'une fréquence de décharge des neurones de DRG relativement plus lente (Renganathan et al. 2001; Herzog et al. 2003). Ces résultats ne sont cependant pas surprenants car dans les neurones des ganglions cervicaux $Na_v1.7$ est responsable de la fréquence de décharge relativement rapide (Rush *et al.* 2006).

Selon leur vitesse de conduction, les neurones nociceptifs sont généralement classifiés en fibres C (plus lentes) et en fibres Aδ (plus rapides car finement myélinisées) (Julius and Basbaum 2001). Cependant, le profil d'expression protéique de ces fibres a permis la création de plusieurs sous catégories. Au sein des fibres C, il est ainsi possible de distinguer les neurones non peptidergiques et les neurones peptidergiques (Stucky and Lewin 1999). Les neurones non peptidergiques représentent approximativement 70% des neurones, formant ainsi la majorité des fibres C. Ces neurones diffèrent aussi par leur lieu de projection dans la moelle épinière. En effet, les neurones non peptidergiques projettent dans la lamina II de la corne dorsale de la moelle épinière alors que les neurones peptidergiques projettent dans la lamina I (Braz *et al.* 2005). Ces neurones diffèrent aussi par les canaux Na^+ qu'ils expriment, les neurones non peptidergiques exprimant préférentiellement $Na_v1.8$. Mon projet de doctorat a aussi permis de révéler un fait intéressant, l'expression de $Na_v1.3$ est intimement liée à la présence de $Na_v1.7$ dans les neurones de petits diamètres des DRG. L'analyse statistique de la composition en ARN_m de ces neurones a aussi révélé qu'ils sont répartis en au moins 3 groupes distincts. Le premier groupe exprimant préférentiellement $Na_v1.8$ et $Na_v1.9$, le second groupe exprimant principalement $Na_v1.7$ et le dernier groupe exprimant de façon similaire les différents sous-types de canaux sodiques.

Il a été observé que l'expression, les cinétiques et la dépendance au voltage sont modifiées dans les modèles de douleurs neuropathiques et d'inflammation (Vijayaragavan *et al.* 2004; Stamboulian *et al.* 2010). Ces changements sont responsables de l'hyperexcitabilité de plusieurs types de neurones et

notamment des neurones afférents primaires (Waxman *et al.* 1994; McGowan *et al.* 2009; Novakovic *et al.* 1998; Gold *et al.* 2003). En extrapolant les résultats de notre étude aux modifications observés dans les douleurs pathologiques, il est possible d'améliorer la compréhension de l'hyperexcitabilité neuronale. En effet, nos résultats supportent l'hypothèse selon laquelle la surexpression de $Na_v1.7$ diminue le seuil d'activation des PAs dans les douleurs neuropathiques (Black *et al.* 2004; Cummins *et al.* 2004). Nous avons montré que l'expression relative des différents isoformes de canaux Na^+ module partiellement les propriétés électriques des neurones. La compréhension fine de l'impact des canaux Na^+ sur le profil électrophysiologique des neurones de DRG est un outil important dans la compréhension des mécanismes menant au développement et au maintien des douleurs pathologiques. Cependant, il est connu que d'autres canaux influences les propriétés électrophysiologiques des PAs. Par exemple, les canaux K^+ et les canaux Ca^{2+} influencent la fréquence de décharge, la durée et les cinétiques des PAs (Deister *et al.* 2009; Winlove and Roberts 2012). Ainsi, les propriétés des PAs proviennent d'un équilibre entre les différents canaux présent à la membrane cellulaire dans lequel les canaux Na^+ jouent un rôle majeure.

Plusieurs études avaient précédemment lié l'expression relative des canaux Na^+ aux différences électrophysiologiques observées entre les sous populations neuronales composant le DRG (Craner *et al.* 2002; Berta *et al.* 2008; Lampert *et al.* 2006). L'expression de divers isoformes avait aussi été reliée avec les changements induits lors des douleurs pathologiques (Craner *et al.* 2002; Black *et al.* 2004; Chahine *et al.* 2008). Néanmoins, les études précédentes utilisaient la quantification des ARN_m ou des protéines de la totalité des neurones de DRG. Il était donc difficile d'établir un lien direct entre les modifications des ARNm et le profil électrophysiologiques étant donné la diversité des neurones présents (Berta *et al.* 2008; Strickland *et al.* 2008). Par ailleurs, les études d'immunohistochimie et hybridation *in situ* ne peuvent pas

se corréler avec l'électrophysiologie à cause des contraintes expérimentales (Black *et al.* 2004; Novakovic *et al.* 1998). Notre étude de la modulation des canaux Na^+ permet de corréler l'expression des canaux Na^+ au profil électrophysiologique d'une même cellule. Mon projet de doctorat constitue donc la première étude permettant de montrer un lien direct entre le profil électrophysiologique et la composition des canaux Na^+.

Effet du BAB sur les canaux Na^+

Dans la seconde partie, nous avons étudié la spécificité de l'anesthésie provoquée par le BAB. Lorsqu'il est injecté de façon péridurale, cet anesthésique local permet d'obtenir une réduction des douleurs chroniques chez les patients résistant aux traitements conventionnels tels que les TCA et les opiacés. De plus, l'utilisation de cette substance ne semble pas provoquer d'effets secondaires (aucun effet moteur) (Korsten *et al.* 1991). L'efficacité du BAB survient après quatre injections d'une suspension de BAB à 5%. La sélectivité de la voie nociceptive sur la voie motrice serait en partie due au confinement de l'anesthésique dans l'espace péridural. Ce dernier ne traverse pas la barrière hématoencéphalique (Grouls *et al.* 2000). L'efficacité du BAB peut durer plusieurs semaines. Ainsi confiné dans l'espace péridural, sa faible solubilité et son coefficient de partage provoquent un faible relargage en solution du BAB. Cela pourrait expliquer un effet prolongé pouvant durer plusieurs semaines.

Comme les canaux Na^+ exprimés dans les neurones moteurs et les neurones nociceptifs sont souvent distincts, nous avons donc émis l'hypothèse que la spécificité de l'analgésie provenait d'une plus grande affinité du BAB envers les canaux exprimés dans les neurones nociceptifs. Ces derniers expriment préférentiellement les canaux $Na_v1.7$ et $Na_v1.8$. $Na_v1.6$ est quant à lui préférentiellement exprimé dans les fibres motrices et les fibres sensitives non nociceptives. Pour étudier les effets spécifiques du BAB sur les canaux Na^+,

nous avons utilisé des cellules HEK293 exprimant de façon stable les canaux $Na_v1.6$, $Na_v1.7$ et $Na_v1.8$ ainsi que des neurones dissociés de DRG.

Nous avons montré une modulation différentielle par le BAB des différents canaux Na^+. L'affinité du BAB pour $Na_v1.8$ est significativement plus forte que pour $Na_v1.6$. Nous avons aussi montré que le BAB affecte plus fortement l'inactivation lente des canaux $Na_v1.7$ et $Na_v1.8$. Ce paramètre étant un facteur prépondérant dans l'excitabilité neuronale (Faber *et al.* 2012a; Hildebrand *et al.* 2011b; Han *et al.* 2012; Blair and Bean 2003; Khodorov 1991). La présence de 1µM de BAB réduit l'amplitude des PAs produits par les neurones de petits diamètres de DRG lors des trains de potentiels d'actions. Cette diminutions serait probablement causée par l'augmentation de l'inactivation lente (Vijayaragavan *et al.* 2001; Tripathi *et al.* 2006). Le BAB provoque aussi une inhibition dose-dépendante de la fréquence des PAs dans les neurones de DRG. Nous avons ainsi montré que l'effet anesthésique du BAB et la spécificité de l'anesthésie sont en partie provoqués par l'inhibition des canaux $Na_v1.7$ et $Na_v1.8$ préférentiellement à $Na_v1.6$. De plus, nous avons montré que le BAB favorise grandement l'entrée des canaux en inactivation lente, constituant très probablement son mécanisme d'action principal.

Effet des SSRI sur les canaux Na^+

Dans la troisième partie, nous avons approfondie l'étude pharmacologique des canaux Na^+ des neurones nociceptifs. Nous avons ainsi étudié l'implication des canaux Na^+ dans l'anesthésie provoquée par les SSRI. Bien que leurs mécanismes d'action soient mal compris, et compte tenu de leur innocuité, ces molécules sont fréquemment utilisées en troisième ligne dans le traitement des douleurs pathologiques et la fibromyalgie (Lee and Chen 2010). Une partie de l'anesthésie est provoquée par l'augmentation de l'activité des voies inhibitrices descendantes. Cependant, les canaux Na^+ ont précédemment été identifiés comme cible des SSRI (Lenkey *et al.* 2010; Dick *et al.* 2007). Notre hypothèse

était donc que le mécanisme d'action des SSRI menant à l'anesthésie était en partie provoqué par l'inhibition des canaux Na^+. Nous avons utilisé trois SSRI utilisés en clinique (paroxétine, fluoxétine et citalopram) et étudié leurs effets sur les canaux $Na_v1.7$ et $Na_v1.8$ exprimés de façon hétérologue dans des cellules HEK293. Les trois SSRI testés provoquent une inhibition tonique. La paroxétine présente la plus grande affinité suivie de la fluoxétine et finalement le citalopram. Ces résultats concordent avec les études montrant que le citalopram est le SSRI le plus sélectif (David *et al.* 2003). La paroxétine et la fluoxétine ont des effets similaires sur les canaux Na^+. Ils accélèrent l'entrée en inactivation lente, montrent un bloque fréquence-dépendant important et ralentissent la récupération des canaux Na^+ avec un effet plus important sur $Na_v1.7$. La façon dont ces SSRI modulent les canaux Na^+ est semblable à ce qui peut être observé avec différents anesthésiques locaux tel que la lidocaine (Chevrier *et al.* 2004). Nous suggérons donc que, dans certaines conditions, la modulation des canaux Na^+ puisse participer à l'anesthésie provoquée par les SSRI.

Pourquoi étudier les canaux sodiques?

Les canaux Na^+ sont essentiels dans la genèse et la transmission de la réponse nociceptive. Ils constituent ainsi une base moléculaire importante dans ces processus physiologiques et/ou pathologiques. La diversité des propriétés électrophysiologiques ainsi que leur expression différentielle soutient une spécialisation des fonctions des canaux sodiques (Hu *et al.* 2009; Chahine *et al.* 2005). Les différentes sous-unités α des canaux Na^+ présentes dans les neurones sensitifs périphériques collaborent à l'électrogénèse et participent la diversité des profils électrophysiologiques de ces neurones. Malgré les progrès de la compréhension du rôle des différents canaux Na^+, de nombreuses questions demeurent. En effet, les rôles spécifiques de chacun et la synergie existant entre les différents canaux Na^+ pour moduler l'excitabilité de ces neurones sont encore mal compris. De plus, les effets exacts de leur

modulation en réponse à la lésion des nerfs et l'inflammation provoquant l'hyperexcitabilité des neurones sont méconnus.

La régulation et les paramètres biophysiques des différents canaux sodiques jouent un rôle déterminant dans l'excitabilité des neurones. De multiples évidences provenant des canalopathies affectant $Na_v1.7$, $Na_v1.8$ et $Na_v1.9$ démontrent que des modifications dans les paramètres biophysiques peuvent mener à l'hyperexcitabilité des neurones périphériques (Price and Dussor 2013; Cang *et al.* 2009). De plus, la perte de fonction de $Na_v1.7$ mène à l'insensibilité congénitale à la douleur. Les canaux Na^+ responsables de l'électrogénèse spécifiquement dans les neurones périphériques semblent des cibles de choix pour le traitement des douleurs pathologiques (Gilron and Dickenson 2014; Theile and Cummins 2011).

Traitement des douleurs pathologiques

De nombreux médicaments utilisés pour traiter la douleur existent. Malgré cela, plusieurs patients résistants aux traitements conventionnels demeurent un défi pour les médecins. Une des avenues possibles pour le développement pharmacologique des anesthésiques est la découverte de nouveaux bloqueurs sélectifs et spécifiques aux canaux Na^+ présents dans les neurones nociceptifs. Plusieurs études démontrent l'efficacité des bloqueurs spécifiques de $Na_v1.7$ et $Na_v1.8$ (Ekberg *et al.* 2006; Jarvis *et al.* 2007; McGowan *et al.* 2009). Cependant, plusieurs défis doivent être relevés. Les bloqueurs des canaux sodiques disponibles présentent une faible sélectivité envers les différents canaux sodiques entraînant plusieurs effets secondaires indésirables tel que le dédoublement de la vision, la confusion et la somnolence (Waxman and Zamponi 2014). La compréhension des mécanismes d'inhibition doit donc être mieux comprise pour faciliter le criblage de ces molécules.

Choix des modèles et limites

Nous avons choisi d'étudier les rôles des canaux Na^+ dans l'électrogénèse des neurones de DRG étant donné les propriétés de ces neurones. Le corps cellulaire se retrouve dans les DRG juxtaposés à la moelle épinière, facilitant ainsi la dissociation et la culture. Cela facilite l'enregistrement de ces neurones par les différentes techniques d'électrophysiologie. De plus, la composition relativement restreinte des différents canaux Na^+ exprimés par ces neurones a permis une bonne quantification tout en permettant d'étudier la collaboration entre différents canaux Na^+.

Quoique le modèle et le choix de la technique soient appropriés pour le type d'étude que nous avons effectué dans la première partie de cette thèse, il demeure plusieurs limites à notre méthode. En effet, la limite de détection de la PCR quantitative sur les cellules unique a peut-être sous-estimé la présence de certains canaux Na^+. De plus, la diversité des canaux Na^+ que cette technique permettait de quantifier est restreinte et ne nous permettait pas de tester tous les sous-types connus, ainsi $Na_v1.1$ et $Na_v1.2$ n'ont pas été testés. Il est donc possible que des canaux Na^+ en quantité non négligeable, participant à l'excitabilité de ces neurones, n'aient pas été quantifiés. Finalement, nous avons montré que les protéines sont corrélées de façon linéaire aux ARN_m dans des rats contrôles. Cependant, il faudrait effectuer à nouveau les validations afin de déterminer si cette corrélation demeure dans les différents modèles neuropathiques où une certaine variabilité des ARN_m est observée.

L'étude des composés pharmacologiques sur les canaux Na^+ exprimés de façon hétérologue permet d'identifier les effets spécifiques à chaque canal Na^+. Cela permet ainsi une meilleure compréhension des mécanismes d'inhibition. Cependant, l'expression hétérologue ne permet pas l'étude dans des conditions physiologiques et certains mécanismes de modulation et de régulation ne sont pas présents dans ces cellules.

Conclusion

Le premier objectif de cette thèse était de comprendre comment les différentes sous-unités α des canaux Na^+ interagissent afin de moduler l'activité électrique des neurones sensitifs périphériques. Cela permet notamment une meilleure compréhension des mécanismes permettant de provoquer les multiples profils électrophysiologiques. Nous avons montré que les différents canaux Na+ modulent effectivement l'activité électrique des neurones. Il serait maintenant intéressant de déterminer comment les modifications de l'expression de canaux Na^+ affectent l'excitabilité des petits neurones de DRG.

Dans les chapitres 3 et 4, nous nous sommes intéressés à la modulation pharmacologique des canaux Na^+. Le but était de comprendre comment les molécules au pouvoir anesthésiques modulent les canaux Na^+ pour provoquer l'anesthésie. Pour ce faire, nous avons étudié l'inhibition provoquée par le BAB sur les canaux Na^+ présents dans les neurones périphériques. Nous avons observé que le BAB module différemment les canaux Na^+. Il provoque une inhibition fréquence dépendante et un déplacement de la dépendance au voltage de l'inactivation vers les potentiels plus hyperpolarisés des canaux $Na_v1.6$, $Na_v1.7$ et $Na_v1.8$. De plus, le BAB favorise l'entrée en inactivation lente des canaux $Na_v1.7$ et $Na_v1.8$, mais n'a qu'un effet négligeable sur l'entrée en inactivation lente de $Na_v1.6$. Cela est possiblement responsable de la sélectivité de l'anesthésie sans effet sur les voies motrices. Le mécanisme à la base de l'anesthésie provoqué par les SSRIs demeure tout de même partiellement incompris. Il comprend entre autres la suractivation des voies inhibitrices descendantes. Nous avons montré que les SSRI inhibent les canaux Na^+ et que, par conséquent, une partie l'anesthésie provoquée par les SSRIs peut passer par l'inhibition des canaux Na^+.

La compréhension fine des mécanismes provoquant la modulation des canaux Na^+ et leur influence sur l'excitabilité neuronale sont des outils primordiaux dans la compréhension des mécanismes menant au développement et au

maintien des douleurs pathologiques. La compréhension de l'anesthésie provoquée par la modulation pharmacologique des canaux Na^+ pourrait permettre l'élaboration de nouvelles stratégies thérapeutiques ciblant différentes propriétés des canaux Na^+.

References

Abdulla, M., Khaled, S.S., Khaled, Y.S. and Kapoor, H. 2014. Congenital insensitivity to pain in a child attending a paediatric fracture clinic. J. Pediatr. Orthop. B

Acharfi, S., Baroudi, G., Napolitano, C., Priori, S.G., Del Bufalo, A., Mok, N.S. *et al*. 2002. Novel biophysical mechanisms implicated in Brugada syndrome. Can. J. Cardiol. **18**(Suppl.B): 197B

Aggarwal, S.K. and MacKinnon, R. 1996. Contribution of the S4 segment to gating charge in the *Shaker* K^+ channel. Neuron **16**(6): 1169-1177

Akopian, A.N., Sivilotti, L. and Wood, J.N. 1996. A tetrodotoxin-resistant voltage-gated sodium channel expressed by sensory neurons. Nature **379**(6562): 257-262

Akopian, A.N., Souslova, V., England, S., Okuse, K., Ogata, N., Ure, J. *et al*. 1999. The tetrodotoxin-resistant sodium channel SNS has a specialized function in pain pathways. Nat. Neurosci. **2**(6): 541-548

Aley, K.O., Messing, R.O., Mochly-Rosen, D. and Levine, J.D. 2000. Chronic hypersensitivity for inflammatory nociceptor sensitization mediated by the epsilon isozyme of protein kinase C. J. Neurosci. **20**(12): 4680-4685

Amaya, F., Wang, H., Costigan, M., Allchorne, A.J., Hatcher, J.P., Egerton, J. *et al*. 2006. The voltage-gated sodium channel Na(v)1.9 is an effector of peripheral inflammatory pain hypersensitivity. J. Neurosci. **26**(50): 12852-12860

Argoff, C. 2011. Mechanisms of pain transmission and pharmacologic management. Curr. Med. Res. Opin. **27**(10): 2019-2031

Armstrong, C.M. and Hille, B. 1998. Voltage-gated ion channels and electrical excitability. Neuron **20**(3): 371-380

Augustine, G.J., Chikaraishi, D.M., Ehlers, M.D., Einstein, G., Fitzpatrick, D., Hall, W.C. *et al*. 2001. Neuroscience. **Second Edition**

Backx, P.H., Yue, D.T., Lawrence, J.H., Marban, E. and Tomaselli, G.F. 1992. Molecular localization of an ion-binding site within the pore of mammalian sodium channels. Science **257**(5067): 248-251

Bang, S., Yang, T.J., Yoo, S., Heo, T.H. and Hwang, S.W. 2012. Inhibition of sensory neuronal TRPs contributes to anti-nociception by butamben. Neurosci. Lett. **506**(2): 297-302

Baron, R., Binder, A. and Wasner, G. 2010. Neuropathic pain: diagnosis, pathophysiological mechanisms, and treatment. Lancet Neurol. **9**(8): 807-819

Barry, J., Gu, Y., Jukkola, P., O'Neill, B., Gu, H., Mohler, P.J. *et al*. 2014. Ankyrin-G directly binds to kinesin-1 to transport voltage-gated Na+ channels into axons. Dev. Cell **28**(2): 117-131

Beckh, S. 1990. Differential expression of sodium channel mRNAs in rat peripheral nervous system and innervated tissues. FEBS Lett. **262**(2): 317-322

Beekwilder, J.P., O'Leary, M.E., van den Broek, L.P., van Kempen, G.T., Ypey, D.L. and Van den Berg, R.J. 2003. Kv1.1 channels of dorsal root ganglion neurons are inhibited by *n*-butyl-*p*-aminobenzoate, a promising anesthetic for the treatment of chronic pain. J. Pharmacol. Exp. Ther. **304**(2): 531-538

Beekwilder, J.P., Winkelman, D.L., van Kempen, G.T., Van den Berg, R.J. and Ypey, D.L. 2005. The block of total and N-type calcium conductance in mouse sensory neurons by the local anesthetic n-butyl-p-aminobenzoate. Anesth. Analg. **100**(6): 1674-1679

Benn, S.C., Costigan, M., Tate, S., Fitzgerald, M. and Woolf, C.J. 2001. Developmental expression of the TTX-resistant voltage-gated sodium channels $Na_v1.8$ (SNS) and $Na_v1.9$ (SNS2) in primary sensory neurons. J. Neurosci. **21**(16): 6077-6085

Berta, T., Poirot, O., Pertin, M., Ji, R.R., Kellenberger, S. and Decosterd, I. 2008. Transcriptional and functional profiles of voltage-gated Na(+) channels in injured and non-injured DRG neurons in the SNI model of neuropathic pain. Mol. Cell Neurosci. **37**(2): 196-208

Black, J.A., Dib-Hajj, S., McNabola, K., Jeste, S., Rizzo, M.A., Kocsis, J.D. *et al*. 1996. Spinal sensory neurons express multiple sodium channel alpha-subunit mRNAs. Brain Res. Mol. Brain Res. **43**(1-2): 117-131

Black, J.A., Liu, S., Tanaka, M., Cummins, T.R. and Waxman, S.G. 2004. Changes in the expression of tetrodotoxin-sensitive sodium channels within dorsal root ganglia neurons in inflammatory pain. Pain **108**(3): 237-247

Black, J.A., Renganathan, M. and Waxman, S.G. 2002. Sodium channel Na(v)1.6 is expressed along nonmyelinated axons and it contributes to conduction. Brain Res. Mol. Brain Res. **105**(1-2): 19-28

Blackburn-Munro, G. and Fleetwood-Walker, S.M. 1999. The sodium channel auxiliary subunits $\beta1$ and $\beta2$ are differentially expressed in the spinal cord of neuropathic rats. Neuroscience **90**(1): 153-164

Blair, N.T. and Bean, B.P. 2002. Roles of tetrodotoxin (TTX)-sensitive Na^+ current, TTX-resistant Na^+ current, and Ca^{2+} current in the action potentials of nociceptive sensory neurons. J. Neurosci. **22**(23): 10277-10290

Blair, N.T. and Bean, B.P. 2003. Role of tetrodotoxin-resistant Na^+ current slow inactivation in adaptation of action potential firing in small-diameter dorsal root ganglion neurons. J. Neurosci. **23**(32): 10338-10350

Bourin, M., Chenu, F. and Hascoet, M. 2009. The role of sodium channels in the mechanism of action of antidepressants and mood stabilizers. Curr. Drug Targets. **10**(11): 1052-1060

Brachet, A., Leterrier, C., Irondelle, M., Fache, M.P., Racine, V., Sibarita, J.B. *et al*. 2010. Ankyrin G restricts ion channel diffusion at the axonal initial segment before the establishment of the diffusion barrier. J. Cell Biol. **191**(2): 383-395

Brackenbury, W.J., Djamgoz, M.B. and Isom, L.L. 2008. An emerging role for voltage-gated Na+ channels in cellular migration: regulation of central nervous system development and potentiation of invasive cancers. Neuroscientist. **14**(6): 571-583

Braz, J.M., Nassar, M.A., Wood, J.N. and Basbaum, A.I. 2005. Parallel "pain" pathways arise from subpopulations of primary afferent nociceptor. Neuron **47**(6): 787-793

Bustin, S.A. 2004. A to Z of Quantitative PCR.

Caffrey, J.M., Eng, D.L., Black, J.A., Waxman, S.G. and Kocsis, J.D. 1992. Three types of sodium channels in adult rat dorsal root ganglion neurons. Brain Res. **592**(1-2): 283-297

Caldwell, J.H., Schaller, K.L., Lasher, R.S., Peles, E. and Levinson, S.R. 2000. Sodium channel Na(v)1.6 is localized at nodes of Ranvier, dendrites, and synapses. Proc. Natl. Acad. Sci. U. S. A **97**(10): 5616-5620

Cang, C.L., Zhang, H., Zhang, Y.Q. and Zhao, Z.Q. 2009. PKCepsilon-dependent potentiation of TTX-resistant Nav1.8 current by neurokinin-1 receptor activation in rat dorsal root ganglion neurons. Mol. Pain **5**: 33

Cantrell, A.R., Tibbs, V.C., Yu, F.H., Murphy, B.J., Sharp, E.M., Qu, Y. *et al*. 2002. Molecular mechanism of convergent regulation of brain Na^+ channels by protein kinase C and protein kinase A anchored to AKAP-15. Mol. Cell. Neurosci. **21**(1): 63-80

Catterall, W.A. 1986. Molecular properties of voltage-sensitive sodium channels. Annu. Rev. Biochem. **55**: 953-985

Catterall, W.A. 2000. From ionic currents to molecular mechanisms: the structure and function of voltage-gated sodium channels. Neuron **26**(1): 13-25

Catterall, W.A., Goldin, A.L. and Waxman, S.G. 2005. International Union of Pharmacology. XLVII. Nomenclature and structure-function relationships of voltage-gated sodium channels. Pharmacol. Rev. **57**(4): 397-409

Cestèle, S. and Catterall, W.A. 2000. Molecular mechanisms of neurotoxin action on voltage-gated sodium channels. Biochimie **82**(9-10): 883-892

Chahine, M., Chatelier, A., Babich, O. and Krupp, J.J. 2008. Voltage-gated sodium channels in neurological disorders. CNS. Neurol. Disord. Drug Targets. **7**(2): 144-158

Chahine, M. and O'Leary, M.E. 2011. Regulatory Role of Voltage-Gated Na Channel beta Subunits in Sensory Neurons. Front Pharmacol. **2**: 70

Chahine, M., Ziane, R., Vijayaragavan, K. and Okamura, Y. 2005. Regulation of Na(v) channels in sensory neurons. Trends Pharmacol. Sci. **26**(10): 496-502

Chatelier, A., Mercier, A., Tremblier, B., Theriault, O., Moubarak, M., Benamer, N. *et al*. 2012. A distinct de novo expression of Nav1.5 sodium channels in human atrial fibroblasts differentiated into myofibroblasts. J. Physiol **590**(Pt 17): 4307-4319

Cheng, J.K. and Ji, R.R. 2008. Intracellular signaling in primary sensory neurons and persistent pain. Neurochem. Res. **33**(10): 1970-1978

Chevrier, P., Vijayaragavan, K. and Chahine, M. 2004. Differential modulation of Nav1.7 and Nav1.8 peripheral nerve sodium channels by the local anesthetic lidocaine. Br. J. Pharmacol. **142**(3): 576-584

Choi, J.S., Zhang, L., Dib-Hajj, S.D., Han, C., Tyrrell, L., Lin, Z. *et al*. 2009. Mexiletine-responsive erythromelalgia due to a new Na(v)1.7 mutation showing use-dependent current fall-off. Exp. Neurol. **216**(2): 383-389

Cox, J.J., Reimann, F., Nicholas, A.K., Thornton, G., Roberts, E., Springell, K. *et al*. 2006. An *SCN9A* channelopathy causes congenital inability to experience pain. Nature **444**(7121): 894-898

Craner, M.J., Klein, J.P., Renganathan, M., Black, J.A. and Waxman, S.G. 2002. Changes of sodium channel expression in experimental painful diabetic neuropathy. Ann. Neurol. **52**(6): 786-792

Cregg, R., Momin, A., Rugiero, F., Wood, J.N. and Zhao, J. 2010. Pain channelopathies. J. Physiol **588**(Pt 11): 1897-1904

Cummins, T.R., Aglieco, F., Renganathan, M., Herzog, R.I., Dib-Hajj, S.D. and Waxman, S.G. 2001. Nav1.3 sodium channels: rapid repriming and slow closed-state inactivation display quantitative differences after expression in a mammalian cell line and in spinal sensory neurons. J. Neurosci. **21**(16): 5952-5961

Cummins, T.R., Dib-Hajj, S.D., Black, J.A., Akopian, A.N., Wood, J.N. and Waxman, S.G. 1999. A novel persistent tetrodotoxin-resistant sodium current in SNS-null and wild-type small primary sensory neurons. J. Neurosci. **19**(24): RC43

Cummins, T.R., Dib-Hajj, S.D., Herzog, R.I. and Waxman, S.G. 2005. Nav1.6 channels generate resurgent sodium currents in spinal sensory neurons. FEBS Lett. **579**(10): 2166-2170

Cummins, T.R., Dib-Hajj, S.D. and Waxman, S.G. 2004. Electrophysiological properties of mutant Nav1.7 sodium channels in a painful inherited neuropathy. J. Neurosci. **24**(38): 8232-8236

Cummins, T.R., Howe, J.R. and Waxman, S.G. 1998. Slow closed-state inactivation: a novel mechanism underlying ramp currents in cells expressing the hNE/PN1 sodium channel. J. Neurosci. **18**(23): 9607-9619

Cummins, T.R., Sheets, P.L. and Waxman, S.G. 2007. The roles of sodium channels in nociception: Implications for mechanisms of pain. Pain **131**(3): 243-257

Cummins, T.R. and Waxman, S.G. 1997. Downregulation of tetrodotoxin-resistant sodium currents and upregulation of a rapidly repriming tetrodotoxin-sensitive sodium current in small spinal sensory neurons after nerve injury. J. Neurosci. **17**(10): 3503-3514

Cunha, S.R. and Mohler, P.J. 2009. Ankyrin protein networks in membrane formation and stabilization. J. Cell Mol. Med. **13**(11-12): 4364-4376

David, D.J., Bourin, M., Jego, G., Przybylski, C., Jolliet, P. and Gardier, A.M. 2003. Effects of acute treatment with paroxetine, citalopram and venlafaxine in vivo on noradrenaline and serotonin outflow: a microdialysis study in Swiss mice. Br. J. Pharmacol. **140**(6): 1128-1136

Debono, D.J., Hoeksema, L.J. and Hobbs, R.D. 2013. Caring for patients with chronic pain: pearls and pitfalls. J. Am. Osteopath. Assoc. **113**(8): 620-627

Deffois, A., Fage, D. and Carter, C. 1996. Inhibition of synaptosomal veratridine-induced sodium influx by antidepressants and neuroleptics used in chronic pain. Neurosci. Lett. **220**(2): 117-120

Deister, C.A., Chan, C.S., Surmeier, D.J. and Wilson, C.J. 2009. Calcium-activated SK channels influence voltage-gated ion channels to determine the precision of firing in globus pallidus neurons. J. Neurosci. **29**(26): 8452-8461

Delemotte, L., Tarek, M., Klein, M.L., Amaral, C. and Treptow, W. 2011. Intermediate states of the Kv1.2 voltage sensor from atomistic molecular dynamics simulations. Proc. Natl. Acad. Sci. U. S. A **108**(15): 6109-6114

Dempsey, E.C., Newton, A.C., Mochly-Rosen, D., Fields, A.P., Reyland, M.E., Insel, P.A. *et al*. 2000. Protein kinase C isozymes and the regulation of diverse cell responses. Am. J. Physiol. **279**(3): L429-L438

Deschênes, I., Trottier, E. and Chahine, M. 1999. Cysteine scanning analysis of the IFM cluster in the inactivation gate of a human heart sodium channel. Cardiovasc. Res. **42**(2): 521-529

Deuis, J.R., Zimmermann, K., Romanovsky, A.A., Possani, L.D., Cabot, P.J., Lewis, R.J. *et al*. 2013. An animal model of oxaliplatin-induced cold allodynia reveals a crucial role for Nav1.6 in peripheral pain pathways. Pain **154**(9): 1749-1757

Dharmshaktu, P., Tayal, V. and Kalra, B.S. 2012. Efficacy of antidepressants as analgesics: a review. J. Clin. Pharmacol. **52**(1): 6-17

Dib-Hajj, S.D., Black, J.A., Cummins, T.R., Kenney, A.M., Kocsis, J.D. and Waxman, S.G. 1998a. Rescue of α-SNS sodium channel expression in small dorsal root ganglion neurons after axotomy by nerve growth factor in vivo. J. Neurophysiol. **79**(5): 2668-2676

Dib-Hajj, S.D., Black, J.A. and Waxman, S.G. 2009. Voltage-gated sodium channels: therapeutic targets for pain. Pain Med. **10**(7): 1260-1269

Dib-Hajj, S.D., Fjell, J., Cummins, T.R., Zheng, Z., Fried, K., LaMotte, R. *et al*. 1999. Plasticity of sodium channel expression in DRG neurons in the chronic constriction injury model of neuropathic pain. Pain **83**(3): 591-600

Dib-Hajj, S.D., Tyrrell, L., Black, J.A. and Waxman, S.G. 1998b. NaN, a novel voltage-gated Na channel, is expressed preferentially in peripheral sensory neurons and down-regulated after axotomy. Proc. Natl. Acad. Sci. USA **95**(15): 8963-8968

Dib-Hajj, S.D., Yang, Y., Black, J.A. and Waxman, S.G. 2013. The Na(V)1.7 sodium channel: from molecule to man. Nat. Rev. Neurosci. **14**(1): 49-62

Dib-Hajj, S.D., Yang, Y. and Waxman, S.G. 2008. Genetics and molecular pathophysiology of Na(v)1.7-related pain syndromes. Adv. Genet. **63**: 85-110

Dick, I.E., Brochu, R.M., Purohit, Y., Kaczorowski, G.J., Martin, W.J. and Priest, B.T. 2007. Sodium channel blockade may contribute to the analgesic efficacy of antidepressants. J. Pain **8**(4): 315-324

Djouhri, L., Fang, X., Okuse, K., Wood, J.N., Berry, C.M. and Lawson, S.N. 2003. The TTX-resistant sodium channel Nav1.8 (SNS/PN3): expression and correlation with membrane properties in rat nociceptive primary afferent neurons. J. Physiol **550**(Pt 3): 739-752

Djouhri, L. and Lawson, S.N. 2004. Abeta-fiber nociceptive primary afferent neurons: a review of incidence and properties in relation to other afferent A-fiber neurons in mammals. Brain Res. Brain Res. Rev. **46**(2): 131-145

Dworkin, R.H., O'Connor, A.B., Backonja, M., Farrar, J.T., Finnerup, N.B., Jensen, T.S. *et al*. 2007. Pharmacologic management of neuropathic pain: evidence-based recommendations. Pain **132**(3): 237-251

Eberhardt, M., Nakajima, J., Klinger, A.B., Neacsu, C., Huhne, K., O'Reilly, A.O. *et al*. 2014. Inherited pain: sodium channel Nav1.7 A1632T mutation causes erythromelalgia due to a shift of fast inactivation. J. Biol. Chem. **289**(4): 1971-1980

Ekberg, J., Jayamanne, A., Vaughan, C.W., Aslan, S., Thomas, L., Mould, J. *et al*. 2006. muO-conotoxin MrVIB selectively blocks Nav1.8 sensory neuron specific sodium channels and chronic pain behavior without motor deficits. Proc. Natl. Acad. Sci. U. S. A **103**(45): 17030-17035

England, S., Bevan, S. and Docherty, R.J. 1996. PGE_2 modulates the tetrodotoxin-resistant sodium current in neonatal rat dorsal root ganglion neurones via the cyclic AMP-protein kinase A cascade. J. Physiol. **495**(Pt 2): 429-440

Estacion, M., Dib-Hajj, S.D., Benke, P.J., te Morsche, R.H., Eastman, E.M., Macala, L.J. *et al*. 2008. NaV1.7 gain-of-function mutations as a continuum: A1632E displays physiological changes associated with erythromelalgia and paroxysmal extreme pain disorder mutations and produces symptoms of both disorders. J. Neurosci. **28**(43): 11079-11088

Faber, C.G., Hoeijmakers, J.G., Ahn, H.S., Cheng, X., Han, C., Choi, J.S. *et al*. 2012a. Gain of function Nanu1.7 mutations in idiopathic small fiber neuropathy. Ann. Neurol. **71**(1): 26-39

Faber, C.G., Lauria, G., Merkies, I.S., Cheng, X., Han, C., Ahn, H.S. *et al*. 2012b. Gain-of-function Nav1.8 mutations in painful neuropathy. Proc. Natl. Acad. Sci. U. S. A **109**(47): 19444-19449

Fang, X., Djouhri, L., Black, J.A., Dib-Hajj, S.D., Waxman, S.G. and Lawson, S.N. 2002. The presence and role of the tetrodotoxin-resistant sodium channel $Na_{v1.9\ (NaN)\ in\ nociceptive\ primary\ afferent\ neurons}$. J. Neurosci. **22**(17): 7425-7433

Fang, X., Djouhri, L., McMullan, S., Berry, C., Waxman, S.G., Okuse, K. *et al*. 2006. Intense isolectin-B4 binding in rat dorsal root ganglion neurons distinguishes C-fiber nociceptors with broad action potentials and high Nav1.9 expression. J. Neurosci. **26**(27): 7281-7292

Favre, I., Moczydlowski, E. and Schild, L. 1996. On the structural basis for ionic selectivity among $Na^{+,\ K+,\ and\ Ca2+\ in\ the\ voltage-gated\ sodium\ channel}$. Biophys. J. **71**(6): 3110-3125

Fertleman, C.R., Baker, M.D., Parker, K.A., Moffatt, S., Elmslie, F.V., Abrahamsen, B. *et al*. 2006. SCN9A mutations in paroxysmal extreme pain disorder: allelic variants underlie distinct channel defects and phenotypes. Neuron **52**(5): 767-774

Finan, P.H., Goodin, B.R. and Smith, M.T. 2013. The association of sleep and pain: an update and a path forward. J. Pain **14**(12): 1539-1552

Fitzgerald, E.M., Okuse, K., Wood, J.N., Dolphin, A.C. and Moss, S.J. 1999. cAMP-dependent phosphorylation of the tetrodotoxin-resistant voltage-dependent sodium channel SNS. J. Physiol. **516**(Pt 2): 433-446

Fornaro, M., Lee, J.M., Raimondo, S., Nicolino, S., Geuna, S. and Giacobini-Robecchi, M. 2008. Neuronal intermediate filament expression in rat dorsal root ganglia sensory neurons: an in vivo and in vitro study. Neuroscience **153**(4): 1153-1163

Frohnwieser, B., Chen, L.Q., Schreibmayer, W. and Kallen, R.G. 1997. Modulation of the human cardiac sodium channel alpha-subunit by cAMP-dependent protein kinase and the responsible sequence domain. J. Physiol **498 (Pt 2)**: 309-318

Fukuoka, T., Kobayashi, K., Yamanaka, H., Obata, K., Dai, Y. and Noguchi, K. 2008. Comparative study of the distribution of the alpha-subunits of voltage-gated sodium channels in normal and axotomized rat dorsal root ganglion neurons. J. Comp Neurol. **510**(2): 188-206

Fukuoka, T., Yamanaka, H., Kobayashi, K., Okubo, M., Miyoshi, K., Dai, Y. *et al*. 2012. Re-evaluation of the phenotypic changes in L4 dorsal root ganglion neurons after L5 spinal nerve ligation. Pain **153**(1): 68-79

Galer, B.S., Harle, J. and Rowbotham, M.C. 1996. Response to intravenous lidocaine infusion predicts subsequent response to oral mexiletine: a prospective study. J. Pain Symptom. Manage. **12**(3): 161-167

Garrison, S.R., Weyer, A.D., Barabas, M.E., Beutler, B.A. and Stucky, C.L. 2014. A gain-of-function voltage-gated sodium channel 1.8 mutation drives intense hyperexcitability of A- and C-fiber neurons. Pain

Gilron, I. and Dickenson, A.H. 2014. Emerging drugs for neuropathic pain. Expert. Opin. Emerg. Drugs

Gold, M.S. 1999. Tetrodotoxin-resistant Na^+ currents and inflammatory hyperalgesia. Proc. Natl. Acad. Sci. USA **96**(14): 7645-7649

Gold, M.S. and Flake, N.M. 2005. Inflammation-mediated hyperexcitability of sensory neurons. Neurosignals. **14**(4): 147-157

Gold, M.S., Levine, J.D. and Correa, A.M. 1998. Modulation of TTX-R I_{Na} by PKC and PKA and their role in PGE_2-induced sensitization of rat sensory neurons *in vitro*. J. Neurosci. **18**(24): 10345-10355

Gold, M.S., Reichling, D.B., Shuster, M.J. and Levine, J.D. 1996. Hyperalgesic agents increase a tetrodotoxin-resistant Na^+ current in nociceptors. Proc. Natl. Acad. Sci. USA **93**(3): 1108-1112

Gold, M.S., Weinreich, D., Kim, C.S., Wang, R., Treanor, J., Porreca, F. *et al*. 2003. Redistribution of $Na_v1.8$ in uninjured axons enables neuropathic pain. J. Neurosci. **23**(1): 158-166

Goldberg, Y.P., MacFarlane, J., MacDonald, M.L., Thompson, J., Dube, M.P., Mattice, M. *et al*. 2007. Loss-of-function mutations in the Nav1.7 gene underlie congenital indifference to pain in multiple human populations. Clin. Genet. **71**(4): 311-319

Goldman, D.E. 1943. POTENTIAL, IMPEDANCE, AND RECTIFICATION IN MEMBRANES. J. Gen. Physiol **27**(1): 37-60

Gosselin-Badaroudine, P., Moreau, A. and Chahine, M. 2013. Na 1.5 mutations linked to dilated cardiomyopathy phenotypes: Is the gating pore current the missing link? Channels (Austin.) **8**(1)

Greenbaum, D., Colangelo, C., Williams, K. and Gerstein, M. 2003. Comparing protein abundance and mRNA expression levels on a genomic scale. Genome Biol. **4**(9): 117

Grieco, T.M., Malhotra, J.D., Chen, C., Isom, L.L. and Raman, I.M. 2005. Open-channel block by the cytoplasmic tail of sodium channel β4 as a mechanism for resurgent sodium current. Neuron **45**(2): 233-244

Grouls, R., Korsten, E., Ackerman, E., Hellebrekers, L., van, Z.A. and Breimer, D. 2000. Diffusion of n-butyl-p-aminobenzoate (BAB), lidocaine and bupivacaine through the human dura-arachnoid mater in vitro. Eur. J. Pharm. Sci. **12**(2): 125-131

Gudrun, T. 2006. The E-Method: a highly accurate technique for gene-expression analysis. Nature Methods **3**(7)

Guy, H.R. and Seetharamulu, P. 1986. Molecular model of the action potential sodium channel. Proc. Natl. Acad. Sci. USA **83**(2): 508-512

Hains, B.C., Klein, J.P., Saab, C.Y., Craner, M.J., Black, J.A. and Waxman, S.G. 2003. Upregulation of sodium channel Nav1.3 and functional involvement in neuronal hyperexcitability associated with central neuropathic pain after spinal cord injury. J. Neurosci. **23**(26): 8881-8892

Hains, B.C., Saab, C.Y., Klein, J.P., Craner, M.J. and Waxman, S.G. 2004. Altered sodium channel expression in second-order spinal sensory neurons contributes to pain after peripheral nerve injury. J. Neurosci. **24**(20): 4832-4839

Han, C., Hoeijmakers, J.G., Ahn, H.S., Zhao, P., Shah, P., Lauria, G. *et al*. 2012. Nav1.7-related small fiber neuropathy: impaired slow-inactivation and DRG neuron hyperexcitability. Neurology **78**(21): 1635-1643

Han, C., Vasylyev, D., Macala, L.J., Gerrits, M.M., Hoeijmakers, J.G., Bekelaar, K.J. *et al*. 2014. The G1662S NaV1.8 mutation in small fibre neuropathy: impaired inactivation underlying DRG neuron hyperexcitability. J. Neurol. Neurosurg. Psychiatry **85**(5): 499-505

Heinemann, S.H., Terlau, H. and Imoto, K. 1992a. Molecular basis for pharmacological differences between brain and cardiac sodium channels. Pflügers Arch. **422**(1): 90-92

Heinemann, S.H., Terlau, H., Stühmer, W., Imoto, K. and Numa, S. 1992b. Calcium channel characteristics conferred on the sodium channel by single mutations. Nature **356**(6368): 441-443

Henry, M.A., Freking, A.R., Johnson, L.R. and Levinson, S.R. 2007. Sodium channel Nav1.6 accumulates at the site of infraorbital nerve injury. BMC. Neurosci. **8**: 56

Herzog, R.I., Cummins, T.R., Ghassemi, F., Dib-Hajj, S.D. and Waxman, S.G. 2003. Distinct repriming and closed-state inactivation kinetics of $Na_{v1.6}$ and Nav1.7 sodium channels in mouse spinal sensory neurons. J. Physiol.

Herzog, R.I., Cummins, T.R. and Waxman, S.G. 2001. Persistent TTX-resistant Na^+ current affects resting potential and response to depolarization in simulated spinal sensory neurons. J. Neurophysiol. **86**(3): 1351-1364

Hildebrand, M.E., Mezeyova, J., Smith, P.L., Salter, M.W., Tringham, E. and Snutch, T.P. 2011a. Identification of sodium channel isoforms that mediate action potential firing in lamina I/II spinal cord neurons. Mol. Pain **7**: 67

Hildebrand, M.E., Smith, P.L., Bladen, C., Eduljee, C., Xie, J.Y., Chen, L. *et al*. 2011b. A novel slow-inactivation-specific ion channel modulator attenuates neuropathic pain. Pain **152**(4): 833-843

Ho, C. and O'Leary, M.E. 2011. Single-cell analysis of sodium channel expression in dorsal root ganglion neurons. Mol. Cell Neurosci. **46**(1): 159-166

Ho, C., Zhao, J., Malinowski, S., Chahine, M. and O'Leary, M.E. 2012. Differential expression of sodium channel beta subunits in dorsal root ganglion sensory neurons. J. Biol. Chem. **287**(18): 15044-15053

Hodgkin, A.L. and Huxley, A.F. 1939. Action potentials recorded from inside a nerve fibre. Nature **144**: 710-711

Hu, W., Tian, C., Li, T., Yang, M., Hou, H. and Shu, Y. 2009. Distinct contributions of Na(v)1.6 and Na(v)1.2 in action potential initiation and backpropagation. Nat. Neurosci. **12**(8): 996-1002

Huang, J., Han, C., Estacion, M., Vasylyev, D., Hoeijmakers, J.G., Gerrits, M.M. *et al*. 2014. Gain-of-function mutations in sodium channel NaV1.9 in painful neuropathy. Brain

Huang, J., Yang, Y., Zhao, P., Gerrits, M.M., Hoeijmakers, J.G., Bekelaar, K. *et al*. 2013. Small-fiber neuropathy Nav1.8 mutation shifts activation to hyperpolarized potentials and increases excitability of dorsal root ganglion neurons. J. Neurosci. **33**(35): 14087-14097

Hudmon, A., Choi, J.S., Tyrrell, L., Black, J.A., Rush, A.M., Waxman, S.G. *et al*. 2008. Phosphorylation of sodium channel Na(v)1.8 by p38 mitogen-activated protein kinase increases current density in dorsal root ganglion neurons. J. Neurosci. **28**(12): 3190-3201

Igwe, O.J. and Chronwall, B.M. 2001. Hyperalgesia induced by peripheral inflammation is mediated by protein kinase C βII isozyme in the rat spinal cord. Neuroscience **104**(3): 875-890

Isom, L.L. 2001. Sodium channel beta subunits: anything but auxiliary. Neuroscientist. **7**(1): 42-54

Isom, L.L. and Catterall, W.A. 1996. Na+ channel subunits and Ig domains. Nature **383**(6598): 307-308

Jarvis, M.F., Honore, P., Shieh, C.C., Chapman, M., Joshi, S., Zhang, X.F. *et al*. 2007. A-803467, a potent and selective Nav1.8 sodium channel blocker, attenuates neuropathic and inflammatory pain in the rat. Proc. Natl. Acad. Sci. U. S. A **104**(20): 8520-8525

Jin, S.X., Zhuang, Z.Y., Woolf, C.J. and Ji, R.R. 2003. p38 mitogen-activated protein kinase is activated after a spinal nerve ligation in spinal cord microglia and dorsal root ganglion neurons and contributes to the generation of neuropathic pain. J. Neurosci. **23**(10): 4017-4022

Jin, X. and Gereau IV, R.W. 2006. Acute p38-mediated modulation of tetrodotoxin-resistant sodium channels in mouse sensory neurons by tumor necrosis factor-α. J. Neurosci. **26**(1): 246-255

Julius, D. and Basbaum, A.I. 2001. Molecular mechanisms of nociception. Nature **413**(6852): 203-210

Kambouris, N.G., Hastings, L.A., Stepanovic, S., Marban, E., Tomaselli, G.F. and Balser, J.R. 1998. Mechanistic link between lidocaine block and inactivation probed by outer pore mutations in the rat μ1 skeletal muscle sodium channel. J. Physiol. **512**((Pt 3)): 693-705

Kazen-Gillespie, K.A., Ragsdale, D.S., D'Andrea, M.R., Mattei, L.N., Rogers, K.E. and Isom, L.L. 2000. Cloning, localization, and functional expression of sodium channel β1A subunits. J. Biol. Chem. **275**(2): 1079-1088

Kellenberger, S., West, J.W., Catterall, W.A. and Scheuer, T. 1997. Molecular analysis of potential hinge residues in the inactivation gate of brain type IIA Na^+ channels. J. Gen. Physiol. **109**(5): 607-617

Kerr, B.J., Souslova, V., McMahon, S.B. and Wood, J.N. 2001. A role for the TTX-resistant sodium channel Nav 1.8 in NGF-induced hyperalgesia, but not neuropathic pain. Neuroreport **12**(14): 3077-3080

Khaliq, Z.M., Gouwens, N.W. and Raman, I.M. 2003. The contribution of resurgent sodium current to high-frequency firing in Purkinje neurons: an experimental and modeling study. J. Neurosci. **23**(12): 4899-4912

Khodorov, B.I. 1991. Role of inactivation in local anesthetic action. Ann. N. Y. Acad. Sci. **625**: 224-248

Kim, C.H., Oh, Y., Chung, J.M. and Chung, K. 2001. The changes in expression of three subtypes of TTX sensitive sodium channels in sensory neurons after spinal nerve ligation. Brain Res. Mol. Brain Res. **95**(1-2): 153-161

Kim, C.H., Oh, Y., Chung, J.M. and Chung, K. 2002. Changes in three subtypes of tetrodotoxin sensitive sodium channel expression in the axotomized dorsal root ganglion in the rat. Neurosci. Lett. **323**(2): 125-128

Kim, E.K. and Choi, E.J. 2010. Pathological roles of MAPK signaling pathways in human diseases. Biochim. Biophys. Acta **1802**(4): 396-405

Kontis, K.J., Rounaghi, A. and Goldin, A.L. 1997. Sodium channel activation gating is affected by substitutions of voltage sensor positive charges in all four domains. J. Gen. Physiol. **110**(4): 391-401

Korsten, H.H.M., Ackerman, E.W., Grouls, R.J.E., van Zundert, A.A.J., Boon, W.F., Bal, F. *et al*. 1991. Long-lasting epidural sensory blockade by n-butyl-p-aminobenzoate in the terminally ill intractable cancer pain patient. Anesthesiology **75**(6): 950-960

Kretschmer, T., Nguyen, D.H., Beuerman, R.W., Happel, L.T., England, J.D., Tiel, R.L. *et al*. 2002. Painful neuromas: a potential role for a structural transmembrane protein, ankyrin G. J. Neurosurg. **97**(6): 1424-1431

Lai, J., Gold, M.S., Kim, C.S., Bian, D., Ossipov, M.H., Hunter, J.C. *et al*. 2002. Inhibition of neuropathic pain by decreased expression of the tetrodotoxin-resistant sodium channel, NaV1.8. Pain **95**(1-2): 143-152

Lampert, A., Hains, B.C. and Waxman, S.G. 2006. Upregulation of persistent and ramp sodium current in dorsal horn neurons after spinal cord injury. Exp. Brain Res. **174**(4): 660-666

Lee, Y.C. and Chen, P.P. 2010. A review of SSRIs and SNRIs in neuropathic pain. Expert. Opin. Pharmacother. **11**(17): 2813-2825

Leipold, E., Liebmann, L., Korenke, G.C., Heinrich, T., Giesselmann, S., Baets, J. *et al*. 2013. A de novo gain-of-function mutation in SCN11A causes loss of pain perception. Nat. Genet. **45**(11): 1399-1404

Lenkey, N., Karoly, R., Kiss, J.P., Szasz, B.K., Vizi, E.S. and Mike, A. 2006. The mechanism of activity-dependent sodium channel inhibition by the antidepressants fluoxetine and desipramine. Mol. Pharmacol. **70**(6): 2052-2063

Lenkey, N., Karoly, R., Lukacs, P., Vizi, E.S., Sunesen, M., Fodor, L. *et al*. 2010. Classification of drugs based on properties of sodium channel inhibition: a comparative automated patch-clamp study. PLoS. One. **5**(12): e15568

Leo, S., D'Hooge, R. and Meert, T. 2010. Exploring the role of nociceptor-specific sodium channels in pain transmission using Nav1.8 and Nav1.9 knockout mice. Behav. Brain Res. **208**(1): 149-157

Lerche, H., Peter, W., Fleischhauer, R., Pika-Hartlaub, U., Malina, T., Mitrovic, N. *et al*. 1997. Role in fast inactivation of the IV/S4-S5 loop of the human muscle Na^+ channel probed by cysteine mutagenesis. J. Physiol. **505**(Pt 2): 345-352

Lin, D.M., Loveall, B., Ewer, J., Deitcher, D.L. and Sucher, N.J. 2007. Characterization of mRNA expression in single neurons. Methods Mol. Biol. **399**: 133-152

Lindia, J.A. and Abbadie, C. 2003. Distribution of the voltage gated sodium channel Na(v)1.3-like immunoreactivity in the adult rat central nervous system. Brain Res. **960**(1-2): 132-141

Lipkind, G.M. and Fozzard, H.A. 1994. A structural model of the tetrodotoxin and saxitoxin binding site of the Na^+ channel. Biophys. J. **66**(1): 1-13

Lopez-Santiago, L.F., Pertin, M., Morisod, X., Chen, C., Hong, S., Wiley, J. *et al*. 2006. Sodium channel $\beta 2$ subunits regulate tetrodotoxin-sensitive sodium channels in small dorsal root ganglion neurons and modulate the response to pain. J. Neurosci. **26**(30): 7984-7994

Maier, T., Guell, M. and Serrano, L. 2009. Correlation of mRNA and protein in complex biological samples. FEBS Lett. **583**(24): 3966-3973

Maingret, F., Coste, B., Padilla, F., Clerc, N., Crest, M., Korogod, S.M. *et al*. 2008. Inflammatory mediators increase Nav1.9 current and excitability in nociceptors through a coincident detection mechanism. J. Gen. Physiol **131**(3): 211-225

Malemud, C.J. 2009. Focus on pain mechanisms and pharmacotherapy in the treatment of fibromyalgia syndrome. Clin. Exp. Rheumatol. **27**(5 Suppl 56): S86-S91

Malhotra, J.D., Kazen-Gillespie, K., Hortsch, M. and Isom, L.L. 2000. Sodium channel β subunits mediate homophilic cell adhesion and recruit ankyrin to points of cell-cell contact. J. Biol. Chem. **275**(15): 11383-11388

Mantegazza, M., Yu, F.H., Catterall, W.A. and Scheuer, T. 2001. Role of the C-terminal domain in inactivation of brain and cardiac sodium channels. Proc. Natl. Acad. Sci. USA **98**(26): 15348-15353

Marshall, O. 2007. Graphical design of primers with PerlPrimer. Methods Mol. Biol. **402**: 403-414

Matthews, E.A., Wood, J.N. and Dickenson, A.H. 2006. Na(v) 1.8-null mice show stimulus-dependent deficits in spinal neuronal activity. Mol. Pain **2**: 5

McCarthy, R.J., Kerns, J.M., Nath, H.A., Shulman, M. and Ivankovich, A.D. 2002. The antinociceptive and histologic effect of sciatic nerve blocks with 5% butamben suspension in rats. Anesth. Analg. **94**(3): 711-716

McGowan, E., Hoyt, S.B., Li, X., Lyons, K.A. and Abbadie, C. 2009. A peripherally acting Na(v)1.7 sodium channel blocker reverses hyperalgesia and allodynia on rat models of inflammatory and neuropathic pain. Anesth. Analg. **109**(3): 951-958

McPhee, J.C., Ragsdale, D.S., Scheuer, T. and Catterall, W.A. 1995. A critical role for transmembrane segment IVS6 of the sodium channel alpha subunit in fast inactivation. J. Biol. Chem. **270**(20): 12025-12034

Mohler, P.J., Rivolta, I., Napolitano, C., Lemaillet, G., Lambert, S., Priori, S.G. *et al*. 2004. Nav1.5 E1053K mutation causing Brugada syndrome blocks binding to ankyrin-G and expression of Nav1.5 on the surface of cardiomyocytes. Proc. Natl. Acad. Sci. U. S. A **101**(50): 17533-17538

Mohler, P.J., Schott, J.J., Gramolini, A.O., Dilly, K.W., Guatimosim, S., DuBell, W.H. *et al*. 2003. Ankyrin-B mutation causes type 4 long-QT cardiac arrhythmia and sudden cardiac death. Nature **421**(6923): 634-639

Moldovan, M., Alvarez, S., Romer, R.M. and Krarup, C. 2013. Axonal voltage-gated ion channels as pharmacological targets for pain. Eur. J. Pharmacol. **708**(1-3): 105-112

Moore, B.A., Stewart, T.M., Hill, C. and Vanner, S.J. 2002. TNBS ileitis evokes hyperexcitability and changes in ionic membrane properties of nociceptive DRG neurons. Am. J. Physiol Gastrointest. Liver Physiol **282**(6): G1045-G1051

Moreau, A., Gosselin-Badaroudine, P. and Chahine, M. 2014. Biophysics, pathophysiology, and pharmacology of ion channel gating pores. Front Pharmacol. **5**: 53

Morgan, K., Stevens, E.B., Shah, B., Cox, P.J., Dixon, A.K., Lee, K. *et al*. 2000. β3: an additional auxiliary subunit of the voltage-sensitive sodium channel that modulates channel gating with distinct kinetics. Proc. Natl. Acad. Sci. USA **97**(5): 2308-2313

Moulin, D.E., Clark, A.J., Gilron, I., Ware, M.A., Watson, C.P., Sessle, B.J. *et al*. 2007. Pharmacological management of chronic neuropathic pain - consensus statement and guidelines from the Canadian Pain Society. Pain Res. Manag. **12**(1): 13-21

Murphy, B.J., Rossie, S., De Jongh, K.S. and Catterall, W.A. 1993. Identification of the sites of selective phosphorylation and dephosphorylation of the rat brain Na^+ channel α subunit by cAMP-dependent protein kinase and phosphoprotein phosphatases. J. Biol. Chem. **268**(36): 27355-27362

Nassar, M.A., Baker, M.D., Levato, A., Ingram, R., Mallucci, G., McMahon, S.B. *et al*. 2006. Nerve injury induces robust allodynia and ectopic discharges in Nav1.3 null mutant mice. Mol. Pain **2**: 33

Nassar, M.A., Levato, A., Stirling, L.C. and Wood, J.N. 2005. Neuropathic pain develops normally in mice lacking both Nav1.7 and Nav1.8. Mol. Pain **1**: 24

Nassar, M.A., Stirling, L.C., Forlani, G., Baker, M.D., Matthews, E.A., Dickenson, A.H. *et al*. 2004. Nociceptor-specific gene deletion reveals a major role for Nav1.7 (PN1) in acute and inflammatory pain. Proc. Natl. Acad. Sci. USA **101**(34): 12706-12711

Norregaard, J., Volkmann, H. and Danneskiold-Samsoe, B. 1995. A randomized controlled trial of citalopram in the treatment of fibromyalgia. Pain **61**(3): 445-449

Novakovic, S.D., Tzoumaka, E., McGivern, J.G., Haraguchi, M., Sangameswaran, L., Gogas, K.R. *et al*. 1998. Distribution of the tetrodotoxin-resistant sodium channel PN3 in rat sensory neurons in normal and neuropathic conditions. J. Neurosci. **18**(6): 2174-2187

Obata, K., Yamanaka, H., Dai, Y., Mizushima, T., Fukuoka, T., Tokunaga, A. *et al*. 2004. Activation of extracellular signal-regulated protein kinase in the dorsal root ganglion following inflammation near the nerve cell body. Neuroscience **126**(4): 1011-1021

Ogata, N. and Tatebayashi, H. 1993. Kinetic analysis of two types of Na^+ channels in rat dorsal root ganglia. J. Physiol. **466**: 9-37

Oh, Y., Sashihara, S., Black, J.A. and Waxman, S.G. 1995. Na^+ channel β1 subunit mRNA: differential expression in rat spinal sensory neurons. Brain Res. Mol. Brain Res. **30**(2): 357-361

Ohno, K., Yokota, A., Hirofuji, S., Kanbara, K., Ohtsuka, H. and Kinoshita, M. 2010. Altered expression of sodium channel distribution in the dorsal root ganglion after gradual elongation of rat sciatic nerves. J. Orthop. Res. **28**(4): 481-486

Patapoutian, A., Tate, S. and Woolf, C.J. 2009. Transient receptor potential channels: targeting pain at the source. Nat. Rev. Drug Discov. **8**(1): 55-68

Pérez-garcía, M.T., Chiamvimonvat, N., Marban, E. and Tomaselli, G.F. 1996. Structure of the sodium channel pore revealed by serial cysteine mutagenesis. Proc. Natl. Acad. Sci. USA **93**(1): 300-304

Pertin, M., Ji, R.R., Berta, T., Powell, A.J., Karchewski, L., Tate, S.N. *et al*. 2005. Upregulation of the voltage-gated sodium channel β2 subunit in neuropathic pain models: characterization of expression in injured and non-injured primary sensory neurons. J. Neurosci. **25**(47): 10970-10980

Pless, S.A., Galpin, J.D., Niciforovic, A.P. and Ahern, C.A. 2011. Contributions of counter-charge in a potassium channel voltage-sensor domain. Nat. Chem. Biol. **7**(9): 617-623

Porreca, F., Lai, J., Bian, D., Wegert, S., Ossipov, M.H., Eglen, R.M. *et al*. 1999. A comparison of the potential role of the tetrodotoxin-insensitive sodium channels, PN3/SNS and NaN/SNS2, in rat models of chronic pain. Proc. Natl. Acad. Sci. USA **96**(14): 7640-7644

Poulin, H., Bruhova, I., Timour, Q., Theriault, O., Beaulieu, M., Frassati, D. *et al*. 2014. Fluoxetine Blocks Nav1.5 Channels Via a Mechanism Similar to That of Class 1 Antiarrhythmics. Mol. Pharmacol.

Price, T.J. and Dussor, G. 2013. AMPK: An emerging target for modification of injury-induced pain plasticity. Neurosci. Lett. **557 Pt A**: 9-18

Priest, B.T., Murphy, B.A., Lindia, J.A., Diaz, C., Abbadie, C., Ritter, A.M. *et al*. 2005. Contribution of the tetrodotoxin-resistant voltage-gated sodium channel NaV1.9 to sensory transmission and nociceptive behavior. Proc. Natl. Acad. Sci. U. S. A **102**(26): 9382-9387

Qin, N., D'Andrea, M.R., Lubin, M.L., Shafaee, N., Codd, E.E. and Correa, A.M. 2003. Molecular cloning and functional expression of the human sodium channel β_{1B} subunit, a novel splicing variant of the $\beta 1$ subunit. Eur. J. Biochem. **270**(23): 4762-4770

Ragsdale, D.S., McPhee, J.C., Scheuer, T. and Catterall, W.A. 1994. Molecular determinants of state-dependent block of Na^+ channels by local anesthetics. Science **265**(5179): 1724-1728

Ragsdale, D.S., McPhee, J.C., Scheuer, T. and Catterall, W.A. 1996. Common molecular determinants of local anesthetic, antiarrhythmic, and anticonvulsant block of voltage-gated Na^+ channels. Proc. Natl. Acad. Sci. USA **93**(17): 9270-9275

Raman, I.M. and Bean, B.P. 1997. Resurgent sodium current and action potential formation in dissociated cerebellar Purkinje neurons. J. Neurosci. **17**(12): 4517-4526

Raouf, R., Quick, K. and Wood, J.N. 2010. Pain as a channelopathy. J. Clin. Invest **120**(11): 3745-3752

Raphael, J.H., Southall, J.L. and Kitas, G.D. 2003. Adverse effects of intravenous lignocaine therapy in fibromyalgia syndrome. Rheumatology. (Oxford) **42**(1): 185-186

Ratcliffe, C.F., Westenbroek, R.E., Curtis, R. and Catterall, W.A. 2001. Sodium channel $\beta 1$ and $\beta 3$ subunits associate with neurofascin through their extracellular immunoglobulin-like domain. J. Cell Biol. **154**(2): 427-434

Renganathan, M., Cummins, T.R. and Waxman, S.G. 2001. Contribution of $Na_v1.8$ sodium channels to action potential electrogenesis in DRG neurons. J. Neurophysiol. **86**(2): 629-640

Richmond, J.E., Featherstone, D.E., Hartmann, H.A. and Ruben, P.C. 1998. Slow inactivation in human cardiac sodium channels. Biophys. J. **74**(6): 2945-2952

Rogers, M., Tang, L., Madge, D.J. and Stevens, E.B. 2006. The role of sodium channels in neuropathic pain. Semin. Cell Dev. Biol. **17**(5): 571-581

Rosenberg, M. 2003. Goodman and Gilman's The Pharmacological Basis of Therapeutics, 10th Edition. Anesth. Prog. **50**(4): 190-191

Roskell, N.S., Beard, S.M., Zhao, Y. and Le, T.K. 2011. A meta-analysis of pain response in the treatment of fibromyalgia. Pain Pract. **11**(6): 516-527

Rossie, S. and Catterall, W.A. 1989. Phosphorylation of the alpha subunit of rat brain sodium channels by cAMP-dependent protein kinase at a new site containing Ser686 and Ser687. J. Biol. Chem. **264**(24): 14220-14224

Rowbotham, M.C., Davies, P.S., Verkempinck, C. and Galer, B.S. 1996. Lidocaine patch: double-blind controlled study of a new treatment method for post-herpetic neuralgia. Pain **65**(1): 39-44

Roza, C., Laird, J.M., Souslova, V., Wood, J.N. and Cervero, F. 2003. The tetrodotoxin-resistant Na+ channel Nav1.8 is essential for the expression of spontaneous activity in damaged sensory axons of mice. J. Physiol **550**(Pt 3): 921-926

Rush, A.M., Bräu, M.E., Elliott, A.A. and Elliott, J.R. 1998. Electrophysiological properties of sodium current subtypes in small cells from adult rat dorsal root ganglia. J. Physiol. **511**(Pt 3): 771-789

Rush, A.M., Cummins, T.R. and Waxman, S.G. 2007. Multiple sodium channels and their roles in electrogenesis within dorsal root ganglion neurons. J. Physiol. **579**(Pt 1): 1-14

Rush, A.M., Dib-Hajj, S.D., Liu, S., Cummins, T.R., Black, J.A. and Waxman, S.G. 2006. A single sodium channel mutation produces hyper- or hypoexcitability in different types of neurons. Proc. Natl. Acad. Sci. U. S. A **103**(21): 8245-8250

Rush, A.M. and Waxman, S.G. 2004. PGE(2) increases the tetrodotoxin-resistant Na(v)1.9 sodium current in mouse DRG neurons via G-proteins. Brain Res. **1023**(2): 264-271

Saarto, T. and Wiffen, P.J. 2007. Antidepressants for neuropathic pain. Cochrane. Database. Syst. Rev. (4): CD005454

Sandkuhler, J. 2009. Models and mechanisms of hyperalgesia and allodynia. Physiol Rev. **89**(2): 707-758

Schafranski, M.D., Malucelli, T., Machado, F., Takeshi, H., Kaiber, F., Schmidt, C. *et al*. 2009. Intravenous lidocaine for fibromyalgia syndrome: an open trial. Clin. Rheumatol. **28**(7): 853-855

Schild, J.H. and Kunze, D.L. 2012. Differential distribution of voltage-gated channels in myelinated and unmyelinated baroreceptor afferents. Auton. Neurosci. **172**(1-2): 4-12

Scholz, A. 2002. Mechanisms of (local) anaesthetics on voltage-gated sodium and other ion channels. Br. J. Anaesth. **89**(1): 52-61

Scholz, J. and Woolf, C.J. 2007. The neuropathic pain triad: neurons, immune cells and glia. Nat. Neurosci. **10**(11): 1361-1368

Sculptoreanu, A. and De Groat, W.C. 2007. Neurokinins enhance excitability in capsaicin-responsive DRG neurons. Exp. Neurol. **205**(1): 92-100

Sculptoreanu, A., De Groat, W.C., Buffington, C.A. and Birder, L.A. 2005. Abnormal excitability in capsaicin-responsive DRG neurons from cats with feline interstitial cystitis. Exp. Neurol. **193**(2): 437-443

Shah, B.S., Gonzalez, M.I., Bramwell, S., Pinnock, R.D., Lee, K. and Dixon, A.K. 2001a. Beta3, a novel auxiliary subunit for the voltage gated sodium channel is upregulated in sensory neurones following streptozocin induced diabetic neuropathy in rat. Neurosci. Lett. **309**(1): 1-4

Shah, B.S., Stevens, E.B., Gonzalez, M.I., Bramwell, S., Pinnock, R.D., Lee, K. *et al*. 2000. beta3, a novel auxiliary subunit for the voltage-gated sodium channel, is expressed preferentially in sensory neurons and is upregulated in the chronic constriction injury model of neuropathic pain. Eur. J. Neurosci. **12**(11): 3985-3990

Shah, B.S., Stevens, E.B., Pinnock, R.D., Dixon, A.K. and Lee, K. 2001b. Developmental expression of the novel voltage-gated sodium channel auxiliary subunit β3, in rat CNS. J. Physiol. **534**(Pt 3): 763-776

Sheets, P.L., Jackson, J.O., Waxman, S.G., Dib-Hajj, S.D. and Cummins, T.R. 2007. A Nav1.7 channel mutation associated with hereditary erythromelalgia contributes to neuronal hyperexcitability and displays reduced lidocaine sensitivity. J. Physiol **581**(Pt 3): 1019-1031

Shirahata, E., Iwasaki, H., Takagi, M., Lin, C., Bennett, V., Okamura, Y. *et al*. 2006. Ankyrin-G regulates inactivation gating of the neuronal sodium channel, Nav1.6. J. Neurophysiol. **96**(3): 1347-1357

Shulman, M., Harris, J.E., Lubenow, T.R., Nath, H.A. and Ivankovich, A.D. 2000. Comparison of epidural butamben to celiac plexus neurolytic block for the treatment of the pain of pancreatic cancer. Clin. J. Pain **16**(4): 304-309

Shulman, M., Lubenow, T.R., Nath, H.A., Blazek, W., McCarthy, R.J. and Ivankovich, A.D. 1998. Nerve blocks with 5% butamben suspension for the treatment of chronic pain syndromes. Reg Anesth. Pain Med. **23**(4): 395-401

Sindrup, S.H., Bjerre, U., Dejgaard, A., Brosen, K., Aaes-Jorgensen, T. and Gram, L.F. 1992. The selective serotonin reuptake inhibitor citalopram relieves the symptoms of diabetic neuropathy. Clin. Pharmacol. Ther. **52**(5): 547-552

Sindrup, S.H., Gram, L.F., Brosen, K., Eshoj, O. and Mogensen, E.F. 1990. The selective serotonin reuptake inhibitor paroxetine is effective in the treatment of diabetic neuropathy symptoms. Pain **42**(2): 135-144

Smith, M.R., Smith, R.D., Plummer, N.W., Meisler, M.H. and Goldin, A.L. 1998. Functional analysis of the mouse Scn8a sodium channel. J. Neurosci. **18**(16): 6093-6102

Smith, R.D. and Goldin, A.L. 1996. Phosphorylation of brain sodium channels in the I-II linker modulates channel function in *Xenopus* oocytes. J. Neurosci. **16**(6): 1965-1974

Smith, R.D. and Goldin, A.L. 1998. Functional analysis of the rat I sodium channel in *Xenopus* oocytes. J. Neurosci. **18**(3): 811-820

Song, X.J., Zhang, J.M., Hu, S.J. and LaMotte, R.H. 2003. Somata of nerve-injured sensory neurons exhibit enhanced responses to inflammatory mediators. Pain **104**(3): 701-709

Stahlberg, A., Hakansson, J., Xian, X., Semb, H. and Kubista, M. 2004. Properties of the reverse transcription reaction in mRNA quantification. Clin. Chem. **50**(3): 509-515

Stamboulian, S., Choi, J.S., Ahn, H.S., Chang, Y.W., Tyrrell, L., Black, J.A. *et al*. 2010. ERK1/2 mitogen-activated protein kinase phosphorylates sodium channel Na(v)1.7 and alters its gating properties. J. Neurosci. **30**(5): 1637-1647

Stevens, M., Peigneur, S. and Tytgat, J. 2011. Neurotoxins and their binding areas on voltage-gated sodium channels. Front Pharmacol. **2**: 71

Strickland, I.T., Martindale, J.C., Woodhams, P.L., Reeve, A.J., Chessell, I.P. and McQueen, D.S. 2008. Changes in the expression of NaV1.7, NaV1.8 and NaV1.9 in a distinct population of dorsal root ganglia innervating the rat knee joint in a model of chronic inflammatory joint pain. Eur. J. Pain **12**(5): 564-572

Stucky, C.L. and Lewin, G.R. 1999. Isolectin B(4)-positive and -negative nociceptors are functionally distinct. J. Neurosci. **19**(15): 6497-6505

Stühmer, W., Conti, F., Suzuki, H., Wang, X.D., Noda, M., Yahagi, N. *et al*. 1989. Structural parts involved in activation and inactivation of the sodium channel. Nature **339**(6226): 597-603

Sucher, N.J., Deitcher, D.L., Baro, D.J., Warrick, R.M. and Guenther, E. 2000. Genes and channels: patch/voltage-clamp analysis and single-cell RT-PCR. Cell Tissue Res. **302**(3): 295-307

Sumpton, J.E. and Moulin, D.E. 2014. Fibromyalgia. Handb. Clin. Neurol. **119**: 513-527

Takahashi, N., Kikuchi, S., Dai, Y., Kobayashi, K., Fukuoka, T. and Noguchi, K. 2003. Expression of auxiliary beta subunits of sodium channels in primary afferent neurons and the effect of nerve injury. Neuroscience **121**(2): 441-450

Tao, X., Lee, A., Limapichat, W., Dougherty, D.A. and MacKinnon, R. 2010. A gating charge transfer center in voltage sensors. Science **328**(5974): 67-73

Terlau, H., Heinemann, S.H., Stühmer, W., Pusch, M., Conti, F., Imoto, K. *et al*. 1991. Mapping the site of block by tetrodotoxin and saxitoxin of sodium channel II. FEBS Lett. **293**(1-2): 93-96

Thakor, D.K., Lin, A., Matsuka, Y., Meyer, E.M., Ruangsri, S., Nishimura, I. *et al*. 2009. Increased peripheral nerve excitability and local NaV1.8 mRNA up-regulation in painful neuropathy. Mol. Pain **5**: 14

Theile, J.W. and Cummins, T.R. 2011. Recent developments regarding voltage-gated sodium channel blockers for the treatment of inherited and acquired neuropathic pain syndromes. Front Pharmacol. **2**: 54

Theriault, O., Poulin, H., Sculptoreanu, A., De Groat, W.C., O'Leary, M.E. and Chahine, M. 2014. Modulation of peripheral Na(+) channels and neuronal firing by n-butyl-p-aminobenzoate. Eur. J. Pharmacol. **727**: 158-166

Tikhonov, D.B. and Zhorov, B.S. 2005. Modeling P-loops domain of sodium channel: homology with potassium channels and interaction with ligands. Biophys. J. **88**(1): 184-197

Toledo-Aral, J.J., Moss, B.L., He, Z.J., Koszowski, A.G., Whisenand, T., Levinson, S.R. *et al*. 1997. Identification of PN1, a predominant voltage-dependent sodium channel expressed principally in peripheral neurons. Proc. Natl. Acad. Sci. USA **94**(4): 1527-1532

Treede, R.D., Jensen, T.S., Campbell, J.N., Cruccu, G., Dostrovsky, J.O., Griffin, J.W. *et al*. 2008. Neuropathic pain: redefinition and a grading system for clinical and research purposes. Neurology **70**(18): 1630-1635

Trelle, S., Reichenbach, S., Wandel, S., Hildebrand, P., Tschannen, B., Villiger, P.M. *et al*. 2011. Cardiovascular safety of non-steroidal anti-inflammatory drugs: network meta-analysis. BMJ **342**: c7086

Trescot, A.M., Datta, S., Lee, M. and Hansen, H. 2008. Opioid pharmacology. Pain Physician **11**(2 Suppl): S133-S153

Tripathi, P.K., Trujillo, L., Cardenas, C.A., Cardenas, C.G., de Armendi, A.J. and Scroggs, R.S. 2006. Analysis of the variation in use-dependent inactivation of high-threshold tetrodotoxin-resistant sodium currents recorded from rat sensory neurons. Neuroscience **143**(4): 923-938

Van den Berg, R.J., Van Soest, P.F., Wang, Z., Grouls, R.J. and Korsten, H.H. 1995. The local anesthetic n-butyl-p-aminobenzoate selectively affects inactivation of fast sodium currents in cultured rat sensory neurons. Anesthesiology **82**(6): 1463-1473

Van den Berg, R.J., Wang, Z., Grouls, R.J.E. and Korsten, H.H.M. 1996. The local anesthetic, *n*-butyl-*p*-aminobenzoate, reduces rat sensory neuron excitability by differential actions on fast and slow Na^+ current components. Eur. J. Pharmacol. **316**(1): 87-95

Vanoye, C.G., Gurnett, C.A., Holland, K.D., George, A.L., Jr. and Kearney, J.A. 2014. Novel SCN3A variants associated with focal epilepsy in children. Neurobiol. Dis. **62**: 313-322

Vanoye, C.G., Kunic, J.D., Ehring, G.R. and George, A.L., Jr. 2013. Mechanism of sodium channel NaV1.9 potentiation by G-protein signaling. J. Gen. Physiol **141**(2): 193-202

Vargas-Alarcon, G., Alvarez-Leon, E., Fragoso, J.M., Vargas, A., Martinez, A., Vallejo, M. *et al*. 2012. A SCN9A gene-encoded dorsal root ganglia sodium channel polymorphism associated with severe fibromyalgia. BMC. Musculoskelet. Disord. **13**: 23

Veldkamp, M.W., Viswanathan, P.C., Bezzina, C., Baartscheer, A., Wilde, A.A.M. and Balser, J.R. 2000. Two distinct congenital arrhythmias evoked by a multidysfunctional Na^+ channel. Circ. Res. **86**(9): E91-E97

Vijayaragavan, K., Boutjdir, M. and Chahine, M. 2004. Modulation of nav1.7 and nav1.8 peripheral nerve sodium channels by protein kinase a and protein kinase C. J. Neurophysiol. **91**(4): 1556-1569

Vijayaragavan, K., O'Leary, M.E. and Chahine, M. 2001. Gating properties of $Na_v1.7$ and $Na_v1.8$ peripheral nerve sodium channels. J. Neurosci. **21**(20): 7909-7918

Wallace, R.H., Scheffer, I.E., Barnett, S., Richards, M., Dibbens, L., Desai, R.R. *et al*. 2001. Neuronal sodium-channel alpha1-subunit mutations in generalized epilepsy with febrile seizures plus. Am. J. Hum. Genet. **68**(4): 859-865

Wang, J., Ou, S.W., Wang, Y.J., Kameyama, M., Kameyama, A. and Zong, Z.H. 2009. Analysis of four novel variants of Nav1.5/SCN5A cloned from the brain. Neurosci. Res. **64**(4): 339-347

Wang, Q., Chen, S., Chen, Q., Wan, X., Shen, J., Hoeltge, G.A. *et al*. 2004. The common *SCN5A* mutation R1193Q causes LQTS-type electrophysiological alterations of the cardiac sodium channel. J. Med. Genet. **41**(5): e66

Wang, S.Y. and Wang, G.K. 1997. A mutation in segment I-S6 alters slow inactivation of sodium channels. Biophys. J. **72**(4): 1633-1640

Wang, W., Atianjoh, F., Gauda, E.B., Yaster, M., Li, Y. and Tao, Y.X. 2011. Increased expression of sodium channel subunit Nav1.1 in the injured dorsal root ganglion after peripheral nerve injury. Anat. Rec. (Hoboken.) **294**(8): 1406-1411

Waxman, S.G. 2013. Painful Na-channelopathies: an expanding universe. Trends Mol. Med. **19**(7): 406-409

Waxman, S.G., Kocsis, J.D. and Black, J.A. 1994. Type III sodium channel mRNA is expressed in embryonic but not adult spinal sensory neurons, and is reexpressed following axotomy. J. Neurophysiol. **72**(1): 466-470

Waxman, S.G. and Zamponi, G.W. 2014. Regulating excitability of peripheral afferents: emerging ion channel targets. Nat. Neurosci. **17**(2): 153-163

Weller, C.M., Pelzer, N., de, V.B., Lopez, M.A., De, F.O., Pascual, J. *et al*. 2014. Two novel SCN1A mutations identified in families with familial hemiplegic migraine. Cephalalgia

Whitaker, W.R., Faull, R.L., Waldvogel, H.J., Plumpton, C.J., Emson, P.C. and Clare, J.J. 2001. Comparative distribution of voltage-gated sodium channel proteins in human brain. Brain Res. Mol. Brain Res. **88**(1-2): 37-53

Winkelman, D.L., Beck, C.L., Ypey, D.L. and O'Leary, M.E. 2005. Inhibition of the A-type K+ channels of dorsal root ganglion neurons by the long-duration anesthetic butamben. J. Pharmacol. Exp. Ther. **314**(3): 1177-1186

Winlove, C.I. and Roberts, A. 2012. The firing patterns of spinal neurons: in situ patch-clamp recordings reveal a key role for potassium currents. Eur. J. Neurosci. **36**(7): 2926-2940

Wittmack, E.K., Rush, A.M., Hudmon, A., Waxman, S.G. and Dib-Hajj, S.D. 2005. Voltage-gated sodium channel Nav1.6 is modulated by p38 mitogen-activated protein kinase. J. Neurosci. **25**(28): 6621-6630

Wolfe, F., Smythe, H.A., Yunus, M.B., Bennett, R.M., Bombardier, C., Goldenberg, D.L. *et al*. 1990. The American College of Rheumatology 1990 Criteria for the Classification of Fibromyalgia. Report of the Multicenter Criteria Committee. Arthritis Rheum. **33**(2): 160-172

Woolf, C.J. 2004. Pain: moving from symptom control toward mechanism-specific pharmacologic management. Ann. Intern. Med. **140**(6): 441-451

Woolf, C.J. and Ma, Q. 2007. Nociceptors--noxious stimulus detectors. Neuron **55**(3): 353-364

Wu, L., Nishiyama, K., Hollyfield, J.G. and Wang, Q. 2002. Localization of Nav1.5 sodium channel protein in the mouse brain. Neuroreport **13**(18): 2547-2551

Xiao, H.S., Huang, Q.H., Zhang, F.X., Bao, L., Lu, Y.J., Guo, C. *et al*. 2002. Identification of gene expression profile of dorsal root ganglion in the rat peripheral axotomy model of neuropathic pain. Proc. Natl. Acad. Sci. U. S. A **99**(12): 8360-8365

Xie, W., Strong, J.A., Ye, L., Mao, J.X. and Zhang, J.M. 2013. Knockdown of sodium channel NaV1.6 blocks mechanical pain and abnormal bursting activity of afferent neurons in inflamed sensory ganglia. Pain **154**(8): 1170-1180

Xiong, W., Li, R.A., Tian, Y. and Tomaselli, G.F. 2003. Molecular motions of the outer ring of charge of the sodium channel: do they couple to slow inactivation? J. Gen. Physiol. **122**(3): 323-332

Yamagishi, T., Janecki, M., Marban, E. and Tomaselli, G.F. 1997. Topology of the P segments in the sodium channel pore revealed by cysteine mutagenesis. Biophys. J. **73**(1): 195-204

Yamane, H., De Groat, W.C. and Sculptoreanu, A. 2007. Effects of ralfinamide, a Na+ channel blocker, on firing properties of nociceptive dorsal root ganglion neurons of adult rats. Exp. Neurol. **208**(1): 63-72

Yang, N., George, A.L., Jr. and Horn, R. 1996. Molecular basis of charge movement in voltage-gated sodium channels. Neuron **16**(1): 113-122

Yang, N.B. and Horn, R. 1995. Evidence for voltage-dependent S4 movement in sodium channels. Neuron **15**(1): 213-218

Yang, Y., Wang, Y., Li, S., Xu, Z., Li, H., Ma, L. *et al*. 2004. Mutations in SCN9A, encoding a sodium channel alpha subunit, in patients with primary erythermalgia. J. Med. Genet. **41**(3): 171-174

Yoshimura, N., Seki, S., Novakovic, S.D., Tzoumaka, E., Erickson, V.L., Erickson, K.A. *et al*. 2001. The involvement of the tetrodotoxin-resistant sodium channel $na_v1.8$ (PN3/SNS) in a rat model of visceral pain. J. Neurosci. **21**(21): 8690-8696

Yu, F.H., Westenbroek, R.E., Silos-Santiago, I., McCormick, K.A., Lawson, D., Ge, P. *et al*. 2003. Sodium channel β4, a new disulfide-linked auxiliary subunit with similarity to β2. J. Neurosci. **23**(20): 7577-7585

Yu, F.H., Yarov-Yarovoy, V., Gutman, G.A. and Catterall, W.A. 2005. Overview of molecular relationships in the voltage-gated ion channel superfamily. Pharmacol. Rev. **57**(4): 387-395

Zhang, X.Y., Wen, J., Yang, W., Wang, C., Gao, L., Zheng, L.H. *et al*. 2013. Gain-of-Function Mutations in SCN11A Cause Familial Episodic Pain. Am. J. Hum. Genet. **93**(5): 957-966

Zhao, J., O'Leary, M.E. and Chahine, M. 2011. Regulation of Nav1.6 and Nav1.8 peripheral nerve Na+ channels by auxiliary beta-subunits. J. Neurophysiol. **106**(2): 608-619

Zhao, Z.Q., Chiechio, S., Sun, Y.G., Zhang, K.H., Zhao, C.S., Scott, M. *et al*. 2007. Mice lacking central serotonergic neurons show enhanced inflammatory pain and an impaired analgesic response to antidepressant drugs. J. Neurosci. **27**(22): 6045-6053

Zheng, T., Kakimura, J., Matsutomi, T., Nakamoto, C. and Ogata, N. 2007. Prostaglandin E2 has no effect on two components of tetrodotoxin-resistant Na+ current in mouse dorsal root ganglion. J. Pharmacol. Sci. **103**(1): 93-102

Zhou, D., Lambert, S., Malen, P.L., Carpenter, S., Boland, L.M. and Bennett, V. 1998. AnkyrinG is required for clustering of voltage-gated Na channels at axon initial segments and for normal action potential firing. J. Cell Biol. **143**(5): 1295-1304

Zhou, J., Yi, J., Hu, N.N., George, A.L., Jr. and Murray, K.T. 2000. Activation of protein kinase A modulates trafficking of the human cardiac sodium channel in *Xenopus* oocytes. Circ. Res. **87**(1): 33-38

Zimmermann, K., Leffler, A., Babes, A., Cendan, C.M., Carr, R.W., Kobayashi, J. *et al*. 2007. Sensory neuron sodium channel Nav1.8 is essential for pain at low temperatures. Nature **447**(7146): 855-858

Annexe

J Physiol 590.17 (2012) pp 4307–4319

The Journal of Physiology

A distinct *de novo* expression of $Na_v1.5$ sodium channels in human atrial fibroblasts differentiated into myofibroblasts

Aurélien Chatelier[1], Aurélie Mercier[1], Boris Tremblier[1], Olivier Thériault[2], Majed Moubarak[1], Najate Benamer[1], Pierre Corbi[3], Patrick Bois[1], Mohamed Chahine[2] and Jean François Faivre[1]

[1]*Institut de Physiologie et Biologie Cellulaires, FRE 3511, CNRS/Université de Poitiers, Poitiers, France*
[2]*Institut universitaire en santé mentale de Québec, Université Laval, Québec, Canada*
[3]*Service de chirurgie cardio-thoracique, CHU Poitiers, France*

Key point

- Fibroblasts play a major role in heart physiology. In pathological conditions, they can lead to cardiac fibrosis when they differentiate into myofibroblasts.
- This differentiated status is associated with changes in expression profile leading to neo-expression of proteins such as ionic channels.
- The present study investigates electrophysiological changes associated with fibroblast differentiation focusing on voltage-gated sodium channels in human atrial fibroblasts and myofibroblasts.
- We show that human atrial fibroblast differentiation in myofibroblasts is associated with *de novo* expression of voltage gated sodium current. Multiple arguments support that this current is predominantly supported by the $Na_v1.5$ α-subunit which may generate a persistent sodium entry into myofibroblasts.
- Our data revealed that $Na_v1.5$ α-subunit expression is not restricted to cardiac myocytes within the atrium. Since fibrosis is one of the fundamental mechanisms implicated in atrial fibrillation, it is of great interest to investigate how this channel could influence myofibroblasts function.

Abstract Fibroblasts play a major role in heart physiology. They are at the origin of the extracellular matrix renewal and production of various paracrine and autocrine factors. In pathological conditions, fibroblasts proliferate, migrate and differentiate into myofibroblasts leading to cardiac fibrosis. This differentiated status is associated with changes in expression profile leading to neo-expression of proteins such as ionic channels. The present study investigates further electrophysiological changes associated with fibroblast differentiation focusing on the activity of voltage-gated sodium channels in human atrial fibroblasts and myofibroblasts. Using the patch clamp technique we show that human atrial myofibroblasts display a fast inward voltage gated sodium current with a density of 13.28 ± 2.88 pA pF^{-1} whereas no current was detectable in non-differentiated fibroblasts. Quantitative RT-PCR reveals a large amount of transcripts encoding the $Na_v1.5$ α-subunit with a fourfold increased expression level in myofibroblasts when compared to fibroblasts. Accordingly, half of the current was blocked by 1 μM of tetrodotoxin and immunocytochemistry experiments reveal the presence of $Na_v1.5$ proteins. Overall, this current exhibits similar biophysical characteristics to sodium currents found in cardiac myocytes except for the window current that is enlarged for potentials between -100 and -20 mV. Since fibrosis is one of the fundamental mechanisms implicated in atrial fibrillation, it is of great interest to investigate how this current could influence myofibroblast properties. Moreover, since

DOI: 10.1113/jphysiol.2012.233593

several $Na_v1.5$ mutations are related to cardiac pathologies, this study offers a new avenue on the fibroblasts involvement of these mutations.

(Received 2 April 2012; accepted after revision 10 July 2012; first published online 16 July 2012)
Corresponding author A. Chatelier: FRE CNRS/Université de Poitiers no. 3511, Pôle Biologie Santé, Bâtiment B36, 1 rue Georges Bonnet, BP 633, 86022 Poitiers Cedex. Email: aurelien.chatelier@univ-poitiers.fr

Abbreviations BDM, 2,3-butanedione 2-monoxime; *k*, Boltzmann steepness coefficient; qPCR, quantitative PCR; RT-qPCR, reverse transcriptase-quantitative polymerase chain reaction; α-SMA, α-smooth muscle actin; TTX, tetrodotoxin; $V_{1/2}$, membrane potential at half-maximal activation or inactivation; VGSC, voltage gated sodium channel.

Introduction

Fibroblasts represent the most abundant cell type founded in cardiac tissue. Although these cells have received less attention than cardiomyocytes, they are important players in many processes such as control of extracellular matrix renewal and production of various paracrine and autocrine factors (Brilla *et al.* 1995; Ellmers *et al.* 2002; Baudino *et al.* 2006). Within the heart, at least two fibroblast populations can be distinguished depending on their tissue localization in the atria or the ventricles. Atrial and ventricular fibroblasts display fundamental differences in their morphology, gene expression profiles and proliferation properties (Burstein *et al.* 2008). It was hypothesized that these characteristics explain, at least in part, the greater propensity of atria to fibrosis compared to the ventricles (Nakajima *et al.* 2000; Verheule *et al.* 2004; Xiao *et al.* 2004). This susceptibility is important since fibrosis and tissue remodelling is one of the fundamental mechanisms implicated in atrial fibrillation (Allessie *et al.* 2002; Burstein & Nattel, 2008), the most common sustained arrhythmia in human (for review see Schotten *et al.* 2011).

In pathological situations such as heart failure, both atrial and ventricular fibroblasts proliferate, migrate and differentiate into myofibroblasts that synthesize excessive extracellular matrix proteins leading to cardiac fibrosis (Weber *et al.* 1994; Swynghedauw, 1999; Manabe *et al.* 2002). This differentiation into myofibroblasts is accompanied by changes in gene expression pattern leading notably to neo-expression of proteins such as α-smooth muscle actin (α-SMA) (Baudino *et al.* 2006). Whereas fibroblasts and myofibroblasts have long been considered as non-excitable cells, studies focused on their electrophysiological properties have emerged in the past decade (for reviews see Yue *et al.* 2011; Vasquez *et al.* 2011). Ventricular fibroblasts express several potassium channels (Chilton *et al.* 2005; Shibukawa *et al.* 2005; Benamer *et al.* 2009; Li *et al.* 2009*a*) and non-selective cationic channels (Rose *et al.* 2007). Voltage gated sodium channels (VGSCs) and chloride channels have also been recently reported in commercially available cultured ventricular fibroblasts (Li *et al.* 2009*a*). Beside the well-characterized role of these channels in excitable cells, there is increasing evidence that VGSCs are also expressed and contribute to cellular functions in non-excitable cells. For example, they appear to be important modulators of cancer cell invasion processes (Roger *et al.* 2003; Gillet *et al.* 2009), human endothelial cells angiogenic abilities (Andrikopoulos *et al.* 2011) or microglia and epidermal keratinocytes secretion properties (Zhao *et al.* 2008; Black *et al.* 2009). VGSCs are composed of one α-subunit, which forms the core of the channel, and several β-subunits, which modulate their expression levels and gating properties (Catterall, 1986; Fozzard & Hanck, 1996; Armstrong & Hille, 1998). In their study on ventricular fibroblasts, Li *et al.* (2009*a*) found that five different VGSC α subunits were heterogeneously expressed within the cultured cells.

Atrial fibroblasts have been less studied than ventricular fibroblasts. Electrophysiological studies report that they express a stretch activated non-selective cationic current (Kamkin *et al.* 2003*a*), a voltage-dependent proton current (El Chemaly *et al.* 2006) and the non-selective cationic channel TRPM7 (Du *et al.* 2010).

Since fibroblasts and myofibroblasts are involved in several physiological and physiopathological processes, it is important to distinguish ionic channel expression within their differentiated state. For example, we have shown that potassium channels, and notably SUR2/Kir6.1, appear progressively over ventricular fibroblast differentiation into myofibroblast and modulate cell proliferation and secretion properties (Benamer *et al.* 2009). Similarly, in atria, it was shown that TRPM7 plays an essential role in human atrial fibroblast proliferation and differentiation (Du *et al.* 2010).

Based on the observations that fibrosis depends on differentiation of fibroblasts into myofibroblasts (Vasquez *et al.* 2011) and is more likely to occur within atria (Yue *et al.* 2011), the present study aimed at investigating electrophysiological changes associated with human atrial fibroblast differentiation. We focused our study on the activity of VGSCs in human atrial fibroblasts or myofibroblast primary cultures. Using reverse transcriptase-quantitative polymerase chain reaction (RT-qPCR), Western blot, immunocytochemistry and the patch clamp technique, we characterized the molecular identity and electrophysiological properties of VGSCs in these cells. The physiological and physiopathological impact of VGSCs in cardiac fibroblasts will be discussed.

Table 1. Characteristics of patients.

Patient	Pathology	Age	Sex	Time of culture tested (days)
1	AAA	56	F	12<
2	AVS	79	F	12<
3	CAS	69	F	12<
4	MVE + CAS	83	F	12<
5	AVS	73	M	12<
6	CAS	56	F	12<
7	AI	60	M	<7 and 12<
8	AAA	59	M	<7 and 12<
9	CAS	66	M	<7 and 12<
10	AVS	74	M	<7 and 12<
11	CAS	64	M	7< and >12
12	CAS	64	M	7< and >12
13	CAS	72	M	<7
14	CAS	70	F	<7
15	CAS	72	F	<7
16	AVS	70	M	<7

AAA, ascending aortic aneurysm; AI, aortic insufficiency; AVS, aortic valve stenosis; CAS, coronary artery stenosis; MVE, mitral valve endocarditis; F, female; M, male. 12<, cells were used after 12 days of culture. <7 and 12<, cells were used before 7 days or after 12 days of culture. 7< and >12, cells were used between 7 and 12 days of cultutre. <7, cells were used before 7 days of culture.

Methods

Ethical approval

All procedures were approved by the human research committee, 'comité de protection des personnes Ouest III', at the University of Poitiers and were carried out in accordance with the *Declaration of Helsinki*. Informed consent was obtained from each patient.

Patients

Right atrial human appendages were obtained from 16 patients (67.9 ± 1.9 years old, 9 males and 7 females) undergoing a cardiac bypass surgery. Sinus rhythm was present in all cases. Myocardial samples were removed during cannulation for cardiopulmonary bypass with extra-corporal circulation, a routine procedure comprising normal management of the patients. Characteristics of patients are given in Table 1.

Isolation and culture of human atrial fibroblasts

Cardiac cells, consisting of smooth muscle cells, endothelial cells, fibroblasts and cardiomyocytes, were dissociated as previously described (Hatem *et al.* 1997; Ancey *et al.* 2002; El Chemaly *et al.* 2006). Heart tissue was minced in calcium-free Krebs solution containing (mmol l^{-1}): NaCl 35, KCl 7.75, KH_2PO_4 1.18, Na_2HPO_4 20, Hepes 10, glucose 10, $NaHCO_3$ 25, saccharose 70, 2,3-butanedione 2-monoxime (BDM) 30, and EGTA 0.5 (pH was adjusted to 7.4 with NaOH), and enzymatically dissociated afterwards over several digestion steps. The first one was performed for 25 min with tissues maintained in the same solution without BDM or EGTA and supplemented with 0.5% bovine serum albumin (BSA), 200 IU ml^{-1} collagenase (type V, Sigma-Aldrich Co., Saint-Quentin Fallavier, France), and 6 IU ml^{-1} protease (type XXIV, Sigma-Aldrich). Two other 20 min digestion steps followed using the same enzymatic solution but containing only collagenase (400 IU ml^{-1}). All steps were carried out with solutions gently shaken in a water bath maintained at 37°C in a 95% O_2 and 5% CO_2 atmosphere. This was followed by gentle stirring of the tissue in a washing buffer containing (mmol l^{-1}): NaCl 130, KCl 4.8, KH_2PO_4 1.2, Hepes 25, glucose 5, EGTA 0.15 and BSA 2% (pH was adjusted to 7.4 with NaOH). Dissociated cells were submitted to successive filtration and centrifugation steps to eliminate cell debris, cardiomyocytes, endothelial and smooth muscle cells as described in previous studies (Louault *et al.* 2008; Benamer *et al.* 2009). Human atrial fibroblasts were cultured afterwards in Dulbecco's Modified Eagle's medium (DMEM; Biowhittaker, Emerainville, France) supplemented with 10% fetal bovine serum (Biowest, Nuaillé, France), 1% antibiotics (100 IU mol^{-1} penicillin-G-Na; 50 IU ml^{-1} streptomycin sulfate), and 1% insulin (10^{-7} mol l^{-1}). The culture was incubated at 37°C in a humidified, 5% CO_2-enriched atmosphere. The culture medium was replaced every 48 h. For patch clamp experiments, just after cell dissociation fibroblasts were seeded directly in 35 mm dishes (NunclonΔ polystyrene surface) kept in culture without trypsin steps until patch clamp experiments. For Western blots and RT-qPCR just after cell dissociation fibroblasts were seeded in 92 mm dishes (NunclonΔ polystyrene surface) and kept in culture without trypsin steps until Western blot or RT-qPCR experiments.

Western blots

Fibroblasts in primary culture were washed with cold phosphate-buffered saline (PBS) and lysed by scraping the cells into a lysis buffer (in mmol l^{-1}: Tris-HCl 50, NaCl 150, EDTA 5, 0.05% Igepal, 1% deoxycholic acid, 1% Triton X-100, 0.1% SDS) containing protease inhibitors (Protease Inhibitor Cocktail, Sigma-Aldrich). Cell lysates were then incubated for 30 min on ice and centrifuged at 1750 *g* for 10 min at 4°C. Soluble cell lysates were denatured 30 min at 37°C in 2× sample buffer (in mmol l^{-1}): Tris-HCl 126, SDS 4%, glycerol

20%, bromophenol blue 0.02%, β-mercaptoethanol 5%. Protein samples (10 μg), obtained from fibroblasts in primary culture, were separated by SDS-PAGE using 8% polyacrylamide gels and transferred to nitrocellulose membranes. Membranes were blocked 1 h in TBS-Tween blocking solution (in mmol l^{-1}: Tris-HCl 100, NaCl 150 and Tween-20 0.1%) with 5% non-fat milk and then probed overnight at 4°C with primary antibodies. Because of the small amount of tissue and so the limited number of atrial fibroblasts obtained after dissociation, the use of the specific anti-human $Na_v1.5$ antibody was not possible in our conditions for Western blot experiments. Therefore, we used the powerful primary antibodies rabbit polyclonal anti-SP19 (1:1000, Alomone Labs Ltd, Jerusalem, Israel) that recognizes all VGSC subunits. β-Actin was probed by mouse monoclonal anti-β-actin (1:10000, Sigma). Membranes were washed and incubated for 1 h at room temperature with specific anti-rabbit or anti-mouse horseradish peroxidase-conjugated secondary antibodies (1:5000, Interchim, Montluçon, France). Membranes were revealed with enhanced chemiluminescence (ECL) chemiluminescent substrate (GE Healthcare, Velizy-Villacoublay, France).

Immunofluorescence staining

Fibroblasts were cultured on coverslips and grown in DMEM. The cells were fixed with PBS with 3% paraformaldehyde for 10 min, permeabilized by 20 min incubation in PBS containing 0.1% Triton X-100, and blocked in PBS containing 5% BSA. Samples were then incubated overnight at 4°C with primary antibodies in PBS containing 5% BSA, after which they were incubated for 1 h at room temperature with the appropriate secondary antibody in the same solution. Coverslips were rinsed and mounted using fluorescence mounting medium (Vectashield, Vector Laboratories, Inc., Burlingame, CA, USA) on glass microscope slides and examined by confocal microscopy.

Primary antibodies used were anti-fibronectin rabbit polyclonal antibody 1/100 (Santa Cruz Biotechnology, Inc., Santa Cruz, CA, USA) to identify fibroblasts, anti-α-SMA monoclonal mouse antibody (Dako, Trappes, France) 1/100 to characterize myofibroblasts and anti-human $Na_v1.5$ rabbit antibody (Alomone) 1/200 to label $Na_v1.5$ sodium channels. Secondary antibody used were Alexa fluor 488 chicken anti-rabbit IgG (1/1000), Alexa Fluor 555 donkey anti-mouse (1/200) and Alexa fluor donkey 568 anti-rabbit IgG (1/400) from Molecular Probes (Invitrogen, Saint Aubin, France). The specificity of secondary antibodies was confirmed by the absence of a signal in preparations when the primary antibody was omitted. Nuclear staining was obtained using TO-PRO-3 (Invitrogen).

Patch clamp experiments

The measurements were carried out at room temperature (~22°C). Fire-polished, patch electrodes (~2 MΩ) were pulled from borosilicate glass capillaries using a vertical micropipette puller (Narishige, Tokyo, Japan). The pipettes were coated with the silicone elastomer HIPEC R6101 (Dow-Corning, Midland, MI, USA) to minimize capacitance. Voltage clamp experiments were performed using an Axopatch 200B amplifier with a CV 203BU headstage (Molecular Devices, Sunnyvale, CA, USA). Series resistance compensation was performed to values >80% to minimize voltage errors. Voltage command pulses were generated by a personal computer equipped with an analog–digital converter (Digidata 1200, Molecular Devices) using pCLAMP software v8.0 (Molecular Devices). Linear leak currents and capacitance artefacts were removed using *P*/*N* leak subtraction. Sodium currents were filtered at 5 kHz and digitized at 20 kHz. Cell capacitance was recorded as a telegraph readout of cell capacitance compensation using Axopatch 200B and pCLAMP. The digitized currents were stored on a computer for later off-line analysis. To avoid clamp problems, only recordings that exhibit an access resistance lower than 5 MΩ were kept for biophysical parameters analysis. The patch pipettes were filled with (mM): 35 NaCl, 105 CsF, 0.1 EGTA, and 10 Hepes. The pH was adjusted to 7.4 using CsOH. The bath solution contained (mM): 150 NaCl, 2 KCl, 1.5 $CaCl_2$, 1 $MgCl_2$, 10 glucose, and 10 Hepes. The pH was adjusted to 7.4 using NaOH. In these conditions, theoretical reversal potential was expected to be around 37 mV. However, the particular myofibroblast shape, which is extremely flat, probably restricted the sodium diffusion from the pipette solution to the intracellular compartment leading to a more positive reversal potential. A −7 mV correction of the liquid junction potential between the patch pipette and the bath solutions was performed.

Currents were recorded using the whole-cell configuration of the patch clamp technique. Sodium currents were generated by clamping cell membrane from a holding potential of −120 mV to potentials ranging from −100 mV to 40 mV for 50 ms in 10 mV increments with 3 s stimulus intervals. Fast and slow decay time constants were obtained by fitting current traces with a double exponential equation. The voltage dependence of activation was determined from the relative membrane conductance as a function of potential using the formula $G_{Na} = I_{Na}/(V_m - V_{rev})$, where G_{Na} is peak conductance and I_{Na} is peak sodium current for the test potential V_m. V_{rev} is the estimated reversal potential of the sodium current obtained by the extrapolation of the current–voltage relationship. The resulting sodium ion conductance was normalized to the maximum response for each

cell. The activation data were fitted with a Boltzmann equation: $G/G_{max} = 1/(1 + \exp[(V - V_{1/2})/k])$, where G_{max} represents the maximum conductance and $V_{1/2}$ and k represent the half-maximum voltage of activation and the Boltzmann steepness coefficient, respectively.

The voltage dependence of inactivation was obtained by measuring the peak Na^+ current during a 20 ms test pulse to −20 mV, which followed a 500 ms pre-pulse to membrane potentials between −120 and 0 mV from a holding potential of −120 mV. Peak inward currents, I, were measured and normalized to the maximum response, I_{max}, of each cell. The inactivation data were also fitted with a Boltzmann equation.

Real-time reverse transcription polymerase chain reaction (RT-qPCR)

Total RNA from human cardiac fibroblasts was isolated using RNAble reagent (Eurobio, Courtaboeuf, France) followed by chloroform extraction and isopropanol precipitation. RNA integrity was evaluated by ethydium bromide staining on a 1% agarose gel. Total RNA was quantified by assessing optical density at 260 and 280 nm (NanoDrop ND-100, Labtech France, Palaiseau, France). cDNA was synthesized using the $Pd(N)_6$ random hexamer primer (GE Healthcare Life Sciences). Ten microlitres of total RNA (1–2 μg) was added to 12 μl of reaction mixture (100 mmol l^{-1} Tris-HCl pH 8.3, 150 mmol l^{-1} KCl, 6.25 mmol l^{-1} $MgCl_2$, 20 mmol l^{-1} DTT, 2 mmol l^{-1} dNTPs (Invitrogen) and 2.4 μg Random Primer $p(dN)_6$ (GE Healthcare Life Sciences). RNA were denatured at 65°C during 2 min and then added to 40 U RNAse inhibitor (RNaseOUT, Invitrogen) and 400 U M-MLV reverse transcriptase (Invitrogen) to 25 μl final volume. cDNA was synthesized at 37°C for 1 h and then added with 50 μl sterile water. Remaining enzymes were heat-deactivated (100°C, 2 min).

qPCR assays were carried out using SYBR green I detection dye on a LC480 platform (Roche) using the vendor's specifications. Primers were designed using PerlPrimer v1.1.19. All qPCR samples were run at least in duplicate, and for each plate we applied a non-template control (NTC) and positive control for each primer pair to control every qPCR run.

Analysis has been done with the lightcycler software LightCycler® 480 SW 1.5 using the second derivative method. Run-to-run variation has been adjusted using a known standard and quantification was corrected for efficiency calculated with the standard curves. Human heart APEX ($Na_v1.4$, $Na_v1.5$, GAPDH) and human cortex ($Na_v1.1$, $Na_v1.2$, $Na_v1.3$, $Na_v1.7$, $Na_v1.8$, $Na_v1.9$, Nax) mRNA has been used for RT-PCR. cDNA was amplified by PCR using specific primer and DNA dilution was used for standard curves. The specificity of the amplification for each run was controlled with a melting curve analysis and was performed directly following the PCR by continuously reading the fluorescence while slowly heating the reaction from 65°C to 95°C.

HEK293T cell transfection

HEK293T cells were grown in high glucose DMEM supplemented with fetal bovine serum (10%), L-glutamine (2 mM), penicillin (100 U ml^{-1}) and streptomycin (10 mg ml^{-1}). The cells were incubated in a 5% CO_2 humidified atmosphere after being transfected with wild-type human $Na_v1.5$ cDNA (1.5 μg) and human β1 subunit (1.5 μg) using the calcium phosphate method as previously described (Margolskee *et al.* 1993). The human sodium channel β1 subunit and CD8 were inserted in the pIRES bicistronic vector in the form of pCD8-IRES-β1. Using this strategy, transfected cells that bound beads also expressed the β1 subunit protein. Before performing patch-clamp experiments, 2 day post-transfection cells were incubated for 5 min in medium containing anti-CD8 coated beads (Dynabeads CD8, Invitrogen, Dynal AS, Oslo, Norway). The unattached beads were removed by washing with extracellular solution. Cells expressing CD8 were distinguished from non-transfected cells by visualizing beads fixed on the cell membrane by light microscopy. Using this strategy, transfected cells that bound beads also expressed the β1 subunit protein.

Data analysis

Data were analysed using a combination of pCLAMP software v8.0 (Molecular Devices), Microsoft Excel and SigmaPlot 8.0 (SPS, Chicago, IL, USA).

Data are presented as means ± standard error of the mean (SEM). Differences between mean values were evaluated by Student's t test or one-way analysis of variance (ANOVA) with values of $P < 0.05$ indicating a significant difference.

Results

Appearance of a voltage gated sodium current in human atrial fibroblast cultures

Human atrial fibroblast differentiation into myofibroblast in culture was evaluated through expression of α-SMA observed by immunofluorescence labelling (Fig. 1*A*). Experiments carried out after 7 days of culture show a clear staining of fibronectin, a specific marker of fibroblastic cells. At this time of culture no specific labelling of α-SMA, a specific marker of myofibroblasts, was observed whereas this protein is strongly expressed after 12 days. This indicates that the differentiation of human atrial fibroblasts into myofibroblasts occurs between 7 and 12 days of culture in our conditions. To investigate the presence of VGSCs during fibroblast differentiation, western

blot experiments were performed after 5 or 15 days of culture (Fig. 1*B*). At 5 days of culture the VGSC protein was absent whereas it was expressed in myofibroblasts of 15 days of culture. To test whether this expression was correlated to the presence of a fast inward sodium current during fibroblast differentiation, whole-cell patch clamp experiments were performed after different times of culture. Before 8 days, no cell ($n = 7$ cells/4 patients) presented a fast inward sodium current whereas 75% of cells ($n = 12$ cells/2 patients) showed this current between 8 and 12 days of culture (Fig. 1*C*). This proportion reached 100% of cells ($n = 22$ cells/7 patients) after 12 days. No relation between the VGSC current appearance and the pathology or the sex of the patients was observed.

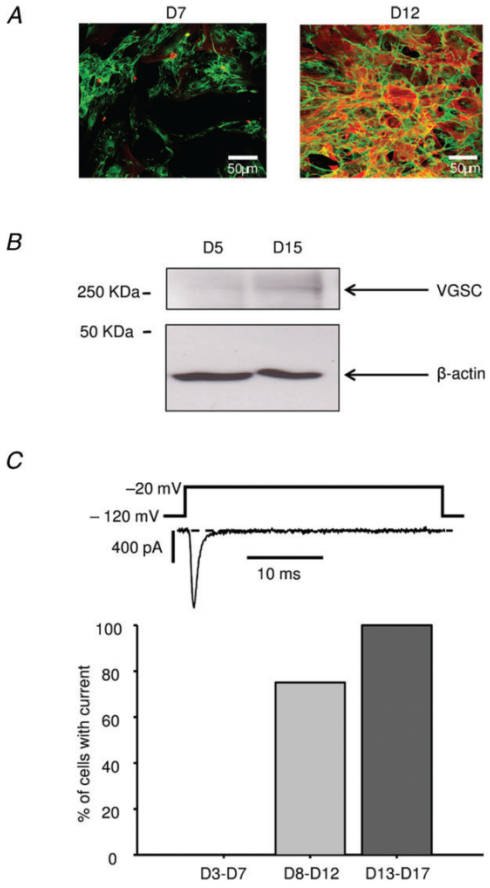

Figure 1. Appearance of a fast inward voltage gated sodium current with human atrial fibroblast differentiation
A, cells were stained after 7 (left panel) or 12 (right panel) days of culture with anti-fibronectin (green labelling) and anti-α-SMA (red labelling) antibodies. *B*, Western blot, representative of 3 experiments, performed with protein preparations obtained from human atrial fibroblasts at 5 and 15 days of culture using antibodies to VGSC and β-actin. *C*, percentage of cells that exhibit a voltage gated transient inward current after 3–7 days (D3–D7, $n = 7$), 8–12 days (D8–D12, $n = 12$) or 13–17 days (D13–D17, $n = 22$) of culture. An example of current after 15 days of culture is shown (top panel).

Biophysical properties of human atrial myofibroblasts VGSC current

Whole cell patch-clamp recordings of the human atrial myofibroblasts using voltage steps from a holding potential of -120 mV produced typical fast activation and fast inactivating currents (Fig. 2*A*). Whereas no current was observed at -20 mV after 5 days of culture (0.05 ± 0.18 pA pF^{-1}, $n = 5$), current density increased to 4.60 ± 1.19 pA pF^{-1} ($n = 3$) after 10 days and reached 13.28 ± 2.88 pA pF^{-1} ($n = 8$) after 15 days ($P < 0.01$, one-way ANOVA). However, sodium currents recorded

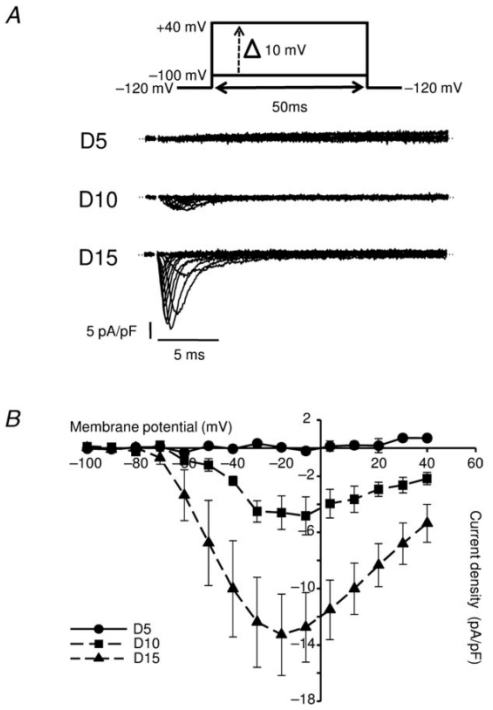

Figure 2. Whole-cell properties of VGSCs recorded in human atrial fibroblasts
A, representative traces of whole cell currents recorded after 5 (D5), 10 (D10) or 15 (D15) days of fibroblast culture using the protocol shown on top. *B*, current density–voltage relationship recorded after 5 (circles, $n = 5$), 10 (squares, $n = 3$) and 15 (triangles, $n = 8$) days of culture. Currents were elicited as described in *A*.

after 10 ($n = 3$) and 15 ($n = 8$) days of culture display current–voltage curves with similar voltage sensitivity (Fig. 2*A* and *B*). Sodium current activation occurs for potentials positive to −70 mV and the peak current was observed at a potential closed to −20 mV. The reversal potential estimated at D15 by extrapolation of the linear part of current–voltage relationship was 71.0 ± 6.4 mV ($n = 8$). The voltage dependence of activation recorded at D15 was determined as described in Methods (Fig. 3*A*). The activation begins at −70 mV and is maximal for potentials greater than 0 mV. When the data are fitted with a Boltzmann function, the midpoint for activation ($V_{1/2}$) and the Boltzmann steepness coefficient (k) are respectively −41.7 ± 4.0 mV and 7.6 ± 0.8 mV ($n = 8$). The availability was determined at D15 from the normalized peak current amplitude of standard test pulses at −20 mV and plotted *versus* prepulse voltages (Fig. 3*A*). The smooth curve fits a Boltzmann function as described in Methods with a midpoint ($V_{1/2}$) and a Boltzmann steepness coefficient (k) of −83.9 ± 3.1 mV and −7.8 ± 0.7 mV, respectively ($n = 5$).

The overlap of the activation and inactivation curves identifies a voltage range where a proportion of sodium channels can enter into an activated state without being fully inactivated ('window current'; Fig. 3*B*). The steady-state availability of channels within this window of voltages is calculated as the product of the fitted steady-state activation and inactivation parameters as described previously (Huang *et al.* 2010). This availability is a biphasic function and is very small for potentials below −100 mV and above −20 mV. Between these potentials, there is a non-negligible probability to have persistent opened channels with a peak value of 0.37% obtained at −60 mV.

The time courses of current decay elicited at depolarized voltages were fitted using a double exponential function. The resulting fast and slow time constants were plotted *versus* voltage (Fig. 3*C*) and were 2.8 ± 0.5 ms and 13.9 ± 3.3 ms at −40 mV, respectively ($n = 8$).

$Na_v1.5$ and β_1 subunits are good candidates for the myofibroblast VGSC current

In order to identify VGSC α and β subunit transcripts expressed in fibroblasts and myofibroblasts, RT-qPCR was carried out on cells from three different patients obtained before 8 and after 13 days of culture, respectively. Figure 4*A* illustrates the expression pattern of nine of the sodium channel α subunits. Interestingly, amongst these screened transcripts, only $Na_v1.2$ and $Na_v1.5$ were detected in fibroblasts with an expression level of $Na_v1.5$ sevenfolds higher than $Na_v1.2$. In myofibroblasts, other isoforms were detected such as $Na_v1.3$, 1.6 and 1.7 whereas $Na_v1.2$ expression was unchanged. On the other hand, $Na_v1.5$ presented a fourfold increased expression level and was at least eightfold higher than other α subunit transcripts. Subunits like $Na_v1.1$, 1.4, 1.8, 1.9 or the atypical Na_x were not detected in fibroblasts or myofibroblasts.

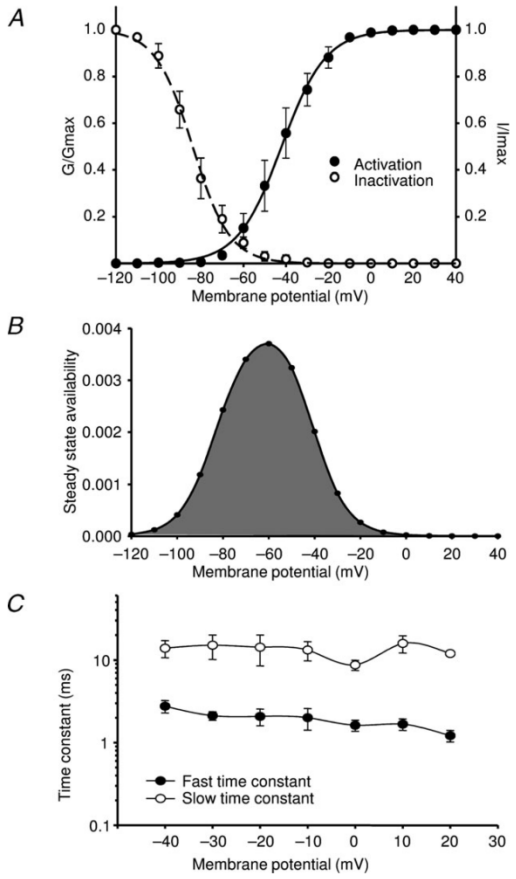

Figure 3. Biophysical properties of VGSCs recorded in human atrial myofibroblasts after 15 days in culture
A, voltage dependence of activation (filled circles, $n = 8$) and inactivation (open circles, $n = 5$) fitted with a Boltzmann function (see Methods). Sodium conductance (G) was calculated from the *I–V* curve experiments (Figure 2A). This conductance was normalized to maximum conductance (G_{max}) obtained during the *I–V* curve and plotted *versus* imposed membrane potential. Steady state inactivation was assayed as described in Methods and plotted *versus* membrane pre-pulse potential. *B*, the overlap of activation and inactivation of sodium channels defines a range of voltages (window) where the channels could be partially activated without being fully inactivated. The availability of channels at a stable potential is calculated as the product of the activation and the inactivation Boltzmann functions (Huang *et al.* 2010). *C*, fast (filled circles) and slow (open circles) inactivation time constants as a function of membrane potential. The decay phases of currents elicited as described in Fig. 2*A* ($n = 8$) were fitted with a double exponential to estimate the open state inactivation time constants.

β subunit transcripts are also expressed in fibroblasts and myofibroblasts (Fig. 4*B*). The major β subunit was β_1 with quantities that doubled with fibroblast differentiation. Small amounts of β_3 and β_4 were also present whereas β_2 was absent.

Human atrial myofibroblast VGSC current is predominantly supported by the $Na_v1.5$ α subunit

Based on the RT-qPCR results (Fig. 4*A*), $Na_v1.5$ is the more abundant transcript in myofibroblasts. Because this is the only detected transcript which codes for a TTX resistant α-subunit, the cells were perfused with 1 μM TTX to investigate whether the current recorded in myofibroblasts was sensitive to TTX. Figure 5*A* and *B* shows that the perfusion of 1 μM of TTX produced a significant and reversible reduction of the sodium current to $41.8 \pm 8.0\%$ of the control amplitude ($n = 4$, $P < 0.01$, one-way ANOVA). To compare the reduction of current observed to the $Na_v1.5$ TTX sensitivity, we used HEK293T cells transiently transfected with both human α-$Na_v1.5$ and β_1 subunits. In our conditions, 1 μM TTX decreased $Na_v1.5$ current to $47.98 \pm 9.83\%$ of the control ($n = 3$, $P < 0.01$, one-way ANOVA), which is not significantly different from the reduction observed in myofibroblasts. The $Na_v1.5$ α subunit expression in myofibroblasts was finally investigated by immunofluorescence experiments (Fig. 5*C*). Cells incubated with specific $Na_v1.5$ antibodies after 15 days of culture exhibited a clear staining that confirmed the presence of the protein whereas it was absent at 5 days of culture.

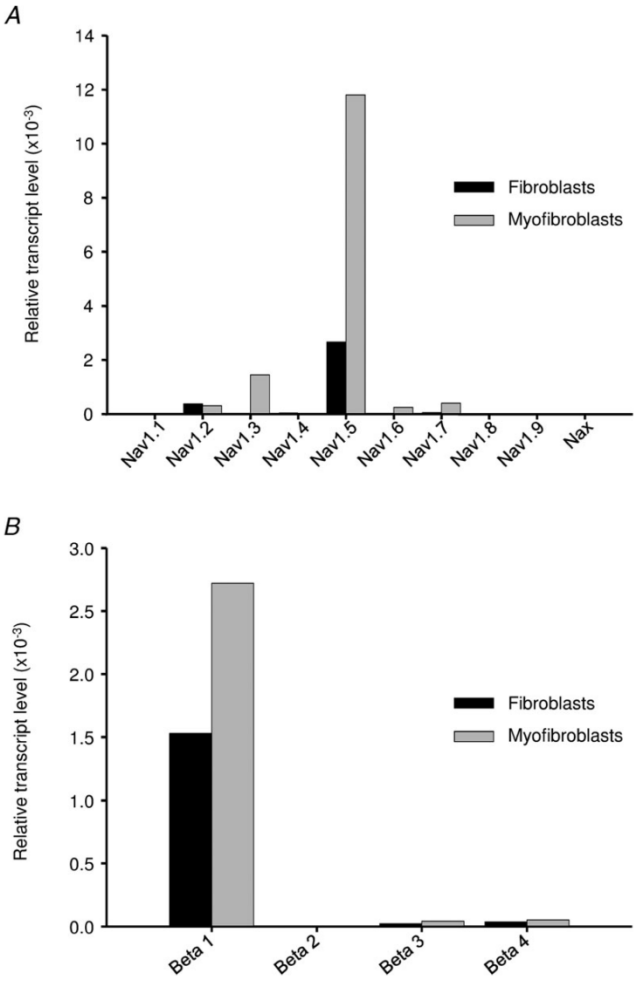

Figure 4. mRNA expression levels of VGSC subunits in human atrial fibroblasts and myofibroblasts
Relative quantities *versus* GAPDH of Na_v α (*A*) and β (*B*) subunit transcripts evaluated by real-time reverse transcription polymerase chain reaction (RT-qPCR) using mRNA extract from human atrial fibroblasts after 3–7 (fibroblasts) or 13–17 (myofibroblasts) days of culture.

Discussion

This study investigates for the first time changes in the expression pattern of VGSCs associated with human atrial fibroblasts differentiation. We show that human atrial fibroblasts differentiation into myofibroblasts is accompanied by the neo-expression of rapid voltage gated sodium current. Electrophysiological properties of this current are similar to sodium channels found in cardiac myocytes and there is strong evidence that this current is supported by $Na_v1.5$ α-subunit, the typical cardiac VGSC traditionally characterized in cardiomyocytes.

Fibroblasts differentiation was studied in culture as described in previous studies (Baudino *et al.* 2006; Teunissen *et al.* 2007; Benamer *et al.* 2009; Benamer *et al.* 2011). In our experimental conditions, the cells expressed α-SMA, a typical marker of myofibroblasts (Wang *et al.* 2003; Miragoli *et al.* 2006; Miragoli *et al.* 2007; Zlochiver *et al.* 2008), between 7 and 12 days of culture. This suggests that human atrial fibroblasts in culture differentiate into myofibroblasts within this period of time. The differentiation process is slower than that described previously in our laboratory using mouse ventricular fibroblasts (Benamer *et al.* 2009; Benamer *et al.* 2011). Since the present study was realized in the same conditions, we suggest that the differentiation kinetics depend on either the species and/or on the origin of the fibroblast (atrial or ventricular).

Investigating the VGSC α-subunit candidates revealed that $Na_v1.2$, $Na_v1.3$, $Na_v1.5$, $Na_v1.6$ and $Na_v1.7$ transcripts are present. The use of the real time RT-qPCR technique on diverse cell differentiation states allowed us to compare the expression levels of all sodium channel isoforms found in human genome within fibroblasts or myofibroblasts. The differentiation process is accompanied by an increased expression of the cardiac $Na_v1.5$ transcripts and by a slight *de novo* expression of neuronal transcripts such as $Na_v1.3$, $Na_v1.6$ and $Na_v1.7$. However, neuronal VGSCs are weakly expressed compared to $Na_v1.5$. According to our results, there is no transcript of $Na_v1.3$, $Na_v1.6$ and $Na_v1.7$ in fibroblasts whereas they were detected in a previous study of Li *et al.* (2009*a*). At least two hypotheses may account for this discrepancy. First, Li's study used a commercially available fibroblast cell line culture with several passages. As a consequence, it is reasonable to postulate that the cells they handled were (at least in major part) myofibroblasts, rather than fibroblasts. The detection of $Na_v1.3$, $Na_v1.6$ and $Na_v1.7$ would thus correspond to myofibroblast transcripts as in our study. Moreover, there may be differences between the expression pattern of ventricular (as in Li's study) and atrial (as in ours) fibroblasts. Amongst detected transcripts in

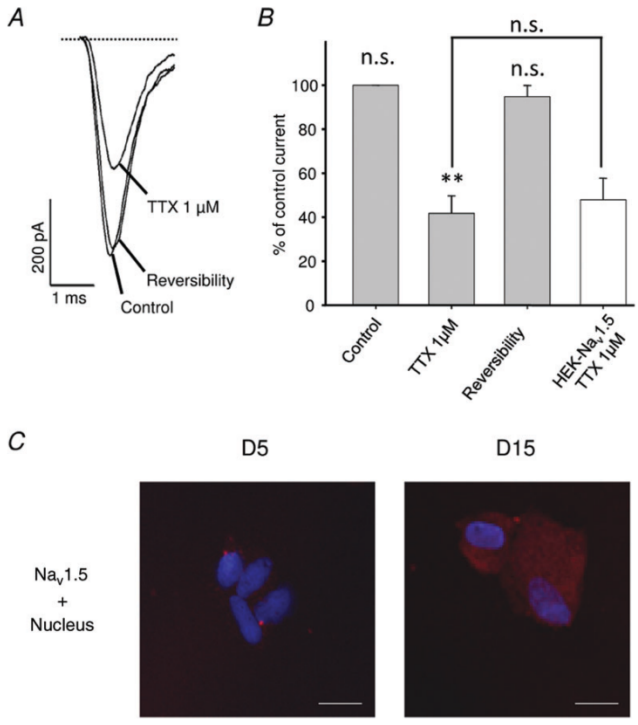

Figure 5. Molecular identity of the VGSC α-subunit recorded in human atrial myofibroblasts
A, representative example of the effect of TTX at 1 μM on fibroblast sodium current. Currents were elicited by a standard test pulse from a holding potential of –120 mV to a test pulse of −20 mV for 50 ms. TTX was perfused until current stabilization and washout with a control perfusion to check reversibility. *B*, effects of 1 μM TTX ($n = 4$) on the voltage gated sodium current evoked as described in *A* on myofibroblasts (grey bars) or HEK293 cells transiently transfected with $Na_v1.5 + \beta_1$ subunits (white bar). *C*, fibroblasts (5 days of culture; D5) and myofibroblasts (15 days of culture; D15) observed in fluorescence. Cells were stained with anti-$Na_v1.5$ antibody and the nuclei were stained using TO-PRO-3. Scale bar corresponds to 20 μm.

myofibroblasts, $Na_v1.5$ is the only one translated in a TTX resistant subunit (Catterall *et al.* 2005). In this study, 1 μM blocked almost 50% of the current as observed in $Na_v1.5$ transfected HEK293T cells. This result strongly suggests that $Na_v1.5$ is the α-subunit responsible of the current. Whereas real time RT-qPCR and TTX results, combined with immunofluorescence experiments, do not rule out the presence of TTX sensitive isoforms, they clearly indicate that the $Na_v1.5$ α-subunit represents the major part of the human myofibroblast's VGSC. Moreover, based on the TTX sensitivity and kinetics of the current we can also exclude a calcium channels component.

In the present study, it would have been interesting to compare sodium current from myofibroblasts and atrial myocytes of the same patients. Unfortunately, whereas cardiomyocytes and fibroblasts can be obtained using the same protocol, it is difficult to obtain both cell types at the same time since enzymatic digestion has to be adapted to the cells desired. Comparing the VGSC current of the present study to those observed in mammalian cardiomyocytes revealed similar but not identical biophysical properties (Schneider *et al.* 1994; Li *et al.* 2009*b*; Sato *et al.* 2009; Mishra *et al.* 2011; Lin *et al.* 2011). For example, the window current delimited by the area between the activation and inactivation is larger in myofibroblasts. This defines a range of potentials where the sodium channels can be activated without being fully inactivated, leading to a persistent entry of sodium ions in myofibroblasts. How relevant can a steady-state availability of 0.37% at -60 mV be? A recent study showed that $Na_v1.5$ Y1767C mutant which presents a value of 0.13% is implicated in long QT syndrome development (Huang *et al.* 2010). It is therefore reasonable to envisage that the persistent entry of sodium in myofibroblasts through the window current may have a significant impact on their function.

According to the window current characterized in our study, the persistent sodium entry strongly depends on membrane potential. Despite that fibroblast and myofibroblasts are not considered to be excitable, different studies have shown membrane potential variations of these cells. In human and rat atrial fibroblasts, the resting membrane potential is close to -15 mV (Kiseleva *et al.* 1998; Kamkin *et al.* 1999). At this potential, the persistent entry of sodium predicted with the Boltzmann product would be negligible (see Fig. 3*B*). On the other hand, several phenomena lead to a negative shift of fibroblast membrane potential recorded in atrial tissue. Indeed, experiments realized on rat atrial fibroblasts revealed a stretch-dependent strong hyperpolarization of membrane potential that was maximal 8 days after myocardial infarction and recovered after 30 days (Kiseleva *et al.* 1998; Kamkin *et al.* 2002). Another study realized in the same cardiac tissue showed that reoxygenation after hypoxia also induced a hyperpolarization of rat atrial fibroblast membrane potential (Kamkin *et al.* 2003*b*). Whereas it is difficult to test the effect of these post-traumatic conditions on membrane potential in human atrial tissue, it is reasonable to envisage that similar mechanisms could take place. In rat, these potentials, predominantly between -50 mV and -60 mV, correspond to the peak of the sodium window current described in the present study. As a consequence, such a cell polarity may induce a persistent sodium entry. In rat myofibroblasts, the sodium–calcium exchanger has been shown to be implicated in migration and proliferation processes (Raizman *et al.* 2007). It is therefore plausible that the persistent sodium current could lead to similar effects through an increase in intracellular calcium due to the reverse mode of the sodium–calcium exchanger. It would be interesting to investigate whether $Na_v1.5$ could influence myofibroblast proliferation, migration and secretion properties as observed in other cell types (Roger *et al.* 2003; Zhao *et al.* 2008; Gillet *et al.* 2009; Andrikopoulos *et al.* 2011). Moreover, an increase in calcium has recently been related to fibrogenesis in human atrial fibrillation (Du *et al.* 2010). In this study, intracellular calcium modulation was mediated by TRPM7 expression in human atrial fibroblasts and was modulated with fibroblast differentiation. Our study raises the possibility that $Na_v1.5$, through the reverse mode of the sodium–calcium exchanger, participates in such an increase in intracellular calcium in myofibroblasts and could be implicated in human atrial fibrosis and fibrillation.

In summary, we show for the first time the presence of a rapid voltage gated sodium current in human atrial myofibroblasts with electrophysiological characteristics similar to sodium channels found in excitable cells. Multiple arguments support that this sodium current is predominantly supported by the $Na_v1.5$ α subunit, which may generate a persistent sodium entry into myofibroblasts. Since fibrosis is one of the fundamental mechanisms implicated in atrial fibrillation, it is of great interest to investigate how this current could influence myofibroblasts proliferation, migration and secretion properties. Moreover, several $Na_v1.5$ mutations are related to cardiac pathologies (Amin *et al.* 2010) such as Long QT, Brugada syndrome or Lenegre disease. This study raises the possibility that some cardiac consequences of such mutations may be due to myofibroblast alterations. For example, a SCN5A mutation associated with lone atrial fibrillation has recently been characterized as a gain of function mutation that enhances the sodium window current (Li *et al.* 2009*c*). Since atrial fibrosis is strongly related to atrial fibrillation, it would be interesting to question the impact of this mutation on atrial myofibroblast physiology.

In conclusion, this study provides a new direction in research on the cardiac role of wild-type $Na_v1.5$ as well as the consequences of $Na_v1.5$ pathological mutations.

Therefore, investigating the expression and role of $Na_v1.5$ sodium channels of myofibroblasts in the atria during the remodelling in pathologies such as atrial fibrillation is warranted.

References

Allessie M, Ausma J & Schotten U (2002). Electrical, contractile and structural remodeling during atrial fibrillation. *Cardiovasc Res* **54**, 230–246.

Amin AS, Tan HL & Wilde AA (2010). Cardiac ion channels in health and disease. *Heart Rhythm* **7**, 117–126.

Ancey C, Corbi P, Froger J, Delwail A, Wijdenes J, Gascan H, Potreau D & Lecron JC (2002). Secretion of IL-6, IL-11 and LIF by human cardiomyocytes in primary culture. *Cytokine* **18**, 199–205.

Andrikopoulos P, Fraser SP, Patterson L, Ahmad Z, Burcu H, Ottaviani D, Diss JK, Box C, Eccles SA & Djamgoz MB (2011). Angiogenic functions of voltage-gated Na^+ channels in human endothelial cells: modulation of vascular endothelial growth factor (VEGF) signaling. *J Biol Chem* **286**, 16846–16860.

Armstrong CM & Hille B (1998). Voltage-gated ion channels and electrical excitability. *Neuron* **20**, 371–380.

Baudino TA, Carver W, Giles W & Borg TK (2006). Cardiac fibroblasts: friend or foe? *Am J Physiol Heart Circ Physiol* **291**, H1015–H1026.

Benamer N, Fares N, Bois P & Faivre JF (2011). Electrophysiological and functional effects of sphingosine-1-phosphate in mouse ventricular fibroblasts. *Biochem Biophys Res Commun* **408**, 6–11.

Benamer N, Moha Ou MH, Demolombe S, Cantereau A, Delwail A, Bois P, Bescond J & Faivre JF (2009). Molecular and functional characterization of a new potassium conductance in mouse ventricular fibroblasts. *J Mol Cell Cardiol* **46**, 508–517.

Black JA, Liu S & Waxman SG (2009). Sodium channel activity modulates multiple functions in microglia. *Glia* **57**, 1072–1081.

Brilla CG, Maisch B, Zhou G & Weber KT (1995). Hormonal regulation of cardiac fibroblast function. *Eur Heart J* **16 Suppl C**, 45–50.

Burstein B, Libby E, Calderone A & Nattel S (2008). Differential behaviors of atrial versus ventricular fibroblasts: a potential role for platelet-derived growth factor in atrial-ventricular remodeling differences. *Circulation* **117**, 1630–1641.

Burstein B & Nattel S (2008). Atrial fibrosis: mechanisms and clinical relevance in atrial fibrillation. *J Am Coll Cardiol* **51**, 802–809.

Catterall WA (1986). Molecular properties of voltage-sensitive sodium channels. *Annu Rev Biochem* **55**, 953–985.

Catterall WA, Goldin AL & Waxman SG (2005). International Union of Pharmacology. XLVII. Nomenclature and structure-function relationships of voltage-gated sodium channels. *Pharmacol Rev* **57**, 397–409.

Chilton L, Ohya S, Freed D, George E, Drobic V, Shibukawa Y, Maccannell KA, Imaizumi Y, Clark RB, Dixon IM & Giles WR (2005). K^+ currents regulate the resting membrane potential, proliferation, and contractile responses in ventricular fibroblasts and myofibroblasts. *Am J Physiol Heart Circ Physiol* **288**, H2931–H2939.

Du J, Xie J, Zhang Z, Tsujikawa H, Fusco D, Silverman D, Liang B & Yue L (2010). TRPM7-mediated Ca^{2+} signals confer fibrogenesis in human atrial fibrillation. *Circ Res* **106**, 992–1003.

El Chemaly A, Guinamard R, Demion M, Fares N, Jebara V, Faivre JF & Bois P (2006). A voltage-activated proton current in human cardiac fibroblasts. *Biochem Biophys Res Commun* **340**, 512–516.

Ellmers LJ, Knowles JW, Kim HS, Smithies O, Maeda N & Cameron VA (2002). Ventricular expression of natriuretic peptides in Npr1(–/–) mice with cardiac hypertrophy and fibrosis. *Am J Physiol Heart Circ Physiol* **283**, H707–H714.

Fozzard HA & Hanck DA (1996). Structure and function of voltage-dependent sodium channels: comparison of brain II and cardiac isoforms. *Physiol Rev* **76**, 887–926.

Gillet L, Roger S, Besson P, Lecaille F, Gore J, Bougnoux P, Lalmanach G & Le Guennec JY (2009). Voltage-gated sodium channel activity promotes cysteine cathepsin-dependent invasiveness and colony growth of human cancer cells. *J Biol Chem* **284**, 8680–8691.

Hatem SN, Benardeau A, Rucker-Martin C, Marty I, de CP, Villaz M & Mercadier JJ (1997). Different compartments of sarcoplasmic reticulum participate in the excitation-contraction coupling process in human atrial myocytes. *Circ Res* **80**, 345–353.

Huang H, Priori SG, Napolitano C, O'Leary ME & Chahine M (2010). Y1767C, a novel SCN5A mutation induces a persistent sodium current and potentiates ranolazine inhibition of Nav1.5 channels. *Am J Physiol Heart Circ Physiol* **300**, H288–299.

Kamkin A, Kiseleva I & Isenberg G (2003*a*). Activation and inactivation of a non-selective cation conductance by local mechanical deformation of acutely isolated cardiac fibroblasts. *Cardiovasc Res* **57**, 793–803.

Kamkin A, Kiseleva I, Wagner KD, Lammerich A, Bohm J, Persson PB & Gunther J (1999). Mechanically induced potentials in fibroblasts from human right atrium. *Exp Physiol* **84**, 347–356.

Kamkin A, Kiseleva I, Wagner KD, Lozinsky I, Gunther J & Scholz H (2003*b*). Mechanically induced potentials in atrial fibroblasts from rat hearts are sensitive to hypoxia/reoxygenation. *Pflugers Arch* **446**, 169–174.

Kamkin A, Kiseleva I, Wagner KD, Pylaev A, Leiterer KP, Theres H, Scholz H, Gunther J & Isenberg G (2002). A possible role for atrial fibroblasts in postinfarction bradycardia. *Am J Physiol Heart Circ Physiol* **282**, H842–H849.

Kiseleva I, Kamkin A, Pylaev A, Kondratjev D, Leiterer KP, Theres H, Wagner KD, Persson PB & Gunther J (1998). Electrophysiological properties of mechanosensitive atrial fibroblasts from chronic infarcted rat heart. *J Mol Cell Cardiol* **30**, 1083–1093.

Li GR, Sun HY, Chen JB, Zhou Y, Tse HF & Lau CP (2009*a*). Characterization of multiple ion channels in cultured human cardiac fibroblasts. *PLoS One* **4**, e7307.

Li GR, Sun HY, Zhang XH, Cheng LC, Chiu SW, Tse HF & Lau CP (2009*b*). Omega-3 polyunsaturated fatty acids inhibit transient outward and ultra-rapid delayed rectifier K^+ currents and Na^+ current in human atrial myocytes. *Cardiovasc Res* **81**, 286–293.

Li Q, Huang H, Liu G, Lam K, Rutberg J, Green MS, Birnie DH, Lemery R, Chahine M & Gollob MH (2009*c*). Gain-of-function mutation of Nav1.5 in atrial fibrillation enhances cellular excitability and lowers the threshold for action potential firing. *Biochem Biophys Res Commun* **380**, 132–137.

Lin X, Liu N, Lu J, Zhang J, Anumonwo JM, Isom LL, Fishman GI & Delmar M (2011). Subcellular heterogeneity of sodium current properties in adult cardiac ventricular myocytes. *Heart Rhythm* **8**, 1923–1930.

Louault C, Benamer N, Faivre JF, Potreau D & Bescond J (2008). Implication of connexins 40 and 43 in functional coupling between mouse cardiac fibroblasts in primary culture. *Biochim Biophys Acta* **1778**, 2097–2104.

Manabe I, Shindo T & Nagai R (2002). Gene expression in fibroblasts and fibrosis: involvement in cardiac hypertrophy. *Circ Res* **91**, 1103–1113.

Margolskee RF, McHendry-Rinde B & Horn R (1993). Panning transfected cells for electrophysiological studies. *Biotechniques* **15**, 906–911.

Miragoli M, Gaudesius G & Rohr S (2006). Electrotonic modulation of cardiac impulse conduction by myofibroblasts. *Circ Res* **98**, 801–810.

Miragoli M, Salvarani N & Rohr S (2007). Myofibroblasts induce ectopic activity in cardiac tissue. *Circ Res* **101**, 755–758.

Mishra S, Undrovinas NA, Maltsev VA, Reznikov V, Sabbah HN & Undrovinas A (2011). Post-transcriptional silencing of SCN1B and SCN2B genes modulates late sodium current in cardiac myocytes from normal dogs and dogs with chronic heart failure. *Am J Physiol Heart Circ Physiol* **301**, H1596–1605.

Nakajima H, Nakajima HO, Salcher O, Dittie AS, Dembowsky K, Jing S & Field LJ (2000). Atrial but not ventricular fibrosis in mice expressing a mutant transforming growth factor-β_1 transgene in the heart. *Circ Res* **86**, 571–579.

Raizman JE, Komljenovic J, Chang R, Deng C, Bedosky KM, Rattan SG, Cunnington RH, Freed DH & Dixon IM (2007). The participation of the Na^+-Ca^{2+} exchanger in primary cardiac myofibroblast migration, contraction, and proliferation. *J Cell Physiol* **213**, 540–551.

Roger S, Besson P & Le Guennec JY (2003). Involvement of a novel fast inward sodium current in the invasion capacity of a breast cancer cell line. *Biochim Biophys Acta* **1616**, 107–111.

Rose RA, Hatano N, Ohya S, Imaizumi Y & Giles WR (2007). C-type natriuretic peptide activates a non-selective cation current in acutely isolated rat cardiac fibroblasts via natriuretic peptide C receptor-mediated signalling. *J Physiol* **580**, 255–274.

Sato PY, Musa H, Coombs W, Guerrero-Serna G, Patino GA, Taffet SM, Isom LL & Delmar M (2009). Loss of plakophilin-2 expression leads to decreased sodium current and slower conduction velocity in cultured cardiac myocytes. *Circ Res* **105**, 523–526.

Schneider M, Proebstle T, Hombach V, Hannekum A & Rudel R (1994). Characterization of the sodium currents in isolated human cardiocytes. *Pflugers Arch* **428**, 84–90.

Schotten U, Verheule S, Kirchhof P & Goette A (2011). Pathophysiological mechanisms of atrial fibrillation: a translational appraisal. *Physiol Rev* **91**, 265–325.

Shibukawa Y, Chilton EL, Maccannell KA, Clark RB & Giles WR (2005). K^+ currents activated by depolarization in cardiac fibroblasts. *Biophys J* **88**, 3924–3935.

Swynghedauw B (1999). Molecular mechanisms of myocardial remodeling. *Physiol Rev* **79**, 215–262.

Teunissen BE, Smeets PJ, Willemsen PH, De Windt LJ, Van der Vusse GL & Van Bilsen M (2007). Activation of PPARdelta inhibits cardiac fibroblast proliferation and the transdifferentiation into myofibroblasts. *Cardiovasc Res* **75**, 519–529.

Vasquez C, Benamer N & Morley GE (2011). The cardiac fibroblast: functional and electrophysiological considerations in healthy and diseased hearts. *J Cardiovasc Pharmacol* **57**, 380–388.

Verheule S, Sato T, Everett T 4th, Engle SK, Otten D, Rubart-von der Lohe M, Nakajima HO, Nakajima H, Field LJ & Olgin JE (2004). Increased vulnerability to atrial fibrillation in transgenic mice with selective atrial fibrosis caused by overexpression of TGF-β1. *Circ Res* **94**, 1458–1465.

Wang J, Chen H, Seth A & McCulloch CA (2003). Mechanical force regulation of myofibroblast differentiation in cardiac fibroblasts. *Am J Physiol Heart Circ Physiol* **285**, H1871–H1881.

Weber KT, Sun Y, Tyagi SC & Cleutjens JP (1994). Collagen network of the myocardium: function, structural remodeling and regulatory mechanisms. *J Mol Cell Cardiol* **26**, 279–292.

Xiao HD, Fuchs S, Campbell DJ, Lewis W, Dudley SC Jr, Kasi VS, Hoit BD, Keshelava G, Zhao H, Capecchi MR & Bernstein KE (2004). Mice with cardiac-restricted angiotensin-converting enzyme (ACE) have atrial enlargement, cardiac arrhythmia, and sudden death. *Am J Pathol* **165**, 1019–1032.

Yue L, Xie J & Nattel S (2011). Molecular determinants of cardiac fibroblast electrical function and therapeutic implications for atrial fibrillation. *Cardiovasc Res* **89**, 744–753.

Zhao P, Barr TP, Hou Q, Dib-Hajj SD, Black JA, Albrecht PJ, Petersen K, Eisenberg E, Wymer JP, Rice FL & Waxman SG (2008). Voltage-gated sodium channel expression in rat and human epidermal keratinocytes: evidence for a role in pain. *Pain* **139**, 90–105.

Zlochiver S, Munoz V, Vikstrom KL, Taffet SM, Berenfeld O & Jalife J (2008). Electrotonic myofibroblast-to-myocyte coupling increases propensity to reentrant arrhythmias in two-dimensional cardiac monolayers. *Biophys J* **95**, 4469–4480.

Author contributions

A.C., P.C., P.B., M.C. and J.F.F. contributed to the conception and design of the experiments. A.C., A.M., B.T., O.T., M.M. and N.B. performed data collection, analysis and/or interpretation. A.C.,

P.B., M.C. and J.F.F. drafted or critically revised the manuscript. qPCR experiments were done at the Institut Universitaire en Sant Mentale de Qubec (Qubec, Canada). All other experiments were performed at the Institut de Physiologie et Biologie Cellulaire (Poitiers, France). All authors approved the final version submitted.

Acknowledgements

The authors are grateful to Christophe Magaud for his expert technical assistance and to ImageUp microscopic platform for fluorescence imaging. This work was supported in part by the Fondation de France. The authors declare no conflict of interest in relation to this article.

Translational perspective

Fibroblasts play a major role in heart physiology. They are at the origin of the extracellular matrix renewal and production of various paracrine and autocrine factors. In pathological conditions, fibroblasts proliferate, migrate and differentiate into myofibroblasts leading to cardiac fibrosis. This differentiated status is associated with changes in gene expression profile, leading to neo-expression of proteins such as ionic channels. We demonstrate that the activity of voltage-gated sodium channels increases as human atrial fibroblasts differentiate into myofibroblasts. It can be hypothesized that during the fibrosis process characterized by fibroblast differentiation the sodium channel modulation in these non-excitable cells may contribute to a pathological phenotype. Since fibrosis is one of the fundamental mechanisms involved in atrial fibrillation, it may be of great interest to investigate how this current could influence myofibroblast proliferation, migration and secretion properties. On the other hand, several sodium channel mutations are related to cardiac pathologies such as long QT, Brugada syndrome and Lenegre disease. This study raises the possibility that some cardiac consequences of such mutations may be due to myofibroblasts in addition to cardiac muscular cell alteration. In conclusion, this study provides a new direction in research on the cardiac role of sodium channels.

Molecular Pharmacology Fast Forward. Published on July 15, 2014 as doi:10.1124/mol.114.093104

Fluoxetine Blocks $Na_v1.5$ Channels Via a Mechanism Similar to That of Class 1 Antiarrhythmics

Hugo Poulin, Iva Bruhova, Quadiri Timour, Olivier Theriault, Jean-Martin Beaulieu, Dominique Frassati, and Mohamed Chahine

Centre de recherche, Institut universitaire en santé mentale de Québec, Quebec City, QC, Canada (H.P., O.T., J.-M.B., M.C.); The State University of New York at Buffalo, Buffalo, NY, USA (I.B.); Laboratoire de Pharmacologie Médicale, EA 4612 Neurocardiologie, Université Lyon 1, Lyon, France (Q.T.); Department of Psychiatry and Neuroscience, Université Laval, Quebec City, QC, Canada (J.-M.B.); Pôle Dapela, Département de l'autisme et des psychoses d'évolution lente de l'adulte, Centre Hospitalier Le Vinatier, Bron, France (D.F.); Department of Medicine, Université Laval, Quebec City, QC, Canada (M.C.)

Fluoxetine blocks $Na_v1.5$ channels

Correspondence to:
Mohamed Chahine, Ph.D.
Centre de recherche
Institut universitaire en santé mentale de Québec
2601 chemin de la Canardière
Quebec City, QC, Canada G1J 2G3
Telephone: 1-418-663-5747, #4723
Fax: 1-418-663-8756
Email: mohamed.chahine@phc.ulaval.ca

Number of pages: **35**

Number of figures: **6**

Number of tables: **1**

Number of references: **47**

Word count in the abstract: **249**

Word count in the introduction: **492**

Word count in the discussion: **1710**

Abbreviations: CNS, central nervous system; DAT, dopamine transporter; HP, holding potential; IC50, dose producing 50% maximum current inhibition; OCD, obsessive compulsive disorders; MAT, monoamine transporter; NET, norepinephrine transporter; SCD, sudden cardiac death; SERT, serotonin transporter; SSRI, selective serotonin re-uptake inhibitor

Abstract

The voltage-gated $Na_v1.5$ channel is essential for the propagation of action potentials in the heart. Malfunctions of this channel are known to cause hereditary diseases. It is a prime target for class 1 antiarrhythmic drugs and a number of antidepressants. The purpose of the present study was to investigate the $Na_v1.5$ blocking properties of fluoxetine, a selective serotonin re-uptake inhibitor. $Na_v1.5$ channels were expressed in HEK-293 cells, and Na^+ currents were recorded using the patch-clamp technique. Dose-response curves of racemic fluoxetine (IC_{50} = 39 μM) and its optical isomers had similar IC_{50} (40 and 47 μM for the (+) and (–) isomer, respectively). Norfluoxetine, a fluoxetine metabolite, had a higher affinity than fluoxetine, with an IC_{50} of 29 μM. Fluoxetine inhibited currents in a frequency-dependent manner, shifted steady-state inactivation to more hyperpolarized potentials, and slowed the recovery of $Na_v1.5$ from inactivation. Mutating a phenylalanine (F1760) and a tyrosine (Y1767) in DIVS6, significantly reduced the affinity of fluoxetine and its frequency-dependent inhibition. We used a non-inactivating $Na_v1.5$ mutant to show that fluoxetine displays open-channel block behavior. The molecular model of fluoxetine in $Na_v1.5$ was in agreement with mutational experiments, in which F1760 and Y1767 were found to be the key residues in binding fluoxetine. We concluded that fluoxetine blocks $Na_v1.5$ by binding to the class 1 antiarrhythmic site. The blocking of cardiac Na^+ channels should be taken into consideration when prescribing fluoxetine alone, or in association with other drugs that may be cardiotoxic or for patients with conduction disorders.

Introduction

Fluoxetine (Prozac) is a selective serotonin re-uptake inhibitor (SSRI) (Wong *et al.*, 1995) that is widely prescribed for the treatment of Central Nervous System (CNS)-linked cognitive, emotional, and behavioral disorders. Since its discovery in 1974 (Wong *et al.*, 1974), the beneficial psychotropic effects of fluoxetine have led to its being used to treat disorders other than depression, including obsessive compulsive disorders (OCD) and bulimia nervosa (Wong *et al.*, 1995). The multiple side effects of fluoxetine (Sghendo and Mifsud, 2012) have raised questions about its supposed selective 5-HT-mediated effect. While fluoxetine inhibits serotonin transporter (SERT) in the low nanomolar range (Torres *et al.*, 2003), its therapeutic effect appears only at a much higher plasma and brain concentrations (Muscettola *et al.*, 1978; Bolo *et al.*, 2000). At low micromolar concentrations, fluoxetine also targets other proteins and inhibits several types of ion channels and receptors, including the nicotinic acetylcholine receptor (Hennings *et al.*, 1999; Eisensamer *et al.*, 2003), voltage-gated Ca^{2+} channels (Deák *et al.*, 2000; Pacher *et al.*, 2000), volume-regulated anion channels (Maertens *et al.*, 2002), neuronal Na^+ channels (Lenkey *et al.*, 2006), and hERG, a cardiac K^+ channel (Thomas *et al.*, 2002). The inhibition of the hERG K^+ channel by fluoxetine occurs via two different mechanisms: (i) direct channel blockade and (ii) disruption of channel protein trafficking (Rajamani *et al.*, 2006). This may explain some of the cardiovascular side effects observed during chronic fluoxetine treatments, including bradycardia and QT prolongation (Pacher and Kecskemeti, 2008; Timour *et al.*, 2012). Dysfunctions of $Na_V1.5$, which are responsible for the rapid upstroke of the action potential caused by the rapid entry of Na^+ ions into cardiomyocytes, also lead to arrhythmia complications. The

prolongation of QT intervals may be due to the improper inactivation of the $Na_v1.5$ as in Romano-Ward syndrome (LQT3), while the reduction of Na^+ currents through $Na_v1.5$ may lead to arrhythmias such as Brugada syndrome (Herbert and Chahine, 2006). The major cause of the higher mortality rate in psychiatric patients *versus* the general population is sudden cardiac death (SCD), which mainly results from arrhythmias that occur during treatments with psychotropic drugs. It has been reported that fluoxetine decreases the maximum rate of rise of the depolarization phase (V_{max}) of ventricular cell preparations (Pacher *et al.*, 2000; Magyar *et al.*, 2003), but little is known about the direct effect of fluoxetine on the biophysical properties of $Na_v1.5$.

In the present study, we investigated the electrophysical properties of fluoxetine (racemic and enantiomers) and its metabolite norfluoxetine, as well as other psychotropic drugs, on $Na_v1.5$ stably expressed in HEK-293 cells. We showed that racemic fluoxetine, its metabolite norfluoxetine, and its enantiomers act as potential antagonists of human $Na_v1.5$ unlike the other classes of antidepressants tested.

We also studied the effect of the F1760C and Y1767C mutations of the class I antiarrhythmic binding site on the use-dependent blockade of cardiac Na^+ channels by fluoxetine and showed that fluoxetine behaves like a class I antiarrhythmic drug.

Materials and Methods

Cell cultures

Human embryonic kidney (HEK-293) cells stably expressing human $Na_v1.5$ were used as previously described (Huang *et al.*, 2011). In brief, the cells were grown under standard tissue culture conditions (5% CO_2, 37°C) in high-glucose DMEM supplemented with 10% FBS, 2 mM L-glutamine, 100 U/ml of penicillin, and 10 mg/ml of streptomycin (Gibco-BRL Life Technologies, Burlington, ON). For experiments with the F1760C, Y1767C, and L409C/A410W mutants, the HEK-293 cells were transiently transfected with the pcDNA3.1 vector containing mutant $Na_v1.5$ cDNA (5 μg) or with the empty vector pIRES/CD8 (5 μg) in 10 cm petri dishes using the calcium phosphate method as previously described (Huang *et al.*, 2011). Transfected cells were briefly preincubated with CD8 antibody-coated beads (Dynabeads M450 CD8-a, (Life Technologies Inc., Burlington, ON, Canada) before recording currents. HEK-293 cells expressing the pIRES/CD8 vector were decorated with CD8 beads, which were used to identify cells for recording Na^+ currents.

Whole-cell patch-clamp recordings

Macroscopic Na^+ currents from HEK-293 cells were recorded using the whole-cell patch-clamp technique. Patch-clamp recordings were obtained using low-resistance, fire-polished electrodes (<1 MΩ) made from 8161 Corning borosilicate glass coated with Sylgard (Dow-Corning, Midland, MI) to minimize electrode capacitance. Currents were recorded using an Axopatch 200 amplifier with the pClamp software (Molecular Devices Sunnyvale, CA). The series resistance was 70-80% compensated. Whole-cell currents

were filtered at 5 kHz, digitized at 10 kHz, and stored on a microcomputer equipped with an analog-to-digital converter (Digidata 1300, Molecular Devices). The cells were allowed to stabilize for 5 min after the whole-cell configuration was established before recording the currents. The experiments were performed at room temperature (22°C). The pipettes were filled with an intracellular solution composed of 35 mM NaCl, 105 mM CsF, 10 mM EGTA, and 10 mM Cs-HEPES. The pH was adjusted to 7.4 with CsOH. The external solution was composed of 150 mM NaCl, 2 mM KCl, 1.5 mM $CaCl_2$, 1 mM $MgCl_2$, 10 mM glucose, and 10 mM HEPES. The pH was adjusted to 7.4 with NaOH.

The drugs were applied using a constantly running ValveLink8.2® gravity-driven perfusion system (Automate Scientific, Berkeley, CA) equipped with a glass syringe with a 250 μM tip. Different concentrations of the same drug were applied on the same cell. We used silicone-free tubing since we had observed changes in fluoxetine concentrations when silicon tubing was used, most likely because fluoxetine adheres to silicone, which can change the applied concentrations considerably.

The peak current amplitudes at different drug concentrations were subtracted from the value obtained with the control solution and were normalized to the control value in order to obtain the dose-response curves and IC_{50} values. Each point on the dose-response curves represents the mean of inhibition calculated from all recorded cells at a specific drug concentration. The values were fit to a Hill equation of the following form:

$$(I_{control} - I_{fluoxetine})/I_{control} = ax^b/(c^b + x^b),$$

where I is the peak current, a is the maximum inhibition, b is the Hill coefficient, c is the IC_{50}, and x is the concentration of agonist. To obtain activation curves, Na^+ conductance (G_{Na}) was calculated from the peak current (I_{Na}) using the following equation: $G_{Na} =$

$I_{Na}/(V - E_{Na})$, where V is the test potential and E_{Na} is the reversal potential. Normalized G_{Na} values were plotted against the test potentials. To obtain the inactivation curves, the peak current was normalized to the maximal value and was plotted against the conditioning pulse potential. Steady-state activation and inactivation curves were fit to a Boltzmann equation of the following form:

$$G/G_{max}\ (or\ I/I_{max}) = 1/[1 + \exp\ (V_{1/2} - V/k_v],$$

where G is the conductance, I is the current, $V_{1/2}$ is the voltage at which the channels are half-maximally activated or inactivated, and k_v is the slope factor. To determine the recovery from inactivation, the test pulse peak current (I_{test}) was normalized to the corresponding prepulse current (I_{cont}). I_{test}/I_{cont} was plotted against the pulse interval and was fitted to a double or triple exponential function of the following form:

$$I/I_{max} = A_1(1 - \exp\ (-t/\tau_1)) + A_2(1 - \exp\ (-t/\tau_2))$$

or

$$I/I_{max} = A_1(1 - \exp\ (-t/\tau_1)) + A_2(1 - \exp\ (-t/\tau_2)) + A_3(1 - \exp\ (-t/\tau_3)),$$

where τ_1, τ_2 and τ_3 are the time constants, t is the time and A_1, A_2 and A_3 are the amplitudes of the time constants.

The results were analyzed using a combination of pCLAMP software v10.2 (Molecular Devices), Microsoft Excel, and SigmaPlot v11.0 (SSPSS, Chicago, IL).

Statistical analysis

Results are expressed as means ± SEM. Statistical significance was calculated using Student's unpaired t test, and the level of statistical significance was set at $P < 0.05$. The

statistical significances for the IC_{50} were calculated using R software and the *drc* package (The R Foundation for Statistical Computing, Vienna, Austria).

Drugs

Racemic fluoxetine, S (+) fluoxetine, S (–) fluoxetine, norfluoxetine, and (+) fenfluramine were from Sigma-Aldrich (St. Louis, MO). Nisoxetine and methylphenidate were from Tocris Bioscience (Bristol, UK). Stock solutions (5 mM) were prepared in water and were diluted in the external solution prior to use.

Homology modeling of fluoxetine binding site in the $Na_v1.5$

The human cardiac $Na_v1.5$ was modeled in the closed and open states based on the closed Na_vAb (3RVY.pdb) and open Na_vMs (3ZJZ.pdb) X-ray structures (Payandeh *et al.*, 2011; Bagnéris *et al.*, 2013). To describe the symmetric positions of residues in four homologous domains in the channel, we used a universal residue-labeling scheme (Zhorov and Tikhonov, 2004). A residue is labeled by its domain number (1-4), segment (i, inner helix S6; o, outer helix S5; p, P-loop), and the relative number from the N end of a transmembrane helix or from the DEKA-locus positions 1p50, 2p50, etc. For example, $F^{4i15(1760)}$ designates phenylalanine in the domain IV inner helix, 15 positions downstream from the start of the segment. In some cases, the sequence-based residue number is included in the label in parentheses.

The alignment of bacterial Na_vAb and Na_vMs with eukaryotic sodium channels was taken as previously proposed (Payandeh *et al.*, 2011; McCusker *et al.*, 2012; Tikhonov and Zhorov, 2012). An insertion downstream from the DEKA locus was proposed (Tikhonov and Zhorov, 2012), however, in our models, this insertion was not introduced

as the ligand was docked in the pore and residues above the DEKA locus would not affect ligand binding. The models contained the pore region (S5, P, and S6) of the human $Na_v1.5$. The closed model also contained the L4-5 linker (the linker between domain 4 and 5) because it is available in the X-ray structure. The extracellular linkers between P-loops and transmembrane helices were truncated to match the length of the X-ray structure templates, which does not affect ligand docking in the inner pore as they are distant. Ionizable residues were modeled as neutral, but the ionizable residues of DEKA locus were modeled as charged. S-fluoxetine was modeled as protonated, since its ammonium group has a pKa of ~10.

All calculations were performed using the ZMM program (www.zmmsoft.com, ZMM Software Inc., Flamborough, Ontario, Canada). The nonbonded energy was calculated using the AMBER force field (Weiner *et al.*, 1984, 1986) with a cutoff distance of 8 Å. Atomic charges at fluoxetine were calculated with the MOPAC software using the semi-empirical method AM1 (Dewar *et al.*, 1985). The hydration energy was calculated by using the implicit-solvent method (Lazaridis and Karplus, 1999). Electrostatic energy was calculated using the environment- and distance-dependent dielectric function without desolvation energy (Garden and Zhorov, 2010). The DEKA locus was loaded with an explicit water molecule, which was initially constrained to the Asp and Lys side chains, subsequently once constraints were removed, the water did not move away from the DEKA locus. The Monte Carlo minimization (MCM) method (Li and Scheraga, 1987) was used to optimize the models. All torsional angles of the protein and ligand were allowed to vary during energy calculations, while bond angles were rigid in the protein and flexible in the ligand. To prevent large deviations of the channel

models from the X-ray structure templates during energy minimizations, the α-carbons of the model were constrained to the template using a flat-bottom energy function that allows atoms to deviate penalty-free up to 1 Å, but imposes a penalty of 10 kcal mol^{-1} $Å^{-1}$ for larger deviations. All molecular images were created using MVM. No specific energy terms were used for cation-π interactions, which were accounted for with partial negative charges at the aromatic carbons (Bruhova *et al.*, 2008).

The homology models were first MC-minimized without ligand until the 3000 consecutive energy minimizations did not improve the apparent global minimum found. The optimal binding modes of S-fluoxetine were searched by a two-stage random-docking approach. In the first stage, 60 000 different binding modes of the ligand were randomly generated within a cube with 14 Å edges. This sampling volume covered the entire inner pore including the domain interfaces. Each binding mode was MC-minimized for only 5 steps to remove steric overlaps with the protein. Energetically favorable conformations within 200 kcal/mol from the apparent global minimum were accumulated and then clustered based on ligand generalized coordinates. In the second stage, the 500 energetically best conformations found in the first stage were further MC-minimized for 1000 MC-minimization steps. The energetically most favorable ligand-receptor complexes within 4 kcal/mol were collected and analyzed.

Results

Fluoxetine and its optical isomers block the $Na_v1.5$ channel

We studied the effect of fluoxetine on $Na_v1.5$ stably expressed in HEK-293 cells. Figure 1A shows an example of whole-cell current traces before (control) and after superfusion of 25 and 100 μM racemic fluoxetine. Fluoxetine inhibited Na^+ currents, with a maximum blockade occurring at 100 μM. The inhibition was partially reversible. The superfusion of increasing concentrations of fluoxetine (1, 10, 25, 50, 100, and 200 μM) showed that the blockade by fluoxetine was dose dependent. The dose-response curves (Fig. 1B) showed that the sensitivities of the optical isomers were similar, with an IC_{50} of 39.4 μM for racemic fluoxetine, and 40.0 μM and 46.7 μM for the (+) and (–) isomers, respectively. When the cells were maintained at a holding potential of -90 mV instead of -140 mV, where a proportion of the channels are inactivated, the affinity of racemic fluoxetine for $Na_v1.5$ significantly increased with an IC_{50} of 4.7 μM. Surprisingly, norfluoxetine, a fluoxetine metabolite, displayed a significantly higher affinity than fluoxetine, with an IC50 of 29.5 μM at holding potential of -140 mV. Surprisingly, norfluoxetine, a fluoxetine metabolite, displayed a significantly higher affinity than fluoxetine, with an IC50 of 29.5 μM at holding potential of -140 mV.

The effects of three other monoamine transporters (MAT) -targeting drugs were also tested using HEK-293 cells stably expressing $Na_v1.5$. The norepinephrin reuptake inhibitor, nisoxetine, the dopamine reuptake inhibitor, methylphenidate, and fenfluramine, which like fluoxetine, targets SERT, were all less effective in blocking the channels than fluoxetine, with IC_{50} of 104.5, 618.7 and 203.5 μM, respectively at a holding potential of -140 mV (Fig. 1C). The inhibition potency of these three compounds

was also increased at a holding potential of -90 mV, with IC_{50} of 20.2, 239.5 and 65.5 μM for nisoxetine, methylphenidate and fenfluramine, respectively (Fig. 1C).

Effect of fluoxetine on the steady-state gating properties of $Na_v1.5$ channels

The availability of Na^+ channels following depolarization depends on a number of parameters, including the membrane potential. Fewer channels become available as the membrane potential progressively becomes more depolarized. This is due to the buildup of channels in the inactivated non-conducting state. We studied this phenomenon using a double-pulse protocol: a 500 ms conditioning pulse to voltages ranging from –140 mV to 0 mV, and a test pulse to –30 mV. The current measured following the test pulse is an indicator of the fraction of available channels. The normalized currents following the test pulse were plotted against the conditioning voltage (Fig. 2A). Fluoxetine (30 μM) significantly shifted the $V_{1/2}$ of inactivation of $Na_v1.5$ by 6.7 mV toward more hyperpolarized voltages and resulted in a less steep slope factor (Table 1 and Fig. 2A).

We also investigated the effect of fluoxetine on the steady-state activation of $Na_v1.5$. The activation curves were derived from I/V curves (see Materials and Methods). The activation curves of $Na_v1.5$ in the absence and presence of 30 μM fluoxetine were plotted against voltage (Fig. 2A). Fluoxetine did not significantly shift the midpoint of steady-state activation but had a little effect on the slope factor by reducing its steepness.

Fluoxetine slows the recovery from inactivation of $Na_v1.5$ channels

A prominent characteristic of many class 1 antiarrhythmics is their ability to slow the recovery from inactivation of drug-modified Na^+ channels. We used a two-pulse protocol

to investigate the effect of fluoxetine on the recovery from inactivation. We used a 40 ms, –30 mV conditioning pulse and a 20 ms, –30 mV test pulse, with an interval ranging from 0.1 to 4000 ms to induce recovery from inactivation. The amplitudes of the Na^+ currents measured following the test pulse were then normalized to the control currents and were plotted against the duration of the recovery interval. Channels that recovered from inactivation displayed a progressive increase in currents following the increase in the recovery interval (Fig. 2B). The recovery from inactivation of $Na_v1.5$ after fluoxetine treatment was strongly slowed with the appearance of a third time constant. In comparison, the control curve had a τ_1 and τ_2 of 1.50 and 9.13 ms, respectively, while the fluoxetine had a τ_1, τ_2 and τ_3 of 1.63, 14.90 and 1598.23 ms, respectively (Table 1).

Fluoxetine blocks $Na_v1.5$ channels in a use-dependent manner

During depolarization, Na^+ channels cycle from the resting to the activated and inactivated states. However, when they are subjected to a train of depolarizing pulses, the number of channels available to open is reduced because they are gradually trapped in the inactivated state. This phenomenon is referred to as use-dependence or "frequency-dependent" current reduction. In the presence of a drug, further decreases in currents are likely due to the accumulation of drug-modified channels. For example, lidocaine, a class 1 antiarrhythmic drug, is known to cause the use-dependent inhibition of Na^+ channels. We tested the effect of rapid pulsing on $Na_v1.5$ by applying a series of 50 short 10 ms depolarizing –30 mV pulses. We first characterized the effect of fluoxetine on $Na_v1.5$/WT, and then on the $Na_v1.5$/F1760C and $Na_v1.5$/Y1767C mutant channels. We previously reported that these highly conserved residues of the D4S6 directly contribute

to local anesthetic binding to cardiac channels (O'Leary and Chahine, 2002). As shown in Figure 3A, in the absence of fluoxetine, there was no significant change in the availability of $Na_v1.5$/WT channels when they were pulsed up to 10 Hz. However, in the presence of 30 μM fluoxetine, the availability of $Na_v1.5$/WT channels was dramatically reduced by 44% (P50/P1) when they were pulsed at 2 Hz (Fig. 3B-C) in comparison with the control without drug. When 5 and 10 Hz pulses were used, 30 μM fluoxetine reduced the currents of the $Na_v1.5$/WT by 58% and 67%, respectively compared to the control without drug. To further investigate the role of class 1 antiarrhythmic binding in the current block caused by fluoxetine, we inserted the F1760C or Y1767C mutation into $Na_v1.5$. As shown in Figure 3B-C, 30 μM fluoxetine reduced the current by 8%, 15%, and 20% when $Na_v1.5$/F1760C were pulsed at 2, 5, and 10 Hz, respectively, in comparison with the control without drug. The Y1760C mutation almost completely prevented the use-dependent inhibition of fluoxetine, with a maximal current inhibition of 5% when pulsed at 10 Hz. These results indicated that fluoxetine blocks $Na_v1.5$/WT currents in a use-dependent manner, and that the F1760C and Y1767C mutations dramatically reduce the use-dependent inhibition.

Fluoxetine had a lower affinity for $Na_v1.5$/F1760C mutant channels

We studied the effect of the F1760C and Y1767C mutations on the concentration-dependent block of $Na_v1.5$ currents by fluoxetine. Figure 4A shows examples of current traces recorded from $Na_v1.5$/WT and the mutant channels before and after a treatment with 50 μM fluoxetine. As shown in Figure 4B, while the IC_{50} value of fluoxetine for

$Na_v1.5$/Y1767C (50.1 μM) was slightly higher to that of $Na_v1.5$/WT (39.4 μM), the IC_{50} value for $Na_v1.5$/F1760C (82.8 μM) was more than twice that of the WT channel.

Fluoxetine act as an open-channel blocker

To investigate the role of inactivation in the blockade of $Na_v1.5$ by fluoxetine in greater detail, we used $Na_v1.5$/L409C/A410W mutant stably expressed in HEK-293 cells. These channels exhibit a significant reduction in fast inactivation in HEK-293 (Wang *et al.*, 2013). A large persistent current was detected in the absence of fluoxetine (Fig. 5A). We applied different concentrations of fluoxetine and determined the IC_{50} at the peak current and at the end of the test pulse (90-100 ms). The block at the end of the pulse represents the affinity of the fluoxetine for open channels. As shown in Figure 5B, the IC_{50} (3.5 μM) at the end of the pulse was slightly lower than the IC_{50} at the peak current (9.6 μM), suggesting that fluoxetine is an open-channel blocker.

Molecular modeling of fluoxetine in the $Na_v1.5$

To discover the molecular details of the fluoxetine binding site, we have homology modeled the pore domain of the cardiac $Na_v1.5$ in the closed and open states based on the X-ray structures of bacterial Na channels, Na_vAb (Arcobacter butzleri sodium channel) (Payandeh *et al.*, 2011) and Na_vMs (Magnetococcus sp sodium channel) (Bagnéris *et al.*, 2013), respectively (see PDB file in Data Supplement). A random sampling approach was used to search for the energetically most favorable binding modes of fluoxetine in the $Na_v1.5$. 60 000 random orientations of fluoxetine were seeded inside the channel within a volume to cover the entire pore cavity and inner helix interfaces (Fig. 6A, B). After two

rounds of Monte-Carlo energy minimizations, the energetically best fluoxetine complexes bound inside the inner pore. Fluoxetine adopts two distinct binding modes, a horizontal and a vertical binding mode (Fig. 6C-F). These two binding modes were energetically favorable in both the closed and the open channel pore.

Fluoxetine resembles a three-pointed star with a chiral center in the middle linking three arms comprising an ammonium group, a benzene ring, and a trifluoromethyl benzene ring. In both of the two binding modes of fluoxetine, its ammonium group localizes to the channel's central axis under the DEKA locus, near the focus of the P-helices (Figure 1C-F). Just one position upstream of the DEKA locus, a ring of QGFS residues in position p49 (see description of relative number scheme in Methods) favorably interact with fluoxetine since their side chains face downward into the pore. Particularly, $Q^{1p49(372)}$ and $S^{4p49(1712)}$ form favorable electrostatic contacts with fluoxetine's nitrogen, each contributing 4-9% to the ligand-receptor energy. The ammonium group of fluoxetine was also attracted by the two negatively charged residues of the DEKA locus, which outweighed the repulsion from the Lys of the DEKA locus. Further, the backbone carbonyl groups of residues two to three positions upstream of the DEKA locus (positions p47 and p48) also stabilize fluoxetine.

The horizontal and vertical binding modes are distinguished by the two benzene arms of fluoxetine. In the vertical binding mode (Fig. 6 C, E), one benzene arm is parallel and the other arm is perpendicular to the pore axis. In this mode, one benzene ring π-stacks with $Y^{4i22(1767)}$ and the other interacts with $F^{4i15(1760)}$. Y^{4i22} and F^{4i15} were found to be the two most significant residues in binding fluoxetine; each contributes 16-33% to the ligand-receptor energy. In the horizontal binding mode (Fig. 6 D, F), the two benzene

arms point away ~45-90° from the pore axis. The ligand leans against the P-loop and protrudes between the III-IV domain inner helices. Here, one of the benzene rings π-stacks with F^{4i15}, while the other arm extends towards $F^{3p49(1236)}$ and IIIS6. In the horizontal binding mode, F^{4i15} has the strongest interaction with fluoxetine contributing 23-33% to the ligand-receptor energy, while other residues contributed <10%.

The closed Na_vAb-based and open Na_vMs-based models exhibit similar channel geometry, except for the intracellular half of the inner helices of the open state that bend to widen the pore. In both the closed and open channel models, residues in position i15 (which includes F^{4i15}) and position i22 (which includes Y^{4i22}) are pore-facing. Thus, a vertical and a horizontal binding mode of fluoxetine were found in both the closed and open pore. However, in terms of energy, the horizontal binding mode was favored in the closed state, because the fluoxetine experienced ligand strain in the narrower closed pore. On the other hand, the fluoxetine preferred to adopt the vertical binding mode in the open state as it formed better ligand-receptor contacts with F^{4i15} and Y^{4i22}. In summary, the molecular model of fluoxetine in $Na_v1.5$ was in agreement with mutational experiments, suggesting that F1760 and Y1767 are the two key residues for its binding.

Discussion

In the present study, we characterized the effects of fluoxetine, a widely used antidepressant drug, on $Na_v1.5$, the cardiac voltage-gated Na^+ channel.

Our results showed that racemic fluoxetine and its optical isomers are equally effective blockers of $Na_v1.5$ when current were recorded at a holding potential of -140 mV. Similar results have been reported for cardiac voltage-gated Ca^{2+} channels in canine

ventricular cardiomyocytes, where both fluoxetine enantiomers have similar IC_{50} (Magyar *et al.*, 2003). We also conducted dose-response curves experiments for racemic fluoxetine in HEK-293 at a holding potential of -90 mV, which is near the resting potential of cardiomyocytes. These experiments showed that the IC_{50} of fluoxetine is eight time lower at a holding potential of -90 mV compared to -140 mV, going from 39.4 μM to 4.7 μM. In a manner that is hard to explain, these data are in contradiction with those published by Rajamani et al. who reported that fluoxetine does not inhibit Na^+ currents in HEK-293 cells expressing $Na_v1.5$ (Rajamani *et al.*, 2006). However, our IC_{50} of 4.7 μM is very similar with that published by Harmer et al., who reported an IC_{50} of 4.9 μM using IonWorks™ assays from $hNa_v1.5$-expressing CHO cells maintained at a holding potential of -90 mV (Harmer *et al.*, 2011). These results suggest that the holding potential of the cell is very important to the affinity of fluoxetine for the channel, as it has been also shown in rat hippocampi neurons (Lenkey *et al.*, 2006), suggesting that the fluoxetine binds with higher affinity to inactivated than to resting channels.

In the nervous system, fluoxetine primary targets SERT, which, together with dopamine transporter (DAT) and norepinephrine transporter (NET), make up the three major MAT classes. In order to investigate the effect of other MAT-targeting drugs, we investigated the effect of nisoxetine (NET-targeting drug) (Tejani-Butt, 1992), methylphenidate (DAT-targeting drug) (Han and Gu, 2006), and fenfluramine (SERT-targeting drug) (Cosgrove *et al.*, 2010) on $Na_v1.5$ currents. Our results showed that the affinity of these drugs for $Na_v1.5$ is dependent of the holding potential. The IC_{50} of nisoxetine, methylphenidate and fenfluramine are respectively 5, 2.5 and 3 times lower at a holding potential of -90 mV compared to -140 mV. Like the fluoxetine, the decrease of

IC_{50} at more depolarized potential suggests a higher affinity of these three compounds to inactivated than to resting channels. Furthermore, these compounds also exhibited a use-dependent inhibition, especially nisoxetine with a significant current reduction of 26%, 36% and 38% when pulsing at 2, 5 and 10 Hz, respectively (data not shown). However, these three compounds are still less potent than fluoxetine to inhibit $Na_v1.5$.

The present study was designed to investigate the biophysical mechanism of the $Na_v1.5$ block by fluoxetine as well as the possible pro-arrhythmic properties of this drug. A major finding of our work was that fluoxetine shifts the steady-state inactivation curve by 6.7 mV toward more hyperpolarized values, indicating that it binds to the inactivated state of $Na_v1.5$, as is the case with neuronal Na^+ channels (Lenkey *et al.*, 2006). In addition to a tonic block, fluoxetine decreased $Na_v1.5$ currents in a use-dependent manner when pulsing at 2, 5 and 10 Hz, The affinity of fluoxetine for $Na_v1.5$ thus appears to be modulated by the state of the channel, which rapidly switches between the open and inactivated configurations, leading to the progressive accumulation of inactivated $Na_v1.5$. Use-dependence occurs because drug-modified channels slowly recover only at hyper-polarized voltages. Class 1 antiarrhythmic drugs and local anesthetics have a similar effect (Chahine *et al.*, 1992). We thus determined whether fluoxetine could inhibit Na^+ currents by mutating residues in the class 1 antiarrhythmic drug binding site. Amino acids situated near the cytoplasmic ends of the membrane-spanning S6 α-helixes of all four homologous domains (D1S6-D4S6) form the cytoplasmic entrance of the pore and contribute to the binding sites of both the native inactivation gate and class 1 antiarrhythmic drugs. We previously reported that two highly conserved residues of the D4S6 segment (F1760, Y1767) contribute directly to the local anesthetic binding site of

cardiac Na^+ channels (O'Leary and Chahine, 2002). We showed that both mutations (F1760C and Y1767C) markedly reduced the frequency-dependent effect, with the Y1767C mutation having the greatest effect. However, in tonic block, the F1760C increased the IC_{50} of fluoxetine more significantly than the Y1767C. These results showed that these residues of D4S6 are an integral part of the binding site of fluoxetine, as is the case with many class 1 antiarrhythmic drugs. Our data also suggest that F1760 appears to be more involved in binding fluoxetine when the channel is in the resting state, while Y1767 appears to be key for fluoxetine binding when the channel is in the open/inactivated sate.

Molecular modeling fluoxetine in $Na_v1.5$ was in agreement with mutational experiments, in which $F^{4i15(1760)}$ and $Y^{4i22(1767)}$ were found to be the key residues in binding fluoxetine. However, the models predicted that the ligand is able to assume two energetically favorable binding modes. The vertical binding mode was favored in the open state model, while the horizontal mode in the closed state model. This could suggest that open channel block involves both $F^{4i15(1760)}$ and $Y^{4i22(1767)}$ as visualized in the vertical binding mode. With the same assumption, the horizontal binding mode could represent resting channel block with $F^{4i15(1760)}$ as the essential residue. Fluoxetine share similarities to local anesthetics. Both are drugs sensitive to mutations at $F^{4i15(1760)}$ and $Y^{4i22(1767)}$. Structurally, fluoxetine resembles most classical local anesthetics in approximate size and by possessing an ammonium group and a benzene ring. Fluoxetine adopts similar binding modes in the closed channel homology model as QX-314, cocaine, and tetracaine (Bruhova *et al.*, 2008; Tikhonov and Zhorov, 2012). Since fluoxetine can protrude between the III-IV inner helix interface while in the horizontal binding mode, it could

suggest that fluoxetine may enter or exit through the III-IV domain interface pathway from the extracellular side of the membrane as it has been demonstrated with local anesthetics (Qu *et al.*, 1995; Sunami *et al.*, 2001). Experiments with fluoxetine with a quaternarized ammonium could reveal whether the ligand can block from the extracellular side.

The blockade of the $Na_v1.5$ by fluoxetine should be taken into consideration when prescribing this drug. Blocking the cardiac Na^+ channel may cause an intracardiac conduction delay, which may in turn cause a prolongation of the QRS complex on the electrocardiogram (Delk *et al.*, 2007). Given the association between QRS prolongation and mortality, and the potential for drug-induced arrhythmia, caution is required when prescribing fluoxetine (Thanacoody and Thomas, 2005; Delk *et al.*, 2007), especially given that inhibiting the $Na_v1.5$ by as little as 10% may cause a prolongation of the QRS complex in humans (Cordes *et al.*, 2009). However, a question remains as to how to transpose the significance of the IC_{50} value of fluoxetine to a pathophysiological setting. The IC_{50}/fC_{max} ratio, where fC_{max} represents the unbound (free) plasma concentration in a clinical setting, of a drug that evokes a QRS or a change in QT has been proposed as a tool for determining whether a drug can be safely prescribed (Redfern *et al.*, 2003; Harmer *et al.*, 2011). An IC_{50}/fC_{max} ratio above 30 to 100 has been shown to ensure a suitable degree of safety in terms of drug-induced QRS complex prolongation. The fC_{max} for fluoxetine is 93 nM (Harmer *et al.*, 2011). Thereby, when we mimic the membrane potential of cardiomyocytes in patch-clamp by imposing a holding potential of -90 mV to HEK-293 cells, the IC_{50}/fC_{max} ratio is 50. This is within the 30 to 100 margin and it should act as a safety flag for a possible cardiotoxicity.

Furthermore, in the case of fluoxetine, fC_{max} may not be a good indicator of actual plasma concentrations of total $Na_v1.5$ blockers in vivo since norfluoxetine, an active metabolite of fluoxetine, has a higher affinity for $Na_v1.5$ than fluoxetine itself. Given that norfluoxetine has a half-life of more than a week compared to 70 h for a single dose of fluoxetine (Schepens, 1996), there is a possibility of a long-lasting additive effect on cardiac Na^+ channels. In fact, in the calculation of the IC_{50}/fC_{max} ratio, we should take into consideration the unbound (free) plasma concentration of norfluoxetine. Despite the lack of information about the fC_{max} after a single dose, it is known that the plasma concentration of total (unbound and bound) fluoxetine and norfluoxetine at steady state are very similar after chronicle treatment (91 to 302 ng/ml and 72 to 258 ng/ml, respectively) (U.S. Food and Drug Administration). These suggest that the IC_{50}/fC_{max} ratio following fluoxetine treatment is probably underestimated.

In conclusion, caution should be taken when prescribing fluoxetine at same time as other Na^+ channel inhibitors such as class 1 anti-arrhythmic drugs, especially class 1A and 1C drugs. In addition, fluoxetine should be prescribed with extreme care for patients suffering from ventricular conduction disorders or liver disease. Indeed, as the liver is the primary site of fluoxetine metabolism, its impairment, such cirrhosis, affects the elimination half-life of fluoxetine and norfluoxetine (Schenker *et al.*, 1988).

Authorship Contributions:

Conducted experiments: Poulin, Chahine, Beaulieu

Participated in research design: Poulin, Chahine, Beaulieu, Timour, Theriault

Wrote and contributed to the writing of the manuscript: Poulin, Chahine, Beaulieu, Timour, Frassati

References

Bagnéris C, Decaen PG, Hall BA, Naylor CE, Clapham DE, Kay CWM, and Wallace BA (2013) Role of the C-terminal domain in the structure and function of tetrameric sodium channels. *Nat Commun* **4**:1–10.

Bolo NR, Hodé Y, Nédélec JF, Lainé E, Wagner G, and Macher JP (2000) Brain pharmacokinetics and tissue distribution in vivo of fluvoxamine and fluoxetine by fluorine magnetic resonance spectroscopy. *Neuropsychopharmacology* **23**:428–438.

Bruhova I, Tikhonov DB, and Zhorov BS (2008) Access and binding of local anesthetics in the closed sodium channel. *Mol Pharmacol* **74**:1033–1045.

Chahine M, Barchifg RL, Kallentg RG, and Horn R (1992) Lidocaine Block of Human Heartsodium channels expressed in Xenopus oocytes. *J Mol Cell Cardiol* **1236**:1231–1236.

Cordes J, Li C, Dugas J, Austin-LaFrance R, Lightbown I, Engwall M, Sutton M, and Steidl-Nichols J (2009) Translation between in vitro inhibition of the cardiac Nav1.5 channel and pre-clinical and clinical QRS widening. *J Pharmacol Toxicol Methods* **60**:221.

Cosgrove KP, Staley JK, Baldwin RM, Bois F, Plisson C, Al-Tikriti MS, Seibyl JP, Goodman MM, and Tamagnan GD (2010) SPECT imaging with the serotonin transporter radiotracer [123I]p ZIENT in nonhuman primate brain. *Nucl Med Biol* **37**:587–591.

Deák F, Lasztóczi B, Pacher P, Petheö GL, Valéria Kecskeméti, and Spät A (2000) Inhibition of voltage-gated calcium channels by fluoxetine in rat hippocampal pyramidal cells. *Neuropharmacology* **39**:1029–1036.

Delk C, Holstege CP, and Brady WJ (2007) Electrocardiographic abnormalities associated with poisoning. *Am J Emerg Med* **25**:672–687.

Dewar MJS, Zoebisch EG, Healy EF, and Stewart JJP (1985) Development and use of quantum mechanical molecular models. 76. AM1: a new general purpose quantum mechanical molecular model. *J Am Chem Soc* **107**:3902–3909.

Eisensamer B, Rammes G, Gimpl G, Shapa M, Ferrari U, Hapfelmeier G, Bondy B, Parsons C, Gilling K, Zieglgänsberger W, Holsboer F, and Rupprecht R (2003) Antidepressants are functional antagonists at the serotonin type 3 (5-HT3) receptor. *Mol Psychiatry* **8**:994–1007.

Garden DP, and Zhorov BS (2010) Docking flexible ligands in proteins with a solvent exposure- and distance-dependent dielectric function. *J Comput Aided Mol Des* **24**:91–105.

Han DD, and Gu HH (2006) Comparison of the monoamine transporters from human and mouse in their sensitivities to psychostimulant drugs. *BMC Pharmacol* **6**:1–7.

Harmer a R, Valentin J-P, and Pollard CE (2011) On the relationship between block of the cardiac Na^+ channel and drug-induced prolongation of the QRS complex. *Br J Pharmacol* **164**:260–273.

Hennings ECP, Kiss JP, De Oliveira K, Toth PT, and Vizi ES (1999) Nicotinic acetylcholine receptor antagonistic activity of monoamine uptake blockers in rat hippocampal slices. *J Neurochem* **73**:1043–1050.

Herbert E, and Chahine M (2006) Clinical aspects and physiopathology of Brugada syndrome: review of current concepts. *Can J Physiol Pharmacol* **84**:795–802.

Huang H, Priori SG, Napolitano C, O'Leary ME, and Chahine M (2011) Y1767C, a novel SCN5A mutation, induces a persistent Na+ current and potentiates ranolazine inhibition of Nav1.5 channels. *Am J Physiol Heart Circ Physiol* **300**:288–299.

Lazaridis T, and Karplus M (1999) Effective energy function for proteins in solution. *Proteins* **35**:133–152.

Lenkey N, Karoly R, Kiss JP, Szasz BK, Vizi ES, and Mike A (2006) The Mechanism of Activity-Dependent Sodium Channel Inhibition by the Antidepressants Fluoxetine and Desipramine. *Mol Pharmacol* **70**:2052–2063.

Li Z, and Scheraga HA (1987) Monte Carlo-minimization approach to the multiple-minima problem in protein folding. *Proc Natl Acad Sci U S A* **84**:6611–6615.

Maertens C, Droogmans G, Verbesselt R, and Nilius B (2002) Block of volume-regulated anion channels by selective serotonin reuptake inhibitors. *Naunyn Schmiedebergs Arch Pharmacol* **366**:158–165.

Magyar J, Rusznák Z, Harasztosi C, Körtvély A, Pacher P, Bányász T, Pankucsi C, Kovács L, Szûcs G, Nánási PP, and Kecskeméti V (2003) Differential effects of fluoxetine enantiomers in mammalian neural and cardiac tissues. *Int J Mol Med* **11**:535–542.

McCusker EC, Bagnéris C, Naylor CE, Cole AR, D'Avanzo N, Nichols CG, and Wallace BA (2012) Structure of a bacterial voltage-gated sodium channel pore reveals mechanisms of opening and closing. *Nat Commun* **3**:1102;1–8.

Muscettola G, Goodwin FK, Potter WZ, Magda M, Claeys MM, and Markey SP (1978) Imipramine and desipramine in plasma and spinal fluid: relationship to clinical response and serotonin metabolism. *Arch Gen Psychiatry* **35**:621–625.

O'Leary ME, and Chahine M (2002) Cocaine binds to a common site on open and inactivated human heart (Na(v)1.5) sodium channels. *J Physiol* **541**:701–716.

Pacher P, and Kecskemeti V (2008) Cardiovascular Side Effects of New Antidepressants and Antipsychotics: New Drugs, old Concerns? *Curr Pharm Des* **10**:2463–2475.

Pacher P, Magyar J, Szigligeti P, Bányász T, Pankucsi C, Korom Z, Ungvári Z, Kecskeméti V, and Nánási PP (2000) Electrophysiological effects of fluoxetine in mammalian cardiac tissues. *Naunyn Schmiedebergs Arch Pharmacol* **361**:67–73.

Payandeh J, Scheuer T, Zheng N, and Catterall WA (2011) The crystal structure of a voltage-gated sodium channel. *Nature* **475**:353–358, Nature Publishing Group, a division of Macmillan Publishers Limited. All Rights Reserved.

Qu Y, Rogers J, Tanada T, Scheuer T, and Catterall WA (1995) Molecular determinants of drug access to the receptor site for antiarrhythmic drugs in the cardiac Na+ channel. *Proc Natl Acad Sci U S A* **92**:11839–11843.

Rajamani S, Eckhardt LL, Valdivia CR, Klemens C a, Gillman BM, Anderson CL, Holzem KM, Delisle BP, Anson BD, Makielski JC, and January CT (2006) Drug-induced long QT syndrome: hERG K+ channel block and disruption of protein trafficking by fluoxetine and norfluoxetine. *Br J Pharmacol* **149**:481–489.

Redfern WS, Carlsson L, Davis AS, Lynch WG, MacKenzie I, Palethorpe S, Siegl PKS, Strang I, Sullivan AT, Wallis R, Camm AJ, and Hammond TG (2003) Relationships between preclinical cardiac electrophysiology, clinical QT interval prolongation and torsade de pointes for a broad range of drugs: evidence for a provisional safety margin in drug development. *Cardiovasc Res* **58**:32–45.

Schenker S, Bergstrom RF, Wolen RL, and Lemberger L (1988) Fluoxetine disposition and elimination in cirrhosis. *Clin Pharmacol Ther* **44**:353–359.

Schepens R (1996) Fluoxetine. *IPCS INCHEM [Online] http//www.inchem.org/documents/pims/pharm/pim651.htm#SectionTitle65%20%20Elimination%20and%20excretion* **Online**.

Sghendo L, and Mifsud J (2012) Understanding the molecular pharmacology of the serotonergic system: using fluoxetine as a model. *J Pharm Pharmacol* **64**:317–325.

Sunami A, Glaaser IW, and Fozzard HA (2001) Structural and gating changes of the sodium channel induced by mutation of a residue in the upper third of IVS6, creating an external access path for local anesthetics. *Mol Pharmacol* **59**:684–691.

Tejani-Butt SM (1992) [3H]nisoxetine: a radioligand for quantitation of norepinephrine uptake sites by autoradiography or by homogenate binding. *J Pharmacol Exp Ther* **260**:427–436.

Thanacoody HKR, and Thomas SHL (2005) Tricyclic antidepressant poisoning□: cardiovascular toxicity. *Toxicol Rev* **24**:205–214.

Thomas D, Gut B, Wendt-Nordahl G, and Kiehn J (2002) The antidepressant drug fluoxetine is an inhibitor of human ether-a-go-go-related gene (HERG) potassium channels. *J Pharmacol Exp Ther* **300**:543–548.

Tikhonov DB, and Zhorov BS (2012) Architecture and pore block of eukaryotic voltage-gated sodium channels in view of NavAb bacterial sodium channel structure. *Mol Pharmacol* **82**:97–104.

Timour Q, Frassati D, Descotes J, Chevalier P, Christé G, and Chahine M (2012) Sudden death of cardiac origin and psychotropic drugs. *Front Pharmacol* **3**:76;1–9.

Torres GE, Gainetdinov RR, and Caron MG (2003) Plasma membrane monoamine transporters: structure, regulation and function. *Nat Rev Neurosci* **4**:13–25.

U.S. Food and Drug Administration. (n.d.) *Prozac NDA 18-936/S-064 final labeling, March 31, 2009.*, Retrieved March 31, 2014, from www.accessdata.fda.gov/drugsatfda_docs/label/2003/018936s064lbl.pdf.

Wang GK, Russell G, and Wang S (2013) Persistent human cardiac Na (+) currents in stably transfected mammalian cells: Robust expression and distinct open-channel selectivity among Class 1 antiarrhythmics. *Channels (Austin)* **7**:1–12.

Weiner SJ, Kollman PA, Case DA, Singh UC, Ghio C, Alagona G, Profeta S, and Weiner P (1984) A new force field for molecular mechanical simulation of nucleic acids and proteins. *J Am Chem Soc* **106**:765–784, American Chemical Society.

Weiner SJ, Kollman PA, Nguyen DT, and Case DA (1986) An all atom force field for simulations of proteins and nucleic acids. *J Comput Chem* **7**:230–252.

Wong DT, Bymaster FP, and Engleman EA (1995) Minireview prozac (fluoxetine , lilly 110140), the first selective serotonin uptake inhibitor and an antidepressant drug□: twenty years since its first publication. *Life Sci* **57**:411–441.

Wong DT, Horng JS, Bymaster FP, Hauser KL, and Molloy BB (1974) A selective inhibitor of serotonin uptake: Lilly 110140, 3-(p-trifluoromethylphenoxy)-N-methyl-3-phenylpropylamine. *Life Sci* **15**:471–479.

Zhorov BS, and Tikhonov DB (2004) Potassium, sodium, calcium and glutamate-gated channels: pore architecture and ligand action. *J Neurochem* **88**:782–799.

Footnotes

This work was supported by grants from the Canadian Institutes of Health Research [CIHR, MOP-111072]; and the Heart and Stroke Foundation of Quebec (HSFQ). This work was supported also by a research fellowship from the Canadian Institute of Health Research to I.B; and by the National Institutes of Health [NS-064969] through Anthony Auerbach to I.B. Computations were made possible by the facilities of the Center for Computational Research University at Buffalo (CCR: www.ccr.buffalo.edu).

Figure legends:

Figure 1

Tonic block of $Na_v1.5$/WT currents. (A) Superimposed I_{Na} recordings obtained before and after perfusion with two concentrations of racemic fluoxetine from a holding potential of -140 mV. The dashed line represents zero current. (B) Dose-response curves of the inhibitory effect of norfluoxetine and different optical isomers of fluoxetine on $Na_v1.5$/WT currents. HEK-293 cells stably expressing $Na_v1.5$/WT were perfused with different concentrations of norfluoxetine, racemic fluoxetine, S(+) fluoxetine or R(–) fluoxetine. There was no significant difference between the IC_{50} of racemic fluoxetine (IC_{50} = 39.4 ± 2.0 μM, n = 3-7) and its two optical isomers (IC_{50} = 40.0 ± 2.6 μM, n = 6-14 and 46.7 ± 3.1 μM, n = 3-10). However, norfluoxetine had a significant lower IC_{50} (29.5 ± 1.0 μM, n = 8-15). The IC_{50} of fluoxetine was significantly reduced to 4.7 ± 0.5 μM (n = 7-10) when recorded at a holding potential of -90 mV (*B*, open triangle). (C) Dose-response curves of the inhibitory effect of nisoxetine (n = 3-11), methylphenidate (n = 4-9), and fenfluramine (n = 4-6) on $Na_v1.5$/WT currents recorded at a holding potential of -140 or -90 mV. The IC_{50} of the three drugs at a holding potential of -90 mV were significantly lower than those recorded at -140 mV. Insets in *B* and *C* show the IC_{50} for each compound. The values were fitted to a Hill equation. Currents were elicited from a holding potential of –140 mV or -90 mV, and a–30 mV test pulse lasting 50 ms was delivered every 5 s. $***P < 0.001$

Figure 2

Gating properties of $Na_v1.5$/WT treated with fluoxetine. (A) Voltage-dependence of steady-state activation and inactivation of $Na_v1.5$. Cells were perfused with Ringer's solution as a control (activation, n = 14; inactivation, n = 19) or with 30 μM racemic fluoxetine (activation, n = 18; inactivation, n = 17). Activation curves were elicited with 50 ms depolarizing steps from –100 to 80 mV in 10 mV increments. Cells were held at a holding potential of –140 mV. Fluoxetine caused no significant shift in the activation curve. Steady-state inactivation was determined using 4 ms test pulses to –30 mV after a 500 ms prepulse to potentials ranging from –140 mV to 0 mV (see the *inset* under the inactivation curves for the protocol). The application of 30 μM fluoxetine induced a significant –6.7 mV shift of the inactivation curve (***$P < 0.001$) (Table 1). The activation and inactivation curves were fitted to a single Boltzman function (see Materials and Methods). (B) Recovery from inactivation of $Na_v1.5$ in the absence (n = 10) or presence (n = 9) of 30 μM fluoxetine. The cells were depolarized to –30 mV for 40 ms from a holding potential of –140 mV to inactivate all the Na^+ channels. Test pulses were then applied to –30 mV for 20 ms to measure current amplitudes, with an interval ranging from 0.1 to 4000 ms. The resulting curves were fitted to a double (control) or a triple (+ fluoxetine) exponential equation, which yielded two or three time constants (τ_1, τ_2, τ_3). The application of 30 μM fluoxetine strongly slowed the recovery from inactivation with the appearance of a third time constant (Table 1).

Figure 3

Frequency-dependent inhibition. (A) Representative whole-cell traces recorded from $Na_v1.5$/WT (+/- 30 μM fluoxetine), $Na_v1.5$/F1760C (+ 30 μM fluoxetine), and $Na_v1.5$/Y1767C (+ 30 μM fluoxetine) when pulsing at 10 Hz. The dashed line represents zero current. (B) Use-dependent blocks of $Na_v1.5$/WT, $Na_v1.5$/F1760C, and $Na_v1.5$/Y1767C currents in the presence of 30 μM fluoxetine. A 50 pulse train was applied at –30 mV for 10 ms from a holding potential of –140 mV when pulsing at 2 Hz, 5 Hz, and 10 Hz. Peak currents were measured, normalized to the peak amplitude at P_1, and plotted against the corresponding pules. (C) Relative currents amplitudes (P_{50}/P_1) of the 50th sweep recorded from $Na_v1.5$/WT, $Na_v1.5$/F1760C and $Na_v1.5$/Y1767C. After the fluoxetine treatment, $Na_v1.5$/WT (n = 8) currents were significantly reduced by 44%, 58%, and 67% compared to the control when pulsing at 2, 5, and 10 Hz, respectively (***$P < 0.001$). Fluoxetine significantly reduced $Na_v1.5$/F1760C (n = 11) currents by 15% and 20% when pulsing at 5 and 10 Hz (###$P < 0.001$), respectively, and $Na_v1.5$/Y1767C (n = 6) currents by 5% when pulsing at 10 Hz (φ φ $P < 0.01$) compared with control. There was no significant use-dependent inhibition of $Na_v1.5$/WT (n = 7), $Na_v1.5$/F1760C (n = 5), or $Na_v1.5$/Y1767C (n = 6) currents before the fluoxetine treatment. The controls curves of $Na_v1.5$/WT, $Na_v1.5$/F1760C and $Na_v1.5$/Y1767C without fluoxetine treatment were removed from the graphic *B* and *C* for clarity.

Figure 4

Tonic block of $Na_v1.5$/F1760C and $Na_v1.5$/Y1767C by fluoxetine. (A) Representative whole-cell traces recorded from $Na_v1.5$/WT (left), $Na_v1.5$/F1760C (middle), and

$Na_v1.5$/Y1767C (right) channels before and after the application of 50 μM fluoxetine. The dashed line represents zero current. (B) Dose-response curves of the inhibitory effect of racemic fluoxetine on $Na_v1.5$/WT, $Na_v1.5$/F1760C, and $Na_v1.5$/Y1767C. The IC_{50} values of $Na_v1.5$/F1760C (83 μM) and $Na_v1.5$/Y1767C (50 μM) were significantly higher than $Na_v1.5$/WT value (39 μM), $^{**}P < 0.01$ and $^{***}P < 0.001$. The different concentrations of drugs were applied using a perfusion system. Currents were elicited from a holding potential of –140 mV with a 50 ms test pulse at –30 mV delivered every 5 s. Insets in *B* shows the IC_{50} for each compound. Normalized current (I_{Na}) values were fitted to a Hill equation.

Figure 5

Open-channel block of $Na_v1.5$ by fluoxetine. (A) Superimposed I_{Na} recordings obtained following the application of different concentrations of fluoxetine on $Na_v1.5$/L409C/A410W expressing cells. The dashed line represents zero current. (B) Dose-response curves of the inhibitory effect of fluoxetine on $Na_v1.5$/L409C/A410W at the peak current (blue circle) and 90-100 ms after the beginning of the pulse (green square). The IC_{50} value at the end of the pulse (3.5 μM) was significantly lower than the IC_{50} value at the peak current (9.6 μM) ($^{***}P < 0.001$). Currents were elicited from a holding potential of –140 mV with a 50 ms test pulse at 0 mV delivered every 5 s. Normalized current (I_{Na}) values were fitted to a Hill equation. Dotted grey boxes represent the peak current (left boxe) and the 90-100 ms (right boxe) areas used to construct the dose-response curves.

Figure 6

Searching for the binding site of fluoxetine in the closed and open $Na_v1.5$. The P-loops and S6 helices of domains I, II, III, and IV are colored blue, orange, green, and violet, respectively. The outer helices and the L45 linker are shown as gray strands. The side chains of residues in the DEKA locus, $Q^{1p49(372)}$, $S^{4p49(1712)}$, $F^{4i15(1760)}$ and $Y^{4i22(1767)}$ are shown as sticks with yellow carbons. The water molecule at the DEKA locus is rod-shaped. (A and B) The side and extracellular views of the randomly generated starting points of fluoxetine in the closed $Na_v1.5$. Fluoxetine is presented in wire-frame with gray carbons. For clarity, only 6000 of the 60,000 starting points are shown. (C-F) The side views of the lowest energy vertical (C and E) and horizontal (D and F) binding modes of fluoxetine in the closed (C and D) and open (E and F) channel. Fluoxetine is shown in thick sticks with gray carbons. The side chain of $F^{3p49(1236)}$ is shown in D and F. For clarity the outer helices are not shown in C–F (see PDB file in Data Supplement).

Table 1. ***Biophysical properties of Nav1.5 channels***

	$Na_v1.5$/WT Control		$Na_v1.5$/WT Fluoxetine		
	Mean ± sem	***n***	**Mean ± sem**		***n***
Steady-state activation					
$V_{1/2}$, mV	- 43.49 ± 1.46	14	- 41.52 ± 1.17		18
kv	- 6.13 ± 0.32	14	7.28 ± 0.17	**	18
Steady-state inactivation					
$V_{1/2}$, mV	-87.34 ± 0.94	19	- 94.04 ± 1.64	***	17
kv	6.37 ± 0.19	19	7.67 ± 0.29	***	17
Recovery from inactivation					
τ_1	1.50 ± 0.1	10	1.63 ± 0.1		6
A_1	76.3 ± 2.7	10	35.7 ± 2.1		6
τ_2	9.13 ± 1.0	10	14.90 ± 2.6		6
A_2	23.7 ± 0.8	10	22.0 ± 2.1		6
τ_3	–	–	1598.23 ± 41.6		6
A_3	–	–	42.3 ± 1.7		6

$V_{1/2}$, midpoint for activation or inactivation; *kv*, slope factor for activation or inactivation; τ, time constant; *A*, fraction of the τ components (%); *n*, number of cells. Values are means ± sem, $^{**}P < 0.01$, $^{***}P < 0.001$

Figure 1

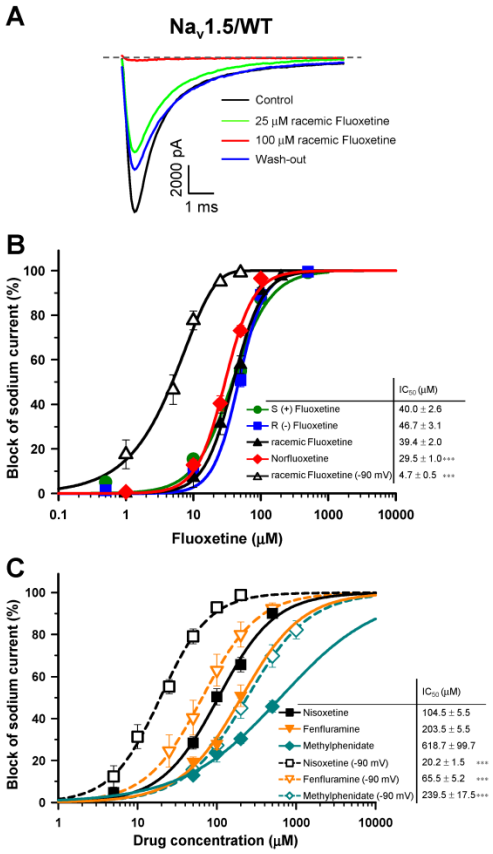
A
Na$_v$1.5/WT
Control
25 µM racemic Fluoxetine
100 µM racemic Fluoxetine
Wash-out
2000 pA
1 ms
B
Block of sodium current (%)
Fluoxetine (µM)
IC$_{50}$ (µM)
S (+) Fluoxetine 40.0 ± 2.6
R (-) Fluoxetine 46.7 ± 3.1
racemic Fluoxetine 39.4 ± 2.0
Norfluoxetine 29.5 ± 1.0***
racemic Fluoxetine (-90 mV) 4.7 ± 0.5 ***
C
Block of sodium current (%)
Drug concentration (µM)
IC$_{50}$ (µM)
Nisoxetine 104.5 ± 5.5
Fenfluramine 203.5 ± 5.5
Methylphenidate 618.7 ± 99.7
Nisoxetine (-90 mV) 20.2 ± 1.5 ***
Fenfluramine (-90 mV) 65.5 ± 5.2 ***
Methylphenidate (-90 mV) 239.5 ± 17.5***

Figure 2

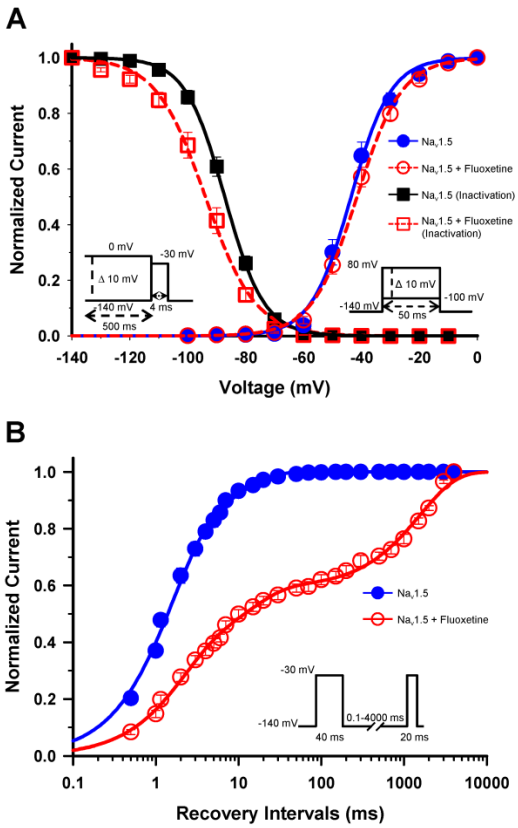
A
Normalized Current
Voltage (mV)
Na,1.5
Na,1.5 + Fluoxetine
Na,1.5 (Inactivation)
Na,1.5 + Fluoxetine (Inactivation)
0 mV
-30 mV
Δ 10 mV
-140 mV
4 ms
500 ms
80 mV
Δ 10 mV
-140 mV
-100 mV
50 ms
B
Normalized Current
Recovery Intervals (ms)
Na,1.5
Na,1.5 + Fluoxetine
-30 mV
-140 mV
0.1-4000 ms
40 ms
20 ms

Figure 3

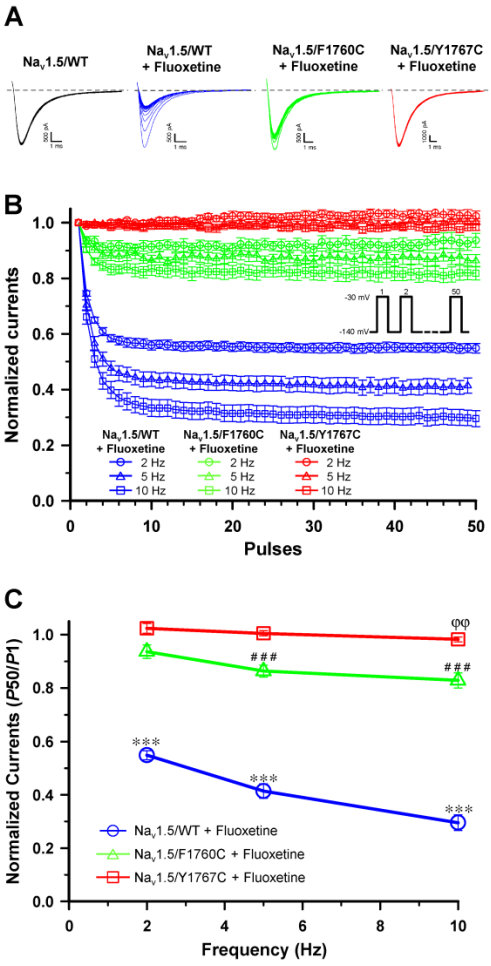
A
Na$_v$1.5/WT
Na$_v$1.5/WT + Fluoxetine
Na$_v$1.5/F1760C + Fluoxetine
Na$_v$1.5/Y1767C + Fluoxetine
B
Normalized currents
Pulses
-30 mV
-140 mV
Na$_v$1.5/WT + Fluoxetine
Na$_v$1.5/F1760C + Fluoxetine
Na$_v$1.5/Y1767C + Fluoxetine
2 Hz
5 Hz
10 Hz
C
Normalized Currents (P50/P1)
Frequency (Hz)
φφ
###
***
Na$_v$1.5/WT + Fluoxetine
Na$_v$1.5/F1760C + Fluoxetine
Na$_v$1.5/Y1767C + Fluoxetine

Figure 4

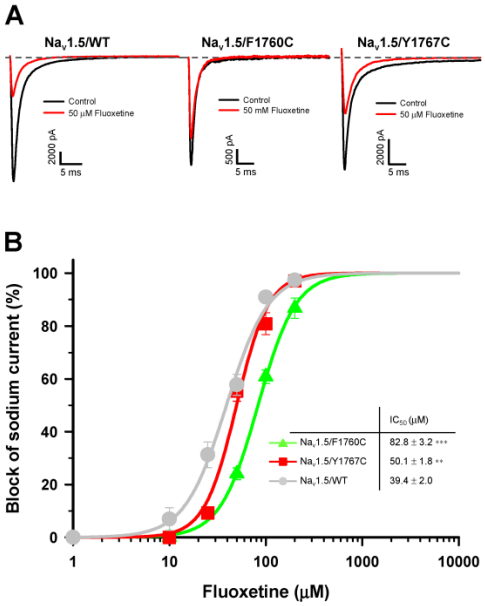
A
Na$_v$1.5/WT
Na$_v$1.5/F1760C
Na$_v$1.5/Y1767C
Control
50 µM Fluoxetine
Control
50 mM Fluoxetine
Control
50 µM Fluoxetine
2000 pA
5 ms
500 pA
5 ms
2000 pA
5 ms
B
Block of sodium current (%)
100
80
60
40
20
0
1
10
100
1000
10000
Fluoxetine (µM)
IC$_{50}$ (µM)
Na$_v$1.5/F1760C 82.8 ± 3.2 ***
Na$_v$1.5/Y1767C 50.1 ± 1.8 **
Na$_v$1.5/WT 39.4 ± 2.0

Figure 5

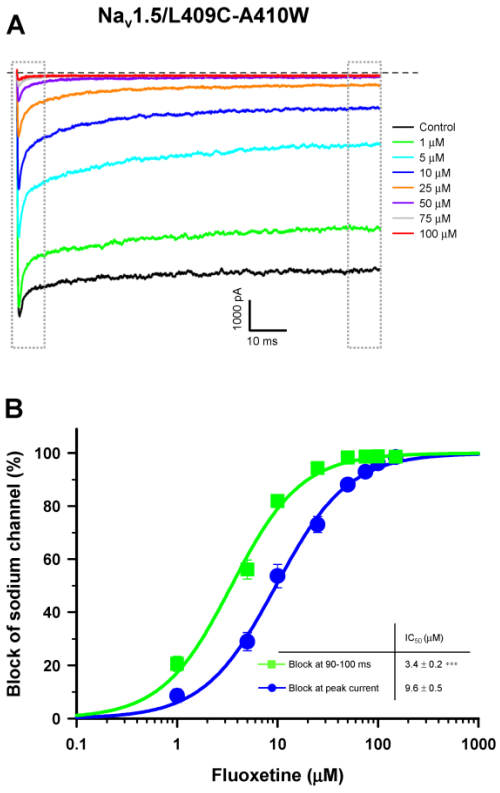
A
Na$_v$1.5/L409C-A410W
Control
1 µM
5 µM
10 µM
25 µM
50 µM
75 µM
100 µM
1000 pA
10 ms
B
Block of sodium channel (%)
100
80
60
40
20
0
0.1
1
10
100
1000
Fluoxetine (µM)
IC50 (µM)
Block at 90-100 ms
3.4 ± 0.2 ***
Block at peak current
9.6 ± 0.5

Figure 6